

**2,4-Dimethylene-1,3-cyclobutanediyl and
2,4-Dimethylenebicyclobutane.
Synthesis, Spectroscopy, and Reactivity
of a Triplet Biradical and Its Covalent Isomer**

Thesis by
Gary James Snyder

In Partial Fulfillment of the Requirements
for the Degree of
Doctor of Philosophy

California Institute of Technology
Pasadena, California

1988
(Submitted December 23, 1987)

©1988
Gary J. Snyder
All Rights Reserved

To My Parents

Acknowledgement

I would first like to thank my advisor, Dennis Dougherty, for his help, encouragement, friendship, and patience. Although my stay at Caltech has been trying at times, I am grateful to have spent it in a research group that has contributed so much to my scientific development. I would also like to thank Dennis for teaching me to say "cooled to 4 K and photolyzed in the cavity of an ESR spectrometer" and for all the golf tips (the don't-do-it-like-this type). Additional thanks are due my undergraduate advisor, Richard Holder (Univ. of New Mexico), who first sparked my interest in physical organic chemistry.

I am also grateful to the members of the Dougherty research group for their friendship and scientific interactions. Specifically, thanks go to Lisa McElwee-White for the moral support she provided in my early years at Caltech and for teaching me to cook microwaveable dinners that fit into little plastic containers. Moon Chang was responsible for instructing me in a multitude of useful and interesting lab techniques, and Aaron "Gomez" Goldberg first introduced me to the wonders of EPR spectroscopy, for which I will be eternally grateful. Later EPR work was greatly aided by Rakesh Jain, Mike Sponsler, and especially Frank Coms. Thanks also go to Julian Pranata for the many helpful discussions on theoretical matters and to David Kaisaki for donating several grams of benzvalene.

Several others also made significant contributions to this project. Janet Marshall is responsible for the emission spectra, and David Smith

invested some time and effort in attempting to measure a fluorescence lifetime. Thanks also go to Al Sylwester for his many words of wisdom, which included "nickel peroxide", and to Tracy Handel for her patience with a certain seemingly endless low-temperature ^{13}C NMR experiment that finally bit the dust. Steve Witt, Dave Blair, and Craig Martin provided valuable assistance with EPR experiments over the years, and Tom Dunn was always available to repair the weak link in the chain of EPR-associated instrumentation.

On a more personal note, life at Caltech would have been much less tolerable if not for the many afternoons of non-competitive (as it turned out) softball with members of the group. A special thanks also goes to my uncle, Roy Snyder, for the occasional use of his sailboat, and to deckhands Brian Masek and Dave Stauffer, who bought most of the beer.

Finally, I would like to acknowledge financial support from the PRF and the NSF, the latter of which provided a pre-doctoral fellowship. I am also very grateful to Linda Cusimano for all the time she spent typing this manuscript and for putting up with the seemingly endless flow of corrections and rewrites.

Abstract

The preparation and direct observation of triplet 2,4-dimethylene-1,3-cyclobutanediyl (1), the non-Kekulé isomer of benzene, is described. The biradical was generated by photolysis of 5,6-dimethylene-2,3-diazabicyclo[2.1.1]hex-2-ene (2) (which was synthesized in several steps from benzvalene) under cryogenic, matrix-isolation conditions. Biradical 1 was characterized by EPR spectroscopy ($|D/hc| = 0.0204 \text{ cm}^{-1}$, $|E/hc| = 0.0028 \text{ cm}^{-1}$) and found to have a triplet ground state. The $\Delta m_s = 2$ transition displays hyperfine splitting attributed to a 7.3-G coupling to the ring methine and a 5.9-G coupling to the exocyclic methylene protons. Several experiments, including application of the magnetophotoselection (mps) technique in the generation of biradical 1, have allowed a determination of the zero-field triplet sublevels as $x = -0.0040$, $y = +0.0136$, and $z = -0.0096 \text{ cm}^{-1}$, where x and y are respectively the long and short in-plane axes and z the out-of-plane axis of 1.

Triplet 1 is yellow-orange and displays highly structured absorption ($\lambda_{\text{max}} = 506 \text{ nm}$) and fluorescence ($\lambda_{\text{max}} = 510 \text{ nm}$) spectra, with vibronic spacings of 1520 and 620 cm^{-1} for absorption and 1570 and 620 cm^{-1} for emission. The spectra were unequivocally assigned to triplet 1 by the use of a novel technique that takes advantage of the biradical's photolability. The absorption has $\epsilon = 7200 \text{ M}^{-1} \text{ cm}^{-1}$ and $f = 0.022$, establishing that the transition is spin-allowed. Further use of the mps technique has demonstrated that the transition is x -polarized, and the excited state is therefore of B_{1g} symmetry, in accord with theoretical predictions.

Thermolysis or direct photolysis of diazene **2** in fluid solution produces 2,4-dimethylenebicyclo[1.1.0]butane (**3**), whose ^1H NMR spectrum (-80°C , CD_2Cl_2) consists of singlets at δ 4.22 and 3.18 in a 2:1 ratio. Compound **3** is thermally unstable and dimerizes with second-order kinetics between -80 and -25°C ($\Delta H^\ddagger = 6.8 \text{ kcal mol}^{-1}$, $\Delta S^\ddagger = -28 \text{ eu}$) by a mechanism involving direct combination of two molecules of **3** in the rate-determining step. This singlet-manifold reaction ultimately produces a mixture of two dimers, 3,8,9-trimethylenetricyclo[5.1.1.0^{2,5}]non-4-ene (**75**) and *trans*-3,10-dimethylenetricyclo[6.2.0.0^{2,5}]deca-4,8-diene (**76t**), with the former predominating. In contrast, triplet-sensitized photolysis of **2**, which leads to triplet **1**, provides, in addition to **75** and **76t**, a substantial amount of *trans*-5,10-dimethylenetricyclo[6.2.0.0^{3,6}]deca-3,8-diene (**77t**) and small amounts of two unidentified dimers.

In addition, triplet biradical **1** ring-closes to **3** in rigid media both thermally (77-140 K) and photochemically. In solution **3** forms triplet **1** upon energy transfer from sensitizers having relatively low triplet energies. The implications of the thermal chemistry for the energy surfaces of the system are discussed.

Table of Contents

Acknowledgement	iv
Abstract	vi
List of Figures	xi
List of Tables	xii
List of Schemes	xiii
 Chapter 1 —Introduction	 1
Structural classes of non-Kekulé hydrocarbons. General theoretical considerations.	3
Experimental studies of non-Kekulé molecules.	5
Simple TMMs.	5
Benzenoid systems.	7
TMEs.	11
2,4-Dimethylene-1,3-cyclobutanediyl (1) as a unique non-Kekulé molecule.	14
The predicted relative energies of singlet and triplet 1.	15
Potential stability and reactivity of 1. Energetics of ring closure.	16
Potential reactivity and structure of 2,4-dimethylene-bicyclo[1.1.0]butane (3).	20
Scope of this work.	22
References and notes.	23
 Chapter 2 —Synthesis, EPR and Electronic Spectroscopy of 2,4-Dimethylene-1,3-cyclobutanediyl	 31
Synthesis.	33
EPR spectroscopy.	49
Assignment of the spectrum to triplet 1.	49
Proton hyperfine splitting.	53
Curie plot.	57
Electronic spectroscopy.	60
Assignment of the spectra to triplet 1.	60

The nature of the electronic transition. -----	65
Assignment of the principal axes and transition moment. Magnetophotoselection. -----	67
The zero-field triplet sublevels. -----	67
The electronic transition dipole moment and vibrational structure. -----	72
Discussion. -----	79
Concerning the singlet-triplet splitting. -----	79
Spin densities and spin polarization. -----	79
Zero-field splitting. -----	83
Magnetophotoselection. The secondary intensity variation. -----	86
Electronic spectroscopy. -----	89
Conclusion. -----	93
Experimental. -----	94
References and notes. -----	131

Chapter 3 —2,4-Dimethylenebicyclo[1.1.0]butane: Preparation, Spectroscopic and Chemical Characterization. Thermal and Photochemical Interconversion of Triplet 2,4-Dimethylene-1,3-cyclobutanediyl and Its Covalent Isomer -----	153
Preparation of dimethylenebicyclobutane (3) and characterization of dimers. -----	155
¹ H NMR spectroscopy of 3 . -----	155
Potential dimers. -----	157
Dimerization in the singlet and triplet manifolds. Spectroscopic assignment of dimers. -----	160
Thermal decomposition of diazene 2 . -----	165
Dimerization in the singlet manifold. -----	169
Dimethylenebicyclobutane dimerization kinetics. -----	169
Intermediacy of 3 in formation of dimers from 2 . -----	169
Dimerization mechanism. -----	174
Dimerization in the triplet manifold. -----	188
Interconversion of triplet 1 and 3 . -----	194

Photochemistry of triplet 1 at 77 K.	194
Photochemistry of 3 .	196
Thermal decay of triplet 1 in rigid media.	197
Discussion.	201
The Berson cascade mechanism.	201
Concerning the possibility of a cascade mechanism for 1 .	204
The dimerization of 3 .	209
Photochemistry of triplet 1 and 3 .	211
Thermal ring closure of triplet 1 .	213
Conclusion.	215
Experimental.	216
References and notes.	267

Appendix 1—Attempted Preparation of 2,4-Dialkyl-1,3-cyclobutanediyls -----

Results. -----	288
Experimental. -----	289
References and notes. -----	293

Appendix 2 —Concerning 2-Oxo-4-methylene-1,3-cyclobutanediyl

Reassignment of the reported EPR spectrum. -----	296
Attempted Synthesis. -----	299
References and notes. -----	300

Appendix 3 Source Listing of Computer Programs

CURIE	-----	303
UVESRDV	-----	304
KINB	-----	311
ABS	-----	313
OSCIL	-----	314

List of Figures

2-1	EPR spectrum of triplet 1. -----	50
2-2	Hyperfine structure of the $\Delta m_s = 2$ transition. -----	54
2-3	Hyperfine structure of the $\Delta m_s = 1$ region. -----	55
2-4	Curie plot. -----	58
2-5	Electronic spectra of triplet 1. -----	61
2-6	Photochemical action spectrum of triplet 1. -----	64
2-7	Relevant orientations and alignments for mps experiments.	68
2-8	Mps in the generation of triplet 1. -----	70
2-9	Mps in the photolysis of triplet 1. -----	73
2-10	Hückel MOs of 1. -----	82
2-11	Zero-field triplet sublevels of 4 and 1. -----	85
2-12	Integrated EPR spectra of Figures 2-8 and 2-9. -----	130
2-13	Simulations of $\Delta m_s = 2$ hyperfine splitting. -----	141
2-14	Calculated Curie Law curves for small S-T gaps. -----	144
3-1	MM2 structures and strain energies of dimers. -----	159
3-2	Arrhenius plot for the decomposition of 2. -----	166
3-3	Decay data for 3 plotted in first- and second-order forms. ----	170
3-4	Eyring plot for the dimerization of 3. -----	171
3-5	Concentrations of 2, 3, 75, and 76t during the thermolysis of 2.	173
3-6	Actual and calculated [3] vs time during the thermolysis of 2.	175
3-7	Dimer ratios vs temperature. -----	187
3-8	Progress of the sensitized photolysis of 2. -----	189
3-9	Arrhenius plot for the decay of triplet 1 at 90-130 K. -----	199
3-10	MM2 geometries of dimers. -----	223
3-11	NMR spectra of 75, 76t, and 77t. -----	227
3-12	Kinetic data for the decay of triplet 1 at 90-130 K. -----	264

List of Tables

1-1	Calculated S-T splitting for 1 . -----	16
1-2	Calculated geometrical parameters for 3 and 45 . -----	21
2-1	EPR zero-field splitting parameters for triplet biradicals. ----	51
2-2	Absorption data for non-Kekulé hydrocarbons and C ₆ H ₆ Kekulé hydrocarbons. -----	91
2-3	Transmittance data for filter combinations. -----	96
2-4	Determination of ϵ for triplet 1 . -----	124
3-1	Product mixtures from thermal and photochemical decompositions of 2 . -----	161
3-2	Activation parameters for diazene thermolyses. -----	167
3-3	Transmittance data for filter combinations. -----	217
3-4	Mass spectral data for dimers and <i>d</i> ₄ -dimers. -----	236
3-5	Decay kinetics of diazene 2 . -----	245
3-6	Dimerization kinetics of 3 . -----	247
3-7	Dimer ratios <i>vs</i> temperature. -----	254
3-8	Sensitized photolysis of 3 . -----	258
3-9	Thermal decay kinetics of triplet 1 in solid CH ₂ Cl ₂ . -----	266
A2-1	Calculated <i>D</i> values for non-Kekulé hydrocarbons and their oxo analogs. -----	297

List of Schemes

2-1	Synthesis of bicyclobutanes 49 and 50 . -----	35
2-2	MTAD addition mechanisms. -----	38
2-3	Synthesis of diazene 2 . -----	41
2-4	General methods for the preparation of diazenes. -----	42
2-5	Synthesis of 2-<i>d</i>₂ . -----	47
2-6	Miscellaneous attempted syntheses. -----	47
3-1	Relevant ¹ H NMR data for cyclopropane derivatives. -----	156
3-2	Potential mechanisms for the dimerization of 3 . -----	176
3-3	Competitive trapping experiments. -----	178
3-4	Potential singlet-manifold dimerization pathways. -----	181
3-5	Conformations of biradical 90 . -----	184
3-6	Potential triplet-manifold dimerization pathways. -----	190
3-7	Conformations of biradical 91 . -----	192
3-8	The Berson cascade mechanism. -----	203

Chapter 1

Introduction

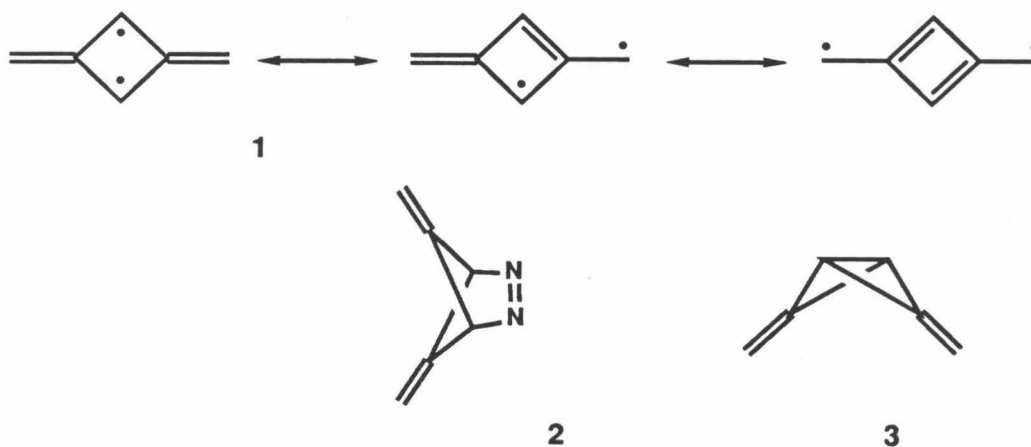
A large variety of thermal and photochemical reactions in organic chemistry are generally believed to involve biradicals as short-lived intermediates, proceed via biradical-like electronic states, or traverse transition structures envisioned as possessing biradical character.^{1,2,3} While this has historically provided much of the motivation for the study of biradicals, the attention of investigators in the field has recently shifted somewhat toward studying biradicals both as novel species in their own right and as potential building blocks for materials with unique magnetic and electrical properties.

One factor that has contributed to this shift in focus is the fact that, unlike localized hydrocarbon biradicals, which have generally proven somewhat elusive, many delocalized biradicals are relatively stable and amenable to direct study. Delocalized biradicals have been referred to as non-Kekulé⁴ molecules, because their unpaired electrons occupy a classical π -system but are topologically prevented from forming a π -bond. A major goal of current work has been to achieve an understanding of the factors that govern stability and spin preference in these systems. Such insight could potentially allow the design of extended systems with many electrons whose mutual interactions are controlled topologically. For example, this idea has recently been applied both theoretically⁵ and experimentally⁶ to the construction of organic ferromagnets.

Of the thermal and photochemical reactions that can potentially proceed via biradical intermediates, few have the opportunity to confine the unpaired electrons to a common π -system. As models for intermediates in these reactions, non-Kekulé hydrocarbons therefore certainly have much less

generality than localized biradicals. However, the wealth of experimental data offered by delocalized biradicals provides valuable benchmarks for theoretical methods that profess to treat homolytic bond cleavage reactions accurately. Moreover, these species constitute important tests of electronic structure theory in a general sense.⁷

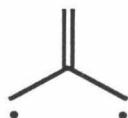
The work described herein concerns the chemistry and spectroscopy of the non-Kekulé isomer of benzene, 2,4-dimethylene-1,3-cyclobutanediyl (alternatively 1,3-dimethylenecyclobutadiene), 1.⁸ We have found that deazetation of diazene 2 enables the generation of this fundamentally unique biradical as well as its covalent isomer 2,4-dimethylenebicyclo[1.1.0]butane (3) under a variety of experimental conditions.



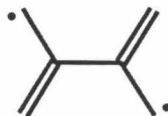
Structural classes of non-Kekulé hydrocarbons. General theoretical considerations.

Most alternant non-Kekulé hydrocarbons that can be conceived fall into two topologically distinct classes whose prototypical members are

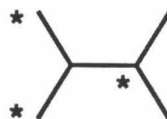
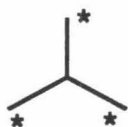
trimethylenemethane (TMM, 4) and tetramethyleneethane (TME, 5). The critical difference between these structures is most easily recognized by



4 TMM



5 TME



applying the "starred-unstarred" atom formalism.⁹ Thus, 4 has two more starred atoms than unstarred, whereas 5 has an equal number of atoms in each set.

Ovchinnikov has derived a simple rule within the framework of valence bond theory, which states that the total spin of such systems is given by $(n^* - n^\circ)/2$ where n^* and n° are the numbers of starred and unstarred atoms.^{5a} TMM (4) is thereby expected to have a triplet ($S=1$) and TME (5) a singlet ($S=0$) ground state.

Simple molecular orbital theory reveals that both 4 and 5 have a pair of degenerate non-bonding MOs and should therefore be triplets by Hund's rule. However, Borden and Davidson have pointed out that NBMO topology can lead to violations of Hund's rule in some cases.¹⁰ For systems in which $n^* > n^\circ$ the NBMOs are confined to the starred set of atoms, but for those with $n^* = n^\circ$ the NBMOs span different sets,¹⁰ and thus are said to be disjoint.¹⁰ In TMM

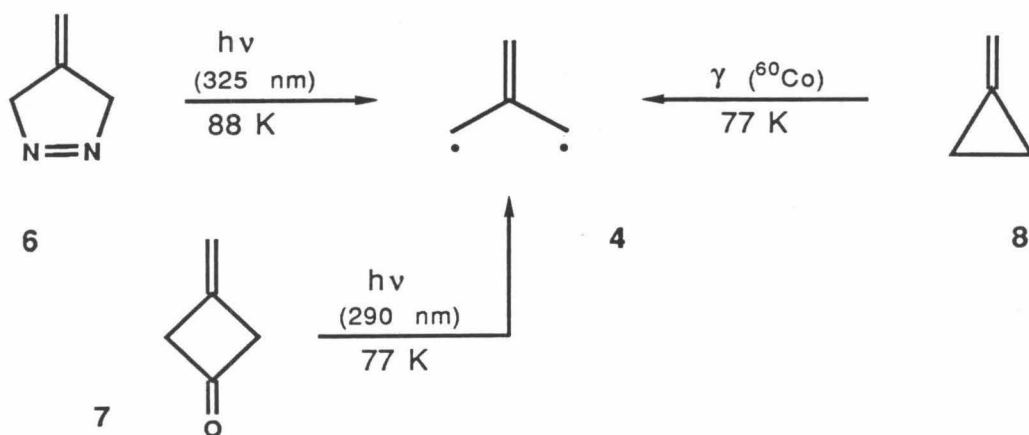
(4) the two NBMOs are not disjoint. While the Pauli principle requires the unpaired electrons of the triplet to occupy different regions of space, the singlet faces no such restriction, and its wavefunction suffers energetically because both non-bonding electrons can appear simultaneously in the same AO.¹⁰ In contrast, singlet TME (5), whose NBMOs are disjoint, avoids these destabilizing interactions, and the triplet and singlet states are expected to be of comparable energies.¹⁰

Experimental studies of non-Kekulé molecules.

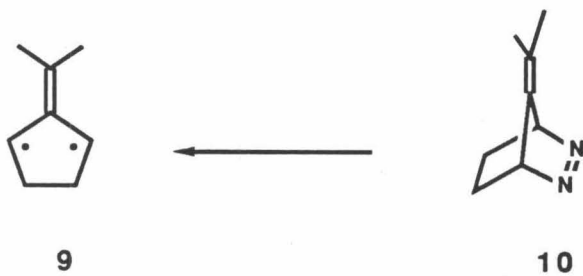
Much of the recent experimental work in this field has focused on the direct spectroscopic observation of these delocalized biradicals. Another experimental goal is the characterization of both the singlet and the triplet states and the determination of the energy gap between them. In keeping with the theoretical arguments above, triplet ground states have consistently been found for biradicals of the TMM genre. However, the ground spin states of TME-type systems are currently a source of controversy, as the experimental findings are frequently at variance with high level theoretical calculations. These systems are discussed below in addition to TMM-type species. It is conceptually useful to divide the members of the TMM family into three structural types: (1) Simple TMMs, (2) *m*-quinodimethane and other benzenoid systems, and (3) dimethylenecyclobutadiene, 1, and other nonbenzenoid systems, a class of which 1 is at present the only member.¹¹

Simple TMMs. The parent hydrocarbon, 4, has been the subject of considerable theoretical attention.¹³ The planar triplet is predicted to be the

ground state by ca. 15 kcal mol⁻¹.¹³ The triplet EPR signal of TMM (4) was first observed by Dowd in 1966 upon irradiation of frozen solutions of pyrazoline 6.¹⁵ The biradical was later prepared by photolysis of 3-methylenecyclobutanone (7)¹⁶ and by γ -radiolysis of methylenecyclopropane (8).¹⁷ TMM was later established to have a triplet ground state by a linear Curie plot (*i.e.*, a plot of its EPR signal intensity *vs* 1/*T*).¹⁸

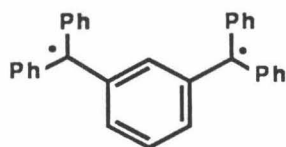


Berson has described an extensive and elegant series of experiments employing ethano-bridged TMMs typified by 9.^{14,19} These ground state triplet biradicals have been generated from the corresponding 1,2-diazeno precursors (e.g., 10) under a variety of conditions, and their chemistry has



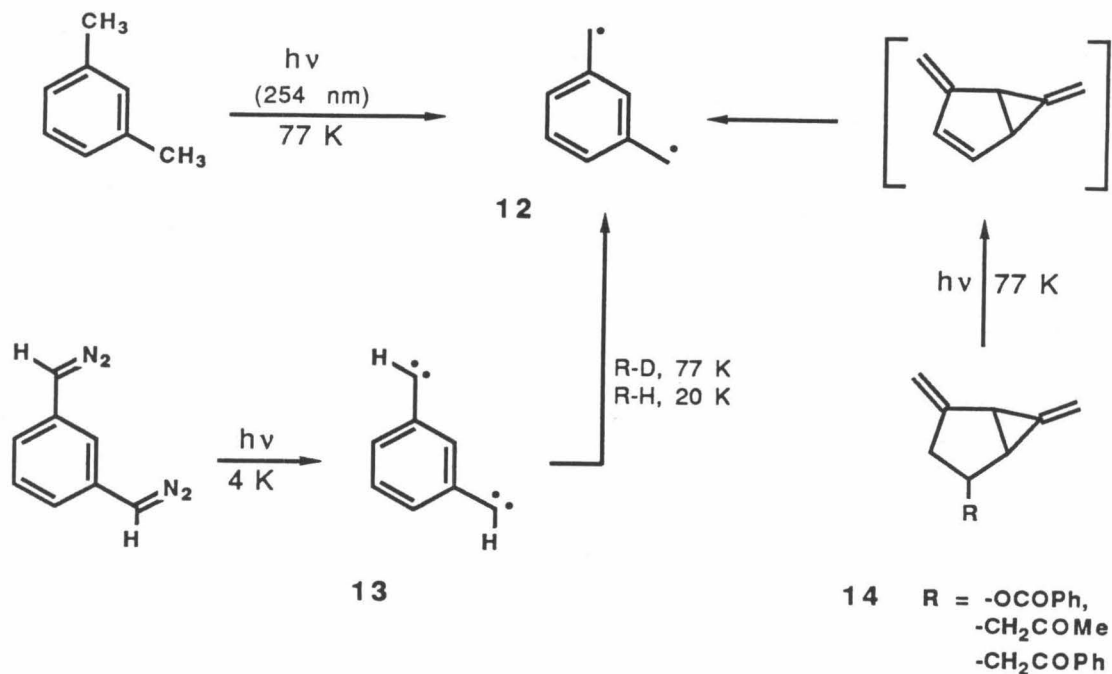
been investigated in detail.^{14,19} Although this structural variation apparently has only a minimal electronic influence on the TMM moiety, it has a profound effect on the stability of the biradical (see below). In fact, **9** is sufficiently stable in its bond-broken form that the chemistry of both singlet and triplet **9** could be studied. This ultimately allowed an experimental determination that the S-T energy gap of **9** at the planar geometry is ≥ 13 kcal mol⁻¹.¹⁴

Benzenoid systems.²⁰ The Schlenk-Brauns hydrocarbon, **11**, a stable *m*-quinodimethane derivative, was reported as early as 1915.²⁰ More recently,

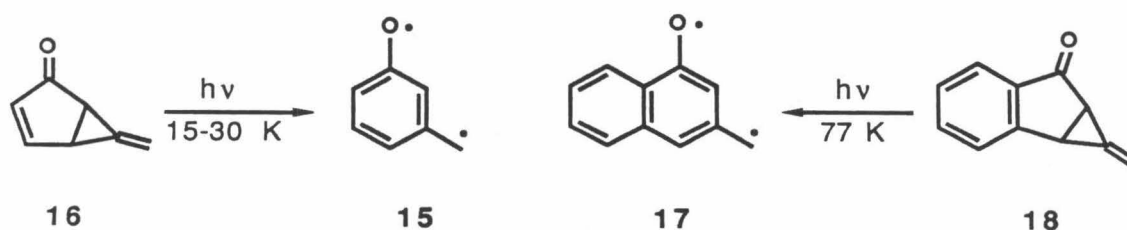


11

Migirdicyan and Baudet prepared the parent *m*-quinodimethane (alternatively *m*-xylylene, **12**) by exhaustive photolysis of *m*-xylene at 77 K and observed it by optical spectroscopy.²¹ Wright and Platz later generated biradical **12** by allowing the (quintet) biscarbene, **13**, to abstract H-atoms from the solvent matrix and observed its triplet EPR signal.²² Goodman and Berson found the same signal to be produced upon Norrish type II photofragmentation of compounds **14**,^{23a} and have also studied the solution-phase chemistry of **12**.²³ The triplet state of **12** is predicted at the ab initio level to be 10 kcal mol⁻¹ below the singlet.²⁴



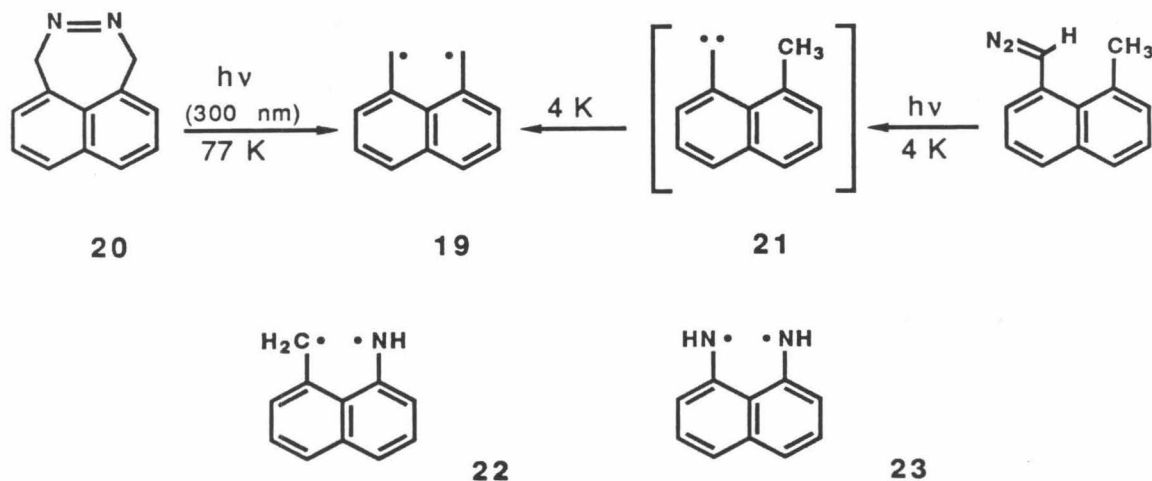
As a test of the influence of heteroatom substitution on the spin preferences of non-Kekulé systems, Berson and coworkers have generated the yellow biradical *m*-quinomethane (15) by photolysis of enone 16^{25,26} and analogously the orange biradical 17 by irradiation of 18.^{25,27} Each of these



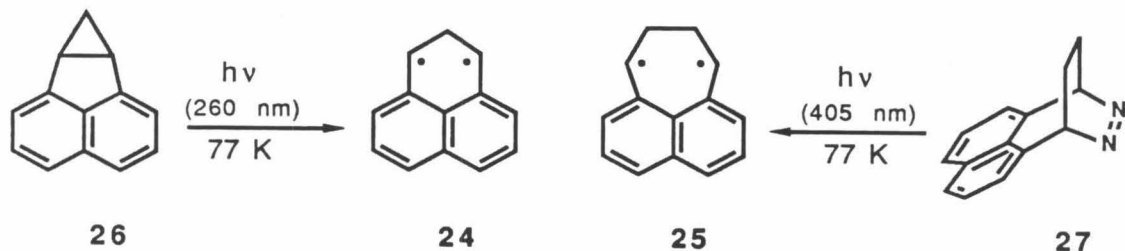
was observed by EPR spectroscopy in frozen solutions, and each has a triplet ground state.^{25,28} Although the results of solution-phase trapping of 15 imply

capture only of the singlet biradical,^{28,29} picosecond absorption spectroscopy has established that at room temperature initial formation of singlet **17** is followed by intersystem crossing to the triplet.³⁰

The 1,8-naphthoquinodimethanes (NQMs) constitute another extensively studied group of non-Kekulé benzenoid hydrocarbons. The parent NQM, **19**, was first generated by Pagni and Dodd by photolysis of diazene **20**.³¹ These workers observed the EPR spectrum of **19** at 77 K,³¹ and Wirz and Pagni later observed the electronic absorption spectrum of this species.³³ Interestingly, Platz succeeded in generating **19** from carbene **21** via a facile intramolecular H-atom abstraction.^{34,35} Similar routes involving the nitrene analogs of **21** afforded **22** and **23**, which were identified by EPR spectroscopy.³⁶ All three biradicals have been demonstrated to be ground state triplets.^{34,36}

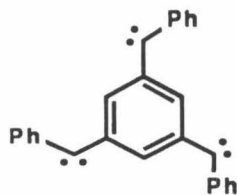
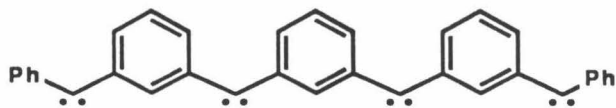


In addition to the parent NQM, **19**, derivatives **24**,³⁷ 1,3- and **25**,³³ 1,4-perinaphthadiyl, have been generated by photolysis of hydrocarbon **26** and diazene **27**, respectively. These biradicals are also found to have triplet ground states by EPR and have been studied by optical spectroscopy.^{33,37}



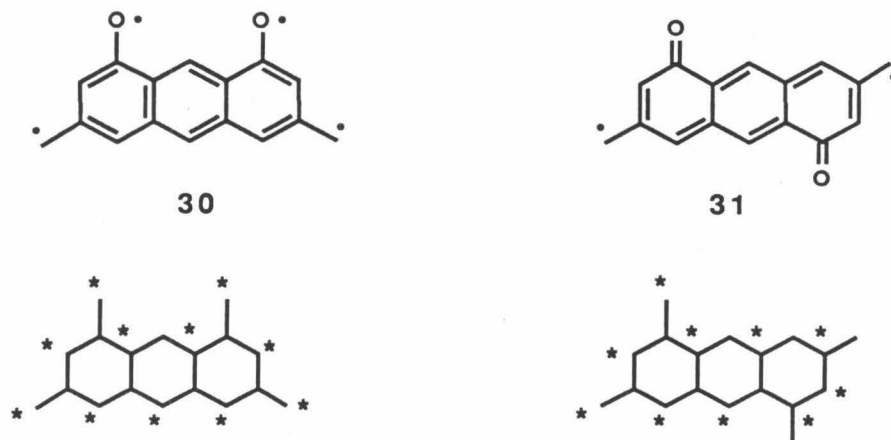
Subsequent to the original observation of biradical **24**, the solution-phase reactivity of this species and a derivative have been examined, but no evidence has been found to indicate that the singlet is a stable structure.³⁸ Interestingly, Fisher and Michl have recently found that at cryogenic temperatures triplet **24** decays via a 1,2-hydrogen shift mechanism that involves quantum mechanical tunnelling.³⁹

In addition to biradicals, the benzenoid classification also encompasses several extended high-spin systems⁴⁰ developed as models for organic ferromagnets. For instance, the *m*-quinodimethane topology has been used to transmit spin information between triplet carbene units. Itoh has reported that triscarbene **28** is a ground state septet,⁴¹ and Itoh and Iwamura have found that **29** has a nonet ground state.⁴² This topology is apparently also the

**28****29**

source of the high-spin coupling present in the oxidized form of the 1,3,5-trisaminobenzene polymer, which has recently been reported as the first organic ferromagnet.^{6a}

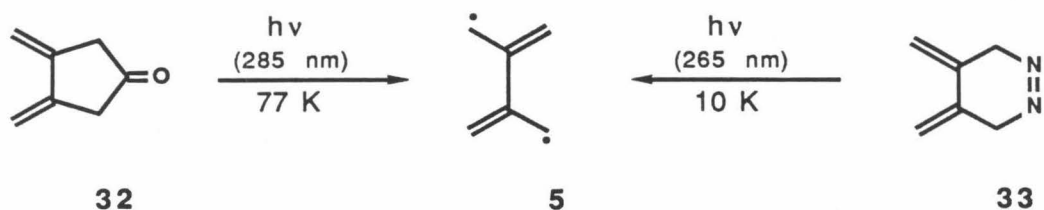
Two additional extended systems of this family, **30** and **31**, have been devised by Berson and coworkers as important tests of ground state spin multiplicity predictions.⁴³ Although these two systems are quite similar in



structure, the topologies of their π -systems are significantly different. Whereas **30** was expected to have a quintet ground state, **31** was expected to be a ground state singlet biradical, since it has $n^* = n^\circ$ and its NBMOs are disjoint.⁴³ Topologically, therefore, **31** is actually a member of the TME class (see below). Experimentally, these red-purple species were generated in a manner analogous to that used to prepare biradicals **15** and **17**. Tetraradical **30** was established to be a ground state quintet, as anticipated, but **31** was found to have a triplet ground state, at variance with the predictions. Later semiempirical calculations by Lahti, Rossi, and Berson, however, found a triplet preference for **31**.¹²

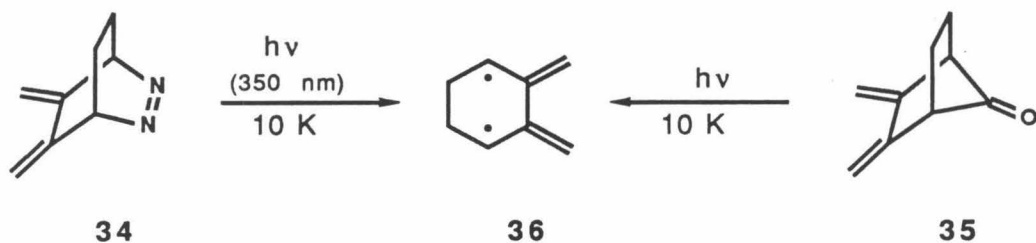
TMEs. The ground spin state of planar TME (**5**) is currently a subject of debate.^{44,45} Dowd first prepared the parent hydrocarbon, **5**, in 1970 by

photolysis of ketone **32** and observed its triplet EPR signal.⁴⁶ A study of the temperature dependence of the EPR signal intensity of **5**, however, awaited its recent generation from the more suitable diazene precursor, **33**.⁴⁷ The linear



Curie plot obtained was taken as evidence that **5** has a triplet ground state;⁴⁷ however, its EPR spectrum – while not ruling out a planar geometry – is more consistent with a perpendicular (D_{2d}) structure.^{47,45}

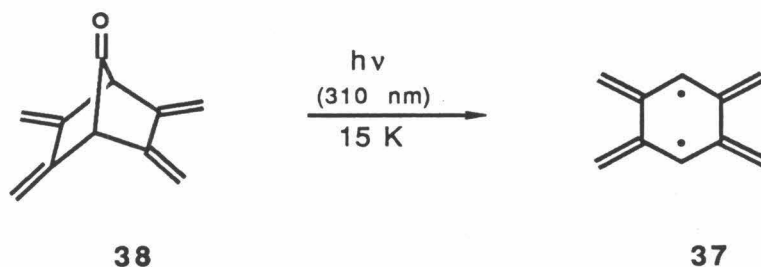
A derivative of TME expected to be more nearly planar was prepared by Roth and Erker.⁴⁸ Irradiation of diazene **34** or ketone **35** produced EPR⁴⁸ and absorption⁴⁹ spectra ascribed to biradical **36**. Roth and coworkers have also



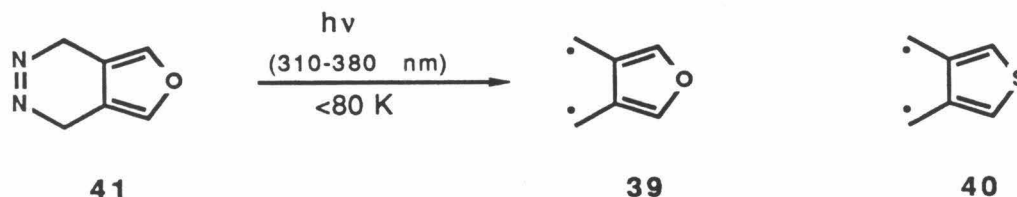
studied the solution-phase chemistry of **36**.^{50,49} In the hope of resolving some of the ambiguity associated with the parent TME, **5**, Dowd and coworkers recently obtained a Curie plot for **36**, and found it to be linear, again implying a triplet ground state.⁴⁵

Also a member of this family is 1,2,4,5-tetramethylenebenzene (**37**). This biradical is formally constructed by uniting two pentadienyl radicals at their

inactive carbons (i.e., those bearing no NBMO coefficients), just as TME (5) is derived by a similar union of two allyl radicals. This species has been predicted by ab initio calculations to have a substantial (5-7 kcal mol⁻¹) singlet preference.⁵¹ The red biradical **37** has recently been generated by irradiation of **38**, and its EPR and visible absorption spectra have been recorded.⁵² Once again, a linear Curie plot revealed that **37** also has a triplet ground state, at variance with the theoretical prediction.⁵²



Yet another TME derivative predicted^{12,53} to have a singlet ground state is 3,4-dimethylenefuran (**39**). Both semiempirical¹² and ab initio⁵³ calculations find that the presence of the oxygen has a minimal effect on the S-T splitting, and, as in the parent TME (**5**), the singlet is favored by a few kcal mol⁻¹. Peters, Berson, and coworkers have recently prepared both the purple



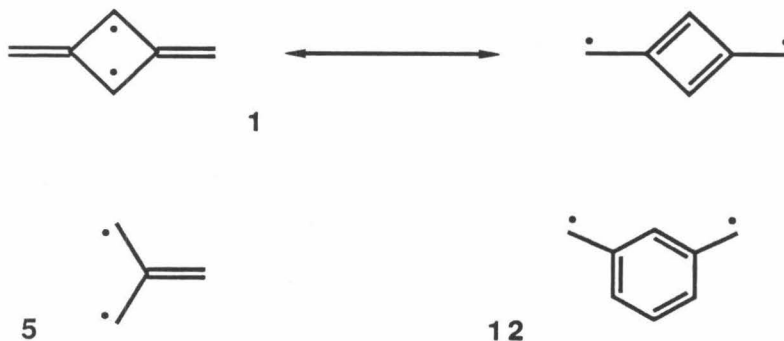
biradical **39** and its thiophene analog **40** from the corresponding diazenes, for example **41**.⁵⁴ Solution-phase flash spectroscopic and trapping studies suggest that only the singlet biradical is generated and captured. Neither

biradical **39** nor **40** gives rise to a triplet EPR signal.⁵⁴ Moreover, the 77 K ¹³C CP/MAS NMR spectrum of **39** displays no paramagnetic contact shift, establishing that **39** (and probably also **40**) has a singlet ground state.⁵⁵

In summary, members of the TME family constitute important tests of the various theoretical models, and their ground spin states are difficult to predict accurately. On the other hand, members of the TMM family should be expected to have substantial triplet preferences (barring, of course, the presence of unusual topologies, extensive heteroatom substitution, or other features that might dramatically influence the relative energies of the two spin states).

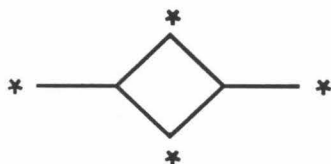
2,4-Dimethylen-1,3-cyclobutanediyl (1) as a unique non-Kekulé molecule.

Biradical **1** can be thought of as both a derivative of the simple TMMs, but with its unpaired spins coupled by two TMM subunits, and – in at least a formal sense – the antiaromatic analog of *m*-quinodimethane (**12**). Although cyclobutadiene-containing resonance structures surely are not the best representations of **1**, their presence may suggest an added dimension in the chemistry and spectroscopy of the biradical. Additionally, biradical **1** is *the* non-Kekulé isomer of benzene, so christened because it incorporates the only possible arrangement of six π -orbitals having both the non-Kekulé topology and a closed cycle of electrons (not to mention its molecular formula).



The predicted relative energies of singlet and triplet 1.

It is important to appreciate that, as a member of the TMM genre and therefore having $n^* - n^{\circ} = 2$, biradical 1 has universally been predicted to have



a triplet ground state. Ovchinnikov's rule^{5a} (see above), of course, predicts a triplet ground state for such systems. Moreover, the NBMOs of 1 cannot be confined to disjoint sets of atoms, so that the triplet should be preferred according to the Borden-Davidson analysis.¹⁰ In fact, a triplet ground state for 1 was predicted by Roberts as early as 1952 on the basis of MO calculations.⁵⁶ Given the theoretical consensus for a triplet ground state and the fact that such predictions have been consistently reliable for TMM-type systems, biradical 1 was therefore not expected to serve as a test of these simple methods of predicting ground state spin multiplicity.⁵⁷

Feller, Davidson, and Borden have carried out ab initio calculations of the relative energies of planar triplet and singlet **1** at various levels of theory.⁵⁸ The calculated values of the S-T splitting are listed in Table 1-1. It should be noted that this study relied on an STO-3G/RHF geometry optimization for the triplet and an STO-3G/TCSCF optimization for the singlet. Such wavefunctions have been found inadequate for geometry optimization of delocalized biradicals,⁶¹ and the UHF- and n -CI-optimized geometries for triplet **1** were found to be significantly different from that obtained at the RHF level.^{61,58,62} Notwithstanding this difficulty, inspection of Table 1-1 suggests that augmenting the split-valence S and T wavefunctions with CI should selectively stabilize the triplet.⁵⁹ Accordingly, we estimate the theoretical S-T gap for **1** as about 15 kcal mol⁻¹.

Table 1-1. Calculated S-T splitting for **1**.^{58,59}

Basis set	Wavefunctions (T/S)	$\Delta E = E(1A_g)^{60} - E(3B_{2u})$
STO-3G	RHF/TCSCF	6.1 kcal mol ⁻¹
	+ CI	13.3
SVP (3s, 2p, 1d/2s)	RHF/TCSCF	7.6

Potential stability and reactivity of **1**. Energetics of ring closure.

Biradicals are species that — in a classical sense — possess a broken bond.⁶³ Accordingly, their thermodynamic and kinetic stability with respect to unimolecular bond formation is of interest from an experimental as well as a theoretical standpoint. Ring closure of singlet biradicals is normally so favorable that these species exist in energy minima that are extremely

shallow at best. Applying conventional spectroscopic methods under cryogenic, matrix-isolation conditions — although a powerful method for characterizing non-Kekulé triplets — generally yields little or no information on the corresponding singlet biradical, the covalent isomers, or the reaction dynamics of the system. It is therefore desirable also to study these systems at higher temperatures in fluid media. Specifically, information about the behavior of delocalized singlet biradicals can sometimes be obtained from chemical trapping^{14,28,29} and time resolved spectroscopic studies^{64,30} under these conditions. Of course, the success of such studies depends on the singlet biradical having a finite lifetime to begin with, and this has seldom been demonstrated for systems with triplet ground states.^{14,28,29}

In fact, biradical 1 incorporates structural features that could offset the energetic advantage of bond formation, thereby making both spin states relatively amenable to study. This point is best illustrated by a comparison to the chemistry of the simple TMMs, which are probably the closest analogs to 1 in terms of structure-reactivity relationships.

Chemical trapping of the parent TMM (4) is relatively difficult.⁶⁵ In competition is ring closure to methylenecyclopropane (8), a reaction with a



4

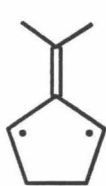


8

barrier of only 7 kcal mol⁻¹ ($\log A \approx 9$) from the ground triplet state.⁶⁶ The ring closure barrier for the singlet biradical is probably, at best, much

smaller; in fact, there is no experimental evidence to suggest that this species exists at an energy minimum on the singlet surface.

Berson and coworkers were able to demonstrate that both triplet and singlet **9** are independently trappable entities.^{14,19,67} These workers deduced that the singlet encounters a 2.3 kcal mol⁻¹ barrier along its preferred closure pathway to **42**.^{14,68} This kinetic barrier is apparently caused by the thermodynamic destabilization of the two possible closure products, **42** and **43**, relative to **9**.^{14,19} Thus, while **4** lies significantly higher in energy than **8**, the ethano-bridged triplet TMM, **9**, was found to be *more* stable than **42** or **43**.^{14,68,69} Because ring closure of **9** is discouraged by a large increase in strain energy, the biradical is said to be "strain-protected."¹⁴

**9****42****43**

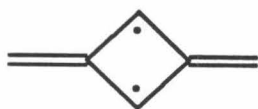
This may also be the case for triplet **1**. Simple thermochemical arguments based on strain and resonance energies can be formulated to estimate the relative energies of triplet **1** and its covalent isomers. The TMM systems discussed above serve as valuable calibration points for this method.

Upon going from **34** to **8** the energy gained by forming a C—C σ -bond, about 80 kcal mol⁻¹,⁷⁰ is partly compensated by the strain energy of **8**, 41 kcal mol⁻¹,⁷¹ and loss of the resonance energy of **34**. Ab initio CI calculations find the energy difference between **34** and **8** to be 15 kcal mol⁻¹.⁷² This allows an

estimate of the ^3TMM resonance energy as $80 - 41 - 15 = 24 \text{ kcal mol}^{-1}$. We can use this value to estimate the relative energies of biradical **9** and its covalent isomers. Closure of **39** to form **42** is accompanied by an increase in strain energy from 5 kcal mol^{-1} ⁷³ for **9** to $27 + 41 = 68 \text{ kcal mol}^{-1}$ ^{74,14} for **42**. By using the above values for C–C bond and TMM resonance energies, we find that ring closure of **39** to **42** is endothermic by $68 - (5 + 80 - 24) = 7 \text{ kcal mol}^{-1}$, in reasonable agreement with the experimental results.^{14,68,69} The strain energy of the anti-Bredt olefin, **43**, is significantly higher than that of **42**,⁷⁵ and it is not formed from biradical **9**.^{14,75,76}

We can apply the same reasoning to the ring closure of triplet **1** to provide dimethylenebicyclobutane (**3**). The 80 kcal mol^{-1} C–C bond energy is offset by a loss of about 41 kcal mol^{-1} of resonance energy (based on the ratio of the Hückel resonance energies for **1** and **4**⁷⁷) and an increase in strain energy. While the strain energy of **1** is about 32 kcal mol^{-1} ,⁷⁸ the strain energy of **3** is more difficult to evaluate. A reasonable estimate would be 41 kcal mol^{-1} for each of the two methylenecyclopropane units⁷¹ and another 9 as a result of their incorporation into a bicyclobutane ring system,⁸⁰ for a total of 91 kcal mol^{-1} . However, **3** is potentially a very unusual molecule, and its stability could be influenced by electronic interactions between the π -bonds and the transannular σ -bond. In fact, *ab initio* calculations by Schleyer⁸¹ indicate that a strain energy (actually a combination of strain and delocalization energies) of $76\text{--}82 \text{ kcal mol}^{-1}$ ⁸² for **3** would be more appropriate. Using 79 kcal mol^{-1} for this value, we estimate that triplet biradical **1** should be $79 - (80 + 32 - 41) = 8 \text{ kcal mol}^{-1}$ more stable than **3**. *Ab initio* calculations by Feller, Davidson, and Borden⁵⁸ find **3** to be virtually isoenergetic with triplet

1.⁸³ (The strain energy of bicyclo[2.1.0]pent-(1,2)-ene has been calculated as 123 kcal mol⁻¹,⁸⁴ disqualifying 44 as a viable participant in the chemistry of 1.)



1



3



44

Biradical 1 is far from being a simple derivative of TMM. However, in terms of its stability with respect to ring closure one might — based on these energetic considerations — expect behavior more like that of the constrained TMM, 9, than that of the parent, 4. For example, if as in the case of singlet 9, singlet 1 encounters a strain-induced barrier to ring closure, the triplet and singlet biradicals could be independently characterizable species. A barrier to closure of the singlet could also allow a determination of the theoretically important S-T gap for 1.

Potential reactivity and structure of 2,4-dimethylenebicyclo[1.1.0]butane (3).

As alluded to above, 3 is an interesting molecule in its own right. Its structure might be expected to be quite different from "ordinary" bicyclobutanes in that its π -bonds not only increase the strain energy of the ring system, but interact electronically with the strained central bond.⁸¹ Ab initio calculations^{58,81} have found geometries for dimethylenebicyclobutane

(3) substantially different from that of the parent hydrocarbon 45. The calculated transannular bond lengths, r , and the angles between the planes of the cyclopropyl groups, θ , are presented in Table 1-2. Although one calculation finds two minima for 3,⁵⁸ on the average, θ is seen to increase by about 15° while r increases by about 0.25 \AA on going from 45 to 3. Moreover, these calculations^{58,81} predict the bridgehead carbons of 3 to be highly inverted, that is, all four atoms bound to them lie on the same side of a plane. One might then describe the central bond as comprising the small lobes of sp^3 -like hybrid orbitals.

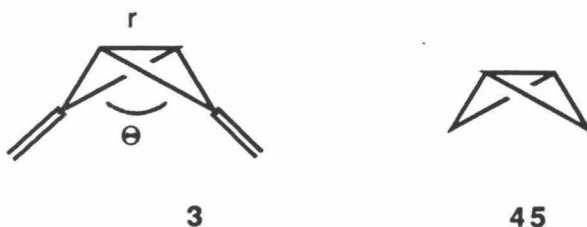


Table 1-2. Calculated geometrical parameters for 3 and 45.

Geometry optimization	r	θ	ref.
3: 3-21G/TCSCF	1.775 \AA	135°	81
STO-3G/TCSCF	1.638	125°	58
	1.882	144°	58
45: 3-21G/TCSCF	1.529	120°	81
STO-3G/TCSCF	1.510	119°	58

Because it is difficult to foresee what unusual reactivity patterns might result from such structural features, our experimental efforts with regard to 3

have been guided more by its predicted energetic relationship to biradical 1. Again, the 9-42 system may serve as the best model for our system in this respect. Compound 42 is observable in solution by low temperature ^1H NMR spectroscopy, and above $-50\text{ }^\circ\text{C}$ it forms dimers via triplet 9.^{68,69} We have found that dimethylenebicyclobutane (3) is similarly observable by low temperature NMR spectroscopy and also forms dimers, but by a fundamentally different mechanism — one that suggests that 3 is indeed a very unusual molecule.

Scope of this work.

Chapter 2 describes the synthesis of biradical 1 and its spectroscopic characterization in rigid media at cryogenic temperatures. As anticipated, biradical 1 is easily observable by EPR spectroscopy and has a triplet ground state. Several EPR experiments have provided a great deal of information concerning the electronic structure of the biradical. In addition, the characterization of triplet 1 by electronic spectroscopy is described.⁸

Chapter 3 deals with dimethylenebicyclobutane (3) and the solution-phase chemistry of triplet 1 and this covalent isomer. Compound 3 undergoes a novel dimerization reaction that attests to its high strain energy and perhaps its unusual structure as well. The thermal and photochemical reactivity of 3 in solution and of triplet 1 in rigid media are also addressed.

References and notes.

1. *Diradicals*; Borden, W. T., Ed.; Wiley: New York, 1982.
2. See, for example, Turro, N. J.; Kraeutler, B. In ref. 1; Ch 6, pp 259-321. Wirz, J. *Pure Appl. Chem.* **1984**, *56*, 1289-1300. Dauben, W. G.; Salem, L.; Turro, N. J. *Acc. Chem. Res.* **1975**, *8*, 41-54. Bonacic-Koutecky, V.; Koutecky, J.; Michl, J. *Angew. Chem., Int. Ed. Engl.* **1987**, *26*, 170-189.
3. Salem, L.; Rowland, C. *Angew. Chem., Int. Ed. Engl.* **1972**, *11*, 92-111.
4. Dewar, M.J.S. *The Molecular Orbital Theory of Organic Chemistry*; McGraw-Hill: New York, 1969; pp 232-233.
5. (a) Ovchinnikov, A.A. *Theor. Chim. Acta* **1978**, *47*, 297-304; *Dokl. Akad. Nauk. SSSR* **1977**, *236*, 928-931. (b) Klein, D.J.; Nelin, C.J.; Alexander, S.; Matsen, F.A. *J. Chem. Phys.* **1982**, *77*, 3101-3108.
6. (a) Torrance, J.B.; Oostra, S.; Nazzari, A. *Synth. Metals* **1987**, *19*, 709-714. (b) See also: Korshak, Y.V.; Medvedeva, T.V.; Ovchinnikov, A.A.; Spector, V.N. *Nature* **1987**, *326*, 370-372.
7. Borden, W. T. In ref. 1; Ch 1, pp 1-72.
8. For preliminary communications of this work, see (a) Snyder, G. J.; Dougherty, D. A. *J. Am. Chem. Soc.* **1985**, *107*, 1774-1775; (b) **1986**, *108*, 299-300.
9. Longuet-Higgins, H. C. *J. Chem. Phys.* **1950**, *18*, 265-274.
10. Borden, W.T.; Davidson, E.R. *J. Am. Chem. Soc.* **1977**, *99*, 4587-4594. See also ref. 7, esp. pp 37-39.
11. Dimethylenecyclooctatetraenes have been addressed theoretically in ref. 12.

12. Lahti, P. M.; Rossi, A. R.; Berson, J. A. *J. Am. Chem. Soc.* **1985**, *107*, 2273-2280.
 13. For leading references, see ref. 7, p 35; ref. 14, pp 173-175; and Borden, W. T.; Davidson, E. R. *Acc. Chem. Res.* **1981**, *14*, 69-76.
 14. Berson, J. A. In ref. 1; Ch 4, pp 151-194.
 15. Dowd, P. *J. Am. Chem. Soc.* **1966**, *88*, 2587-2589.
 16. Dowd, P.; Sachdev, K. *J. Am. Chem. Soc.* **1967**, *89*, 715-716.
 17. Yamaguchi, T.; Irie, M.; Yoshida, H. *Chem. Lett.* **1973**, 975-978.
 18. Baseman, R. J.; Pratt, D. W.; Chow, M.; Dowd, P. *J. Am. Chem. Soc.* **1976**, *98*, 5726-5727.
 19. Berson, J. A. *Acc. Chem. Res.* **1978**, *11*, 446-453.
 20. This field has recently been reviewed by Platz, M. S. In ref. 1, Ch. 5, pp 195-258.
 21. Migirdicyan, E.; Baudet, J. *J. Am. Chem. Soc.* **1975**, *97*, 7400-7404.
 22. Wright, B. B.; Platz, M. S. *J. Am. Chem. Soc.* **1983**, *105*, 628-630.
- These authors succeeded in generating an EPR signal similar to that of 12 by 254-nm photolysis of mesitylene, providing support for the previous assignment of the optical spectra of 12.²¹
23. (a) Goodman, J. L.; Berson, J. A. *J. Am. Chem. Soc.* **1985**, *107*, 5409-5424; **1984**, *106*, 1867-1868; (b) **1985**, *107*, 5424-5428.
 24. Kato, S.; Morokuma, K.; Feller, D.; Davidson, E. R.; Borden, W. T. *J. Am. Chem. Soc.* **1983**, *105*, 1791-1795.
 25. Rule, M.; Matlin, A. R.; Seeger, D. E.; Hilinski, E. F.; Dougherty, D. A.; Berson, J. A. *Tetrahedron* **1982**, *38*, 787-798.

26. Rule, M.; Matlin, A. R.; Hilinski, E. F.; Dougherty, D. A.; Berson, J. A. *J. Am. Chem. Soc.* **1979**, *101*, 5098-5099.
27. Seeger, D. E.; Hilinski, E. F.; Berson, J. A. *J. Am. Chem. Soc.* **1981**, *103*, 720-721.
28. Inglin, T. A.; Berson, J. A. *J. Am. Chem. Soc.* **1986**, *108*, 3394-3402.
29. Matlin, A. R.; Inglin, T. A.; Berson, J. A. *J. Am. Chem. Soc.* **1982**, *104*, 4954-4955.
30. Goodman, J. L.; Peters, K. S.; Lahti, P. M.; Berson, J. A. *J. Am. Chem. Soc.* **1985**, *107*, 276-277.
31. Pagni, R. M.; Burnett, M. N.; Dodd, J. R. *J. Am. Chem. Soc.* **1977**, *99*, 1972-1973. Watson, C.R., Jr.; Pagni, R.M.; Dodd, J.R.; Bloor, J.E. *J. Am. Chem. Soc.* **1976**, *98*, 2551-2562.³²
32. The original assignment of a singlet ground state was demonstrated to be erroneous, and triplet ground states have been established by linear Curie plots. See ref. 20, pp 225-227; ref. 33; ref. 34.
33. Gisin, M.; Rommel, E.; Wirz, J.; Burnett, M. N.; Pagni, R. M. *J. Am. Chem. Soc.* **1979**, *101*, 2216-2218.
34. Platz, M. S. *J. Am. Chem. Soc.* **1979**, *101*, 3398-3399.
35. Platz, M. S. *J. Am. Chem. Soc.* **1980**, *102*, 1192-1194.
36. Platz, M. S.; Carrol, G.; Pierrat, F.; Zayas, J.; Auster, S. *Tetrahedron* **1982**, *38*, 777-785. Platz, M. S.; Burns, J. R. *J. Am. Chem. Soc.* **1979**, *101*, 4425-4426.
37. Muller, J.-F.; Muller, D.; Dewey, H. J.; Michl, J. *J. Am. Chem. Soc.* **1978**, *100*, 1629-1630.³¹

38. Hasler, E.; Gassmann, E.; Wirz, J. *Helv. Chim. Acta* **1985**, *68*, 777-788. Pagni, R. M.; Burnett, M. N.; Hassaneen, H. M. *Tetrahedron* **1982**, *38*, 843-851.
39. Fisher, J. J.; Michl, J. *J. Am. Chem. Soc.* **1987**, *109*, 583-584.
40. Iwamura, H. *Pure Appl. Chem.* **1986**, *58*, 187-196. Itoh, K. *Pure Appl. Chem.* **1978**, *50*, 1251-1259.
41. Takui, T.; Itoh, K. *Chem. Phys. Lett.* **1973**, 120-124.
42. Teki, Y.; Takui, T.; Itoh, K.; Iwamura, H.; Kobayashi, K. *J. Am. Chem. Soc.* **1983**, *105*, 3722-3723. Sugawara, T.; Bandow, S.; Kimura, K.; Iwamura, H.; Itoh, K. *J. Am. Chem. Soc.* **1984**, *106*, 6449-6450.
43. Seeger, D. E.; Lahti, P. M.; Rossi, A. R.; Berson, J. A. *J. Am. Chem. Soc.* **1986**, *108*, 1251-1265. Seeger, D. E.; Berson, J. A. *J. Am. Chem. Soc.* **1983**, *105*, 5144-5146.
44. Du, P.; Borden, W. T. *J. Am. Chem. Soc.* **1987**, *109*, 930-931.
45. Dowd, P.; Chang, W.; Paik, Y. H. *J. Am. Chem. Soc.* **1987**, *109*, 5284-5285.
46. Dowd, P. *J. Am. Chem. Soc.* **1970**, *92*, 1066-1068. The reported *D* value was measured incorrectly.⁴⁷
47. Dowd, P.; Chang, W.; Paik, Y. H. *J. Am. Chem. Soc.* **1986**, *108*, 7416-7417.
48. Roth, W. R.; Erker, G. *Angew. Chem., Int. Ed. Engl.* **1973**, *12*, 503-504.
49. Roth, W. R.; Biermann, M.; Erker, G.; Jelic, K.; Gerhartz, W.; Görner, H. *Chem. Ber.* **1980**, *113*, 586-597.

50. Roth, W. R.; Scholz, B. P.; Breuckmann, R.; Jelich, K.; Lennartz, H.-W. *Chem. Ber.* **1982**, *115*, 1934-1946.
51. Du, P.; Hrovat, D. A.; Borden, W. T.; Lahti, P. M.; Rossi, A. R.; Berson, J. A. *J. Am. Chem. Soc.* **1986**, *108*, 5072-5074.
52. Roth W. R.; Langer, R.; Bartmann, M.; Stevermann, B.; Maier, G.; Reisenauer, H. P.; Sustmann, R.; Müller, W. *Angew. Chem., Int. Ed. Engl.* **1987**, *26*, 256-258.
53. Du, P.; Hrovat, D. A.; Borden, W. T. *J. Am. Chem. Soc.* **1986**, *108*, 8086-8087.
54. Stone, K. J.; Greenberg, M. M.; Goodman, J. L.; Peters, K. S.; Berson, J. A. *J. Am. Chem. Soc.* **1986**, *108*, 8088-8089.
55. Zilm, K. W.; Merrill, R. A.; Greenberg, M. M.; Berson, J. A. *J. Am. Chem. Soc.* **1987**, *109*, 1567-1569.
56. Roberts, J.D.; Streitwieser, A., Jr.; Regan, C.M. *J. Am. Chem. Soc.* **1952**, *74*, 4579-4582.
57. See also: Maynau, D.; Malrieu, J.-P. *J. Am. Chem. Soc.* **1982**, *104*, 3029-3034. Döhnert, D.; Koutecky, J. *J. Am. Chem. Soc.* **1980**, *102*, 1789-1796.
58. Feller, D.; Davidson, E.R.; Borden, W.T. *J. Am. Chem. Soc.* **1982**, *104*, 1216-1218.
59. At Feller, Davidson, and Borden's STO-3G/RHF optimized triplet geometry, we have calculated (using a split-valence basis set) a 1A_g (TCSCF) – $^3B_{2u}$ (RHF) gap of 9.3 kcal mol⁻¹. At GVB (3/6) level for the singlet and GVB (2/4) level for the triplet, this splitting decreased to 4.6 kcal mol⁻¹. Inclusion of CI (all excitations in the n -space) selectively stabilized the triplet,

increasing the gap to 17.0 kcal mol⁻¹. Snyder, G.J.; Goddard, W.A., III; Dougherty, D.A., unpublished results.

60. The planar singlet (¹A_g) was found to be unstable with respect to a slight pyramidalization at the ring methine carbons, with the resulting ¹A₁ (C_{2v}) minimum being 1-2 kcal mol⁻¹ lower in energy than the ¹A_g; however, the instability of ¹A_g may have been an artifact of the STO-3G basis set.⁵⁸

61. Borden, W. T.; Davidson, E. R.; Feller, D. *Tetrahedron* **1982**, *38*, 737-739.

62. Davidson, E.R.; Borden, W.T.; Smith, J. *J. Am. Chem. Soc.* **1978**, *100*, 3299-3302.

63. This idea has been proposed (in a somewhat more elegant form) as one definition of a biradical.²⁵

64. Kelley, D. F.; Rentzepis, P. M. *J. Am. Chem. Soc.* **1983** *105*, 1820-1824. Kelley, D. F.; Rentzepis, P. M.; Mazur, M.; Berson, J. A. *J. Am. Chem. Soc.* **1982**, *104*, 3764-3766.

65. Dowd, P. *Acc. Chem. Res.* **1972**, *5*, 242-248. Dowd, P.; Sengupta, G.; Sachdev, K. *J. Am. Chem. Soc.* **1970**, *92*, 5726-5727.

66. Dowd, P.; Chow, M. *Tetrahedron* **1982**, *38*, 799-807; *J. Am. Chem. Soc.* **1977**, *99*, 6438-6440.

67. (a) Corwin, L.R.; McDaniel, D.M.; Busby, R.J.; Berson, J.A. *J. Am. Chem. Soc.* **1980**, *102*, 276-287. (b) Duncan, C.D.; Corwin, L.R.; Davis, J.H.; Berson, J.A. *J. Am. Chem. Soc.* **1980**, *102*, 2350-2358.

68. Mazur, M.; Berson, J.A. *J. Am. Chem. Soc.* **1982**, *104*, 2217-2222; **1981**, *103*, 684,686.

69. Rule, M.; Mondo, J. A.; Berson, J. A. *J. Am. Chem. Soc.* **1982**, *104*, 2209-2216. Rule, M.; Lazzara, M.G.; Berson, J.A. *J. Am. Chem. Soc.* **1979**, *101*, 7091-7092.

70. The bond dissociation energies for Et-Et, Et-*n*Pr, Et-*i*Pr, *n*Pr-*i*Pr, and *i*Pr-*i*Pr are all within 2 kcal mol⁻¹ of this value. Benson, S. W. *Thermochemical Kinetics*; Wiley: NY, 1976; p. 309. See also, McMillen, D.F.; Golden, D.M. *Ann. Rev. Phys. Chem.* **1982**, *33*, 493-532.

71. Wiberg, K. B. *Angew. Chem., Int. Ed. Engl.* **1986**, *25*, 312-322.

72. Feller, D.; Davidson, E.R.; Borden, W.T. *Isr. J. Chem.* **1983**, *23*, 105-108.

73. This value is an average of those for methylenecyclopentane, 6.1, and cyclopentene, 4.1 kcal mol⁻¹.⁷¹

74. The strain energies of cyclopropane and cyclobutane are taken as 27.5 and 26.5 kcal mol⁻¹ respectively.⁷¹

75. Salinaro, R. F.; Berson, J. A. *J. Am. Chem. Soc.* **1979**, *101*, 7094-7095.

76. Rule, M.; Salinaro, R. F.; Pratt, D. R.; Berson, J. A. *J. Am. Chem. Soc.* **1982**, *104*, 2223-2228.

77. At the Hückel level the resonance energy of TMM (4) is $(2\sqrt{3}-2)\beta$ = 1.46 β , while that of 1 is $(2\sqrt{5}+1)-4\beta$ = 2.47 β . These resonance energies are calculated relative to two localized radical centers and the appropriate numbers of isolated ethylene units.

78. This estimate derives from the observation that each sp² center incorporated into the cyclobutane ring system adds *ca.* 1.5 kcal mol⁻¹ to the strain energy.^{71,79}

79. Schleyer, P.v.R.; Williams, J.E.; Blanchard, K.R. *J. Am. Chem. Soc.* **1970**, *92*, 2377-2386.

80. The strain energy of bicylobutane is taken to be 64 kcal mol⁻¹,⁷¹ 9 kcal mol⁻¹ higher than that of two cyclopropanes.⁷⁴

81. Budzelaar, P.H.M.; Kraka, E.; Cremer, D.; Schleyer, P.v.R. *J. Am. Chem. Soc.* **1986**, *108*, 561-567.

82. (1) The enthalpy change calculated for the isodesmic reaction **3** + 2 cyclopropanes → 2 methylenecyclopropanes (**6**) + bicyclobutane, 9 kcal mol⁻¹,⁸¹ provides a strain (actually strain + resonance) energy of 82 kcal mol⁻¹ for **3**. (2) Analogously, ΔH calculated for **3** + 2 propanes → 2 isobutenes + bicyclobutane, -12 kcal mol⁻¹ ⁸¹ provides a strain energy of 76 kcal mol⁻¹.

83. (a) Feller, Davidson, and Borden⁵⁸ employed an STO-3G geometry optimization to find two minima corresponding to dimethylenebicyclobutane (**3**), (see Table 2-1). The STO-3G/TSCSF-CI energies of these were found to be 2-4 kcal mol⁻¹ higher and their SVP/TCSCF energies 4-5 kcal mol⁻¹ lower than that of planar triplet **1**.

84. Wiberg, K.B.; Bonnevillie, G.; Dempsey, R. *Isr. J. Chem.* **1983**, *23*, 85-92. We are aware of no experimental evidence for the existence of a derivative of this ring system.

Chapter 2

Synthesis, EPR and Electronic Spectroscopy of 2,4-Dimethylene-1,3-cyclobutanediyl

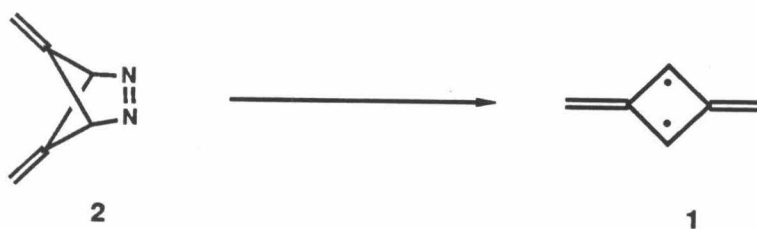
Low temperature matrix-isolation spectroscopy has proven to be a valuable method for the characterization of a variety of reactive species,¹ including both localized²⁻⁴ and delocalized^{5,6} biradicals. The advantages of this technique are twofold. The host matrix prevents the molecules of interest from reacting with one another, and the low temperatures normally employed shut down many undesirable unimolecular reactions.

EPR spectroscopy has been a widely used method for the direct observation and study of triplet biradicals under matrix-isolation conditions.²⁻⁶ We have employed EPR as well as optical spectroscopy in the study of triplet 2,4-dimethylene-1,3-cyclobutanediyl (1) in rigid media at cryogenic temperatures. Our EPR experiments have provided a considerable amount of information concerning the electronic structure of the biradical. Specifically, the hyperfine splitting in the $\Delta m_s = 2$ transition has furnished information on the geometry and spin distribution of triplet 1. Additionally, study of the primary ($\Delta m_s = 1$) region of the EPR spectrum of both isotropic and partially oriented samples of triplet 1 has allowed us to determine the magnitude of the spin-spin dipolar coupling interaction along each of the biradical's magnetic axes. As anticipated, the triplet is the ground spin state of biradical 1.⁷

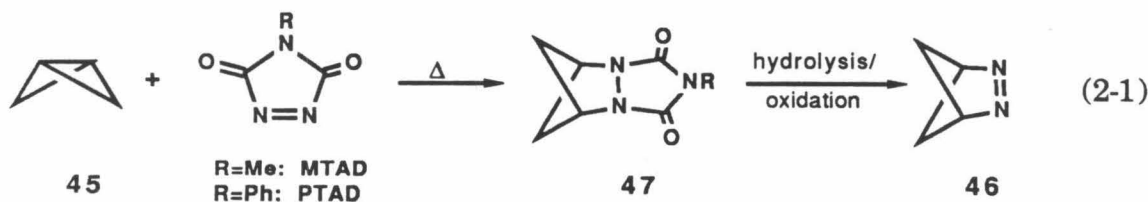
In addition, triplet 1 is yellow-orange and displays highly structured absorption and emission spectra. By applying a novel technique that takes advantage of the biradical's light sensitivity, we have demonstrated conclusively that the triplet state is the source of the optical spectra. Further EPR experiments have established the strength and nature of the electronic transition as well as its polarization.⁷

Synthesis.

Extrusion of nitrogen from azoalkanes is a fairly general method of preparing biradicals and strained hydrocarbons⁸ under a variety of conditions. In particular, biradicals of the trimethylenemethane (TMM) family have been generated from 1,2-diazenes both thermally and photochemically.^{9,11} Thus, diazene **2** presented itself as potentially the best source of biradical **1**.

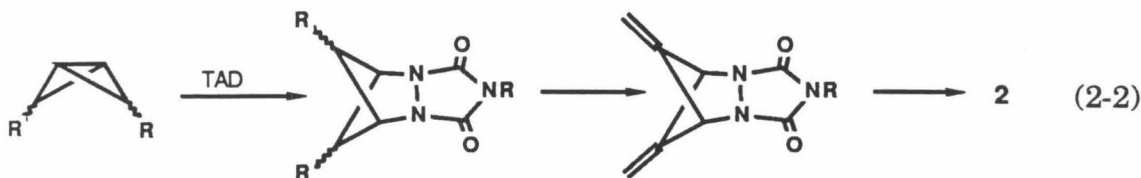


Our basic synthetic approach to **2** was motivated by the recent preparation of 2,3-diazabicyclo[2.1.1]hex-2-ene, **46**, in our laboratory.¹² The key step in this synthesis was the thermal cycloaddition of methyl- or phenyltriazolinedione (MTAD or PTAD) across the central bond of bicyclo[1.1.0]butane, **45** (eqn 2-1). Standard methodology was then used to



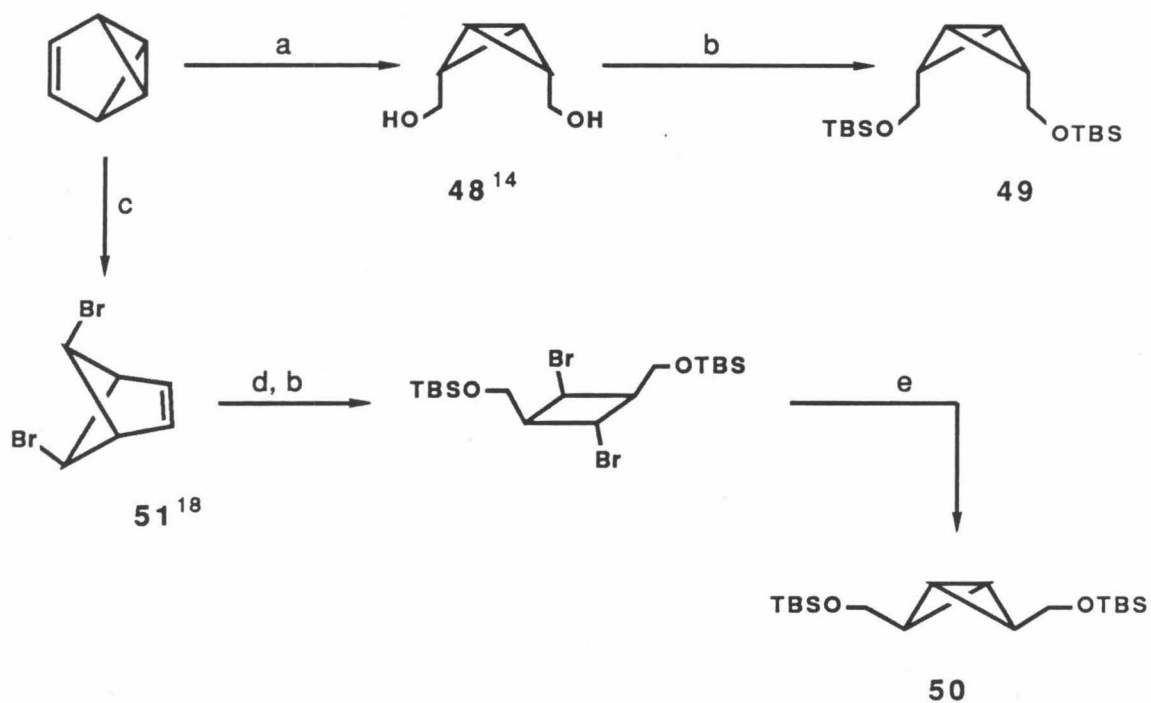
convert the resulting urazole, **47**, to **46**.¹² In addition, accompanying our initial publication of this reaction, Amey and Smart reported gaining entry into the ring system of **47** by thermal and photochemical additions of MTAD and PTAD to various bridgehead-disubstituted bicyclobutanes.¹³ We expected, therefore, that a triazolinedione (TAD) could be added to a

bicyclobutane bearing substituents that would later allow introduction of the diene functionality of **2** (eqn 2-2).



At the outset of our synthesis we found that the only available bicyclobutanes with useful functionality at only the 2 and 4 positions were those recently prepared from benzvalene by Christl and coworkers.^{14,15} Thus, reductive ozonolysis of benzvalene yields **48** (Scheme 2-1),^{14a,b} whose hydroxyl groups can be masked to provide **49**, a viable candidate for the TAD addition. Our laboratory had earlier shown^{12,16,17} that the addition of TAD to bicyclobutane occurs from the *endo* direction. Anticipating that the *endo* substituents of **49** would sterically hinder this process, we developed an alternative sequence (Scheme 2-1) which afforded *exo*-substituted bicyclobutane **50**. Dibromide **51**, the product of formal addition of Br₂ across the transannular bond of benzvalene, was prepared by the method of Roth and Katz.¹⁸ Ozonolytic cleavage of the double bond and subsequent "deprotection" of the transannular bicyclobutane bond by *t*BuLi coupling¹⁹ afforded primarily the thermodynamically more stable²⁰ *exo,exo* epimer, **50**; by ¹H NMR only about 5% of **49** was formed.²¹

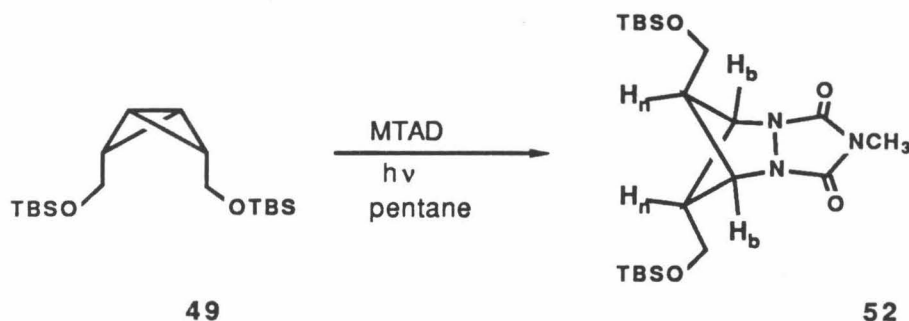
As expected, thermal addition of TAD to **50** was rapid, but **49** was completely inert under comparable reaction conditions (see **Experimental**). However, even under conditions that had previously been found optimal for the formation of **47** (eqn 2-1),¹² the product of the addition to **50** was

Scheme 2-1.^a

^a(a) O_3 , -78°C ; LiAlH_4 , THF, -30°C .¹⁴ (b) $\text{tBuMe}_2\text{SiCl}$, imidazole, CH_2Cl_2 .
 (c) Br_2 , $\text{CCl}_4/\text{Et}_2\text{O}$, 0°C .¹⁸ (d) O_3 , CH_2Cl_2 , -78°C ; LiAlH_4 , THF/ Et_2O , 35°C . (e) tBuLi , Et_2O /pentane, -78°C , Ar.

unfortunately not a cycloadduct analogous to **47**. Instead an intractable mixture of products was obtained. This mixture displayed a complex ^1H NMR spectrum with numerous broad signals, including one in the olefinic region.

We have found, however, that MTAD adds *photochemically* to **49** to provide **52** in 37% yield after chromatography. The stereochemical assignment is firmly established by the observation of a 1.7 Hz coupling between the bridgehead (H_b) and endo (H_n)²³ protons; the exo protons of the endo,endo epimer (**55**, Scheme 2-2) would not be expected to couple to H_b .²⁴ The

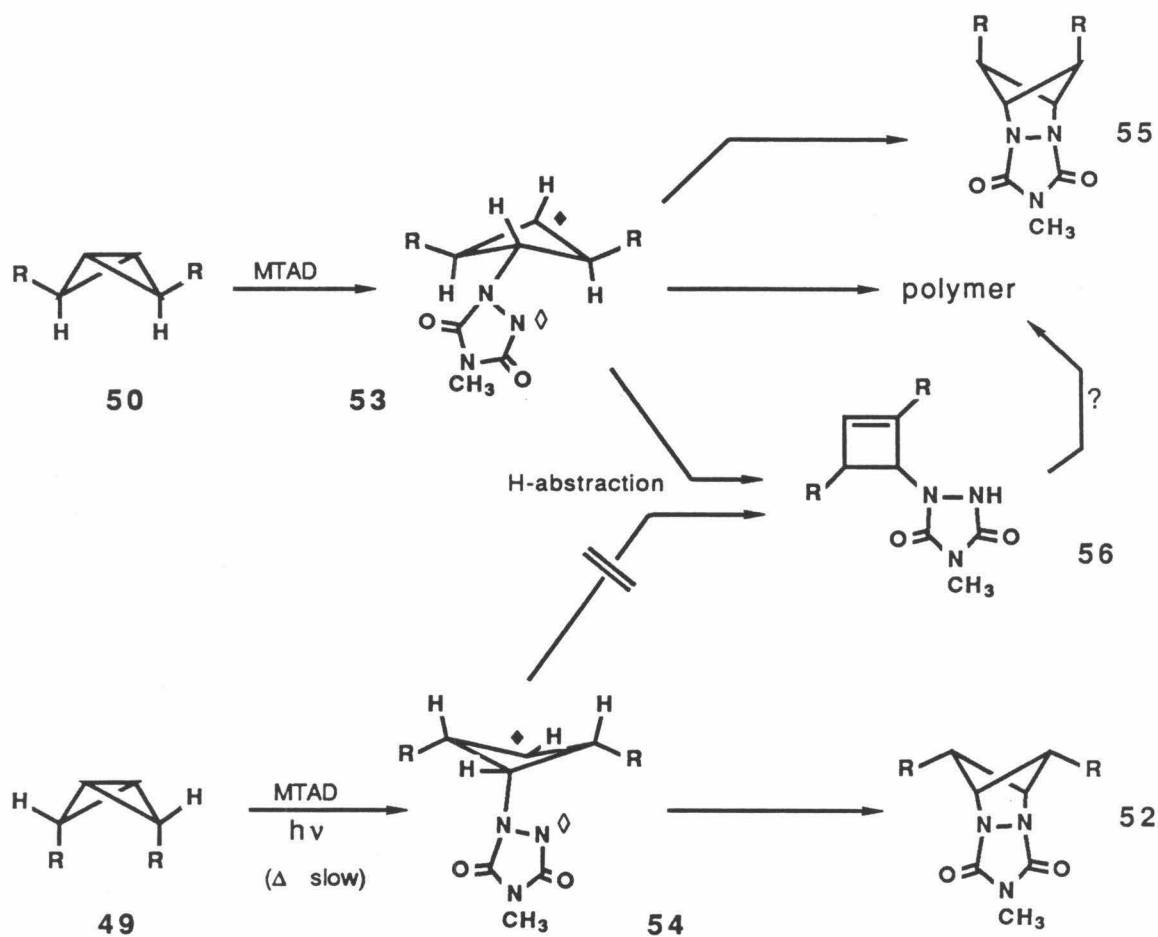


mechanistic implication of this stereochemistry is that of *endo* attack on the central bond of **49** by the photochemically activated MTAD (MTAD^*). This result suggested that MTAD^* was taking the course expected for the thermal attack on **49**, yet overcoming the steric hindrance which foiled our initial attempts at the thermal addition. Upon reinvestigating the failed thermal addition, we found that both MTAD and PTAD can be forced to cycloadd to **49** (iso-octane, 100°C), to form **52** and its *N*-phenyl analog, respectively, albeit in yields estimated as 5% or less. Because the photochemical addition of MTAD to **49** was by far the superior synthetic method we made no effort to optimize the yields of these thermal reactions.

The differing reactions of **49** and **50** with TAD can be rationalized in a straightforward way. Geometrical constraints dictate that the endo addition to bicyclobutanes must be stepwise, and such additions are thought to involve zwitterionic or biradical-like intermediates^{12,25} (Scheme 2-2). We interpret the contrasting results of thermal addition of TAD to **50** and photochemical addition to **49** in terms of intermediates **53** and **54**, respectively, as shown in Scheme 2-2. Two factors are evident which contribute to the failure of **53** to form a cycloadduct. The cyclobutyl ring of **53** certainly prefers to pucker so that all three substituents occupy pseudo-equatorial positions. Closure to **13** then requires a ring flip and the concomitant development of close, non-bonded contacts between the siloxymethyl (R) groups. Additionally, the β -hydrogens are situated such that they can easily be abstracted by the neighboring divalent nitrogen to form an "ene" product, **56**. Whether the pathway to **56** traverses **53** or is concerted,²⁷ this process remains stereochemically viable. Analogs of **56** have been observed in the reactions of TAD with bicyclobutanes.¹³ Although we have made no attempt to isolate non-cycloadducts, the observation of a broad olefinic ¹H NMR resonance suggests that such a process may be occurring (albeit probably accompanied by some sort of polymerization). In contrast to the tribulations of **53**, intermediate **54** seems far more prone to closure. Specifically, puckering of the cyclobutyl ring so as to minimize steric repulsions also places the urazolyl group in a favorable position for closure to **52**. In addition, the β -hydrogens of **56** are unavailable for abstraction.

We can cite two possible mechanisms for the photochemical attack of MTAD on **49**. Visible excitation of MTAD produces an n,n^* state, leaving the

Scheme 2-2.



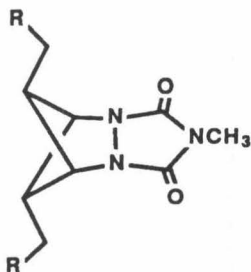
$R = CH_2OTBS$

$\blacklozenge = \cdot, +$

$\diamond = \cdot, -$

azo moiety with free radical character.²⁸ In fact, free radical reactions are frequently observed in MTAD photochemistry.²⁹ Apparently, MTAD* (either singlet or triplet³⁰) is much more reactive toward **49** than ground-state MTAD and can overcome the steric blockade presented by the siloxymethyl groups to form intermediate **54**. Alternatively, the initial step could be electron transfer,³¹ as in the photochemical singlet addition of MTAD to naphthalene.³⁰ Collapse of the radical ion pair to form **54** would probably be less sensitive to steric hindrance than the thermal attack. (It should be noted that such a mechanism may provide a pathway for formation of **53**, either by competitive collapse of the ion pair at the less crowded exo face of $49^{\cdot+}$, or by inversion of $49^{\cdot+}$ to $50^{\cdot+}$ followed by back electron transfer and facile but non-productive reaction of **50** with MTAD (see above). At present we cannot rule out such a competing pathway in the photochemical reaction.)

The conversion of **52** to diazene **2** was then a matter of introducing the double bonds and converting the urazole to the azo functionality. Removal of the TBS groups and transformation of the diol (**57**) to the corresponding dimesylate (**58a**), dibromide (**58b**), and diiodide (**58c**) was easily accomplished. However, the desired elimination could not be effected by the



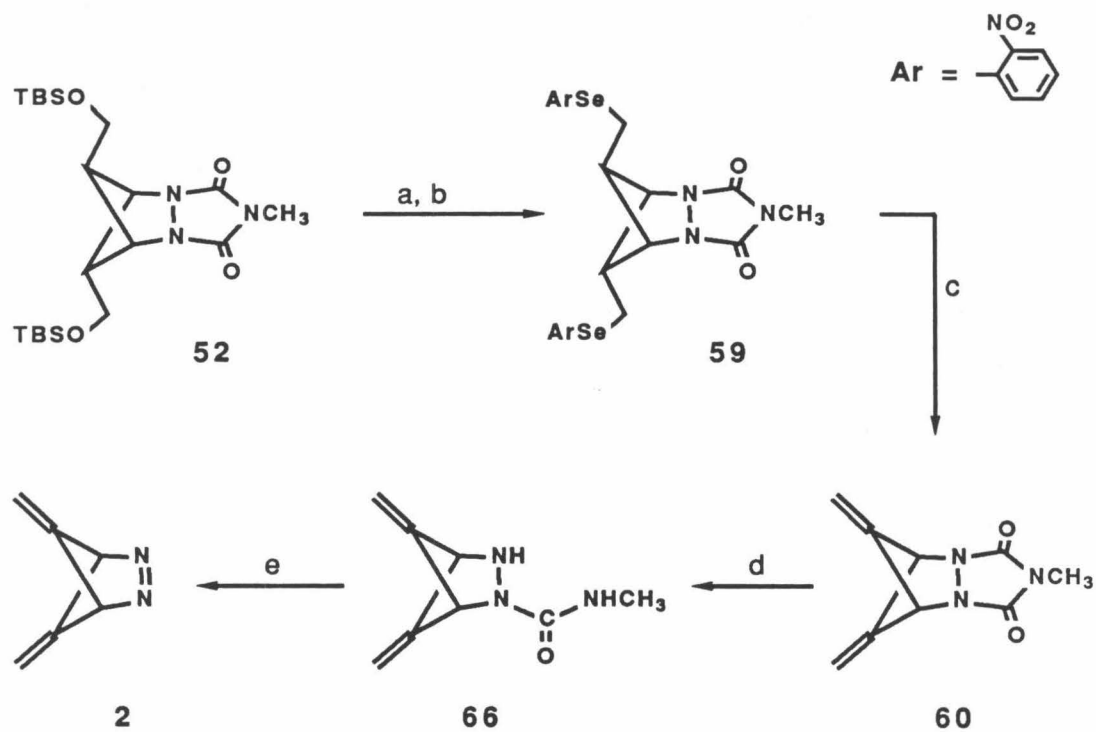
57, R = OH
58a, R = OSO₂CH₃
b, R = Br
c, R = I

usual methods (*t*BuO⁻, DBU, AgF). We therefore turned to selenoxide chemistry. In particular, *o*-nitrophenylselenoxide elimination³⁴ is reported to

be the preferred method for the elimination in normally uncooperative primary isobutyl-type systems^{34b} such as the present one. Conversion of selenide **59** (Scheme 2-3) to the diene, **60**, was accomplished in 66% isolated yield.

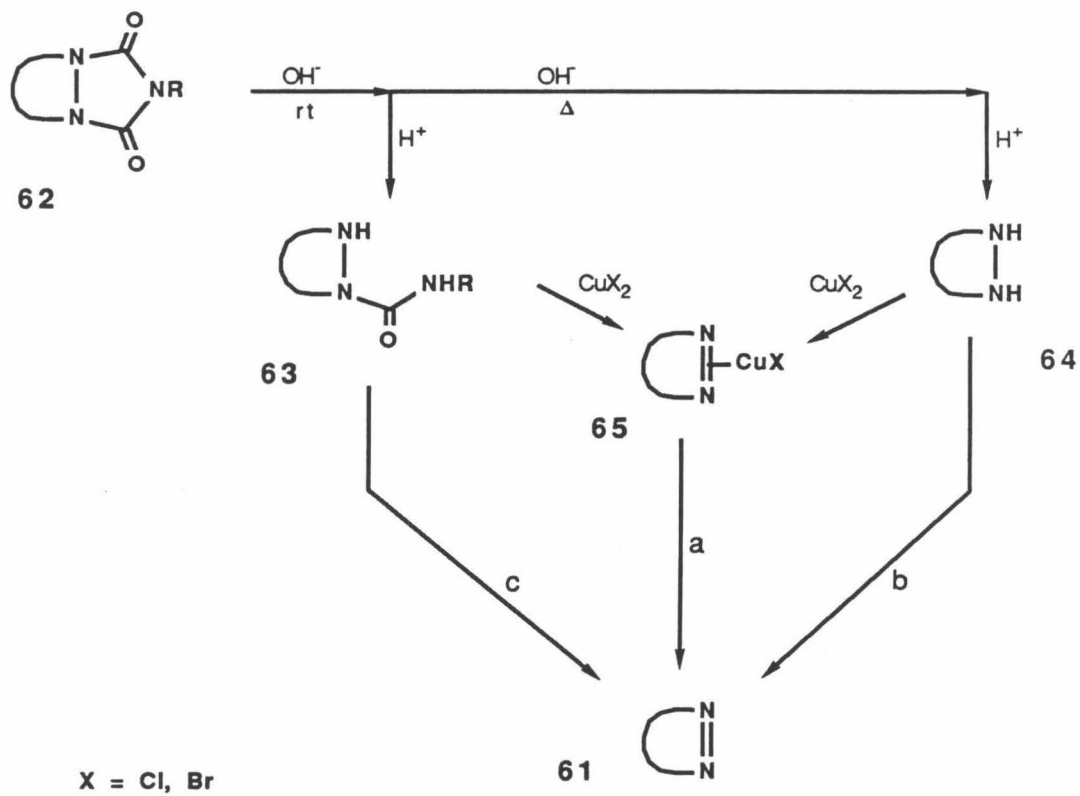
We initially attempted to prepare **2** by subjecting urazole **60** to the standard hydrolysis/oxidation procedure (KOH, ROH, Δ ; CuCl₂; base),³⁶ but this apparently induced a deep-seated rearrangement.³⁷ We suspected that the strain present in the bicyclo[2.1.1] ring system might have been contributing not only to the anticipated thermal instability of **2** but to the lability of the various intermediates in the hydrolysis/oxidation sequence. We therefore directed our attention toward carrying out the conversion under milder hydrolytic conditions and/or making the diazene at very low temperature.

Scheme 2-4 illustrates the general pathways available for the low temperature preparation of azoalkanes, **61**, from urazoles (*R* = methyl or phenyl), **62**. Partial hydrolysis to the semicarbazide, **63**, can normally be effected at room temperature,³⁸ whereas conversion of **62** to the hydrazine, **64**, requires more vigorous conditions.³⁹ (The latter is more easily obtained from the corresponding bis-carbamic ester when such a derivative is available.) In most cases cupric halides are used to oxidize the hydrolysis product(s), whether **63**^{38,40} or **64**, providing a readily isolable complex, **65**.⁴¹ The diazene, **61**, is then liberated by treatment of **65** with aqueous ammonia (or pyridine or aq NaOH). This step (*a* in Scheme 2-4) has been conducted at temperatures as low as $-50\text{ }^{\circ}\text{C}$ (although with difficulty).^{3a} Alternatively, hydrazines (**64**) have been oxidized directly to diazenes (**61**) at low

Scheme 2-3.^a

^a(a) $n\text{Bu}_4\text{N}^+\text{F}^-$, THF. (b) $o\text{NO}_2\text{PhSeCN}$, $n\text{Bu}_3\text{P}$, THF.³⁵ (c) O_3 , CHCl_3 , -60°C ; $i\text{Pr}_2\text{NH}$, CCl_4 , Δ . (d) KOH , $\text{DMSO}/\text{H}_2\text{O}$ (6:1). (e) Nickel peroxide, CH_2Cl_2 , -78°C .

Scheme 2-4.



temperature ($\leq -50\text{ }^{\circ}\text{C}$) with a variety of reagents, most notably MnO_2 ⁴² and $t\text{BuOCl}$ ⁴³⁻⁴⁵ (*b*, Scheme 2-4). Semicarbazides (**63**) have also been oxidized directly to diazenes at ambient temperature (*c*, Scheme 2-4).^{39,41b}

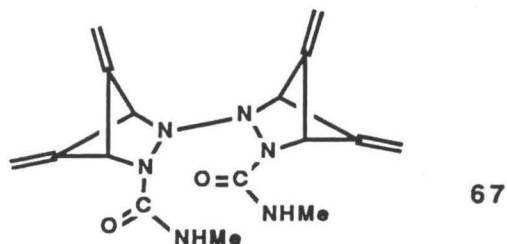
Whereas the hydrolysis in refluxing isopropanol caused rearrangement, hydrolysis of **60** at room temperature in DMSO/ H_2O provided the semicarbazide, **66**, (Scheme 2-3) in 90% yield after purification by preparative-TLC.

After a few futile attempts at converting **66** to the copper complex of the diazene⁴⁸ we tried using MnO_2 to carry out the oxidation. The heterogeneous conditions under which MnO_2 had been used to carry out similar conversions^{39,42} seemed especially suitable for a low-temperature preparation of **2**. Treatment of a solution of the semicarbazide (**66**) in CH_2Cl_2 with MnO_2 ⁴² at $-78\text{ }^{\circ}\text{C}$ for several hours converted a small amount of **66** to **2** as determined by ^1H NMR (see below). Encouraged by this result and the success of Dervan and coworkers in the heterogeneous, low temperature preparation of 1,1-diazenes by treating hydrazine precursors with nickel peroxide,⁴⁹ we decided to try this reagent for the desired oxidation. Thus, treatment of **66** in CH_2Cl_2 with nickel peroxide at $-78\text{ }^{\circ}\text{C}$ results in a conveniently rapid⁵⁰ loss of the semicarbazide, as indicated by TLC analysis of the reaction mixture. Removal of the black solid by filtration and the solvent under vacuum at $-78\text{ }^{\circ}\text{C}$ affords **2** as a white solid.

The ^1H NMR spectrum of **2** in CD_2Cl_2 at $-80\text{ }^{\circ}\text{C}$ reveals singlets at δ 5.48 and 4.75 in a 1:2 ratio. Diazene **2** also displays the characteristic azo group n, n^* transition at 331 nm (CD_2Cl_2 , $\epsilon = 240$; λ_{max} 333 nm in MTHF). This transition energy is quite similar to that of **46** and its derivatives.^{3a, 12}

Diazenes **2** is quite labile thermally, and loses nitrogen with first-order kinetics, which are conveniently monitored by ^1H NMR between -40 and -70 $^\circ\text{C}$. This decomposition affords 2,4-dimethylenebicyclo[1.1.0]butane (**3**), which dimerizes in the same temperature range to produce two stable ($\text{C}_{12}\text{H}_{12}$) products (see Chapter 3).⁵¹ We do note, though, that because thermal decomposition of **2** is so facile, spectroscopic samples of the diazene invariably contain about 20% decomposition products. Most of the decomposition presumably occurs during transfer of cold (-78 $^\circ\text{C}$) solutions of **2**, especially when these solutions are small in volume. ^1H NMR analysis of a typical sample implies that the nickel peroxide oxidation produces diazenes **2** in an overall yield of approximately 30%, based on the amount of **2**, **3**, and dimers present. Aside from these decomposition products the diazene samples normally appear to be exceptionally clean. The oxidation byproducts presumably adhere to the nickel peroxide or are removed along with the reaction solvent.

We have found that, at least at -78 $^\circ\text{C}$,⁵² this oxidation is critically dependent on the activity of the nickel peroxide (see **Experimental**). During our attempts to overcome the activity problems, we apparently induced the formation of two side-products with ^1H NMR signals closely resembling those of the semicarbazide (**66**), but missing the amine proton resonance. The two species, each with eight ^1H NMR signals, are formed in significant but inconsistent quantities and in ratios varying unpredictably from about 1:4 to 4:1. Nickel peroxide is known to oxidatively couple amines,⁵³ and we tentatively assign the species observed as coupled semicarbazides of structure **67**. That two sets of resonances are present suggests that the species are



slowly interconverting conformers of **67** with bilateral symmetry. However, we have observed neither photochemical nor thermal interconversion of the two compounds up to about 0 °C. (Above 0 °C the two species decompose at slightly different rates, producing an uncharacterized mixture of flocculent, yellow or whitish solids.) This explanation would therefore seem to require the presence of one or more abnormally large rotation barriers in addition to the likely hydrogen-bonding interactions between the amide groups. Nevertheless, compound **67** appears at present to be the most reasonable source of the NMR signals observed.

Having tentatively assigned the byproduct as **67**, we began conducting the oxidation of **66** by adding the semicarbazide to the nickel peroxide, rather than vice versa, and this procedure prevents the formation of **67**.

Nickel peroxide is a rather ill-defined substance, and we have no direct evidence concerning the mechanism of the oxidation of **66** to **2**. It is worth noting, however, that nickel peroxide oxidations are generally believed to proceed via free radical mechanisms.⁵³ We suspect that the oxidation is initiated by abstraction of the amine hydrogen of **66**. Diazene **2** could then be produced — at least formally — by simple fragmentation of the amine-centered radical, although some pathway involving nickel-coordinated intermediates may be more reasonable. At any rate, it is certainly reasonable

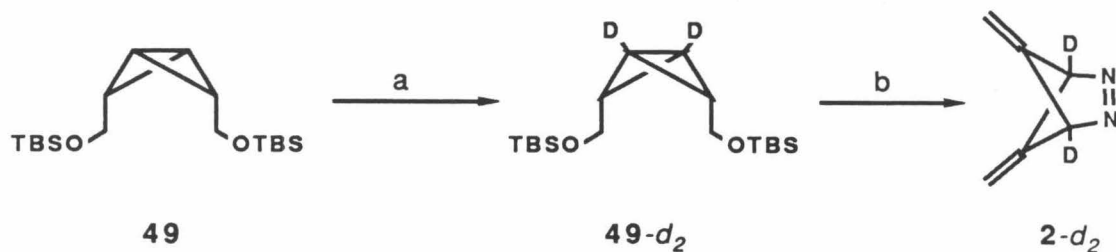
to ascribe the exceptional, low-temperature reactivity of nickel peroxide toward **66** to this free radical-like nature.

More recently, nickel peroxide has been demonstrated to be generally useful for the preparation of 1,2-diazenes from hydrazines,⁴⁴ as well as from phenyl⁵⁴ and methyl^{3a,55} semicarbazides.

Additionally, we required deuterium-labeled diazene for various spectroscopic and chemical studies to be described below and in Chapter 3. Diazene **2-*d*₂** was prepared as shown in Scheme 2-5. The bridgehead protons of bicyclobutanes are reasonably acidic and can easily be exchanged for deuteria by treatment with alkyllithium followed by D₂O.⁵⁶ Accordingly, **49** was treated with *n*BuLi then D₂O three times in order to thoroughly wash out the bridgehead hydrogen. Completion of the synthetic sequence afforded **2-*d*₂** with >99% bridgehead deuterium incorporation.

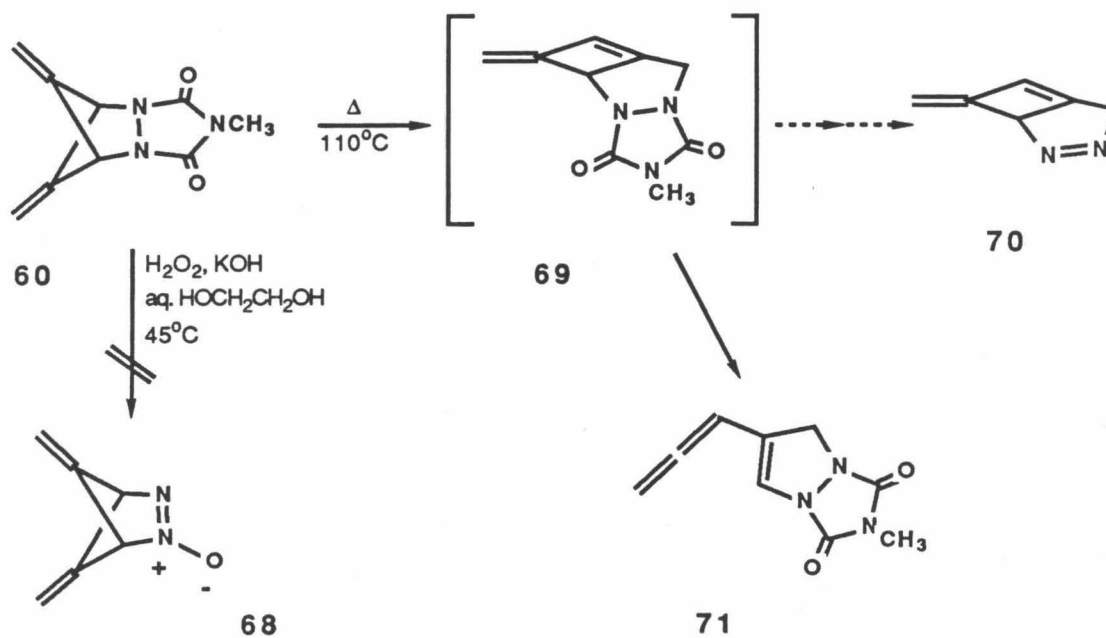
We also attempted to prepare the azoxy compound **68** (Scheme 2-6). Azoxy compounds have been found to extrude N₂O with activation energies from 7⁵⁷ to ≥ 23 kcal mol⁻¹⁵⁸ higher than the corresponding diazenes. Thus, **69** might have been much less thermally sensitive than **2**. However, oxidative hydrolysis of urazole **60** under conditions^{58b, 59} (Scheme 2-6) that converted urazole **5** to the azoxy analog of **3** failed to provide **68**.

Finally, we felt that pyrolysis of urazole **60** might provide either biradical **1** by extrusion of MTAD or the rearranged urazole, **69**, which could be converted to diazene **70** (Scheme 2-6). Indeed, heating **60** at 110 °C provided an isomeric urazole in approximately 10% yield as the only product isolated. The compound displayed the characteristic urazole group MS fragmentation pattern (see **Experimental**) as well as the usual N-methyl singlet in the ¹H

Scheme 2-5.^a

^a(a) $n\text{BuLi}$, $\text{Et}_2\text{O}/\text{hexane}$, rt; D_2O . Three cycles. (b) See Schemes 2-1 and 2-3.

Scheme 2-6.



NMR spectrum. However, the observation of a 6.4 Hz coupling between olefinic methylene and methine protons is inconsistent with the structure of **69**. The ^1H NMR spectrum is consistent with the allene, **71**, though.⁶⁰ This compound could arise via an electrocyclic opening of the cyclobutane ring of **69**.⁶¹ and we therefore suggest that the conversion proceeds as shown in Scheme 2-6.

EPR spectroscopy.

When a frozen solution of diazene **2** is irradiated directly (or triplet-photosensitized) with UV light in the cavity of an EPR spectrometer at 4 to 140 K, the spectrum of Figure 2-1 is observed.⁷ This spectrum is characteristic of a randomly-oriented ensemble of immobilized triplet species^{65,64a} and is described by zero-field splitting (zfs) parameters $|D/hc|=0.0204\text{ cm}^{-1}$ and $|E/hc|=0.0028\text{ cm}^{-1}$.⁶² Given its method of generation, the signal is unequivocally assigned to biradical **1** on the basis of its D value.

Assignment of the spectrum to triplet 1. The D value manifests itself in the width of the primary ($\Delta m_s = 1$) six-line region of a triplet EPR spectrum. This parameter is a gauge of the magnitude of the dipolar coupling between the unpaired spins, which lifts the degeneracy of the triplet sublevels even in the absence of an external magnetic field. The extent of this spin-spin interaction depends critically on the effective separation between the unpaired electrons and is therefore a sensitive probe of their distribution. Table 2-1 lists some representative D values observed for related hydrocarbon biradicals. The D value derived from the spectrum of Figure 1 falls nicely within the range of values of other delocalized biradicals. For comparison we include in Table 2-1 two localized⁷⁵ members of the cyclobutanediyl series,³ a photoexcited triplet state of a covalent isomer of **1**, and a carbene. Also included are the D values calculated by a previously described method that uses the point-charge approximation to evaluate the zfs integrals.⁷⁴ The values listed were calculated by using Hückel wavefunctions.⁷⁴ Unless highly

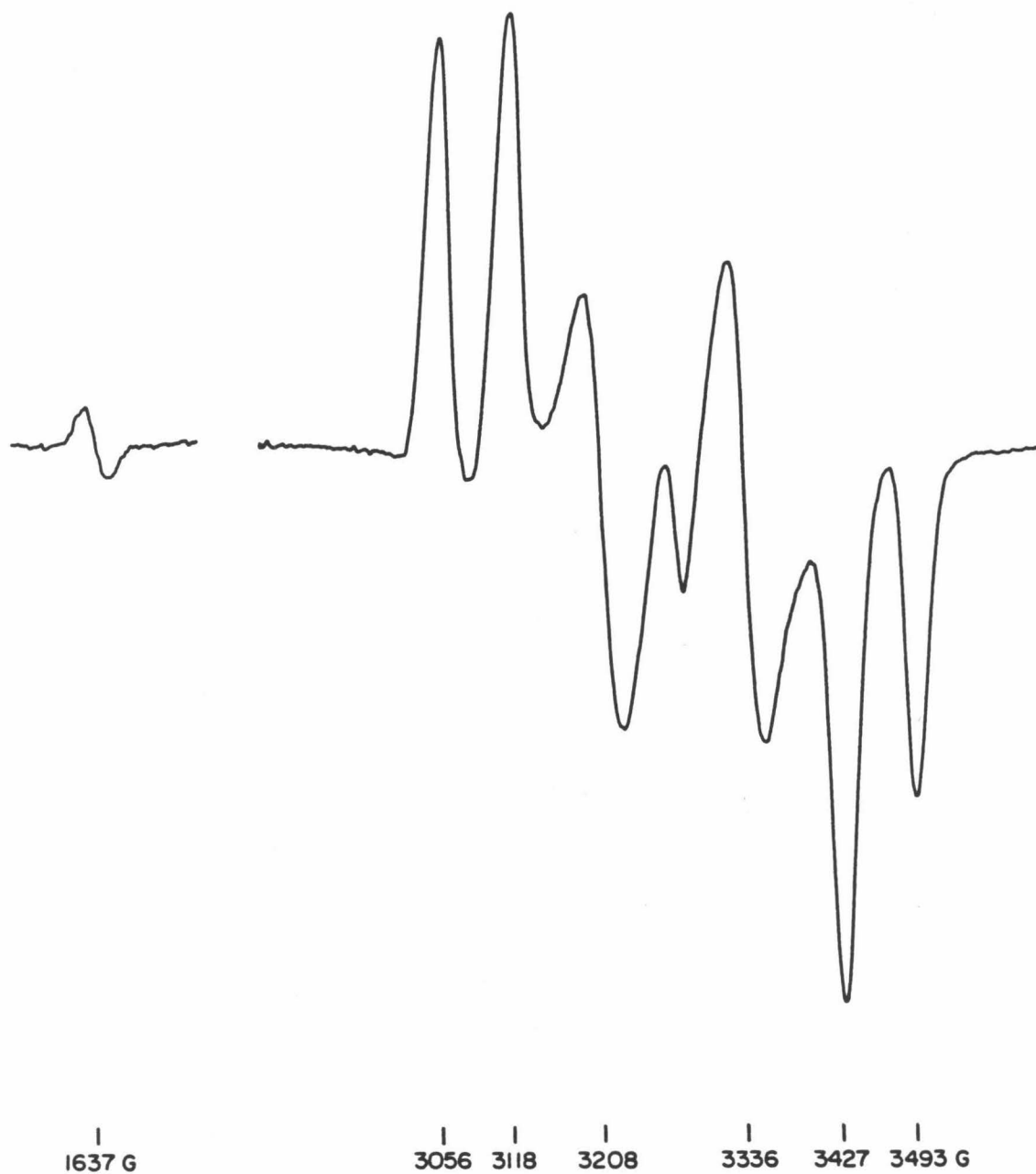



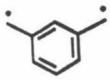



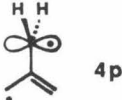
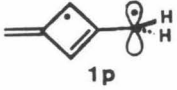
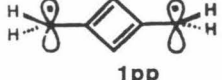


Figure 2-1. First-derivative EPR spectrum of 1 ($|D/hc| = 0.0204 \text{ cm}^{-1}$, $|E/hc| = 0.0028 \text{ cm}^{-1}$)⁶² observed after 1 min of (primarily) sensitized photolysis (1000-W Xe arc lamp; λ 315-415 nm) of 2 in MTHF (2-methyltetrahydrofuran) containing 0.3 M Ph_2CO at 5-6 K. The spectrum was recorded at 9.18 GHz and 0.002 mW microwave power.

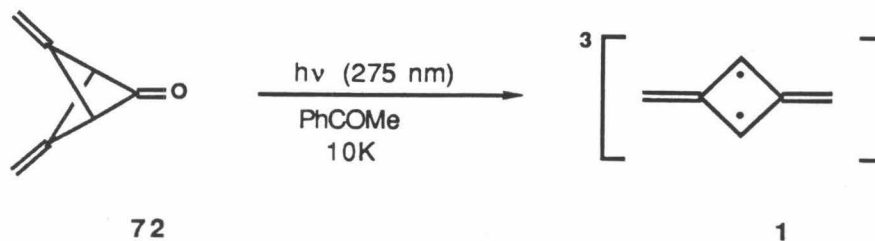
Table 2-1. EPR zero-field splitting parameters for triplet biradicals.

	Experimental		Calculated ^a	Ref.
	D/hc ^b	E/hc ^b	D/hc ^b	
 1	0.0204	0.0028	0.051 ^c	This work
 4	0.0248	<0.0003	0.052 ^d	66
 9	0.0265	0.0055	0.046 ^d	67
 12	0.011	≤0.001	0.032 ^d	68
	0.112	0.005		3
	0.050	0.001		3a
	0.1581	0.0064 ^f		69
Ph ₂ C:	0.405	0.019		70
 4p			0.096	71, this work
 1p			0.080 ^g	This work
 1pp			0.018 ^g	This work

^abased on Hückel wavefunctions. ^bin cm⁻¹. ^ccalculated at the π -CI-optimized geometry of ref. 72b, 73. ^dref. 74. ^ephosphorescent triplet state. ^fthe deviation from hexagonal symmetry is attributed to the influence of the crystalline C₆D₆ host and the quinoidal character of the excited state.⁶⁹ ^gcalculated with 1.48 Å bonds to the perpendicular methylene groups.

correlated wavefunctions are used, it is difficult to calculate D values precisely,⁷⁶ but this method has proven to be quite useful for obtaining *relative* D values among related structures. In relation to the other non-Kekulé hydrocarbons of Table 2-1, it is apparent that both the observed and the calculated D values for **1** are quite consistent with its delocalized structure. The E value is generally treated as a symmetry parameter only — a value of zero being a necessary but insufficient criterion for assigning the signal carrier an axially symmetric structure — and we attach no qualitative significance to the E value observed for **1**.

Along with the D value, the identity of the precursor diazene (**2**) used to generate the EPR signal leaves no doubt that its source is biradical **1**. As testimony to the facility of the photochemical conversion of **2** to **1** we note that the spectrum of Figure 2-1 was generated by only 1 min of sensitized photolysis. This spectrum is completely free of monoradical impurities; the central line near 3270 G is a double-quantum transition, so assigned on the basis of its strong microwave power dependence.⁶⁴ We have also obtained this triplet EPR signal upon photolysis of frozen solutions of **2** in a variety of solvents in addition to MTHF, including Et₂O, 3-methylpentane (3-MP), CH₂Cl₂, acetone, Et₂O/EtOH (4:1), MeOH/EtOH (1:1), and toluene-*d*₈/3-MP (7:1). A final corroborative piece of evidence concerning the assignment of the EPR spectrum of Figure 2-1 was recently provided by Dowd and Paik, who independently generated a weak signal ascribed to **1** by sensitized photolysis of ketone **72**.⁷⁸



Proton hyperfine splitting. Additional information concerning the unpaired electron distribution, and further confirmation of the structure of triplet 1 are provided by the hyperfine splitting in the half-field ($\Delta m_s = 2$) transition.⁷⁹ Figure 2-2 shows both the seven-line pattern observed for 1 and the five-line pattern observed upon replacement of the ring hydrogens with deuteria. Additionally, the second and fifth lines of the $\Delta m_s = 1$ region (3118 and 3427 G in Figure 2-1) display poorly resolved, but discernable hyperfine structure with the same 6-7 G splitting observed in the half-field transition. This hyperfine structure is shown in Figure 2-3.

Electron-nuclear hyperfine as well as electron-electron dipolar interactions in immobilized species are generally anisotropic, and thus dependent on orientation with respect to the applied magnetic field. It is therefore not immediately apparent that the observed structure of the $\Delta m_s = 2$ transition in our randomly-oriented sample should be readily interpretable in terms of conventional hyperfine coupling constants. That it is, in fact, interpretable in the present case as well as in several other hydrocarbon biradicals^{3a,5} results from a convenient combination of effects.

Triplet half-field transitions are inherently anisotropic, as four stationary resonant fields occur in this region.^{79,81} However, this transition is much more isotropic than the $\Delta m_s = 1$, which normally spans several hundred Gauss

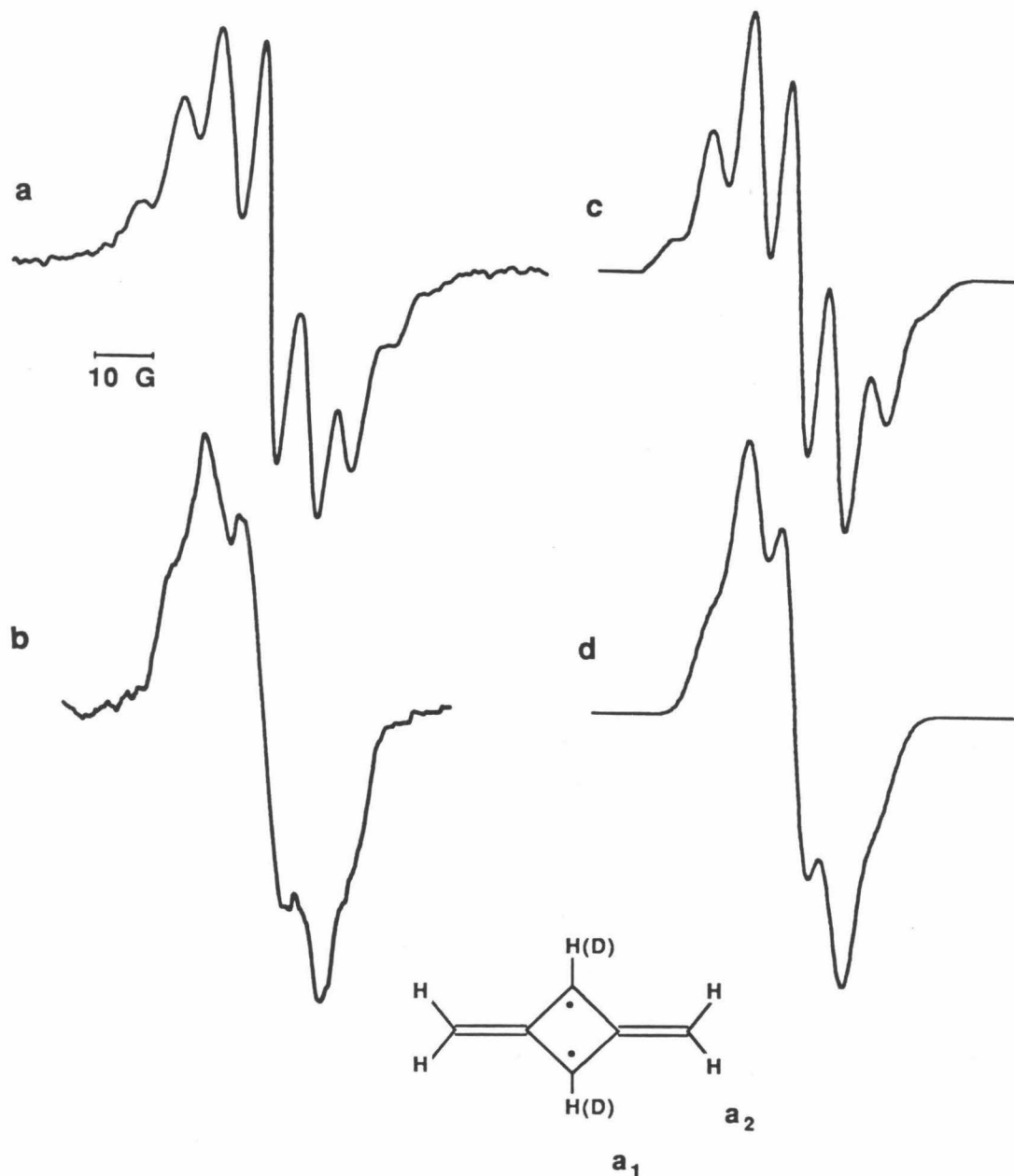


Figure 2-2. Hyperfine structure of the $\Delta m_s = 2$ transition. (a) The 1637 G signal of Figure 2-1 enhanced with 2.0 mW power and 3 G field modulation. (b) The analogous signal of 1- d_2 (obtained under similar conditions of signal generation and measurement). (c,d) Spectra simulated by using isotropic proton coupling constants $a_1 = 7.3$ G and $a_2 = 5.9$ G^{63,80a} and a 5.8 G linewidth.

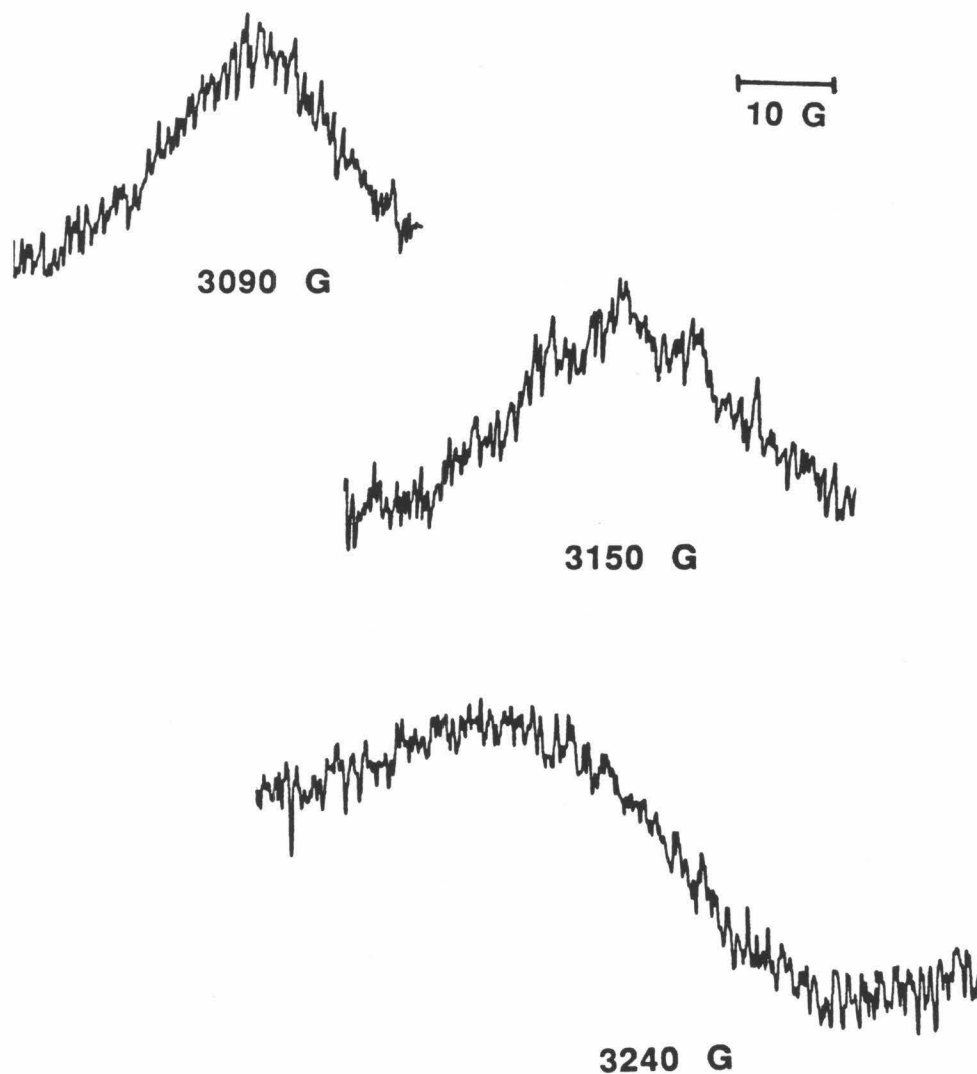


Figure 2-3. The low-field $\Delta m_s = 1$ transitions of 1. The spectra were obtained at 77 K with 2.5-G field modulation and 0.2 mW microwave power (9.27 GHz). (The sample contained a partially-oriented assembly of biradicals; Figure 2-8c.) A sample of 1- d_2 was found to display no resolvable hyperfine splitting in the 3150 G transition.

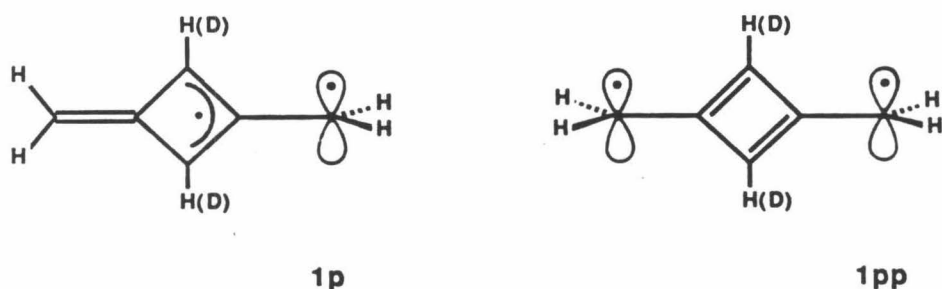
with six such stationary fields. When the D value is small, the $\Delta m_s = 2$ anisotropy is diminished considerably⁸¹; for **1** the four stationary fields are nearly coincident, and the entire transition extends over only 5 G (before the effects of linewidth and proton hyperfine interactions are included).

The hyperfine interactions responsible for the observed splitting in **1** involve coupling to α -protons (*i.e.*, those attached directly to spin-carrying carbons). This coupling represents the sum of both isotropic and anisotropic contributions. The former arise from direct electron-nuclear contact caused by spin polarization of the C—H bond, which places negative spin density at the α -proton. The anisotropic component arises from proton-electron dipolar coupling.⁸² In general, the anisotropic interaction generates a superposition of individual resonances for all possible orientations of a randomly-oriented but non-reorienting species, and the resulting spectral shape is complex. However, if the radical centers are planar the form of the α -proton hyperfine coupling tensor is such that the splitting it produces in a randomly-oriented ensemble has very nearly the isotropic value.⁸³ For example, TMM (**4**) embedded in a polycrystalline methylenecyclopropane host exhibits a splitting⁸⁴ in the $\Delta m_s = 2$ transition that is within 0.3 G of the isotropic value (9.3 G), which was determined accurately from a single crystal study.^{66b} We therefore feel confident in interpreting our hyperfine splitting (Figure 2-2) in terms of isotropic coupling constants, at least on a semiquantitative level.

With this analysis in mind, the observed splitting can be attributed by inspection to interaction with six protons that have comparable coupling constants in **1** and four in **1-d₂**. In fact, computer simulation⁶³ of these spectra reveals that the splitting constants a_1 and a_2 (Figure 2-2), although similar,

are not identical. As shown in Figure 2-2c and d, we have obtained reasonable simulations of both experimental spectra by using splittings of $a_1 = 7.3$ G for two protons (7.3/6.5 for two deuterons) and $a_2 = 5.9$ G for four.^{80a}

We note that the hyperfine structure observed is consistent only with the planar geometry for **1**. Rotation of the terminal methylene groups produces **1p** or **1pp**. The observed removal of the larger (7.3 G) splitting by deuteration



at the methine positions obviates further consideration of **1pp**. With regard to **1p** we note that, to first order, the methylenecyclobutenyl moiety has spin density only at the ring methine positions.⁸⁵ Removal of the larger splitting on going from **1** to **1-d₂** is consistent with this idea. However, the five-line pattern observed for **1-d₂** (Figure 2-2b) requires comparable spin densities on both methylenes and is therefore quite incompatible with structure **1p**. (In further support, we note that the D values calculated for these structures (Table 2-1) are much less consistent with the experimental value than that calculated for the planar geometry.) We conclude that triplet **1** is planar.

Curie plot. Figure 2-4 shows the variation in EPR signal intensity with reciprocal temperature. The data presented were obtained upon first increasing then decreasing the temperature to demonstrate that the intensity

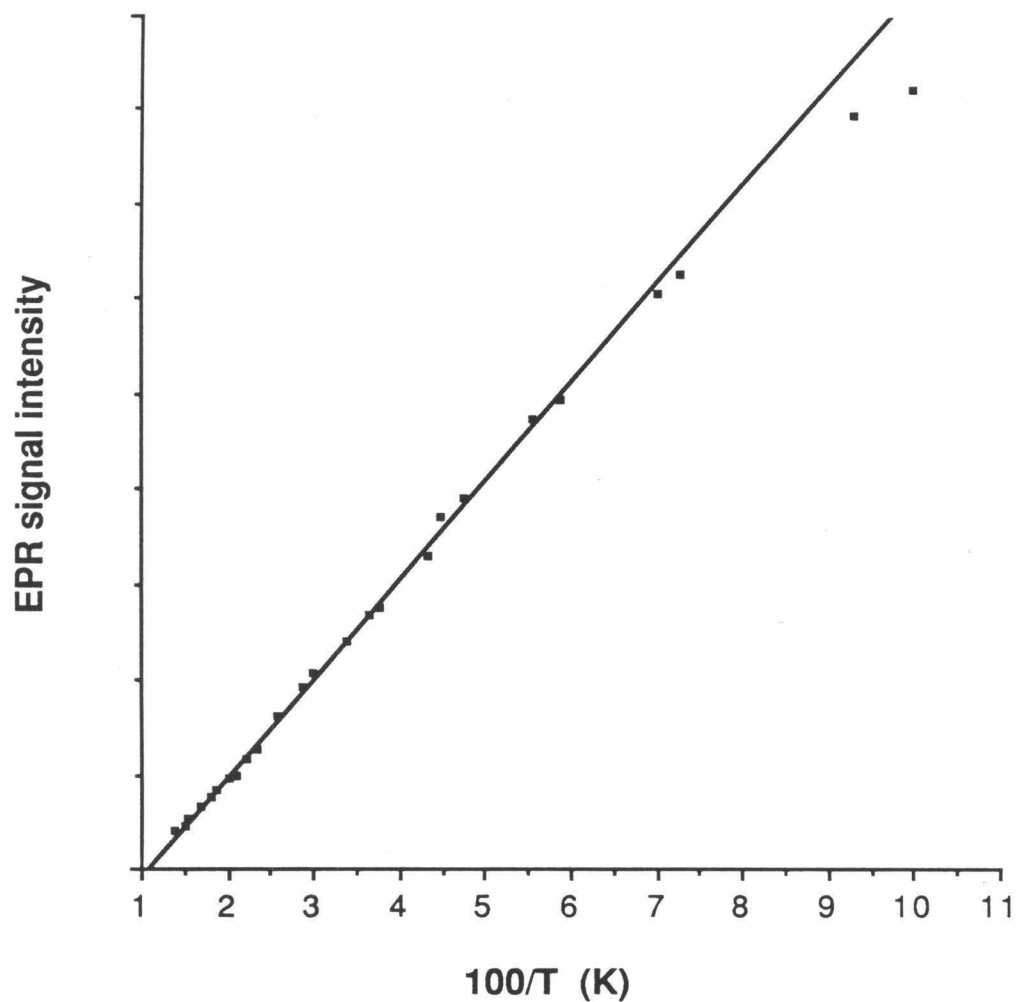


Figure 2-4. Curie Law plot of the first-derivative EPR signal intensity of 1 (in 1:1 EtOH/MeOH) as a function of temperature between 10 and 75 K (the range is limited by the thermal instability of the biradical). Data points were obtained upon both increasing and decreasing the temperature. Because saturation of the EPR signal begins near 15 K at the microwave power used (0.01 mW), points below this temperature (*i.e.*, the last four), were not used in determining the least-squares line. Errors in temperature measurement are discussed in **Experimental**.

change is reversible. Aside from the slight curvature at the low temperature end of the plot, which we attribute to saturation of the signal, the intensity adheres to the Curie Law between 15 and 75 K. This indicates that the triplet is the ground state of 1 or that the singlet and triplet are nearly degenerate.⁸⁶ That theoretical estimates place the singlet well above the triplet energetically makes the latter situation very improbable. We therefore adopt the customary interpretation of a linear Curie plot and assign the triplet as the ground spin state of 1.

Electronic spectroscopy.

During our somewhat injudicious initial attempts to generate 1 by photolyzing 2 in the EPR cavity, we quickly became apprised of the fact that the triplet biradical is quite photosensitive, being irreversibly destroyed by visible light. After preparing 1 by irradiating the diazene with UV light, a simple filter-shuffling experiment established that light of $\lambda < 515$ nm was responsible for destroying the biradical,⁷ suggesting that triplet 1 has a strong electronic transition near 500 nm.

Indeed, when a sample of 2 in MTHF is irradiated with UV light, an intense yellow-orange color appears. In addition, the sample displays a bright, short-lived, green emission that is readily observable when the sample is placed in the UV-vis spectrophotometer beam. Figure 2-5 shows the absorption, emission and excitation spectra of the colored species obtained at 77 K.⁷ The correspondence between the absorption and excitation spectra provides a formal demonstration that the same species is responsible for both the absorption and emission observed.

Assignment of the spectra to triplet 1. We have compelling evidence that the absorption and emission spectra of Figure 2-5 are those of triplet 1. That these spectra arise from 1 (*i.e.*, they are not due to an impurity or by-product) is demonstrated by the coincident formation of the EPR and absorption spectra and their loss upon bleaching the sample with visible light. In addition, both the EPR and absorption spectra decay very slowly ($t_{\frac{1}{2}} = ca.$ 30 hrs) at 77 K in MTHF.⁸⁸ The decay is non-exponential due to a distribution of matrix sites,⁸⁹ which gives rise to a distribution of rate constants. This

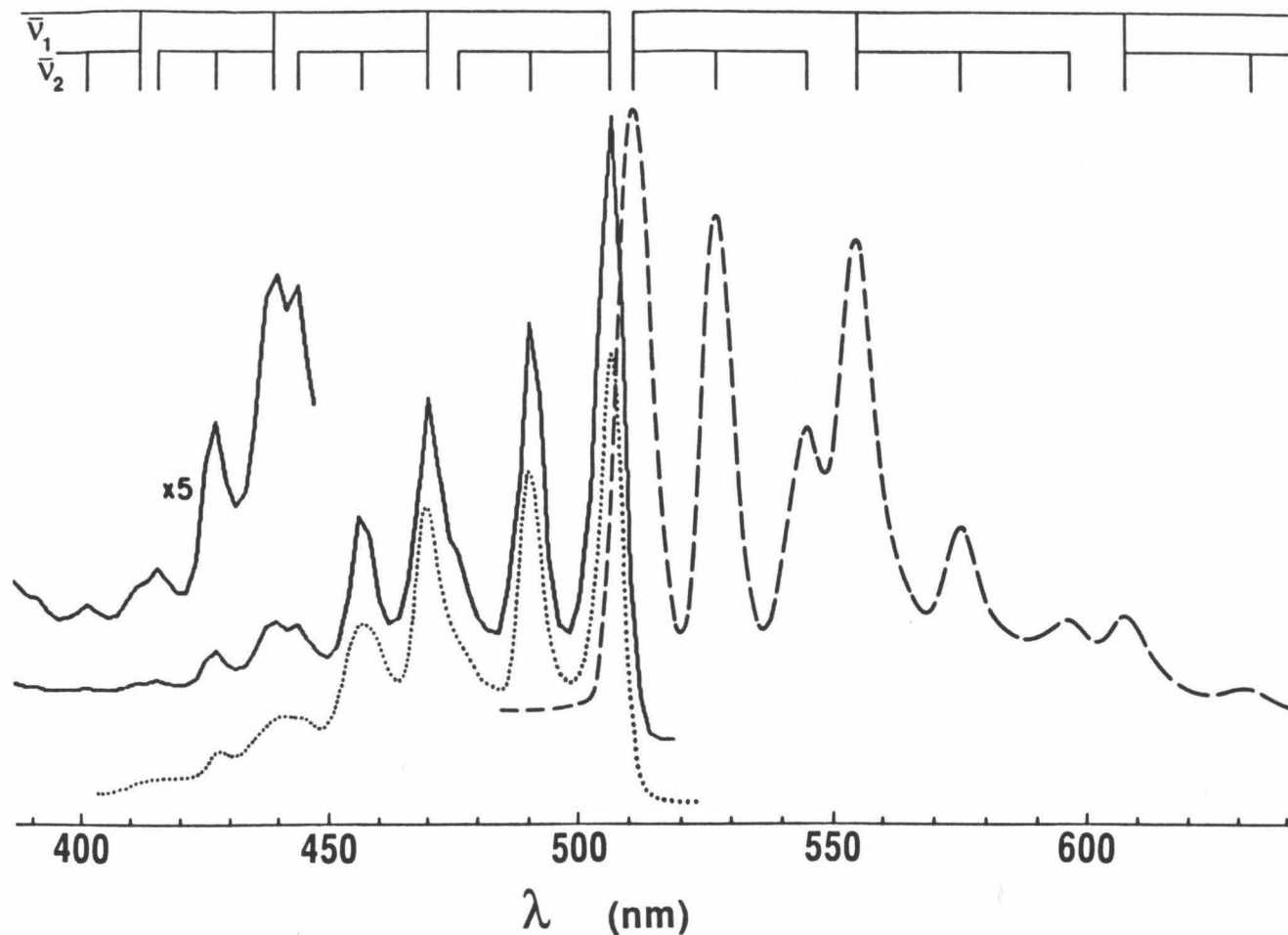


Figure 2-5. Absorption (—), fluorescence (---; $\lambda_{\text{ex}}=440$ nm), and fluorescence excitation (····; $\lambda_{\text{em}}=550$ nm) spectra of triplet 1 in MTHF at 77K. $\lambda_{\text{max}}=506$ and 510 nm for absorption and emission, respectively. Neither the fluorescence nor the excitation spectrum is corrected for decomposition of 1 during the scan (with increasing wavelength in both cases), estimated as 40% in the former spectrum.

kinetic behavior can often be treated by plotting $\ln I$ vs t^\dagger .⁸⁹ Such plots of the EPR and absorption intensities for 1 were linear and provided the same "most probable" rate constant.⁸⁹

These observations do not rule out the possibility that the optical spectra result from a species in rapid equilibrium with triplet 1, singlet 1 being the obvious candidate. The optical spectra were recorded at 77 K, which would allow significant population of a higher lying singlet even if the S-T gap is on the order of a few kcal mol⁻¹. We had observed photodestruction of the EPR signal at 4 K with *ca.* 500-nm light. Although this suggested that triplet 1 is most likely the species responsible for the 77 K optical spectra, the possibility remained that the spectra are instead those of singlet 1. Triplet 1 might then be destroyed at 4 K via a separate absorption near 500 nm that is overwhelmed by the absorption of the singlet biradical at 77 K. Ideally, one would resolve this conflict by simply measuring the absorption spectrum at 4 K, but we could not easily conduct such an experiment.

We have, however, been able to measure an effective absorption spectrum and at the same time explicitly link the optical spectra of Figure 2-5 and the EPR spectrum *at 4 K*. The well-defined vibronic structure of the absorption envelope and the efficient photochemical destruction of triplet 1 suggested that, if the 77 K absorption spectrum persisted at 4 K, monochromatic irradiation of triplet 1 at an absorption peak would produce a detectably faster decay of the EPR signal than irradiation between peaks. An implementation of this experiment is shown in Figure 2-6a. Scanning from higher to lower wavelength (right to left as shown) at a constant rate with a monochromator, the EPR signal intensity falls off rapidly at precisely the wavelengths of the

vibronic peaks of the 77 K absorption spectrum. The signal intensity curve can be converted to an ϵ vs λ spectrum in a straightforward manner.

The rate of photochemical loss of triplet 1, whose concentration, c_T , is proportional to the EPR signal intensity, S , is given by

$$-\frac{dS}{dt} = K I_0(\lambda) A(\lambda) \Phi_r$$

where K is a proportionality constant. The quantum yield for reaction from the excited state, Φ_r , is assumed to be wavelength independent (vibrational relaxation is rapid), while I_0 , the incident light intensity, varies slightly with λ . Expressing absorbance as $\epsilon c_T l$ and gathering constants, we have

$$-\frac{dS}{dt} = K' I_0(\lambda) c_T \epsilon(\lambda).$$

Again relating c_T to signal intensity, we can express ϵ as

$$\epsilon(\lambda) = K'' \left(-\frac{dS}{dt} \right) \left(\frac{1}{S I_0(\lambda)} \right).$$

The incident light intensity, $I_0(\lambda)$, can be approximated as the Xe arc lamp output spectrum, which is easily measured. Finally, since the irradiation wavelength was changed at a constant rate, the λ axis is also a time axis. Therefore, simply differentiating the signal intensity function with respect to λ and dividing by incident light and signal intensities provides a curve proportional to $\epsilon(\lambda)$ vs λ for the EPR signal carrier.

This curve is presented as Figure 2-6b along with the 77 K absorption spectrum (Figure 2-6c) on the same scale for comparison. It is important to appreciate that this EPR-detected photochemical destruction profile, or "photochemical action spectrum" provides an *explicit* link between 77 K absorption spectrum of Figure 2-5 and the EPR signal of Figure 2-1. This connection is quite analogous to that between absorption and emission spectra

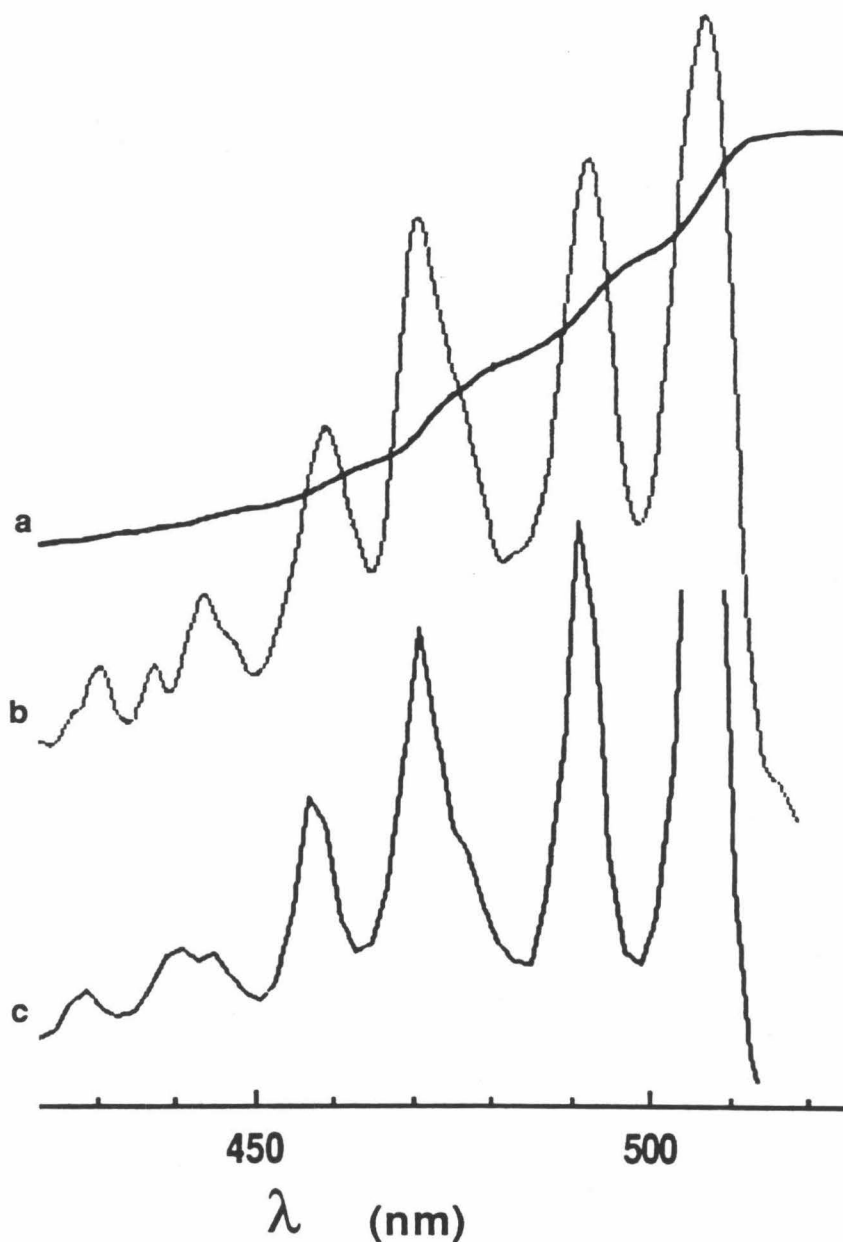


Figure 2-6. Photochemical action spectrum. (a) EPR signal intensity of 1 in MTHF at 4 K, monitored at the low-field γ -transition (3073 G; 9.27 GHz), vs irradiation wavelength. The scan is from right to left as presented and represents photochemical destruction of *ca.* 65% of the triplet 1 initially present. Monochromatic light (*ca.* 3-nm bandpass) from an Xe arc lamp was used, and the irradiation wavelength was decreased from 520 nm at a rate of 6 nm min⁻¹. (b) The function $\epsilon(\lambda) = (-dS/dt)(K/SI_0(\lambda))$ (see text), obtained from curve *a* by smoothing and numerical differentiation. (c) The 77 K absorption spectrum of Figure 2-5.

provided by an excitation spectrum; the action spectrum simply monitors decay rate rather than emission intensity.

Again, we must note that the action spectrum of Figure 2-6b could result from photochemical destruction of the triplet via a rapidly equilibrating, thermally populated singlet state; however, the temperature of the experiment, 4 K, requires the singlet to be nearly degenerate with the triplet.⁹⁰ As mentioned previously, such a near degeneracy is quite improbable, and intervention of the singlet can reasonably be discounted. We accordingly conclude that the optical spectra of Figure 2-5 belong to the EPR signal carrier, triplet 1.

The nature of the electronic transition. Having established the identity of the species responsible for the electronic spectra, we can determine the oscillator strength of the transition by directly relating the intensity of the absorption spectrum to the concentration of triplet 1. Thus, a sample of 2 in an MTHF glass at 77 K was irradiated so as to produce a uniform distribution of biradical with an absorbance of 0.5 at 506 nm (path length 0.35 cm). The concentration of triplet 1 in the sample was then found to be 2×10^{-4} M by comparison of the intensity of the double-integrated EPR signal intensity of 1 with that of a standard free radical sample. Multiple measurements provided an $\epsilon(506 \text{ nm})$ of $7200 (\pm 2000) \text{ M}^{-1} \text{ cm}^{-1}$. Numerical integration of the absorption spectrum then allowed calculation of the transition oscillator strength⁹² as $f=0.022 (\pm 0.006)$. The strength of the absorption indicates that the transition is spin-allowed,⁹³ and therefore that the emission of Figure 2-5 is a fluorescence. (An estimate of the intrinsic fluorescence rate constant

k_f^o , is provided by the relation⁹² $k_f^o(\text{s}^{-1}) = 0.7 \nu_o^2 f$. For (triplet 1)* then $k_f^o = 6 \times 10^6 \text{ s}^{-1}$, corresponding to an intrinsic radiative lifetime of $\tau_f^o = 170 \text{ ns}$.)

The absorption spectrum is virtually independent of solvent (C₇D₈/3-MP (5:1), MTHF, Et₂O, Et₂O/EtOH, MeOH/EtOH (1:1)); the only significant solvent effect we have observed is a *ca.* 1.5-nm blue-shift on going from MTHF (Figure 2-5) to 1:1 MeOH/EtOH. The virtual absence of a solvent effect implies a minimal change in polarity accompanying the excitation, as one might expect for a transition confined to the π -system of planar triplet 1.

The absorption and emission spectra are clearly derived from a single electronic transition coupled to two independent vibrational modes, producing vibronic spacings $\bar{\nu}_1$ and $\bar{\nu}_2$ (Figure 2-5). The highly resolved vibrational structure in these spectra is quite consistent with the rigid structure of the biradical. The striking mirror-image relationship between the two vibronic envelopes (Figure 2-5), the prominence of the 0-0 bands, and the small (150 cm^{-1}) Stokes' shift imply nearly identical geometries for the ground and excited states. Spacing $\bar{\nu}_1$ differs slightly but detectably in the absorption and emission spectra, with values of 1520 and 1570 cm^{-1} for the excited and ground states, respectively. The value of $\bar{\nu}_2$ is measured as *ca.* 620 cm^{-1} in each. Additionally, the absorption spectrum of 1-*d*₂ is experimentally indistinguishable from that of 1, consistent with the expectation (see below) that the active vibrations do not involve the methine C – H bonds.

Assignment of the principal magnetic axes and transition moment.

Magnetophotoselection.

Additional information concerning the electronic structure of triplet 1 is potentially available if the three pairs of $\Delta m_s = 1$ EPR transitions can be assigned to the structural axes of the biradical. We have made such an assignment by (in part) the technique of magnetophotoselection (mps).⁹⁴ In addition, we have used mps to establish the polarization of the optical transition in 1.

The zero-field triplet sublevels. Biradical 1 is of sufficiently high symmetry that the principal axes of the spin-spin dipolar coupling tensor are coincident with the symmetry axes of the molecular frame, as defined in Figure 2-7a. In a rigid, random ensemble of triplet species the resonant field strength for a specific orientation depends on $3\cos^2\theta - 1$, where θ represents the angle between the applied magnetic field direction, H_0 , and one of the principal elements of the dipolar coupling tensor.⁶⁵ Due to this angular dependence, the EPR spectra of such samples are dominated by those species which have one of their principal axes aligned with or *nearly* aligned with H_0 . Thus, a large number of triplet species come into resonance at approximately the same field strength. The resulting abrupt increase in the absorption signal becomes a peak in the derivative spectrum. On the other hand, such groups of similarly-oriented triplets situated such that H_0 lies relatively far from a principal magnetic axis resonate at disparate field strengths. While these orientations contribute to the absorption, they give rise to a more gradual change in the signal intensity, and they consequently produce no

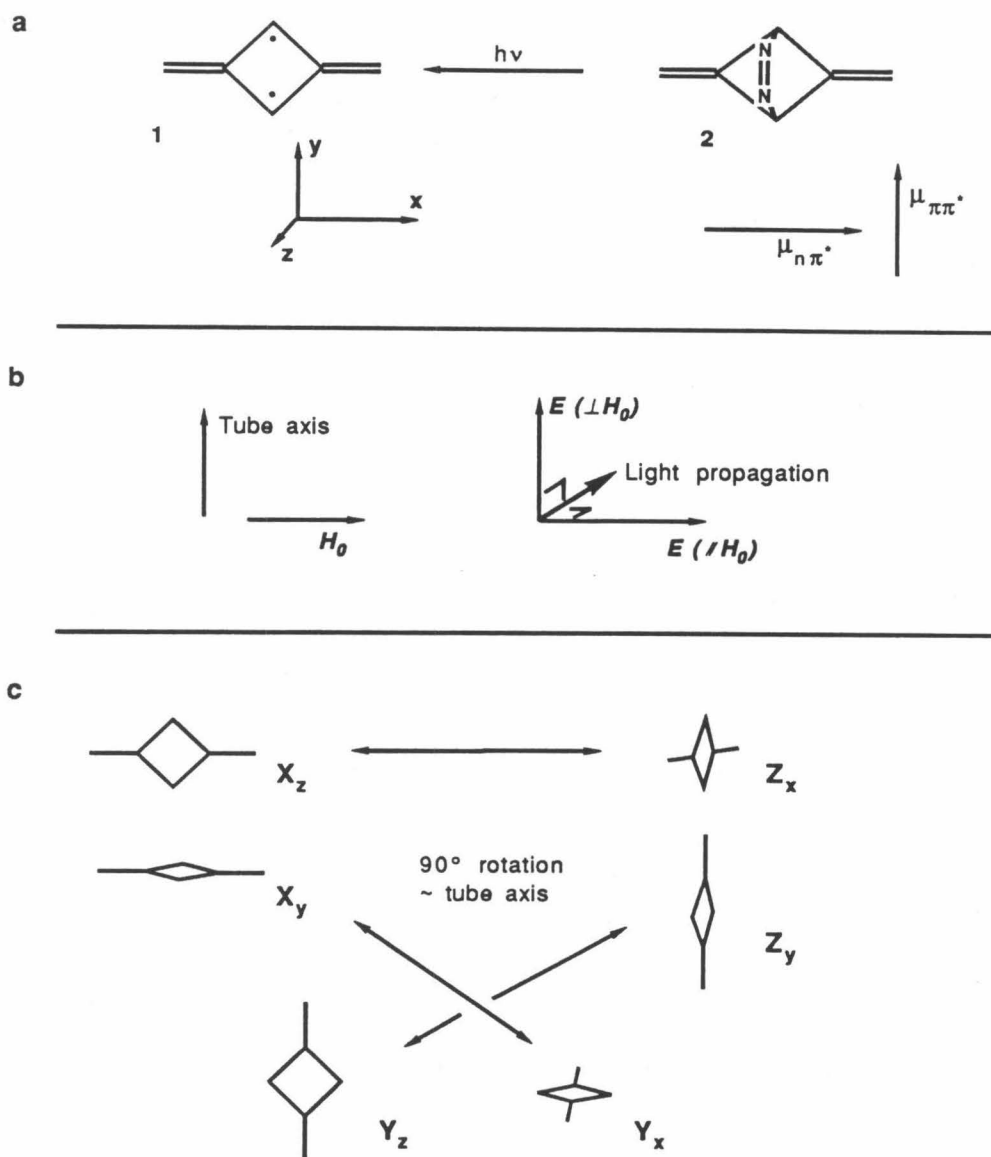


Figure 2-7. (a) The molecular axes defined for biradical 1 and the n, π^* transition dipole moment vector of the azo group of 2. (b) The orientations of the sample tube, static magnetic field, and electric vector of the incident light. (c) The six principal canonical orientations of biradical 1. The orientations are denoted by the molecular axis aligned with H_0 , with subscripts referring to the axis aligned with the incident light beam. Orientations interconverted by a 90° rotation of the sample tube are connected by arrows (rotation interchanges the primary and subscripted axis designations).

prominent feature in the derivative spectrum. Thus, each pair of lines corresponds to a group of orientations with a principal dipolar coupling axis — and for **1** also a molecular symmetry axis — approximately aligned with H_0 .

In order to relate the EPR transitions to the molecular axes, it is necessary to study the EPR spectra of triplets in known orientations. Irradiation of diazene **2** at 333 nm excites the n, π^* transition of the azo chromophore, which is polarized in the direction of the nitrogen p -orbital axes,⁹⁵ as shown in Figure 2-7a. Barring some contortionistic nitrogen extrusion mechanism, the preferred orientation of the biradical formed is then expected to be that in which its x -axis, as defined in Figure 2-7a, lies in the direction of $\mu_{n\pi^*}$ of **2**.

An isotropic distribution of **1** in a rigid medium can conveniently be thought of in terms of the six principal orientations⁹⁶ shown in Figure 2-7c. The orientations are labeled according to the molecular axis of **1** aligned with H_0 (horizontal in the laboratory frame — see Figure 2-7b), with subscripts referring to the biradical axis perpendicular to the page.

Figure 2-8a shows the EPR spectrum of an isotropic distribution of **1** generated by photolyzing a sample of **2** in an MTHF glass at 77 K. When this photolysis is conducted using a polarizer to select UV light with $E \parallel H_0$, biradical orientations X_y and X_z (Figure 2-7b) should be formed preferentially, and the EPR transitions corresponding to the x -axis should be the only ones observed. Figure 2-8b shows the spectrum generated by such a photolysis. The two inner transitions are clearly enhanced relative to the isotropic spectrum. Rotation 90° around the tube axis causes the conversions $X_y \rightarrow Y_x$ and $X_z \rightarrow Z_x$ (rotation interchanges the subscripted and primary labels). As shown in Figure 2-8c, such a rotation, which places the photochemical

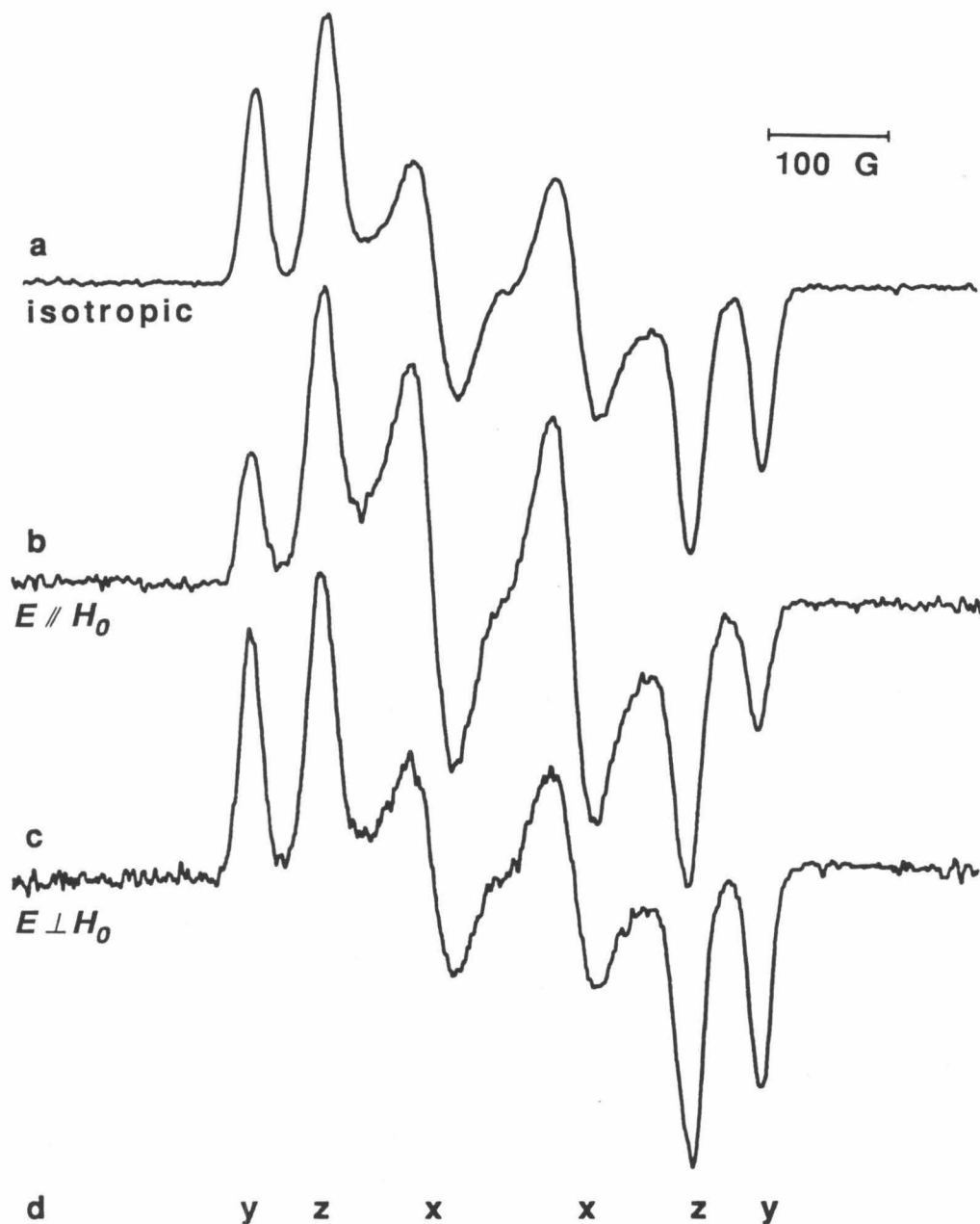


Figure 2-8. Magnetophotoselection experiment performed by irradiating a 77 K sample of **2** in an MTHF glass with linearly polarized 333 (± 4) nm light. (a) The first-derivative EPR signal of an isotropic sample of triplet **1** for comparison. (b) The spectrum observed upon irradiation with $E \parallel H_0$, and (c) the spectrum afforded by rotating the sample 90° relative to its orientation in b, to place the photochemical E imprint $\perp H_0$. (d) Assignment of the transitions in terms of the molecular axes as defined in Figure 2-7a.

imprint of E perpendicular to H_0 , does lead to substantially weakened x -lines relative to y and z . As expected, this latter spectrum is also generated by photolysis with $E \perp H_0$. We therefore assign the inner pair of transitions to the x -axis of **1**. Of course, owing to some scattering and reflection of the UV light, the polarization is not perfect, and all six transitions are present in both spectra. (It is worth noting that there is also a secondary intensity variation between the outer (y and z) peaks (*cf.* Figures 2-8b and c), which is discussed later.)

Additionally, our observation of hyperfine splitting with the isotropic pattern in the middle pair of lines, *i.e.*, the second and fifth $\Delta m_s = 1$ peaks, but none in the outer pair (see Figure 2-3) allows us to assign the middle pair to the biradical z -axis and the outer to the y . As discussed above, α -hyperfine couplings result from a combination of isotropic and anisotropic terms. For **1** the principal axes of the hyperfine coupling tensors for the two types of protons are coincident only in the z direction. Moreover, the anisotropic tensor element in this direction is very nearly zero, effectively leaving only the isotropic contribution.⁹⁷ This leads us to predict that the z -transitions should display the same isotropic splitting pattern observed in the $\Delta m_s = 2$ transition.⁹⁸ (The z -transitions of a randomly oriented sample of TMM (**4**) also display the isotropic splitting pattern for this reason.⁸⁴) The assignments of the $\Delta m_s = 1$ transitions are presented in Figure 2-8d.

Finally, we have established that the D value for **1** is negative. This determination derives from the intensity variations between the low-field and high-field members of each pair of $\Delta m_s = 1$ transitions at very low temperature.⁹⁹ One member of each pair arises from an $m_s = -1 \rightarrow 0$

transition, the other an $m_s=0 \rightarrow 1$ transition.⁶⁵ At sufficiently low temperature the Boltzmann populations of the three states are such that the former transition becomes significantly more probable than the latter.⁹⁹ On going from 77 K (Figure 2-8a) to near 4 K (Figure 2-1) the low-field y -peak and the high-field z - and x -peaks are clearly enhanced. This pattern implies that $D < 0$, the final piece of information necessary to establish the relative energies of the zero-field eigenstates of triplet 1. These are presented below in terms of the molecular axes of the biradical, along with their relationships to the zero-field splitting parameters.⁶⁵

$$\begin{array}{rcl}
 & y & \text{---} +0.0136 \text{ cm}^{-1} \\
 D \left[& & \\
 & x & \text{---} -0.0040 \\
 2E \left[& z & \text{---} -0.0096
 \end{array}$$

The electronic transition dipole moment and vibrational structure. Having assigned the $\Delta m_s = 1$ EPR transitions to the molecular axes of 1, we can exploit the photochemical lability of the biradical to determine its electronic transition moment. When an isotropic sample of 1 (Figure 2-9a) in a good optical quality MTHF glass at 77 K is irradiated with *visible* light, polarized such that $E \parallel H_0$, the spectrum of Figure 2-9b is observed.¹⁰⁰ The virtual absence of the x -transitions implies that biradicals whose x -axes had been aligned with H_0 , namely orientations X_z and X_y (Figure 2-7c), were selectively photolyzed, and accordingly that the electronic transition is x -polarized.¹⁰¹

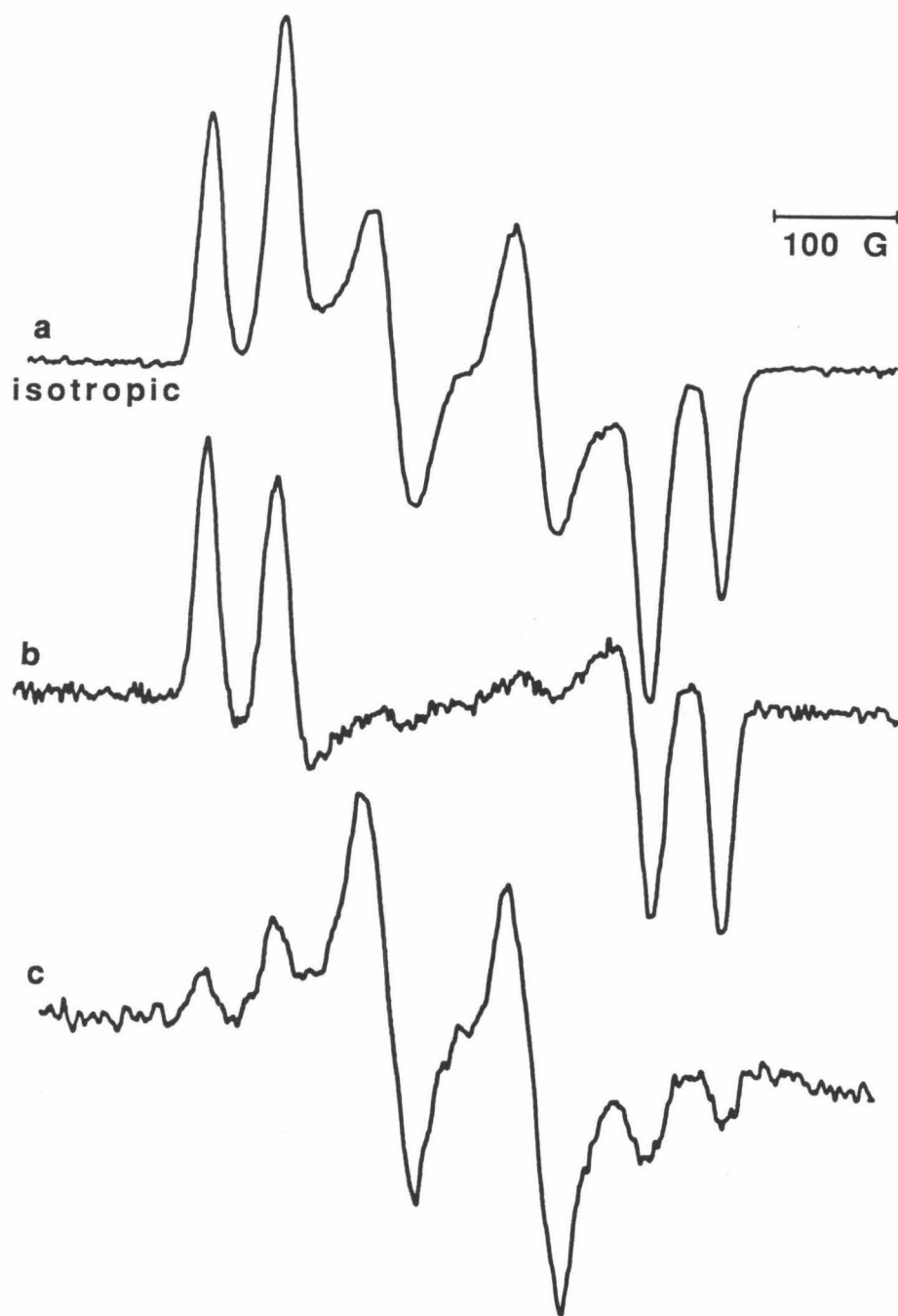


Figure 2-9. (a) The EPR spectrum of an isotropic sample of 1 (Figure 2-8a). (b) The signal produced by photolyzing such an isotropic sample with 490-nm light with $E \parallel H_0$.¹⁰⁰ (c) The signal observed after photolyzing an isotropic sample of 1 with *unpolarized* visible light ($\lambda > 485$ nm) and rotating the sample tube 90° to align the photochemical imprint of the light propagation axis with H_0 .

The spectrum of Figure 2-9b results from a significantly more anisotropic distribution of triplets than that generated by polarized UV-light photolysis of 2 (Figure 2-8b,c). This is a result of two factors: (1) scattering and the resulting depolarization is more important for shorter wavelength light,¹⁰² and (2) the nature of the present experiment, a competitive *destruction* of the different orientations (by polarized *vs* depolarized light) should produce an inherently more anisotropic distribution than the previous competitive *formation* experiment of Figure 2-8.

We have been able to assign the transition moment by a second experiment that is conceptually less obvious but perhaps more interesting than the first. Simple photolysis of an isotropic distribution of 1 with unpolarized visible light should not destroy all orientations equally.⁹⁶ This is, of course, because the **E** vector of the incident light is orthogonal to the direction of its propagation. Consequently, photolysis of an isotropic sample of 1 with unpolarized visible light should destroy all of the biradical orientations except those whose electronic transition dipole moments lie in the direction of the light propagation. Rotating the sample tube 90° then points this molecular axis of the remaining biradicals along H_0 , (see Figure 2-7b,c) and the transition moment is simply read off the EPR spectrum.

Indeed, irradiation of an isotropic sample of 1 in MTHF with low-intensity light of $\lambda > 485$ nm provides a spectrum similar to that of Figure 2-9b, consistent with orientations Z_x and Y_x (Figure 2-7c) having been spared from photolysis. Rotation of the sample tube transforms these into X_z and X_y , and the spectrum of Figure 2-9c is obtained. This confirms that the visible electronic transition of triplet 1 is polarized along the biradical *x*-axis.

(Of course, similar anisotropy should arise from direct photolysis of 2 to generate 1, although the effect should be smaller for the reasons discussed above. The effect is, in fact, observable (see **Experimental**). Thus, the isotropic spectra of Figures of 2-8a and 2-9a were obtained by rotating the sample 90° half-way through the photolysis. True isotropy would require a third photolysis along the tube axis.¹⁰³ However, depolarization effects have most likely rendered the third photolysis superfluous, and we consider the spectra of Figures 2-8a and 2-9a to be very nearly isotropic.)

Our finding that the electronic transition is *x*-polarized allows us to assign the symmetry of the excited state involved. The ground state of 1 is B_{2u} (b_{1u} × b_{3g}; see below). For the transition to be symmetry-allowed (as its oscillator strength suggests), the integral

$$\int \phi_f M \phi_i dq \quad (2-3)$$

must have a totally symmetric integrand.¹⁰⁴ Because the transition involves the *x*-component of the dipole moment operator, *M*, the excited state must be B_{1g} (B_{1g} × *M_x* × B_{2u} = A_g, since *M_x* transforms as B_{3u}).

Such an analysis in terms only of the electronic wavefunctions relies on the transition in question being symmetry-allowed. The absorption intensity observed suggests that this is the case for the transition of triplet 1. However, because the transition actually involves vibronic states, it was not entirely clear under what circumstances and to what extent the vibrational components could influence the polarization of the transition. This issue has been addressed by Albrecht,⁹⁶ and his analysis is summarized in the following discussion.

The transition moment integral is expressed in terms of vibronic wavefunctions ψ , comprising both electronic (ϕ) and vibrational (χ_1 and χ_2) parts. Thus,

$$\psi_{gij} = \phi_g(q, Q) \chi_{1i}(Q) \chi_{2j}(Q)$$

where q and Q are the electronic and nuclear coordinates, respectively. For a transition from the i, j vibrational level of the ground electronic state to the k, l level of the excited state, the transition moment, D , is given by

$$D = \int \int \psi_{ekl} M(q) \psi_{gij} dq dQ$$

or

$$D = \int \int \phi_e \chi_{1k} \chi_{2l} M(q) \phi_g \chi_{1i} \chi_{2j} dq dQ.$$

Thus, it would appear that both electronic and vibrational wavefunctions determine the polarization of a given vibronic transition. However, Albrecht has shown⁹⁶ that this integral can be separated into a symmetry-allowed term

$$D = \int \phi_e M(q) \phi_g dq \int \chi_{1k} \chi_{2l} \chi_{1i} \chi_{2j} dQ \quad (2-4)$$

— which is just the electronic transition moment mentioned above (eqn 2-3) multiplied by the Franck-Condon factor — and a series of symmetry-forbidden terms.⁹⁶ These forbidden terms are integrals that contain non-separable products of both electronic and nuclear wavefunctions. Consequently, these terms give finite intensity to transitions between electronic states that have a vanishing electronic transition moment integral by coupling them via the proper vibrational wavefunctions (e.g., the 254-nm band of benzene arises in this way¹⁰⁴). While the polarization established by the allowed term (eqn 2-4) is determined only by the symmetries of the electronic wavefunctions, the

polarizations of the forbidden terms are governed by the symmetries of the vibrational as well as the electronic wavefunctions. Albrecht has pointed out that the vibronic envelope of a symmetry-allowed transition can therefore contain mixed polarization if the forbidden terms contribute significantly.⁹⁶ Such a phenomenon could be helpful in assigning the symmetries of the active vibrations in an electronic band. We have, however, found no evidence of mixed polarization in the absorption envelope of triplet 1¹⁰¹ consistent with the allowed term (eqn 2-4) being dominant, as anticipated on the basis of the absorption strength. The transition intensity and polarization are therefore determined entirely by the electronic integral (eqn 2-3).

The relative intensities of the vibronic peaks are then established by the Franck-Condon factors

$$\int \chi_{1k} \chi_{2l} \chi_{1i} \chi_{2j} dQ.$$

The absorption (and fluorescence) arises from the ground vibrational state, so χ_{1i} and χ_{2j} are always totally symmetric.^{104,105} For the integral to have a finite value, χ_{1k} χ_{2l} must therefore also belong to the symmetric representation. The regularity of the vibrational progressions (Figure 2-5) require that both χ_{1k} and χ_{2l} be symmetric for each vibronic peak.¹⁰⁶ Wavefunction χ_{1k} , for example, is symmetric (*i.e.*, it belongs to the A_g representation of D_{2h}) for *all* values of k if its vibrational mode is A_g and for *even* values of k if its vibrational mode belongs to another representation.^{105,104} In the latter instance, the vibrational progression corresponding to this mode must arise from vibrational levels $k=0, 2, 4$, etc. The same argument applies to χ_{2l} . Thus, the observed vibronic spacings ($\bar{\nu}_1 =$

1520 cm^{-1} , $\bar{\nu}_2 = 620 \text{ cm}^{-1}$ for absorption – see above) correspond to the vibrational frequencies of the active modes if these modes are A_g and to twice their vibrational frequencies if they belong to another representation.

These assignments, of course, have implications for future matrix-isolation IR spectroscopy of triplet 1. If the 620 and 1570 cm^{-1} (ground state) spacings arise from A_g modes, they will be IR-inactive; if they arise instead from B_{1u} , B_{2u} , or B_{3u} modes, they could appear in the IR spectrum, but they would be found at 310 and 785 cm^{-1} .

Discussion.

Concerning the singlet-triplet splitting. As anticipated triplet biradical **1** has proven to be quite amenable to spectroscopic study, in some respects exceptionally so. That we have been able to observe and study triplet **1** at temperatures as low as 4 K is a consequence of the decided triplet preference, which is quite evident from all the theoretical methods that have been applied to the biradical. It is noteworthy that all our experiments are completely consistent with the expectation of a triplet ground state for **1**. Unfortunately we cannot address the magnitude of the triplet preference, even to the extent of placing a lower limit on the S–T gap. It would appear that our Curie plot might provide such information if the singlet were not far above the triplet in energy; however, these plots are extremely insensitive to thermal population of even a very low-lying singlet. Additionally, the electronic spectroscopy could have been quite informative in this regard had we been able to observe spectra attributable to singlet **1**, but again only spectra arising from the triplet ground state were observed. Having found no evidence to contradict the theoretical predictions that the S–T gap for **1** is *substantial* (i.e., several kcal mol⁻¹) we accept this idea, at least as a working hypothesis.

Spin densities and spin polarization. The determination of the relative spin densities at the ring and exocyclic positions of **1** is especially important from a theoretical standpoint. In particular, an adequate treatment of spin polarization¹⁰⁷ is critical to the calculation of the relative energies of biradical electronic states as well as their geometries.^{107,108} Spin polarization generally makes the spin densities at the radical centers of triplet biradicals

larger than those predicted on the basis of the NBMO coefficients alone. This effect operates by providing correlation of electrons in doubly-occupied MOs with those in the NBMOs. Thus, when the paired electrons are allowed to occupy different regions of space, the one whose spin is opposite that of the unpaired electrons can reduce its Coulomb repulsion with these electrons by confining itself to AOs which do not contribute to the NBMOs; the other paired electron is free to occupy the same AOs as the non-bonding electrons, since its correlation is provided by the Pauli principle. This both reinforces the spin density at the carbons on which the non-bonding electrons reside and places negative spin density on the others.¹⁰⁷

In TMM (4) such an increase in spin density at the methylene positions is apparent from the proton hyperfine splitting observed.¹⁰⁹ Similarly, the hyperfine splitting for 1 reveals the influence of spin polarization. The measured splitting constants, $a_1 = 7.3$ G and $a_2 = 5.9$ G can be related to the spin densities, ρ_1 and ρ_2 , at the ring and methylene carbons, respectively, by the relationship^{110,111}

$$a_i = \frac{1}{2} Q \rho_i$$

where Q is a proportionality constant determined from studies of free radicals.¹¹³ Thus, for 1, $\rho_1 = 0.56$ and $\rho_2 = 0.48$.^{80b} Given the difficulty in the measurement and the assumption that the observed splitting constants represent precisely the isotropic values (as well as some amount of uncertainty in the Q values used), our determination of a_1 and a_2 is certainly less accurate than similar measurements made from single crystal spectra^{114,66b} (or from fluid-media studies). We do, however, place significance on the relative spin densities derived from the measured

splittings. Specifically, spectral simulation reveals that the ratio of spin densities, $\rho_1/\rho_2 = 1.15 \pm 0.1.80b$

Figure 2-10 shows the Hückel MOs of 1. The AO coefficients of the NBMOs derived at this level of theory imply spin densities $\rho_1 = 0.6$ and $\rho_2 = 0.4$ ($\rho_1/\rho_2=1.5$) at the ring and exocyclic radical centers, respectively. It is noteworthy that the higher spin density at the ring carbons is a result of the symmetry properties of the NBMOs. This is because the antisymmetric orbital, b_{3g} , is confined by symmetry to the ring carbons, while its counterpart, $2b_{1u}$, occupies both ring and methylene positions. Our experimental spin densities are qualitatively consistent with this expectation.

However, the experimental numbers indicate that the ratio ρ_1/ρ_2 is much smaller than anticipated. This finding is consistent with qualitative spin polarization arguments. Computationally, spin polarization can be treated by augmenting a single-determinant (RHF) wavefunction with configurations that involve one-electron excitations from a bonding MO to an antibonding MO having the proper phase relationships.¹⁰⁷ In 1, the appropriate correlations of the bonding electrons are provided by $1b_{1u} \rightarrow 3b_{1u}$ and $1b_{2g} \rightarrow 2b_{2g}$ (Figure 2-10) excitations. The latter of these is by far the more energetically favorable, implying that spin polarization involving $1b_{2g}$ should be significantly more important than that involving $1b_{1u}$. Because $1b_{2g}$ has a node at the ring methines, spin polarization of the $1b_{2g}$ electron pair can increase the total spin density only at the exocyclic methylene carbons.¹¹⁵ The experimental results support this argument, as do the results of UHF calculations, which find ρ_1 and ρ_2 to be 0.70 and 0.58, respectively ($\rho_1/\rho_2 = 1.21$).^{116,117}

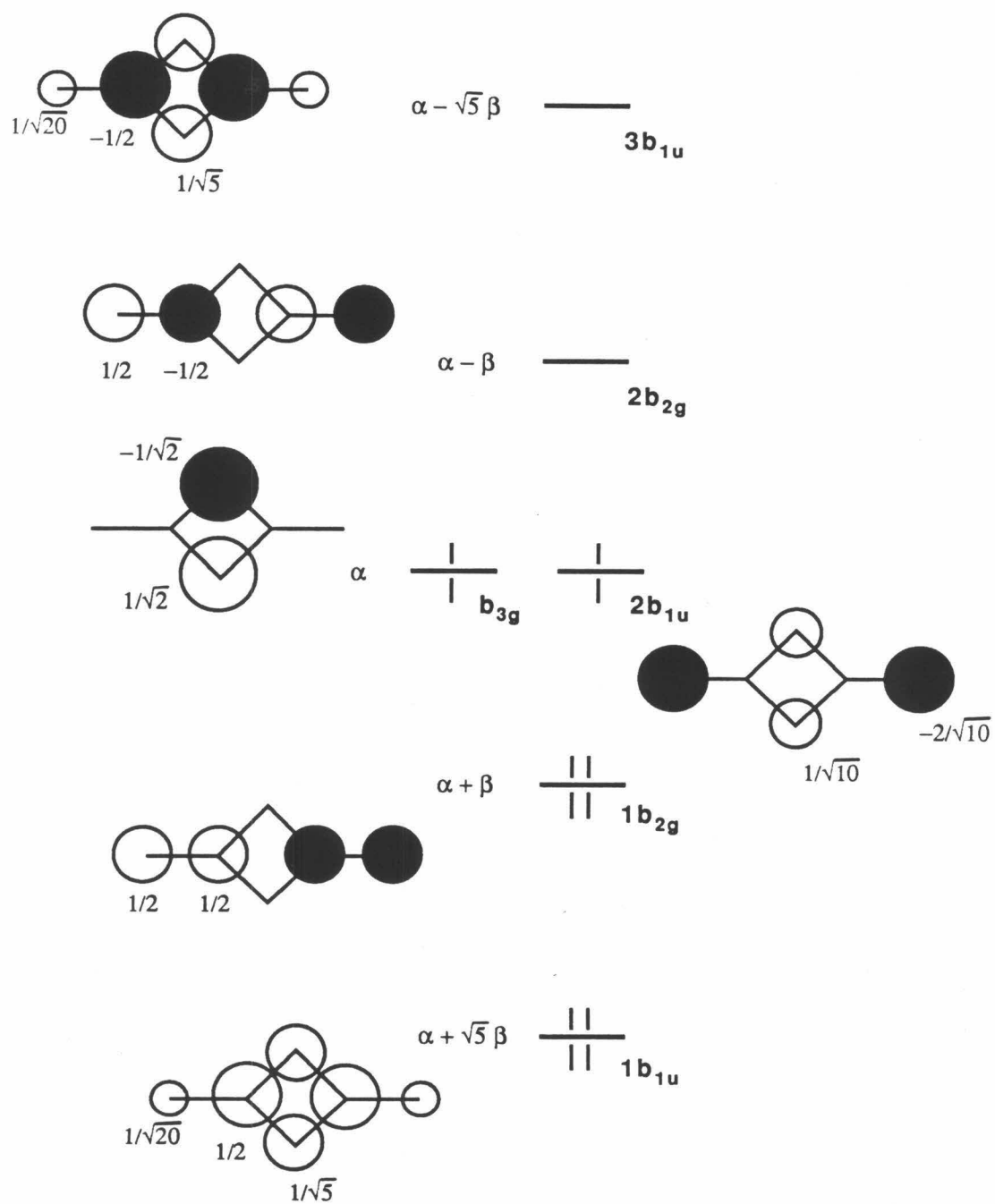


Figure 2-10. The Hückel molecular orbitals of 1,7,2c

We emphasize that because of the experimental uncertainty in our determination of spin densities we hesitate to attach quantitative significance to the individual ρ values reported. However, we believe the ratio of spin densities does have such significance and indicates a preponderant influence of spin polarization at the methylene carbons.

Zero-field splitting. Additional information concerning the electronic structure of triplet 1 is provided by our assignment of the zero-field triplet eigenstates to the symmetry axes of the biradical. However, attempting to relate this information to electronic structural features of 1 — or, more generally, of any biradical with extensively delocalized spins — in a qualitative sense is impractical. There are two primary reasons for this.

The spin-spin dipolar coupling interaction, which is responsible for the zero-field splitting, is best envisioned as the result of each unpaired electron feeling the magnetic field of the other. When the spins are localized, as in the 1,3-cyclobutanediyls,³ for example, the strongest dipolar coupling occurs along the axis connecting the spins, resulting in observed D values that show an excellent correlation with the spin densities at the radical centers.^{3a} In delocalized biradicals, on the other hand, the principal values of the dipolar coupling tensor result from several such interspin vectors oriented at various angles with respect to the principal tensor axes. This makes the principal values more difficult to attribute simply by inspection to specific features of the spin distribution.

In addition, spin polarization¹⁰⁷ (see above) plays a major role in determining the magnitude of the dipolar coupling in delocalized biradicals.⁷⁶

For example, simple Hückel (Table 2-1) or RHF⁷⁶ treatments provide a D value for TMM (4) that is approximately twice the experimental value (Table 2-1). Higher level computational methods¹¹⁸ demonstrate that an adequate treatment of spin polarization is essential for the calculation of D .⁷⁶ This is because of the large contributions made by 1,2-interactions to the dipolar coupling tensor. Spin-spin dipolar coupling displays an r^{-3} dependence, where r is the interelectronic distance. Consequently, the interactions between α and β spins on adjacent centers are magnified relative to the 1,3-interactions between α spins. For TMM the 1,2-interactions make a negative contribution to D ,⁷⁶ thereby effectively canceling a large portion of the dipolar coupling between the unpaired spins on the peripheral carbons.

Spin polarization also has a large effect on the spin-spin dipolar coupling tensor for 1. This is evident from a comparison of the experimental zero-field triplet sublevels with those calculated by using a Hückel wavefunction (Table 2-1). The energy levels of 1 are presented in Figure 2-11 along with those of TMM (4) for comparison. The calculated zero-field splitting patterns for 4 and 1 are quite similar, except that in 4 the x - and y -levels are degenerate by symmetry while in 1 these levels are strongly split. Experimentally, however, one finds that the D values for 4 and 1 have opposite signs. Moreover, for 1 the dominant interaction is in-plane (y), whereas for TMM (4) the z -axis carries the principal tensor element (Figure 2-11). While this seems to suggest that TMM is not a good reference point for 1, these dissimilarities can be attributed simply to the different effects of spin polarization in the two biradicals.

As a result of spin polarization, the experimental zero-field splitting of 4 is reduced relative to the calculated (Hückel) splitting; however, the molecular

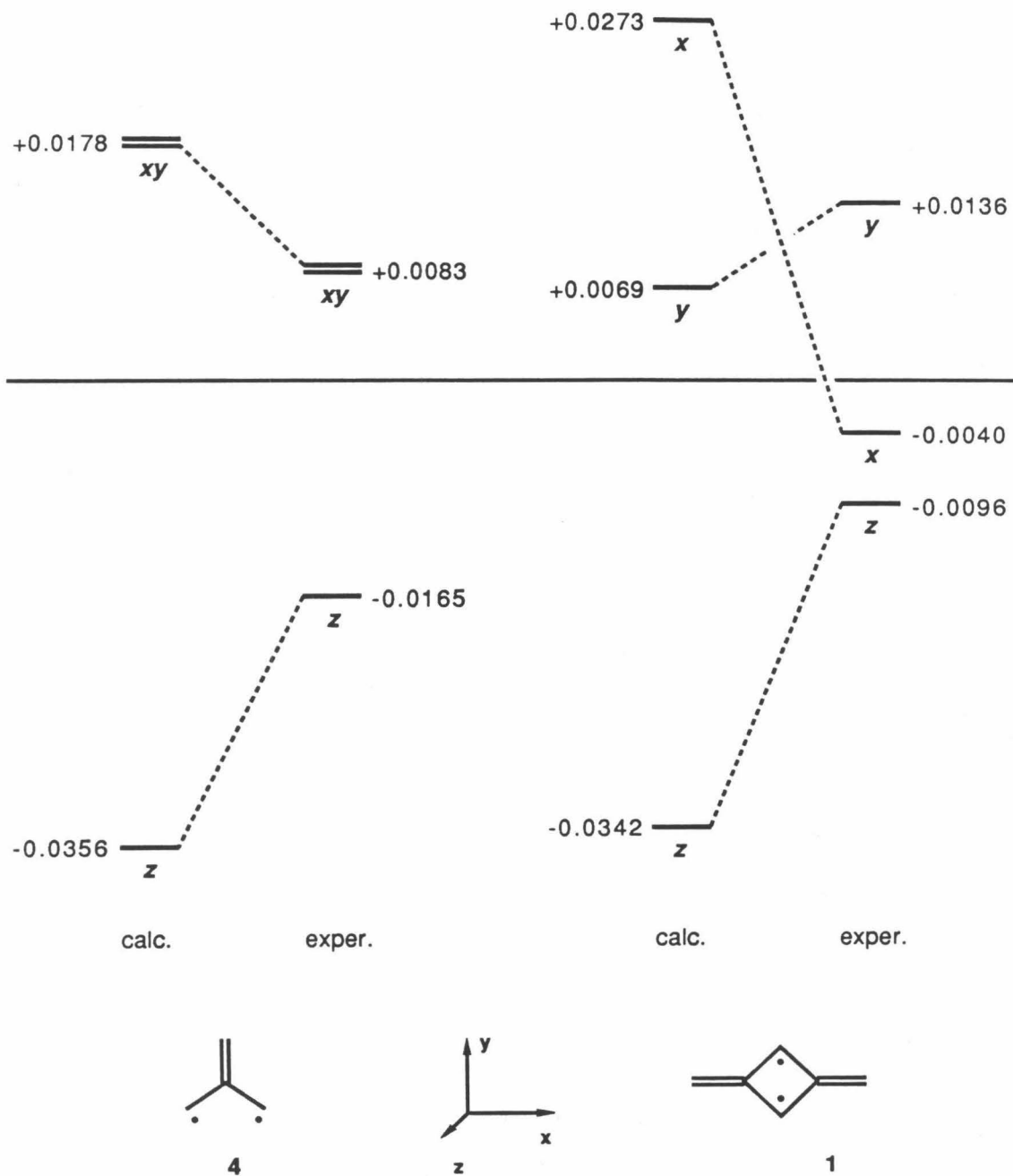
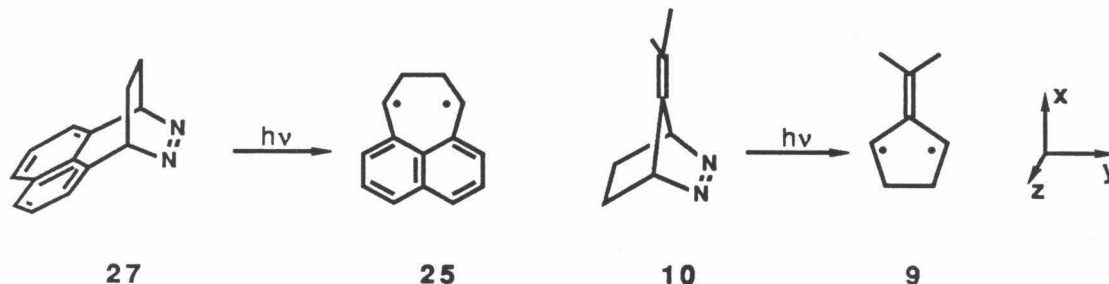


Figure 2-11. Calculated¹¹⁹ and experimental zero-field triplet sublevels for 4^{66,120} and 1 (see text) in units of cm^{-1} .

symmetry requires that the energy level pattern remain the same. For 1 this is not the case. That is, spin polarization need not influence all three calculated energy levels in the same way. Thus, while the shift of the z -level for 1 is quite similar to that of its counterpart in TMM (4), the x - and y -levels are perturbed in very different ways relative to their calculated positions (Figure 2-11). As it turns out, x drops close to z , so that the y -element becomes determinant of D . In light of this result, some amount of caution would appear to be in order when using low-level wavefunctions to predict D values for delocalized biradicals.

Magnetophotoselection. The secondary intensity variation. Two similar magnetophotoselection experiments have appeared in the literature. These involve the generation of 1,4-perinaphthadiyl (25) from diazene 27^{94b} and of TMM derivative 9 from 10.^{94a} Photolysis of diazene 10 with light



having $E // H_0$ produces an EPR spectrum for 9 whose inner pair of transitions is enhanced, just as they are in the analogous spectrum of 1 (Figure 2-8b). To facilitate comparison between 9 and 11, we will define the axes of 9 as shown above. The inner pair of transitions is then assigned to the biradical x -axis on the basis of the known transition dipole moment of the azo group.¹²¹ Interestingly, this system displays a secondary intensity variation between

the z - and y -transitions^{94a} completely analogous to that observed in our system (Figure 2-8). (The **27-25** system does not display such an effect because the E value for **25** is close to zero and its EPR spectrum consequently has only four resolved lines.^{94b})

The analysis of the major intensity change presented above for **1** indicates that, upon going from the $E // H_0$ to the $E \perp H_0$ sample orientation, the assembly $X_y + X_z$ is transformed to $Y_x + Z_x$. Thus, the y - and z -transitions should respond in the same way. However, the $E // H_0$ spectrum of each biradical displays slightly enhanced z -lines; the $E \perp H_0$ spectrum, slightly enhanced y -lines (Figure 2-8, ref. 94a¹²¹). Because the order of the y - and z -lines is reversed for the two biradicals, upon going from $E // H_0$ to $E \perp H_0$ the secondary enhancement shifts from the middle (z) to the outer (y) pair of lines for **1** (Figure 2-8), but from the outer (z) to the middle (y) pair for **9**.^{94a} This establishes that the phenomenon is not simply an artifact of spectral shape changes caused by the primary intensity variation in the inner pair of lines. Rather, the effect must arise from the actual distribution of biradicals produced. Since identifying the source of the effect could provide a method for assigning the $\Delta m_s = 1$ transitions in related systems, or at least a better understanding of the mps experiment, we have considered two possible explanations for it.

Following El-Sayed's analysis of similar secondary intensity variations in EPR spectra of photoexcited aromatic hydrocarbons,^{94d} a mixture of electronic transitions with mutually perpendicular polarizations could be involved. The most obvious candidate for the second excitation in **2** and **10** is the azo group π, π^* , whose transition dipole moment lies along the N—N bond¹²³ (Figure 2-

7a). Excitation of the π, π^* transition of **2** with light of $E // H_0$ should produce biradicals **1** in orientations Y_x and Y_z (Figure 2-7c). If the n, π^* transition contains a component of π, π^* character, the ensemble produced should contain a fraction λ of biradicals in these orientations. The ensemble can then be described as $X_z + X_y + \lambda(Y_z + Y_x)$; rotation of the sample tube transforms this into $Z_x + Y_x + \lambda(Z_y + X_y)$. The secondary intensity variation between the z - and y -transitions would thus arise from $2\lambda Y$ orientations being replaced by λZ . The change observed on going from Figure 2-8b to 2-8c, however, implies exactly the opposite, that is $Z \rightarrow Y$. (The corresponding analysis for the 10-9 system provides the same result.)

The experimental spectra require the second transition to be polarized perpendicular to both the azo $\mu_{n\pi^*}$ and $\mu_{\pi\pi^*}$ vectors (Figure 2-7a). A component dipole moment in this direction would provide $X_z + X_y + \lambda(Z_x + Z_y)$, which rotates to $Z_x + Y_x + \lambda(X_z + Y_z)$, so that $2\lambda Z$ orientations are replaced by λY , consistent with the spectral changes observed. (Again the corresponding analysis holds for the 10-9 system.) However, no transition localized to the azo group n - and π -orbitals can have such a dipole moment. Transitions involving the C—C π -bonds of **2** can carry the required polarization,¹²⁴ though, and one or more of these might admix with the azo n, π^* transition of **2** to produce the observed effect. This explanation is not completely satisfactory, however. Such a mixing of transitions should alter the energy of the azo UV absorption, yet both **2** and **46** (the parent bicyclo[2.1.1]diazene) display the same UV transition energy. Furthermore, diazene **10** appears to have no comparable mechanism for generating the required assembly of biradicals **9**. Although **10** has several potential transitions involving its C—C

double bond that lie in the molecule's mirror plane, none of these appears to have a dipole moment directed along or nearly along what will become the *z*-axis of biradical **9**.

An alternative explanation is a reorientation effect in the nitrogen extrusion step. This would operate by allowing some *Z* orientations, in addition to the *X*, to be produced upon *E* // *H*₀ photolysis of diazene molecules lying, for example, as depicted in Figure 2-7a. Upon loss of N₂, one of the olefinic groups would move into the position formerly occupied by the departing nitrogen. This appears more favorable than the alternative reorientation, which would rotate the hydrocarbon portion of the Figure 2-7a diazene 90° in the plane of the page to generate *Y* orientations. Thus, photolysis of **2** with light of *E* // *H*₀ would produce a biradical assembly $X_y + X_z + \lambda(Z_x + Z_y)$, and the analysis would be just as discussed above. This explanation also holds for the 10-9 system. Biradical **9** would swing either its isopropylidene group or its ethano bridge into the space that had been occupied by the azo group.



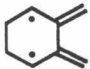
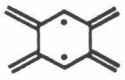
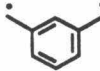


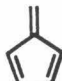



Electronic spectroscopy. The electronic transition energy of triplet **1** (506 nm; 56.5 kcal mol⁻¹) would, at first glance, appear exceptionally low for a molecule with a 6-carbon π -system. However, **1** has a pair of NBMOs, which its fully covalent relatives lack. That its transition occurs at a substantially longer wavelength than the transitions of benzene, fulvene, and 1,2-dimethylenecyclobutene (Table 2-2) is therefore not surprising. In fact, Table 2-2 shows that the triplet-triplet transitions of several non-Kekulé hydrocarbons occur at relatively long wavelengths. It is also worth noting

that the transition displayed by triplet 1 is of considerably longer wavelength than the first moderately strong transition of TMM derivative 9 and of allyl and pentadienyl radicals (Table 2-2), all structures that are formally embedded in the π -system of 1.

The energy, oscillator strength, and polarization of the T-T transition of 1 are all in excellent agreement with the results of PPP-SCF-SCI calculations performed in our laboratory, which find a ${}^3B_{2u} \rightarrow {}^3B_{1g}$ transition at 501-504 nm ($f = 0.01$ - 0.02).¹³⁶ These calculations indicate that the transition involves a combination of $1b_{2g} \rightarrow 2b_{1u}$ and $2b_{1u} \rightarrow 2b_{2g}$ (Figure 2-10) one-electron excitations.¹³⁶ Thus, the excited state is described as $(1/\sqrt{2})[(1b_{1u})^2(1b_{2g})^1(2b_{1u})^2(b_{3g})^1 + (1b_{1u})^2(1b_{2g})^2(b_{3g})^1(2b_{2g})^1]$. The relatively low oscillator strength results from the parity-forbidden nature of the transition.^{126,136}

Given these changes in orbital occupancy we can tentatively assign the vibrations responsible for the double vibronic progression observed (Figure 2-5). The active vibrations generally correspond to the most important geometrical changes induced by the electronic transition.¹³⁷ Qualitative molecular orbital considerations can therefore provide insight into the nature of the vibrations involved. It is reasonable to assume that the active vibrational modes for 1 are confined to the carbon framework, since the C-H bonds lie in the nodal plane of the biradical's π -system. Thus, excitations in the π -system will only directly affect the C-C π -interactions. Our observation of identical absorption spectra for 1 and 1- d_2 is consistent with this idea. The carbon framework has a total of $3n - 6 = 12$ vibrational modes

Table 2-2. Absorption data for triplet non-Kekulé hydrocarbons and C₆H₆ Kekulé hydrocarbons.

	λ^a (ϵ^b) (λ_{\max} (ϵ^b))		Ref.
 1	506 (7200)	MTHF, 77 K	This work
 9	322 (~150) 299 (~250)	EPAc, 79 K	125
 36	480 (900) 427 (2400)	Ar, 10 K; EPAc, 77 K	127
 37	600 (~400) 475 (strong)	Ar, 15 K	128
 12	440 ^d	<i>n</i> -pentane, 77 K	129
	499 (100) 341 (52000)	EPAc, 77 K	130
	263 ^e 254 (200)	gas phase	131
	362 (214) 258 (3980) 243 (12600)	cyclohexane	132
	248 (20000) 212 (100000)	isooctane	133
	409 (weak) 213, 220 (strong) (258 nm) ^f	Ar, 10 K	134
	(285 nm) ^f		

^ain nm. The wavelength of the lowest-energy vibronic band is given. λ_{\max} is included (indented) only if it is different from λ . All the transitions are presumably spin-allowed. ^bM⁻¹cm⁻¹. ^cEt₂O/isopentane/EtOH (5:5:2). ^dfluorescence. ^enot observed. ^fthe wavelengths of absorptions ascribed to allyl and pentadienyl radicals in irradiated polyethylene.¹³⁵

(3 A_g , 2 B_{1g} , 1 B_{2g} , 2 B_{1u} , 2 B_{2u} , and 2 B_{3u}); however, only a few of these appear especially likely to couple with the transition.

Referring to the MO diagram of Figure 2-10, we see that the excitation component $1b_{2g} \rightarrow 2b_{1u}$ (see above) depopulates an olefinic π -orbital, while the component $2b_{1u} \rightarrow 2b_{2g}$ populates the corresponding π^* -orbital. Thus, the excitation should lengthen the bonds to the exocyclic methylene groups, and the corresponding stretching vibration should be activated. We tentatively assign the larger vibrational frequency to such an A_g C—C "double bond" stretching mode. Consistent with the weakening of these bonds in the excited state is the observation of a lower vibrational frequency in the absorption spectrum (1520 cm^{-1}) than in the fluorescence (1570 cm^{-1}). Additionally, because the transition involves an orbital that is bonding across the four-membered ring ($2b_{1u}$), one might expect a ring breathing-type mode to be activated. The set of A_g modes contains two such vibrations, and the 620 cm^{-1} spacing may well correspond to one of these.

Conclusion.

Triplet 1 has turned out to be especially cooperative toward a thorough spectroscopic investigation, even as delocalized biradicals go. Our EPR studies have led to a complete determination of the energies of the zero-field triplet eigenstates in terms of the molecular axes of 1 as well as the relative spin densities at the biradical's methylene and methine carbons. Our finding that triplet 1 has a strong electronic transition and our ability to determine the nature of the excited state involved has been somewhat of an unexpected bonus.

Because the biradical is a small, high-symmetry hydrocarbon that has no heavy-atom substituents, and a wealth of experimental data is now available, triplet 1 is a prime candidate for a detailed theoretical study. In addition, its strong absorption and intense fluorescence should facilitate flash spectroscopic studies of the triplet biradical.

Experimental

General and routine instrumentation.

Reagents were obtained commercially and used without purification unless otherwise noted. THF and MTHF were distilled from sodium benzophenone ketyl immediately before use. Other solvents used in synthetic procedures were reagent grade; those used for EPR and optical spectroscopic studies were "spectro" grade or "gold label." Glassware was base-washed (KOH/EtOH), especially prior to use for reactions involving bicyclobutanes.

Flash chromatography¹³⁸ employed 230-400 mesh silica (EM Science, "silica gel 60"). Large columns were slurry-packed and all others were dry-packed, typically in petroleum ether, then switched to the elution solvent system.

Preparative-scale photolyses were conducted with a pyrex-shrouded Hanovia 450-Watt medium-pressure Hg arc lamp in a water-jacketted immersion well.

NMR spectra were recorded on JEOL FX-90Q or GX-400 spectrometers. ¹H and ¹³C chemical shifts were determined relative to TMS by using the solvent signal as reference. Low-temperature NMR experiments were performed on the 400 MHz instrument and are discussed in more detail in Chapter 3.

IR spectra were measured on a Perkin-Elmer 1310 spectrometer.

Melting points were obtained with the aid of a Thomas-Hoover capillary melting point apparatus and are corrected. Combustion analyses and mass spectra were obtained by the Caltech analytical facility or the U.C. Riverside Mass Spectrometry Lab.

EPR experiments, optical spectroscopy, and photolyses at 77K were conducted by immersing the sample in a liquid N₂-filled quartz finger dewar.

Spectroscopic samples. Sample tubes for spectroscopic studies were Wilmad Glass 701-PQ 5-mm o.d. medium-walled quartz tubes. These were fitted via ground glass joints to high vacuum stopcocks from which they could be conveniently detached with an oxygen-gas flame for use in NMR studies. The inside diameter (i.d.) of these tubes was determined (by measuring the height of a known volume of solvent) to be 0.35-0.36 cm, in accord with the manufacturer's specification. Quartz tubes of 4-mm o.d. were used for EPR studies employing the Oxford cryostat (see below).

The tubes were cleaned by treatment with 5% HF followed by KOH/MeOH (several hours each). After rinsing for several minutes with flowing water, then with acetone, CH₂Cl₂, and finally MeOH the tubes were evacuated to remove the last traces of solvent and pressurized with dry N₂.

Diazene samples were degassed in subdued light on a vacuum line capable of maintaining *ca.* 10⁻³ mm. The samples were alternately frozen in liq. N₂, evacuated, and thawed carefully by lightly stroking the tube to initiate melting of the solvent, then immersing the sample in a CO₂/acetone bath. Three such cycles proved sufficient for the experiments described here. The samples were stored in the dark at 77K or at -100 °C before use.

Photolysis. Cryogenic samples were irradiated with light from an Oriel 1000-Watt "ozone-free" Hg(Xe) or Xe arc lamp (operated at 950-980 Watts) mounted in a (model no. 66023) housing equipped with an *f*/0.7 quartz lens

assembly and water filter. The light was directed through a series of filter glasses in a water-filled chamber and focussed onto the sample. The filter combinations used and their transmittance ranges are listed in Table 2-3.

Table 2-3. Transmittance data for filter combinations.

No.	Filters ^a	Transmittance range ^b	λ_{\max} (Trans)
1	(WG-305)/KG-5/UG-11	$306 < \lambda < 386 \text{ nm}$	355 nm (0.35)
2	#1 + 334 int ^c	$326 < \lambda < 342 \text{ nm}$	335 nm (0.08)
3	WG-305/KG-5/GG-495/NG-4	$485 < \lambda < ca. 775 \text{ nm}^d$	550 nm (0.012)

^a obtained from Schott (3 mm thickness). ^b cutoff values defined as 1% transmittance. ^c 334-nm interference filter obtained from Oriel. ^d cutoff values are defined as 0.1% transmittance for this combination.

Alternatively, the light was focussed onto the entrance slit of an Oriel model 77250 monochromator equipped with a 200-nm-blaze holographic grating and calibrated against the Hg spectral lines.

The Xe lamp output was measured accurately in the wavelength region of interest at 2-3-nm resolution by focussing the monochromator output onto an Oriel model 7104 spectrally neutral 5-mm-diameter thermopile detector.

EPR experiments. Spectra were recorded on a Varian E-line Century Series X-band EPR spectrometer with a TE₁₀₂ cavity ($H_1 \perp H_0$), one end of which consisted of a *ca.* 50%-transmitting photolysis grating. The recorder was interfaced with a Compaq Plus PC, and the digitized data were analyzed with the aid of a double-integration routine¹³⁹ or other programs as required.

Temperatures of 4-80 K were achieved with an Oxford Instruments ESR-900 Continuous Flow Cryostat with liquid helium as the cryogen. Briefly, the helium is drawn through the system by a moderate vacuum, and temperatures above 4 K are obtained by some combination of: (1) restricting the liquid helium flow where it first enters the transfer line, (2) reducing the flow through the vacuum pump, or (3) engaging a heater located just below the sample region. The temperature of the helium stream is monitored continuously by an Au+0.03% Fe *vs* chromel thermocouple located 1 cm below the EPR cavity and controlled by an Oxford model 3120 temperature controller, which allows manual adjustment of the heater power or uses P.I.D. control of the heater to provide a preset thermocouple temperature. We have found, however, that engaging the heater heats the thermocouple junction directly, so that the sample temperature calibration (see below) and the EPR measurements must be conducted with precisely the same heater power. For this reason, we elected to perform the variable temperature experiment (Curie plot) described below with the heater off and the temperature adjustment at the transfer line needle valve only. The consequences of this procedure are discussed under the heading of that experiment.

The sample temperature was measured with a Lake Shore Cryotronics CGR-1-1000 carbon glass resistance sensor. This was immersed in ethylene glycol in a sample tube essentially identical to that used for the EPR measurements and connected via 36-gauge phosphor-bronze leads to a variable μ A current source and a voltmeter. The sensor had been calibrated by the manufacturer against temperature standards at 80 points, which were used to generate resistance *vs* temperature data at 0.2° intervals from 4 to 100 K and

at 2.0° intervals from 100 to 300 K. We found the sensor assembly to provide accurate readings at the boiling points of nitrogen and helium, demonstrating that neither external heat conduction nor heat generated by the applied current compromised the accuracy of the measurement. In this vein we note that our original publication of the spectrum of Figure 2-1 reported an incorrect temperature of 10 K.⁷ This was measured with a primitive thermocouple whose leads evidently conducted more heat to the junction than could be removed by the Air Products Helitrans system in use at the time. We subsequently measured the temperature under similar conditions with the carbon glass resistor and found it to be 5-6 K. We have since obtained spectra essentially identical to that in Figure 2-1 many times with the Oxford system and at temperatures as low as 3.8 K. (We also note that the spectrum of Figure 2-1 was generated by irradiating the sample in only one orientation. However, MTHF glasses stress-fracture at liquid helium temperatures, so that the samples are probably of insufficient optical quality to provide orientationally-enriched samples of 1. This effect is discussed below under the heading "Magnetophotoselection.")

UV-vis absorption spectroscopy. UV-vis spectra were recorded with a Hewlett-Packard 8451A Diode Array Spectrophotometer with a deuterium source and equipped with an HP 85A microcomputer capable of manipulating spectral data according to BASIC instructions. The spectral range was calibrated using the characteristic absorption peaks of a holmium oxide filter, and the λ values reported have been corrected accordingly. Spectra of cryogenic samples in quartz tubes were recorded with air as the reference and

with a single 0.1-sec measurement. Quantitative absorbance values reported were derived from several such measurements. The nominal resolution of the instrument, dictated by the spacing of the diodes, is 2 nm; however, visual interpolation usually allowed reproducible resolution of the maxima for the sharp peaks of Figure 2-5 to better than 0.5 nm with at most ± 0.5 nm uncertainty in their absolute positions.

***Endo,endo*-2,4-bis(hydroxymethyl)bicyclo[1.1.0]butane (48).** A variation of Christl's procedure was developed before his experimental details became available.^{14a} A solution of benzvalene¹⁴⁰ (ca. 13.3 g, 0.171 mol) in 400 ml of ca. 3:1 ether/hexane (similar results have been obtained in ether only) was cooled to -78°C . With magnetic stirring, a stream of O_3 in oxygen (Welsbach ozone generator set to deliver ca. $0.8\text{ mmol O}_3\text{ min}^{-1}$) was bubbled into the solution for 270 min (0.216 mol). The remaining ozone was purged with a stream of N_2 , and the solvent was removed by rotary evaporation as the ozonide mixture warmed to room temperature. When the ozonide approached dryness¹⁴¹ ca. 50 ml of dry THF was added and rotary evaporation continued until ca. 20 ml of solvent remained. The yellow residue was dissolved in 400 ml of THF.

A 5-l three-necked round-bottomed flask was fitted with a gas-tight mechanical stirrer, a thermometer, and a pressure-equalizing addition funnel topped with a gas inlet. The apparatus was dried with a flame under aspirator vacuum, pressurized with N_2 , and cooled. Into the flask were placed 40.0 g (1.05 mol) of LiAlH_4 and 4 l of dry THF. Under a nitrogen atmosphere the slurry was cooled to -35°C with a large-capacity CO_2/iPrOH (-78°C) bath,

and the ozonide solution was placed in the addition funnel. With vigorous stirring this solution was added dropwise over 65 min while the slurry temperature was kept at -35 ± 1 °C. The mixture was then stirred at -35 °C for 60 min and at -31 °C for 30 min before cautious *n,n,3n* work-up¹⁴² below -30 °C. Thus, addition of the first 40 ml of water required 2.5 hours; the following 40 ml of 3 N aq. NaOH and 120 ml of H₂O were introduced over 30 min. The mixture was held at -35 – -40 °C for another hour, allowed to warm slowly, and stirred at room temperature overnight. The yellow mixture was dried over Na₂SO₄, the solids were removed by suction filtration and washed liberally with THF, and the solvent was removed under vacuum to afford 11.3 g of an orange syrup, which by ¹H NMR consisted of 9.9 g (51%) of **48**,¹⁴ the remainder being hemiacetal¹⁴ impurity. Typical (smaller scale) yields were *ca.* 55%. The product was carried forward without purification.

Endo,endo-2,4-bis(*t*-butyldimethylsiloxymethyl)bicyclo[1.1.0]butane (49). The crude diol **48** (9.9 g, 87 mmol) and 33.4 g (491 mmol) of imidazole were dissolved in 1 l of CH₂Cl₂, and 32.5 g (216 mmol) of *t*-butyldimethylsilyl chloride was added.¹⁴³ The reaction was allowed to continue for 100 min at room temperature with magnetic stirring under a CaCl₂ drying tube. The CH₂Cl₂ solution was washed with water (4 x 300 ml) and brine (75 ml), dried (Na₂SO₄), and concentrated under vacuum to afford 35.5 g of clear, amber liquid. By ¹H NMR, the product consisted of *ca.* 25 g (85%) of **49**: ¹H NMR (400 MHz, CDCl₃) δ 3.55 (d, *J* = 6.1 Hz, 4 H, CH₂), 2.70 (m, 2 H, H-2,4), 1.56 (t, *J* = 3.8 Hz, 2 H, H-1,3), 0.86 (s, 18 H, *t*-Bu), 0.02 (s, 12 H, SiMe₂); ¹³C NMR (22.6 MHz, CDCl₃) δ 65.0 (t, CH₂), 56.1 (d, C-2,4), 26.0 (q, *t*Bu), 18.3 (s, *t*Bu),

11.9 (d, C-1,3), -4.9 (q, SiMe₂). Again, we find it more convenient to carry this material forward without purification; the major contaminant, *t*BuMe₂SiOH, is conveniently removed at a later step.

(1 α , 2 α , 3 β , 4 α)-1,3-dibromo-2,4-di(hydroxymethyl)cyclobutane. A cold (0 °C) solution of dibromide 51 in CCl₄ (ca. 150 ml) was prepared from benzvalene¹⁴⁰ (10.55 g, 135 mmol) by the procedure of Roth and Katz¹⁸ and found to have a clean ¹H NMR spectrum identical to that reported.¹⁸ This solution was immediately diluted with 600 ml of -60 °C CH₂Cl₂, and cooled to -78 °C. With magnetic stirring a stream of O₃ in oxygen (ca. 0.8 mmol O₃ min⁻¹) was bubbled into the solution for 190 min (152 mmol). The excess ozone was purged from the blue solution with N₂. The solvent was removed by rotary evaporation as the solution warmed, and the solid ozonide was dissolved in 450 ml of dry THF.

In a dry 2-l three-necked round-bottomed flask bearing a gas-tight mechanical stirrer, a pressure-equalizing addition funnel, and an N₂ inlet-topped ice water condensor, were placed 10.25 g (270 mmol) of LiAlH₄ and 1 l of anhydrous ether. The yellow ozonide solution was filtered and placed in the addition funnel, and the atmosphere in the apparatus was replaced with N₂. The solution was added dropwise with efficient stirring at such a rate as to maintain a brisk reflux (ca. 90 min), and heat was applied to sustain reflux for another 30 min. The reaction was quenched by the *n,n,3n* technique,¹⁴² and the mixture was dried over Na₂SO₄ and filtered. The solvent was removed by rotary evaporation and the oily orange solid triturated with CHCl₃ and air-dried. Recrystallization of the off-white title compound (15.5 g, 42% from

benzvalene) from acetone afforded a white solid: *mp* 138-139 °C; ^1H NMR (400 MHz, acetone- d_6) δ 4.97 (t, $J=7.3$ Hz, 1 H, H-3 144), 4.00 (t, $J=9.2$ Hz, 1 H, H-1 144), 3.77 (dd, $J=11.2$ Hz, 8.3 Hz, 2 H, CH $_2$), 3.68 (dd, $J=11.2$, 5.1 Hz, 4 H, CH $_2$), 2.95 (br m, 4 H, H-2, 4 + OH (D $_2$ O-exchangeable)); ^{13}C NMR (22.6 MHz, acetone- d_6) δ 62.2, 53.5, 52.1, 43.7; MS (EI) m/e (relative intensity) 272, 274, 276 (9, 18, 10; M^+), 241, 243, 245 (6, 9, 5; $\text{M}^+ - \text{CH}_3\text{O}$), 211, 213, 215 (15, 26, 13; $\text{M}^+ - \text{C}_2\text{H}_5\text{O}_2$), 193, 195 (39, 36; $\text{M}^+ - \text{Br}$), 175, 177 (98, 95; $\text{M}^+ - \text{Br}$, H $_2\text{O}$), 145, 147 (91, 100; $\text{M}^+ - \text{Br}$, H $_2\text{O}$, CH $_2\text{O}$); Anal. Calc'd for C $_6$ H $_{10}$ O $_2$ Br $_2$: C, 26.31%; H, 3.68%. Found: C, 26.74%; H, 3.68%.

(1 α , 2 α , 3 β , 4 α)-1,3-dibromo-2,4-di(*t*-butyldimethylsiloxymethyl)cyclobutane. To the dibromodi(hydroxymethyl)cyclobutane (1.00 g, 3.65 mmol), 1.25 g (18.4 mmol) of imidazole, and 200 ml of CH $_2$ Cl $_2$ was added 1.20 g (7.96 mmol) of *t*-butyldimethylsilyl chloride, 143 and the mixture was stirred magnetically under a CaCl $_2$ drying tube at room temperature for 20 hrs. The CH $_2$ Cl $_2$ solution was washed with water (3 x 30 ml) and brine (10 ml), dried (Na $_2$ SO $_4$), filtered through a pad of silica, and concentrated by rotary evaporation. Heating at 70 °C under vacuum for *ca.* 1 hr to remove *t*BuMe $_2$ SiOH afforded 1.65 g (90%) of the title compound as a colorless liquid: ^1H NMR (400 MHz, CDCl $_3$) δ 4.78 (t, $J=7.2$ Hz, 1 H, H-3 144), 3.86 (t, $J=9.2$ Hz, 1 H, H-1 144), 3.79 (dd, $J=10.5$, 8.1 Hz, 2 H, CH $_2$), 3.74 (dd, $J=10.5$, 5.4 Hz, 2 H, CH $_2$), 2.87 (m, 2 H, H-2,4), 0.88 (s, 18 H, *t*Bu), 0.06 (s, 12 H, SiMe $_2$).

Exo,exo-2,4-bis(*t*-butyldimethylsiloxymethyl)bicyclo[1.1.0]butane (50). To a well-stirred solution of 5.05 g (10.1 mmol) of the

dibromodi(siloxymethyl)cyclobutane in 350 ml of anhydrous ether at -78°C under Ar, was added a 2.15 M solution of *t*BuLi in pentane (11.8 ml, 25.4 mmol)¹⁹ via syringe over 4 min. After 3.5 hrs the reaction was quenched by addition of 2.0 ml of water, and the mixture was allowed to warm to room temperature. The solution was washed with water (3 x 100 ml), dried (Na_2SO_4), and concentrated under vacuum to afford 3.46 g of a clear, colorless liquid. By ^1H NMR analysis this product is typically found to contain 50-65% of **50**: ^1H NMR (400 MHz, CDCl_3) δ 3.54 (d, $J=5.1$ Hz, 4 H, CH_2), 1.40 (s, 2 H, H-1,3), 1.15 (t, $J=4.9$ Hz, 2 H, H-2,4), 0.88 (s, 18 H, *t*Bu), 0.04 (s, 12 H, SiMe_2); ^{13}C NMR (100 MHz, CDCl_3) δ 62.3 (t, CH_2), 43.1 (d, C-2,4), 26.0 (q, *t*Bu), 18.4 (s, *t*Bu), 3.3 (d, C-1,3), -5.3 (q, SiMe_2). In addition, ^1H NMR revealed the presence of *ca.* 2-3% of **49**. The remainder of the material was a reaction byproduct tentatively assigned as (1 α , 2 α , 4 α)-1-bromo-2,4-di-(*t*-butyldimethylsiloxymethyl)cyclobutane: ^1H NMR (400 MHz, CDCl_3) δ 4.10 (t, $J=8.4$ Hz, 1 H, H-1), 3.55 (AB-quartet of d, $J=11.0$ Hz (geminal), 4.6 Hz (downfield member), 5.9 Hz (upfield member), $\Delta\nu = \text{ca. } 40$ Hz, 4H, CH_2), 2.57 (m, 9 lines, *ca.* 4-5 Hz separation, 2 H, H-2,4), 2.01 (pseudo-q, $J = \text{ca. } 10$ Hz, 1 H, H-3), 1.68 (pseudo-q, $J = \text{ca. } 10$ Hz, 1 H, H-3). A decoupling experiment supported the peak assignments.

4-Methyl-1,2,4-triazoline-3,5-dione (MTAD). 4-Methylurazole, prepared by literature methods¹⁴⁵ or obtained commercially, was oxidized with N_2O_4 .¹⁴⁶ A typical reaction provided 35 g of MTAD as a red solid which was dried briefly under vacuum and used without further purification.

Reactions of TAD with 49 and 50. Thermal. Solutions of PTAD¹⁴⁶ or MTAD in minimal volumes of THF or ether, respectively, were added via syringe to *ca.* 4-mM solutions of bicyclobutane **50** in CH₂Cl₂¹³ or, more typically, hexane¹² under N₂ at temperatures ranging from 0 to 70 °C. The addition was conducted at such a rate as to maintain a low concentration of TAD, its reaction being monitored qualitatively by disappearance of the red color. Alternatively, a solution of **50** in hexane and the TAD solution were added to the reaction mixture at comparable rates, with addition times ranging from 30 min to 9 hrs. Addition of **50** to a TAD solution or suspension was also attempted. ¹H NMR analysis of the soluble (CDCl₃ or acetone-*d*₆) residue after removal of the reaction solvent in all cases revealed various broad signals, at δ 1.0-4.2, 5.4-5.9 and in the region of the TAD methyl or phenyl group. In all cases the absence of a signal in the δ 4.2-5.4, window, expected for the bridgehead protons of a derivative of **47**, was taken to indicate that no cycloadduct had been produced. While the reaction of **50** with PTAD was rapid and that with MTAD occurred at a reasonable rate at room temperature, **49** could be recovered after 7 hrs at room temperature in the presence of PTAD or after 3 hrs at reflux in hexane in the presence of MTAD.

In contrast, addition of PTAD to a refluxing solution of **49** in isooctane as described above, and removal of the solvent after *ca.* 4 hrs afforded a residue whose ¹H NMR spectrum contained, in addition to numerous broad signals, a small triplet at δ 4.8, assigned as the phenyl analog of **52**. The amount of this adduct present was estimated as, at most, *ca.* 5%, corresponding to *ca.* 2 mg of material. Partial purification of this adduct by preparative-TLC (CH₂Cl₂ and 4:1 (*v/v*) petroleum ether-ether) was attended by a significant loss of material,

but allowed a partial characterization: ^1H NMR (400 MHz, CDCl_3) δ 4.80 (t, $J=1.7$ Hz, 2 H, H-1,7), 3.49 (d, $J=6.6$ Hz, 4 H, CH_2), 2.49 (tt, $J=1.7$, 6.6 Hz, 2 H, H-8,9) – *cf.* spectral data for **52** (below). When the reaction was conducted with MTAD, **52** was produced in a yield comparable to that of the PTAD reaction.

Photochemical. Irradiation of a mixture of **49** and MTAD in CH_2Cl_2 with the 450-Watt Hg arc lamp until the color of the MTAD had dissipated, followed by removal of the solvent, provided a product mixture whose ^1H NMR spectrum resembled that described above with the exceptions of a much smaller olefinic lump and a triplet ($J\approx 2$ Hz) near δ 4.7, attributed to cycloadduct **52** (see below). As judged by the size of this signal in the crude mixture (*vs* an internal standard), the reaction was more successful when pentane was used; the sparingly soluble MTAD was stirred vigorously in this case to effect its dissolution as the reaction proceeded. In the case of PTAD, a *ca.* 0.01-M solution of **49** containing a 7-8-fold excess of PTAD in CH_2Cl_2 was irradiated for 1 hr to provide a crude material whose ^1H NMR spectrum displayed small adduct signals (see above). The yield was estimated to be on the order of 5%, at most. A sufficient quantity of PTAD cannot be dissolved in hydrocarbon solvents at room temperature to conduct the reaction. An attempt to add MTAD to **50** photochemically in competition with their thermal reaction also failed to produce a cycloadduct.

Exo,exo-8,9-bis(t-butyldimethylsiloxymethyl)-4-methyl-2,4,6-triazatricyclo[5.1.1.0^{2,6}]nonane-3,5-dione (52**).** The bicyclobutane (35.5 g

of impure material containing 25 g of **49**, 73 mmol) was split into 11 portions. Each, in turn, was dissolved in 1 l of pentane, and *ca.* half of the requisite 4.25 g (37.6 mmol for each portion of **49**) of MTAD was added. The 450-W Hg arc lamp assembly was immersed in the solution, the vessel was connected to a source of N₂, and the mixture was stirred magnetically for *ca.* 5 min to saturate the solution with MTAD. With efficient stirring the mixture was irradiated for 40 min, the remaining MTAD was added, and the irradiation was continued for another 40 min. The solution was decanted, the sticky solid residue was washed with pentane, and the solvent was removed by rotary evaporation. The combined product, 86 g of a viscous yellow oil, was subjected to flash chromatography on a 10 cm x 5 in silica column. Elution with 2.5 l of 4:1 (*v/v*) petroleum ether-ether provided 17.1 g of a pale yellow liquid. This was heated under vacuum (<1 mm) at 70-80 °C for 1 hr to remove the residual *t*BuMe₂SiOH. The resultant solid was flash chromatographed on a 10 cm x 5 in silica column with 2 l of 19:1, 1.5 l of 5:1, and 1.5 l of 2:1 (*v/v*) petroleum ether-ether eluant to afford 12.4 g (37%) of **52** (*R_f* ≈ 0.3 in 4:1 PE-Et₂O) as a white solid: *mp* 91.5-94.0 °C; ¹H NMR (400 MHz, CDCl₃) δ 4.69 (t, *J*_{1,8} = 1.8 Hz, 2 H, H-1,7), 3.35 (d, *J* = 6.6 Hz, 4 H, CH₂), 3.01 (s, 3H, NCH₃), 2.42 (tt, *J* = 1.8, 6.5 Hz, 2 H, H-8,9), 0.84 (s, 18 H, *t*Bu), -0.01 (s, 12 H, SiMe₂); ¹³C NMR (22.6 MHz, CDCl₃) δ 158.6 (s, C=O), 62.7 (d, C-1,7), 57.1 (t, CH₂), 53.1 (d, C-8,9), 25.8 (q, NCH₃ + *t*Bu), 18.2 (s, *t*Bu), -5.5 (q, SiMe₂); Anal. Calc'd for C₂₁H₄₁O₄N₃Si₂: C, 55.34%; H, 9.07%; N, 9.22%. Found: C, 55.46%; H, 8.94%; N, 9.13%.

Exo,exo-2,4-bis(hydroxymethyl)-4-methyl-2,4,6-triazatricyclo[5.1.1.0^{2,6}]nonane-3,5-dione (57). To a solution of 12.4 g (27.2 mmol) of **52** in 50 ml of THF was added a solution of 22.3 g (70.7 mmol) of tetra-*n*-butylammonium fluoride trihydrate in 85 ml of THF.¹⁴³ After 40 min the orange solution was poured into 200 ml of ether atop a 10 cm x 2.5 in silica column. The sample was loaded onto the column and flash chromatographed with 2 l of 3:1 (*v/v*) ether-methanol eluant to afford an orange oil. This was flash chromatographed on a 10 cm x 5 in ether-packed silica column with 3:1 ether-methanol. The resulting cloudy material was dissolved in THF, filtered by suction through a fine frit, and concentrated under vacuum to 6.2 g of extremely viscous, slightly yellow syrup, which, by ¹H NMR contained 5.40 g (87.5%) of **57** (*R_f*=0.45) and residual tetrabutylammonium contaminant. Crystallization of this material can usually be induced by removal of the last traces of solvent. Further chromatography provides higher purity colorless product; however, the material is typically carried forward without further purification. Preparative TLC (silica, Et₂O-MeOH) provided a spectroscopic sample: ¹H NMR (400 MHz, acetone-*d*₆) δ 4.69 (t, *J*_{1,8}=1.7 Hz, 2 H, H-1,7), 3.79 (t, *J*=5.4 Hz, 2 H (variable integration; D₂O-exchangeable), OH), 3.30 (dd, *J*=6 Hz, 4 H, CH₂), 2.92 (s, 3 H, NCH₃), 2.52 (tt, *J*=1.7, 6.4 Hz, 2 H, H-8,9).

Exo,exo-8,9-bis(methanesulfonatomethyl)-4-methyl-2,4,6-triazatricyclo[5.1.1.0^{2,6}]nonane-3,5-dione (58a). To a stirred solution of diol **57** (0.250 g, 1.10 mmol) in 50 ml of CH₂Cl₂ at 0 °C was added 0.62 ml (0.45 g, 4.5 mmol) of triethylamine (distilled from KOH) followed by 0.255 ml (0.378 g,

3.30 mmol) of methanesulfonyl chloride (distilled).¹⁴⁷ After 3.5 hrs the solution was poured into 20 ml of cold water, and the layers were separated. The organic layer was washed with cold 5% HCl (2 x 15 ml) and saturated NaHCO₃ (15 ml), dried over MgSO₄, and concentrated by rotary evaporation to a yellow solid, which was triturated with ether to afford 0.35 g (83%) of **58a** as a white solid: *mp* 150-153 °C; ¹H NMR (400 MHz, CDCl₃) δ 4.89 (t, *J* = 1.7 Hz, 2 H, H-1,7), 4.00 (d, *J* = 7.3 Hz, 4 H, CH₂), 3.08 (s, 3 H, NCH₃), 3.02 (s, 6 H, OMs), 2.77 (tt, *J* = 1.7, 7.3 Hz, 2 H, H-8,9).

Exo,exo-8,9-bis(bromomethyl)-4-methyl-2,4,6-triazatricyclo-[5.1.1.0^{2,6}]nonane-3,5-dione (58b). Bromine (162 μl, 0.505 g, 3.16 mmol) was added to a suspension of triphenylphosphine (0.85 g, 3.24 mmol) in 3 ml of dry acetonitrile under nitrogen.¹⁴⁸ Ph₃PBr₂ precipitated after the solution had cooled to room temperature. With efficient stirring a solution of 0.36 g (1.58 mmol) of diol **57** in 1.3 ml of CH₃CN was introduced. After *ca.* 10 min the resultant cloudy orange solution was concentrated by rotary evaporation and flash chromatographed on a 2 cm x 6 in silica column with 150 ml of ether as eluent to afford 0.29 g (52%) of **58b** (*R_f* = 0.45) as a white solid. Recrystallization from CH₂Cl₂-ether afforded an analytical sample: *mp* 139.5-140.5 °C; ¹H NMR (400 MHz, CDCl₃) δ 4.80 (t, *J* = 1.7 Hz, 2 H, H-1,7), 3.08, 3.07 (d, *J* = 7.8 Hz, +s, 7 H, CH₂, NCH₃), 2.63 (tt, *J* = 1.7, 7.8 Hz, 2 H, H-8,9); Anal. Calc'd for C₉H₁₁O₂N₃Br₂: C, 30.62%; H, 3.14%; N, 11.90%. Found: C, 30.69%; H, 3.13%; N, 11.86%.

Exo,exo-8,9-bis(iodomethyl)-4-methyl-2,4,6-triazatricyclo[5.1.1.0^{2,6}]-nonane-3,4,-dione (58c). Mesylate 58a (0.15 g, 0.39 mmol), 0.35 g (2.34 mmol) of NaI, and 15 ml of 2-butanone were combined and heated to gentle reflux with stirring for 20 hrs. The mixture was cooled to room temperature and dissolved in 40 ml of 5% aq NaHSO₃. The product was extracted with ether (3 x 30 ml), dried (MgSO₄), concentrated by rotary evaporation, and flash chromatographed on a 2 cm x 5 in silica column with 150 ml of 20:1 (v/v) CH₂Cl₂-ether eluent to provide 0.155 g (89%) of 58c as a white solid: *mp* 137-138 °C (dec); ¹H NMR (400 MHz, CDCl₃) δ 4.68 (t, 1.7 Hz, 2 H, H-1,7), 3.07 (s, 3 H, NCH₃), 2.88 (d, *J* = 8.0 Hz, 4 H, CH₂), 2.59 (tt, *J* = 1.7, 8.0 Hz, 2 H, H-8,9); Anal. Calc'd for C₉H₁₁O₂N₃I₂: C, 24.18%; H, 2.48%; N, 9.40%. Found: C, 24.44%; H, 2.52% N, 9.29%.

Exo,exo-8,9-bis(2-nitrophenylselenomethyl)-4-methyl-2,4,6-triazatricyclo[5.1.1.0^{2,6}]nonane-3,5-dione (59). Diol 57 (2.70 g, 11.9 mmol) was dissolved in 150 ml of dry THF, 13.6 g (59.9 mmol) of *o*-nitrophenylselenocyanate (prepared by literature methods^{34,149} and purified by flash chromatography (silica, CH₂Cl₂) followed by trituration with ether to provide crystalline yellow-orange solid) was added, and the mixture was cooled to 0 °C. With magnetic stirring under a nitrogen atmosphere, 15.3 ml (12.4 g, 61.4 mmol) of tri-*n*-butylphosphine³⁵ was added via syringe over *ca.* 5 min, turning the slurry dark red. After 40 hrs at room temperature the THF was removed completely by rotary evaporation. The remaining material was dissolved in CH₂Cl₂ (*ca.* 60 ml), silica was added, and the solvent was removed, leaving a sticky, solid material. This was applied to a 10 cm x 4.5 in

silica column and flash chromatographed with 2 l of CH₂Cl₂ followed by 1.5 l of 9:1 (v/v) CH₂Cl₂-ether eluent to furnish an orange solid. Trituration with CHCl₃-ether afforded 4.25 g (60%) of **59** (R_f =0.5 in 9:1 CH₂Cl₂-Et₂O) as a yellow solid. An additional trituration provided an analytical sample: UV-vis (CH₂Cl₂) λ_{\max} 256 nm (ϵ 26800), 390 (ϵ 7420); ¹H NMR (400 MHz, CDCl₃) δ 8.27 (d, 2 H, ArH), 7.54, 7.40, 7.34 (pseudo-t, d, pseudo-t, 6 H, ArH), 4.77 (t, J =1.7 Hz, 2 H, H-1,7), 3.07 (s, 3 H, NCH₃), 2.69 (d, J =7.1 Hz, 4 H, CH₂), 2.53 (tt, J =1.7, 7.1 Hz, 2 H, H-8,9); Anal. Calc'd for C₂₁H₁₉O₆N₅Se₂: C, 42.37%; H, 3.22%; N, 11.76%. Found: C, 41.74%; H, 3.15%; N, 11.40%.

8,9-dimethylene-4-methyl-2,4,6-triazatricyclo[5.1.1.0^{2,6}]nonane-3,5-dione (60). Selenide **59** (4.25 g, 7.14 mmol) was dissolved in 900 ml of CHCl₃, and the solution was cooled to -60 °C. With magnetic stirring a stream of O₃ in oxygen (ca. 0.8 mmol O₃ min⁻¹) was bubbled into the solution for 22 min (17.6 mmol) causing it to acquire a blue color. The excess ozone was purged with a stream of N₂ and 5.0 ml (3.61 g, 35.7 mmol) of diisopropylamine was added.

In a dry 5-l three-necked round-bottomed flask equipped with an inlet-topped condensor and a septum were placed 2 l of CCl₄ and 5.0 ml of iPr₂NH (distilled from KOH), and the solution was stirred magnetically and heated to reflux under N₂. To this was added the cold selenoxide solution¹⁵⁰ via a cannula over 1.5 hrs, and the resulting orange solution was allowed to cool after another 15 min. The solution was split into two portions, and each was washed with 5% HCl (500 ml), 5% Na₂CO₃ (500 ml), and brine (50 ml), dried over MgSO₄, and concentrated by rotary evaporation to an orange-red muck.

This was flash chromatographed on two 1:1 charcoal-celite columns: the first, a 5 cm x 4.5 in (90 g) column with 400 ml of CH₂Cl₂ as eluent; the second, a 5 cm x 3 in (60 g) column with 250 ml of CH₂Cl₂. Removal of the solvent provided a yellow-orange solid which was flash chromatographed on a 5 cm x 6.5 in silica column with 1.5 l of 1:1 (v/v) petroleum ether-ether eluent to afford **60** (*R_f* = 0.25) as a slightly yellow solid. This was triturated with ether-pentane (1.5 ml of each) to provide a white solid (0.90 g, 66%). Recrystallization from CH₂Cl₂-hexane furnished an analytical sample: dec *ca.* 152 °C; ¹H NMR (400 MHz, CDCl₃) δ 5.024, 5.019 (2s, 6 H, H-1,7, =CH₂), 3.04 (s, 3 H, NCH₃); ¹H NMR (400 MHz, C₆D₆) δ 4.48 (s, 2 H, H-1,7), 4.35 (s, 4 H, =CH₂), 2.49 (s, 3 H, NCH₃); ¹³C NMR (100 MHz, C₆D₆) δ 161.6 (C=O), 138.2 (C-8,9), 100.1 (=CH₂), 69.3 (C-1,7), 25.7 (NCH₃). An INEPT experiment provided *J*_{CH} (bridgehead) = 189 Hz, *J*_{CH} (=CH₂) = 164 Hz; IR (CH₂Cl₂) 3060 (w), 2940 (w), 1775 (m), 1720 (s), 1445 (m), 1390 (m), 1220 (w), 1165 (m), 1080 (w), 1015 (m), 980 (w), 910 (m), 810 (m) cm⁻¹; UV (MeOH) λ_{max} 210 nm (ε 16800); MS (EI) *m/e* (relative intensity) 191 (36, M⁺), 134 (35, M⁺ - CH₃NCO), 106 (33, M⁺ - CH₃NCO, CO), 79 (34), 78 (55, M⁺ - CH₃NCO, CO, N₂), 77 (29), 65 (33), 64 (29), 52 (100). Anal. Calc'd for C₉H₉O₂N₃: C, 56.54%; H, 4.74%; N, 21.98%. Found: C, 56.50%; H, 4.72%; N, 21.87%.

5,6-Dimethylene-2-(*N*-methylcarbamoyl)-2,3-diazabicyclo[2.1.1]-hexane (66). To a solution of 0.300 g (1.57 mmol) of **60** in 24 ml of 6:1 (v/v) DMSO-water was added 87% KOH (0.360 g, 5.58 mmol), and the solution was stirred under N₂.³⁸ After 2 hrs the solution was acidified with 5% HCl (pH 2-3), causing gas evolution. After another hour *ca.* 15 ml. of saturated aq.

NaHCO₃ was added, followed by enough water to dissolve the precipitated solid, and the product was extracted with CHCl₃ (6 x 30 ml) and dried over MgSO₄. The CHCl₃ was removed by rotary evaporation and the residual DMSO (ca. 15 ml) by distillation (bath temperature 45 °C/<1 mm). The residue was taken up in CH₂Cl₂, applied to a silica preparative-TLC plate (20 cm square x 2 mm thick), and eluted three times with ether. Semicarbazide **66** (*R_f*=0.25-0.40) was recovered with 50 ml of 1:1 (*v/v*) petroleum ether - THF followed by 50 ml of THF, and the solvent was removed under vacuum in subdued light (ca. 24 hrs) to afford 0.234 g (90%) of slightly yellow, extremely viscous syrup (stored under N₂ at -30 °C). Low temperature NMR data are reported here because a slow inversion at the amine center broadens the olefinic ¹³C peaks and causes some ambiguity in the olefinic proton resonances, (*e.g.*, 3:1 peak ratios in some solvents). ¹H NMR (400 MHz, CD₂Cl₂, -60 °C) δ 6.42 (br q, 1 H, amide NH), 4.97 (d, *J*=5.4 Hz, 1 H, amide-bridghead CH), 4.789, 4.785, 4.776, 4.759 (4s, 1 H each, =CH₂), 4.39 (br s, 1 H, amine NH), 4.32 (d, *J*=5.4 Hz, 1 H, amine-bridgehead CH), 2.70 (d, *J*=4.9 Hz, NCH₃); ¹³C NMR (100 MHz, CD₂Cl₂, -60 °C) δ 162.9 (C=O), 141.8, 138.4 (quat), 97.0, 95.4 (=CH₂), 66.8, 65.1 (CH), 26.4 (NCH₃); IR (CH₂Cl₂) 3410 (m), 3270 (w), 3040 (w), 2940 (w), 1670 (s), 1520 (s), 1410 (w), 1370 (w), 1260 (w), 1210 (w), 1155 (w), 1110 (w), 1045 (m), 960 (w), 915 (m), 900 (m), 835 (w), 810 (w), 790 (w). An additional prep-TLC provided an analytical sample: Anal. Calc'd for C₈H₁₁N₃O: C, 58.17%; H, 6.71%; N, 25.44%. Found: C, 57.60%; H, 6.69%; N, 25.03%.

Nickel peroxide was prepared by the method of Nakagawa, *et al.*,¹⁵¹ which provides material with an activity (determined titrimetrically¹⁵¹) of *ca.* 3.5 mmol "available oxygen" (aO) per gram. We have found this oxidant to be unsuitable for our purposes. However, reactivation^{151,49} of this substance with NaOCl yields a solid that can be filtered much more rapidly (with less exposure to air) than the original material and (after thorough drying under vacuum) has an activity of at least 4.5 mmol aO g⁻¹. We have obtained variable results with nickel peroxide that has been stored for more than a few days at -30 °C. After a considerable amount of experience we have concluded that the only foolproof way to ensure the success of the oxidation of **66** is to use freshly-made and freshly-reactivated oxidant.⁵²

2,3-Diaza-5,6-dimethylenebicyclo[2.1.1]hex-2-ene (2). In a dry solid addition ampoule was placed 500 mg (2.25 mmol aO) of fresh nickel peroxide, and the ampoule was fitted to a dry 25-ml pear-shaped flask equipped with a septum. The assembly was flushed with argon, *ca.* 6 ml of CH₂Cl₂ was introduced and cooled to -78 °C, and the nickel peroxide was added to the flask. A solution of 25 mg (0.15 mmol) of the semicarbazide (**66**) in *ca.* 7 ml of CH₂Cl₂ (distilled from CaH₂ under N₂) was placed in a dry 10 ml flask and cooled to -78 °C under positive pressure of argon. With efficient magnetic stirring, the cold semicarbazide solution was added to the nickel peroxide slurry via 30-gauge teflon tubing over *ca.* 5 min. (The reaction was typically analyzed for remaining semicarbazide by TLC. A sample was obtained by filtering an aliquot through a plug of glass wool resting against a constriction in a piece of 20-gauge teflon tubing. If insufficiently active nickel peroxide

had been used, more could be added at this point and the reaction time increased accordingly. The absence of coupling product **67** cannot be conclusively established by TLC analysis, but its presence is often indicated by the appearance of a spot at $R_f \approx 0$ that develops brown upon treatment with vanillin/ H^+ solution.) The reaction was normally allowed to continue for 30 min to 1 hr.

A separate assembly was constructed with warm glassware. This consisted of a 25-ml pear-shaped flask with a high-vacuum valve and a septum-capped sintered glass frit. The frit was equipped with a cooling jacket and a gas inlet arm having a stopcock. While the apparatus was warm a *ca.* 1.5-cm pad of celite was placed on the frit and covered with a small piece of glass wool. The frit and flask were connected through a y-joint to a source of argon and aspirator vacuum.

When the reaction was judged to be complete the frit and flask were cooled to $-78^\circ C$, the celite pad was moistened with *ca.* 2 ml. of CH_2Cl_2 , and the slurry was cannulated through a judiciously short piece of 20-gauge teflon tubing into the frit assembly. The solution was filtered, the celite pad was rinsed with another *ca.* 2 ml of CH_2Cl_2 , and the solvent was removed (to a liq. N_2 trap) at $-78^\circ C$ under vacuum in subdued light over the course of several hours to afford the title diazene (**2**) as a white solid. (An early sample of a few milligrams of **2** decomposed explosively, possibly due to over-exposure to air and/or light; we have since experienced no difficulty in handling milligram quantities of the pure diazene). We use this material without further purification; attempts at recrystallization have generally failed to increase the purity of the sample, but only decrease the yield. We also note that

methylene chloride appears to be by far the best solvent for crystalline diazene **2**. This material is only slightly soluble in the other solvents commonly used (e.g., MTHF). Solutions of **2** in these solvents were made either by first dissolving the crystalline solid in a minimal amount of methylene chloride, by dissolving diazene that had not yet crystallized, or by dissolving material contaminated by a small amount of coupled semicarbazide, **67**. ^1H NMR (400 MHz, CD_2Cl_2 , -80°C) δ 5.48 (s, 2 H, CH), 4.75 (s, 4 H, CH_2); ^1H NMR (400 MHz, C_7D_8 , -80°C): δ 4.66 (s, 2 H, CH); 4.07 (s, 4 H, CH_2); ^{13}C NMR (22.6 MHz, CD_2Cl_2 , -75°C) δ 157.7, 97.0, 82.9. These signals were found to vanish upon warming the sample to -50°C , in accord with the thermal loss of the proton signals. The yield of the reaction was determined by ^1H NMR. Thus, the best diazene samples were found to contain 80-85% **2** and 15-20% dimers, for an overall reaction yield of *ca.* 30%. UV (MTHF) λ_{max} 333 nm; shoulder *ca.* 320 nm. UV (CD_2Cl_2) λ_{max} 331 nm; shoulder *ca.* 320 nm. The samples invariably displayed a large absorption extending up to *ca.* 280 nm. This is not due to **2**, and it presumably arises from the dimeric decomposition products. The ϵ of the diazene in CD_2Cl_2 was determined by making several UV absorbance measurements and determining the concentration of **2** by NMR. Thus, three such measurements provided $\epsilon = (0.146 (\pm 0.01))/(0.35 (\pm 0.01) \text{ cm}) (1.80 (\pm 0.2) \times 10^{-3} \text{ M}) = 230 (\pm 30) \text{ M}^{-1} \text{ cm}^{-1}$; $\epsilon = (0.157 (\pm 0.01))/(0.35 (\pm 0.01) \text{ cm}) (1.86 (\pm 0.2) \times 10^{-3} \text{ M}) = 240 (\pm 30) \text{ M}^{-1} \text{ cm}^{-1}$; and $\epsilon = (0.303 (\pm 0.02))/(0.35 (\pm 0.01) \text{ cm}) (3.69 (\pm 0.2) \times 10^{-3} \text{ M}) = 240 (\pm 20) \text{ M}^{-1} \text{ cm}^{-1}$, for an average of $240 \text{ M}^{-1} \text{ cm}^{-1}$.

Coupled semicarbazide, 67. The two presumed conformers **67a** and **b**, were identified by comparison of $-80\text{ }^{\circ}\text{C}$ 400 MHz ^1H NMR spectra in which they occurred in different ratios, as well as comparison with spectra of their deuterated analogs (from **66-*d*₂**). Warming a sample to $10\text{ }^{\circ}\text{C}$ caused coalescence of the amide proton signals only. After 20 min *ca.* 70% of conformer **b** and 30% of **a** were destroyed. Identical diazene samples stored at $-100\text{ }^{\circ}\text{C}$ for several days are often found to contain different ratios of **a** and **b**, and the ratios sometimes change upon photolysis, but irreproducibly. ^1H NMR (400 MHz, CD_2Cl_2 , $-80\text{ }^{\circ}\text{C}$) **a**: δ 6.41 (q, $J=4.9\text{ Hz}$, 1 H, amide NH), 5.14, 5.05, 4.83, 4.79 (4s, 1 H each, $=\text{CH}_2$), *ca.* 5.04 (d, 1 H, amide-bridgehead CH), 4.51 (d, $J=5.6\text{ Hz}$, 1 H, amine-bridgehead CH), 2.63 (d, $J=4.9\text{ Hz}$, 3 H, NCH_3); **b**: 6.53 (d, $J=4.9\text{ Hz}$, 1 H, amide NH), 5.09, 4.90, 4.77, 4.74 (4s, 1 H each, $=\text{CH}_2$), *ca.* 5.04 (d, 1 H, amide-bridgehead CH), 4.63 (d, $J=5.9\text{ Hz}$, 1 H, amine-bridgehead CH), 2.70 (d, $J=4.9\text{ Hz}$, 3 H, NCH_3).

1,3-*d*₂-Endo,endo-2,4-bis(*t*-butyldimethylsiloxymethyl)bicyclo[1.1.0]-butane (49-*d*₂). A stirred solution of the bicyclobutane (2.40 g of impure material estimated to contain 1.80 g of **49**, 5.25 mmol) in 7 ml of dry ether, under argon, was cooled in an ice bath. To this was added 14.5 ml of a 1.45 M solution of *n*-butyllithium (21.0 mmol) in hexane¹⁴¹ via syringe over *ca.* 5 min, and the orange solution was stirred at room temperature for 6.5 hrs. The solution was then cooled to $0\text{ }^{\circ}\text{C}$ and quenched by the cautious addition of excess D_2O (1.1 ml, 55 mmol), and the resultant mixture was allowed to warm. The solution was dried (Na_2SO_4) and concentrated under vacuum. This procedure was repeated two more times to afford 1.70 g of **49-*d*₂** as a dark

orange liquid. This appeared reasonably pure by ^1H NMR, the spectrum corresponding to that of **49** but lacking the signal of and splitting produced by the bridgehead protons. This material was carried forward without further purification.

1,4- d_2 -2,3-diaza-5,6-dimethylenebicyclo[2.1.1]hex-2-ene (2- d_2). Bicyclobutane **49- d_2** was subjected to the standard reaction sequence (see above). ^1H NMR spectra of the intermediate compounds were consistent with bridgehead deuteration. In addition, a mass spectrum of **60- d_2** displayed a series of peaks corresponding exactly to those assigned (above) to **60** (M^+) and the intermediates generated by the sequential fragmentation of the urazole moiety, at at $m/e + 2$ relative to those of **60**. Specifically, m/e 193 (100), 136 (91), 108 (62), 80 (89), 66 (8), 65 (9), 53 (12), 40 (4). A high-quality ^1H NMR spectrum (400 MHz, CD_2Cl_2) of **2- d_2** allowed an estimate of the extent of deuterium incorporation. The signal of the residual bridgehead protons was only slightly larger than the ^{13}C satellites of the olefinic signal, indicating that the three cycles of $n\text{BuLi}/\text{D}_2\text{O}$ exchange had replaced >99% of the bridgehead hydrogens of **49**.

Thermolysis of urazole 60. A sample of 10 mg of **60** in *ca.* 400 ml of C_6D_6 was placed in a 5-mm o.d. NMR tube, and the sample was degassed and sealed under vacuum. The sample was immersed in a pre-heated (100 °C) oil bath for 4 hrs, the progress of the reaction being monitored intermittently by ^1H NMR.

A white solid (insoluble in CH_2Cl_2 , Me_2CO) had precipitated within the first 30 min of the pyrolysis. The sample was cooled and the benzene- and

CH₂Cl₂-soluble material was applied to a silica preparative-TLC plate and eluted five times with CH₂Cl₂. The major band ($R_f \approx 0.45$) was removed and recovered with ether, the solvent was removed, and the prep-TLC was repeated to afford 1 mg of **70** as a white residue. ¹H NMR (90 MHz, CDCl₃) δ 6.58 (br s, 1 H, olefinic); 5.98 (t, $J=6.4$ Hz, 1 H, allenic); 5.10 (d, $J=6.4$ Hz, 2 H, allenic); 4.43 (br s, 2 H, CH₂); 3.07 (s, 3 H, NCH₃). MS (EI) m/e (relative intensity) 191 (100, M⁺), 134 (32, M⁺ - CH₃NCO), 106 (20, M⁺ - CH₃NCO, CO), 86 (12), 84 (22), 79 (24), 78 (48, M⁺ - CH₃NCO, CO, N₂), 77 (22).

Curie plot. The temperature in the sample region of the cryostat was calibrated against the thermocouple temperature with the carbon glass resistor. The temperature was controlled by adjusting the transfer line needle valve only (see above) in an effort to achieve maximum reproducibility for this particular experiment. In several calibration runs the correlation followed a smooth curve (nearly linear), but the curve shifted unpredictably upon reversing the direction of the temperature change. The absolute uncertainty in the temperature is estimated as *ca.* $\pm 2.5^\circ$ at 30 K, and $\pm 4^\circ$ at 80 K.

For the plot of Figure 2-4 a sample of **2** in 1:1 EtOH/MeOH⁸⁸ was placed in the EPR cavity at 4 K, irradiated with light from the Hg(Xe) arc lamp using filter combination #2 (Table 2-3) and the cavity was shrouded against stray light. The sample was then warmed to 70-80 K for 15 min to allow decay of any biradicals in "fast" matrix sites. The temperature was then lowered in 3 to 6° increments and allowed to stabilize for several minutes at each temperature. The indicated (TC) temperature generally fluctuated no more

than $\pm 0.1^\circ$ during the 2 min scan. All spectra were recorded at 0.01 mW. The onset of saturation was not determined in this run due to our inability to measure the power with sufficient accuracy to generate a quantitatively meaningful intensity *vs* P^\dagger plot, however previous such measurements indicated that this point is *ca.* 15 K. Because the spectral shape was invariant with temperature, and double integration of the spectra had previously been found, therefore, to cause no deviation from linearity in the Curie plot, the reported signal intensity is simply the sum of the intensities of the four *y*- and *z*-peaks of the first-derivative spectrum (Figure 2-1).

Spectra were recorded as the temperature was first decreased, then increased, then decreased again. Anomalous cryostat vacuum readings during measurement of half of the spectra in the first temperature progression and a corresponding break in the plot provided justification for rejecting this entire set. Thus, the points presented in Figure 2-4 represent increasing, then decreasing temperature data. The temperatures used for the plot were derived from the lower-limit of the actual-temperature *vs* TC-temperature calibration curve. A plot made with the upper-limit temperatures also displayed no curvature. Treatment of the sample temperature as such a (nearly) linear function of TC reading (rather than simply assigning each point a large error) is justified by the good correlation of the data of Figure 2-4 and of one other Curie plot we have obtained under similar conditions, as well as the observed calibration curves (see above). We feel that the experiment could not easily be improved with the present equipment (unless we had made provisions to place the sensor in the tube containing the actual spectroscopic sample^{44b}). Even the best conditions we could hope to achieve would not allow

us to further delimit the permissible energy regime of the singlet due to the intrinsic insensitivity of the experiment.⁸⁶

Absorption spectrum of 1. A sample of 2 in MTHF was irradiated with monochromatic 334 (± 10) nm light from a 1000-W Xe arc lamp at 77 K for 1.5 hrs to provide the spectrum of Figure 2-5. Measured peak positions (nm): 505.7 (abs \approx 2), 490.3, 469.5, 456.4, 443, 439, 426.8, 415, 401. (Spectroscopic samples were effectively opaque below *ca.* 280 nm, as mentioned above under the characterization of 2.)

Fluorescence and excitation spectra of 1. Samples of 2 in MTHF were irradiated with monochromatic 334 (± 10) nm light from a 1000-W Xe arc lamp at 77 K for 1 hr to produce an intense yellow-orange color.

The emission spectrometer¹⁵² employed a 150-W Xe arc lamp as the excitation source. The spectrum of Figure 2-5 was recorded with 1.25-mm excitation slits and 2-mm emission slits. The excitation wavelength was 440-445 nm, and a 446-nm cutoff filter protected the PM tube from reflected light. The emission monochromator had been calibrated to the Hg spectral lines, and the wavelength scale was corrected accordingly. The spectrum was also corrected for the variation in the response of the PM tube with wavelength. Measured peak positions (nm): 510, 526, 543, 553, 574, 595, 606, 631. The excitation spectrum was recorded with 1.25-mm excitation and 5-mm emission slits. The emission was monitored at 552 nm and the wavelength scale was arbitrarily shifted 5 nm to compensate for miscalibration of the excitation monochromator.

Decay rate of 1 at 77 K by EPR. A sample of 2 in MTHF was placed in the liq. N₂-filled finger dewar in the EPR cavity, the room lights were dimmed, and the cavity area was shrouded with black cloth. The sample was photolyzed for 15 sec with light from the 1000-W Hg(Xe) arc lamp directed through filter combination #1 (Table 2-3). The rise and decay of the signal were monitored at 3150 G (low field *z*-transition; 9.26 GHz) with 0.5 mW microwave power. The baseline was periodically checked for drift by switching to 2150 G, and the intensity measurements were corrected accordingly. The signal intensity was followed for 1.5 hrs during which time *ca.* 15% of the signal decayed. The slope of a 20-point $\ln I$ vs $t\frac{1}{2}$ plot was 2.3 (± 0.5) $\times 10^{-3}$ sec $^{-\frac{1}{2}}$ corresponding to a most probable rate constant of 9 (± 4) $\times 10^{-7}$ sec $^{-1}$.⁸⁹

Decay rate of 1 at 77 K by UV-vis. The sample used in the EPR experiment above was thawed and refrozen in liq. N₂. The sample was irradiated for 15 sec with the 1000-W Hg(Xe) arc lamp and filter combination #1 (Table 2-3) and quickly transferred to the finger dewar, which had been mounted in the beam of the HP diode array spectrophotometer. The room lights were kept off, the sample area was shrouded with black cloth, and streams of nitrogen were directed at the outer surface of the finger dewar to prevent condensation in the path of the light beam. A 340-nm cutoff filter was placed in front of the light source to prevent photolysis of 2 (photolysis of 1 had been found to be negligible under the conditions used), and spectra were recorded with 0.1-sec measurement time and stored on a floppy disc. The

intensity was measured at each of the four prominent peaks of the spectrum (Figure 2-5) relative to a (sloping) baseline drawn between the edges of the spectrum with the aid of a program written for the HP 85A ("ABS" – Appendix 3). Spectra were recorded over 4 hrs, during which *ca.* 20% of the *I* initially present decayed. Data acquired during the first 30 min displayed a large amount of scatter, presumably due to some movement of the sample before it froze in place. A $\ln I$ vs $t^{\frac{1}{2}}$ plot of the remaining data for the 506-nm peak had a slope of $1.9 (\pm 0.3) \times 10^{-3} \text{ sec}^{-\frac{1}{2}}$ corresponding to a most probable rate constant of $6 (\pm 2) \times 10^{-7} \text{ sec}^{-1}$.⁸⁹ Rates measured with the other vibronic peaks were all within or near this range.

Photochemical action spectrum. A sample of **2** in MTHF was placed in the Oxford cryostat, which was mounted in the EPR cavity. The sample was cooled to 4 K, and photolyzed with 334-nm light from the 1000-W Xe arc lamp (*ca.* 20-nm monochrometer bandpass) for 5-10 min to generate a sufficient concentration of **1**. The signal intensity was monitored at 3073 G (9.27 GHz, 0.5 mW) while the monochrometer wavelength was advanced 1 nm every 10 sec with the slits set for a 2.75-nm bandpass. The data were recorded digitally with a resolution of *ca.* 5.5 points nm⁻¹. With the aid of a FORTRAN program ("UVESRDV" – Appendix 3) written for the IBM-PC/AT the curve was smoothed over a 25-point region by a least-squares procedure,¹⁵³ then differentiated using a 35-point window, which also accomplished a second least-squares smoothing.¹⁵³ The lamp intensity correction was applied as a Gaussian function of lamp intensity data with a 2.5-nm fwhm to approximate the bandpass, centered at each data point. The action spectrum of Figure 2-6

(a and b) was shifted by *ca.* 2 nm (into alignment with the absorption spectrum of Figure 2-6c) to compensate for an apparent miscalibration of the monochrometer (possibly caused by a slight misalignment of the optical arrangement).

Attempts were made to detect a second biradical transition¹³⁶ by scanning down to 260 nm (the practical limit for the Xe lamp used) but no decay of the EPR signal was observed.

Determination of oscillator strength. A sample of 2 in MTHF in a standard 5-mm o.d. EPR tube was irradiated at 77 K for *ca.* 7 min with light from the 1000-W Xe arc lamp that had been directed through filter combination #1 (Table 2-3). The sample tube was placed well away from the optical focal point and rotated during the photolysis to provide a uniform distribution of 1 throughout the MTHF matrix. The sample was stored at 77 K for 3 hrs prior to the analysis in order to avoid the faster portion of the non-exponential decay (see above).

The effective path length of the EPR tube in the UV-vis spectrophotometer beam was measured as 0.35 ± 0.01 cm (roughly in accord with the i.d. specified by the manufacturer) by comparison of a standard solution's absorbance in the tube with that in an ordinary 1-cm cell. The volume contraction of the solvent was measured as *ca.* 20% upon cooling from room temperature to 77 K.

The EPR spin standard consisted of a 5.48×10^{-4} M solution of 2,2,6,6-tetramethylpiperidinyloxy (TEMPO) in MTHF in a tube identical to that containing the biradical sample. The concentration at 77 K was $6.85 (\pm 0.4) \times$

10^{-4} M, the estimated error being based primarily upon the uncertainty in the volume change.

EPR spectra were recorded at 77 K using 0.01 mW power for TEMPO spectra and both 0.01 and 0.1-mW for spectra of 1, thereby avoiding signal saturation in both cases. Several comparisons of 0.01 and 0.1-mW spectra indicated that the accurate power ratio at these settings was 12.8, and the nominal 0.1-mW spectra were scaled to 0.01 mW accordingly. The digitized first-derivative spectra were numerically double-integrated by standard methods¹³⁹ and scaled to a common receiver gain.

The 506-nm absorbance of the sample was determined by recording five spectra as the sample tube was rotated in the finger dewar with respect to the spectrophotometer beam. The absorbance was measured relative to a baseline drawn between the edges of the spectrum with the aid of an HP-85A program ("ABS" – Appendix 3).

Table 2-4. Determination of ϵ for triplet 1.

Measurement	Abs (506 nm) ^a	Double Integral ^b	[1] ^c (M)	ϵ^c (M ⁻¹ cm ⁻¹)
1 UV-vis 1 EPR	0.575 ± 0.03	366 ± 18	$2.10(\pm 0.25) \times 10^{-4}$ M	7820 ± 1600
2 EPR 2 UV-vis	0.423 ± 0.005	344 ± 17	$1.98(\pm 0.24) \times 10^{-4}$ M	6100 ± 1000
3 EPR 3 UV-vis	0.394 ± 0.004	253 ± 30	$1.45(\pm 0.27) \times 10^{-4}$ M	7760 ± 1800

^a the reported errors are standard deviations. ^b the reported errors represent $\pm 5\%$ except for the third, which reflects the disparity of the two measurements that were averaged. ^c the errors are the sums of the relative errors in the contributing values, and thus represent conservative limits.

Three pairs of EPR and absorption measurements were made, at *ca.* 3, 6, and 9.5 hrs after photolysis (see Table 2-4). The second member of the pair followed the first as closely as temporo-spacial constraints permitted, and the order of the two was reversed to compensate for the effects of both intrinsic and adventitious decay of the biradical.

The double-integrated EPR signal intensity of the TEMPO standard, as determined from two separate spectra, was 448 ± 22 , the error reflecting a qualitative observation that the double-integrals (di) are generally reproducible to $\pm 5\%$. The instrument response factor for the TEMPO doublet (free radical) signal, c_D , is then $[\text{TEMPO}]/\text{di} = 1.53 (\pm 0.1) \times 10^{-6}$. Triplet signals are inherently $4/3$ as intense per electron as doublet signals, or $8/3$ as intense per paramagnet.¹⁵⁴ Therefore, the corresponding response factor for the triplet, $c_T = 3/8 c_D$, or $5.74 (\pm 0.4) \times 10^{-7}$.

Absorbance values and double-integrals for the three pairs of measurements on the sample of 1 are reported in Table 2-4. The biradical concentrations were determined by $[1] = c_T(\text{di})$, and $\epsilon = A/(0.35 \pm 0.01 \text{ cm})([1])$. The average of the three values is $7200 \text{ M}^{-1} \text{ cm}^{-1}$. As possible sources of systematic errors, we note that the absorbance values reported could be slightly low due to either exceeding the linear range of the spectrophotometer or hitting the sample tube off center with the beam, both of which would make the measured ϵ too low. However, based on our estimation of the magnitude of these errors (and the values obtained in other inferior experiments, we feel confident that the actual ϵ is within (conservatively) ± 2000 of the stated value, $7200 \text{ M}^{-1} \text{ cm}^{-1}$.

The transition oscillator strength was determined according to the expression⁹²

$$f = 4.3 \times 10^{-9} \int \epsilon d\nu$$

by numerical integration of four absorption spectra over a wavenumber axis in 2-nm steps, with the aid of a program written for the HP-85A ("OSCIL" – Appendix 3). Integration of eight spectra afforded $f=0.022$ with a standard deviation of ± 0.003 ; however, the 27% error limit on ϵ dictates that this error be assigned as ± 0.006 . (This translates into an error of $\pm 1.6 \times 10^6 \text{ s}^{-1}$ on k_f° and $\pm 50 \text{ ns}$ on τ_f° .)

Fluorescence lifetime of 1. Samples of *ca.* $2 \times 10^{-4} \text{ M}$ **1** in MTHF at 77 K were placed in the quartz finger dewar. The pulsed laser system has been described previously.¹⁵⁵ Briefly, the excitation source consisted of a Quanta Ray DCR-1 Q-switched Nd:YAG laser, whose output was frequency-tripled to provide 8-ns pulses of 355-nm light. (The longer wavelength scattered light served to excite the transition of triplet **1**.) The repetition rate was 10 Hz and the *ca.* 3-4-mJ pulses were defocussed in order to prevent rapid photochemical destruction of the biradical. The emission was monitored at 555 nm. Unfortunately, the fluorescence of the biradical was apparently overwhelmed by a large amount of scattered light or light emitted by an impurity, and no meaningful data could be acquired under the experimental conditions used.

Magnetophotoselection. The photolysis setup consisted of, in series, the 1000-W Hg(Xe) arc lamp, the monochrometer, and two quartz lenses having 100 and 175-mm focal lengths. The first of these was adjusted to provide a

parallel light beam and the second to reduce the image of the monochrometer exit slit to approximately the width of the sample at the point of incidence. An Oriel model 27340 polymer sheet-type near-UV/visible linear polarizer was placed between the two lenses and positioned appropriately with a rotatable mount. The monochrometer was found to polarize the light somewhat in the horizontal ($E // H_0$) direction; therefore, for photolyses with unpolarized light, the assembly was replaced with the standard one, in which the (unpolarized) lamp output is directed through an appropriate series of filter glasses and focussed into the EPR cavity. Spectra were recorded with 0.2 mW microwave power at *ca.* 9.25 GHz.

A sample of **2** in MTHF in a 5-mm o.d. quartz tube was frozen in liquid nitrogen to produce an optically transparent glass. The sample was irradiated with monochromatic 333 (± 4) nm light having $E // H_0$ for 30 min to provide the spectrum of Figure 2-8b. Rotation of the sample tube by 90° provided the spectrum of 2-8c. (These spectra were recorded at a common gain.) The double integrals of the two differed by only 2%, demonstrating that the same group of triplets was responsible for the spectra obtained in the two sample tube orientations. Irradiation of a sibling sample instead with $E \perp H_0$ provided a spectrum with relative peak intensities virtually identical to those of Figure 2-8c, and independent of rotation of the sample tube.

The original sample, after having been thawed and refrozen, was irradiated for 7.5 min with the same setup less the polarizer. The tube was rotated 90° and the irradiation was continued for 7.5 min to provide the "isotropic" spectrum of Figures 2-8a and 2-9a. Because the light from the monochrometer carried some polarization, this experiment was repeated

using a third sibling sample, with filter combination #2 (Table 2-3) in its place. After 10 min of irradiation, the spectrum obtained had low-field y -, z -, and x -transition intensities — measured respectively as peak *vs* baseline, peak *vs* neighboring minima, and peak-to-peak, and normalized to the z — of 0.77:1:1.14. Rotation of the sample tube by 90° provided a spectrum with relative intensities 0.84:1:0.78. After another 10 min of photolysis in the new orientation, the spectrum displayed intensities of 0.79:1:1.00. For comparison, the spectrum of Figures 2-8a and 2-9a (generated by photolysis with the monochrometer) has peak intensities of 0.81:1:0.98. Ideally, after two orthogonal photolyses with unpolarized light the X, Y, and Z orientations should be present in a 2:3:3 ratio. Because of depolarization effects, however, the spectra generated by photolyzing with and without the monochrometer represent distributions of biradicals that are very nearly isotropic.

The "isotropic" sample (Figures 2-8a and 2-9a) was irradiated with 490-nm light (8-nm bandpass) with $E \parallel H_0$ for 40 min to provide the spectrum of Figure 2-9b — y , z , and x peak intensities (as defined above): 0.97:1:0.07. Rotation of the sample tube afforded a spectrum having a double-integral within 1% of the previous one and peak intensities 0.72:1:1.91.

An "isotropic" sample of 1 produced by photolyzing *without* the monochrometer (see above) was irradiated for 60 min using filter combination #3 (Table 2-3) to hit only the two lowest-energy vibronic peaks of 1 (see Figure 2-5). A spectrum similar in appearance to that in Figure 2-9b, but less intense, with relative intensities 1.03:1:0.41, was observed. Rotation of the tube provided the spectrum of Figure 2-9c, with peak intensities 0.82:1:5.36.

The integrated EPR spectra of Figures 2-8 and 2-9 are presented as Figure 2-12.

Finally, the absorption spectrum was checked for mixed polarization. A sample of **2** in MTHF at 77 K in the finger dewar was irradiated for 30 min with horizontally polarized monochromatic (334-nm) light. The polarizer was placed in the UV-vis spectrophotometer beam for both the sample and the reference spectra. By rotating both the sample tube and the polarizer, the sample was examined with its photochemical E-imprint aligned with, perpendicular to, and in an end-on orientation relative to the E-vector of the spectrophotometer beam. The relative intensities of the peaks of **2** and **1** varied as expected, demonstrating that the sample was indeed anisotropic. However, the vibronic peaks of the absorption envelope of **1** (Figure 2-5) always appeared in the same relative intensities establishing that all the vibronic transitions carry the same polarization.

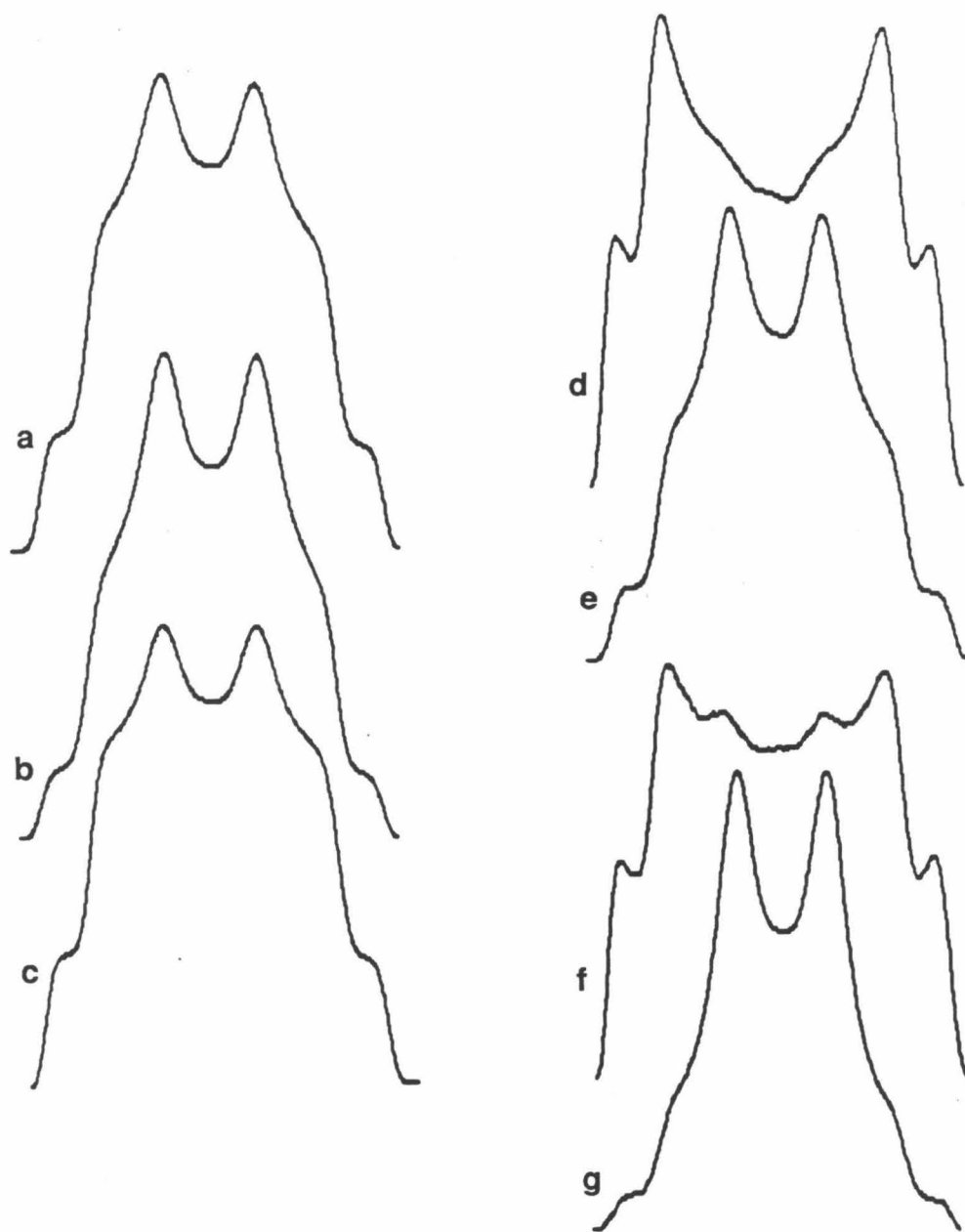


Figure 2-12. Absorption EPR spectra of anisotropic assemblies of triplet 1, obtained by numerical integration¹³⁹ of the spectra of Figures 2-8 and 2-9. The curves correspond to Figures (a) 2-8a (isotropic), (b) 2-8b, (c) 2-8c, (d) 2-9b, (e) 90° rotation of the 2-9b sample, (f) the 2-9c sample before 90° rotation, and (g) 2-9c.

References and notes.

1. See, for example, Chapman, O.L. *Pure Appl. Chem.* **1974**, *40*, 511-523. Dunkin, I.R. *Chem. Soc. Rev.* **1981**, 1-23.
2. Buchwalter, S.L.; Closs, G.L. *J. Am. Chem. Soc.* **1979**, *101*, 4688-4694; **1975**, *97*, 3857-3858.
3. (a) Jain, R.; Sponsler, M.B.; Coms, F.D.; Dougherty, D.A. *J. Am. Chem. Soc.*, in press. (b) Jain, R.; Snyder, G.J.; Dougherty, D.A. *J. Am. Chem. Soc.* **1984**, *106*, 7294-7295.
4. Chapman, O.L.; Chang, C.-C.; Kolc, J. *J. Am. Chem. Soc.* **1976**, *98*, 5703-5705. Sugawara, T.; Bethell, D.; Iwamura, H. *Tet. Lett.* **1984**, 2375-2378. Trozzolo, A.M.; Murray, R.W.; Smolinsky, G.; Yager, W.A.; Wasserman, E. *J. Am. Chem. Soc.* **1963**, *85*, 2526-2527.
5. Jain, R.; McElwee-White, L.; Dougherty, D.A. *J. Am. Chem. Soc.*, submitted for publication.
6. See Chapter 1 of this thesis and references therein.
7. For a preliminary account of this work see Snyder, G.J.; Dougherty, D.A. *J. Am. Chem. Soc.* **1985**, *107*, 1774-1775; **1986**, *108*, 299-300.
8. Engel, P.S. *Chem. Rev.* **1980**, *80*, 99-150. Adam, W.; DeLucchi, O. *Angew. Chem., Int. Ed. Engl.* **1980**, *19*, 762-779. Meier, H.; Zeller, K.-P. *Angew. Chem., Int. Ed. Engl.* **1977**, *16*, 835-851.
9. Berson, J.A. in ref 10, Ch 4, pp. 151-194.
10. *Diradicals*; Borden, W.T., Ed.; Wiley: New York, 1982.
11. Dowd, P. *J. Am. Chem. Soc.* **1966**, *88*, 2587-2589. Crawford, R.J.; Cameron, D.M. *J. Am. Chem. Soc.* **1966**, *88*, 2589-2590.

12. Chang, M.H.; Jain, R.; Dougherty, D.A. *J. Am. Chem. Soc.* **1984**, *106*, 4211-4217. Chang, M.H.; Dougherty, D.A. *J. Org. Chem.* **1981**, *46*, 4092-4093.
13. Amey, R.L.; Smart B.E. *J. Org. Chem.* **1981**, *46*, 4090-4092. See also ref 3a.
14. (a) Leininger, H.; Lanzendörfer, F.; Christl, M. *Chem. Ber.* **1983**, *116*, 669-680. (b) Leininger, H.; Christl, M. *Angew. Chem., Int. Ed. Engl.* **1980**, *19*, 458-459. (c) Leininger, H.; Christl, M.; Wendisch, D. *Chem. Ber.* **1983**, *116*, 681-689.
15. The preparation of 2,4-dicarbomethoxybicyclobutane has been reported by Kelley, F.W., Jr., Ph.D. Thesis, University of Idaho, 1969. However, the reported procedure did not provide viable material in our hands. This bicyclobutane derivative has also been prepared electrochemically: Velluro, A.F.; Griffin, G.W. *J. Org. Chem.* **1966**, *31*, 2241-2243.
16. Chang, M.H.; Dougherty, D.A. *J. Am. Chem. Soc.* **1982**, *104*, 1131-1132.
17. Such backside attack on strained σ -bonds is well precededent: Gassman, P.G. *Acc. Chem. Res.* **1971**, *4*, 128-136.
18. Roth, R.J.; Katz, T.J. *J. Org. Chem.* **1980**, *45*, 961-965; *J. Am. Chem. Soc.* **1972**, *94*, 4770-4771. Roth, R.J. *Synth. Commun.* **1979**, *9*, 751-756.
19. Christl, M.; Lang, R.; Herzog, C. *Tetrahedron* **1986**, *42*, 1585-1596. Christl, M.; Lang, R. *J. Am. Chem. Soc.* **1982**, *104*, 4494-4496.

20. 2,4-*Exo,exo*-dimethylbicyclobutane has been calculated to be *ca.* 13 kcal mol⁻¹ more stable than its *endo,endo* counterpart: Richtsmeier, S.C.; Gassman, P.G.; Dixon, D.A. *J. Org. Chem.* **1985**, *50*, 311-317.

21. Quite consistent with the stereochemical assignments is the characteristic²² upfield NMR shift of the *endo* protons of **50** (δ 1.13) relative to the *exo* protons of **49** (δ 2.70).

22. Wiberg, K.B. *Adv. Alicycl. Chem.* **1968**, *2*, 185. Leftin, J.H.; Gil-Av, E.; Pines, A. *J. Chem. Soc., Chem. Commun.* **1968**, 396-397.

23. Our laboratory's previous *exo-endo* designation^{12,16} was based on the bicyclo[2.1.1]hexane (or tricyclo[5.1.1.0^{2,6}]nonane) ring system, however, IUPAC rules dictate that these labels be reversed when heteroatoms are incorporated into the large bridge as in **46**, **47**, **52**, etc. *Nomenclature of Organic Compounds*; Fletcher, J.H.; Dermer, O.C.; Fox, R.B., Eds.; Advances in Chemistry 126; American Chemical Society: Washington, DC, 1974; pp 114-117.

24. This coupling pattern is dependent on proton-proton dihedral angles which are essentially invariant because the ring system is so rigid. The coupling described is displayed in **47**¹² as well as many bicyclo[2.1.1]hexane derivatives: Wiberg, K.B.; Lowry, B.R.; Nist, B.J. *J. Am. Chem. Soc.* **1962**, *84*, 1594-1597.

25. Evidence for a zwitterionic intermediate in the addition of PTAD to vinyl ethers has been presented: Hall, J.H.; Jones, M.L. *J. Org. Chem.* **1983**, *48*, 822-826. Although, in general, the addition of TAD to olefins is thought to proceed via an aziridinium intermediate,²⁶ the intervention of a similar

species is improbable in the present case. The potentially viable routes for TAD additions to olefins have been discussed.^{26a}

26. (a) Adam, W.; Carballeira, N. *J. Am. Chem. Soc.* **1984**, *106*, 2874-2882. Cheng, C.-C.; Seymour, C.A.; Petti, M.A.; Greene, F.D.; Blount, J.F. *J. Org. Chem.* **1984**, *49*, 2910-2916. (b) Nelsen, S.F.; Kapp, D.L. *J. Am. Chem. Soc.* **1985**, *107*, 5548-5549.

27. See, for example, Hoye, T.R.; Bottorff, K.J.; Caruso, A.J.; Dellaria, J.F. *J. Org. Chem.* **1980**, *45*, 4287-4292.

28. Pocius, A.V.; Yardley, J.T. *J. Am. Chem. Soc.* **1973**, *95*, 721-725; *J. Chem. Phys.* **1974**, *61*, 2779-2792.

29. Hall, J.H. *J. Org. Chem.* **1983**, *48*, 1708-1712. Pirkle, W.H.; Stickler, J.C. *J. Am. Chem. Soc.* **1970**, *92*, 7497-7499. Wamhoff, H.; Wald, K. *Chem. Ber.* **1977**, *110*, 1699-1715. See also: Hall, J.H.; Bigard, W.E.; Fargler, J.M.; Jones, M.L. *J. Org. Chem.* **1982**, *47*, 1459-1462.

30. Kjell, D.P.; Sheridan, R.S. *J. Photochem.* **1985**, *28*, 205-213; *J. Am. Chem. Soc.* **1984**, *106*, 5368-5370.

31. Such an electron transfer appears to be energetically feasible. By applying the Weller equation as suggested by Kjell and Sheridan,³⁰ and substituting an estimate of the oxidation potential for **49** of 1.67 V³² electron transfer from **49** to ¹MTAD* is found to be exothermic by ca. 4 kcal mol⁻¹ (cf. transfer from naphthalene ($E_{\frac{1}{2}}^{\text{ox}} = 1.71$ V), which is calculated to be exothermic by 2-3 kcal mol⁻¹³⁰).

32. By using the oxidation potential for *endo,endo*-2,4-dimethylbicyclobutane, obtained from an empirical correlation between

calculated IP and experimental oxidation potentials. Gassman, P.G.; Mullins, M.J.; Richtsmeier, S.; Dixon, D.A. *J. Am. Chem. Soc.* **1979**, *101*, 5793-5797.

33. Ab initio calculations find the inversion barrier in 45^+ to be ca. 19 kcal mol⁻¹. Hoz, S.; Livneh, M.; Cohen, D. *J. Am. Chem. Soc.* **1987**, *109*, 5149-5156.

34. (a) Sharpless, K.B.; Young, M.W. *J. Org. Chem.* **1975**, *40*, 947-949.
(b) Reich, H.J.; Wollowitz, S.; Trend, J.E.; Chow, F.; Wendelborn, D.F. *J. Org. Chem.* **1978**, *43*, 1697-1705. Clive, D.L.J. *Tetrahedron* **1978**, *34*, 1049-1132.

35. Grieco, P.A.; Gilman, S.; Nishizawa, M. *J. Org. Chem.* **1976**, *41*, 1485-1486.

36. Adam, W.; DeLucchi, O.; Erden, I. *J. Am. Chem. Soc.* **1980**, *102*, 4806-4809. Martin, M.; Roth, W.R. *Chem. Ber.* **1969**, *102*, 811-814. Cookson, R.C.; Gilani, S.S.H.; Stevens, I.D.R. *J. Chem. Soc., C* **1967**, 1905-1909.

37. The major isolable product displayed a ¹H NMR pattern attributed to a monosubstituted olefin (δ 6.66 (dd, J = 11,18 Hz, 1 H), 5.62 (dd, J = 1,18 Hz, 1 H), 5.31 (dd, J = 1,11 Hz, 1 H)) as well as broad and sharp singlets (in a 1:3 ratio) at δ 7.33 and 2.11, respectively.

38. Jösel, R.; Schröder, G. *Lieb Ann. Chem.* **1980**, 1428-1437.

39. See, for example, James, D.R.; Birnberg, G.H.; Paquette, L.A. *J. Am. Chem. Soc.* **1974**, *96*, 7465-7473. Wingard, R.E., Jr.; Russell, R.K.; Paquette, L.A. *J. Am. Chem. Soc.* **1974**, *96*, 7474-7482.

40. Heyman, M.; Bandurco, V.T.; Snyder, J.P. *J. Chem. Soc. Chem. Commun.* **1971**, 297-298.

41. If the diazene is sufficiently labile the complex is apparently bypassed. (a) Askani, R. *Chem. Ber.* **1965**, *98*, 2551-2555. (b) Berson, J.A.; Davis, R.F. *J. Am. Chem. Soc.* **1972**, *94*, 3658-3659.

42. Askani, R.; Wieduwilt, M. *Chem. Ber.* **1976**, *109*, 1887-1897. Berson, J.A.; Olin, S.S. *J. Am. Chem. Soc.* **1970**, *92*, 1086-1087.

43. Flynn, C.R.; Michl, J. *J. Am. Chem. Soc.* **1974**, *96*, 3280-3288; **1973**, *95*, 5802-5803. Rieber, N.; Alberts, J. Lipsky, J.A. Lemal, D.M. *J. Am. Chem. Soc.* **1969**, *91*, 5668-5669. Engel, P.S.; Bishop, D.J. *J. Am. Chem. Soc.* **1975**, *97*, 6754-6762.

44. (a) Dowd, P.; Paik, Y.H. *Tet. Lett.* **1986**, *27*, 2813-2816. (b) Dowd, P.; Chang, W.; Paik, Y.H. *J. Am. Chem. Soc.* **1986**, *108*, 7416-7417.

45. PTAD (-60°C)⁴⁶ and benzoquinones (-70°C)⁴⁷ have also been used.

46. Gisin, M.; Wirz, J. *Helv. Chim. Acta* **1976**, *59*, 2273-2277.

47. Masamune, S.; Nakamura, N.; Spadaro, J. *J. Am. Chem. Soc.* **1975**, *97*, 918-919.

48. We have found no evidence for the intermediacy of **2** in the Cu(II) oxidation. Nickel peroxide oxidation (see below) at room temperature, however, provides the characteristic dimeric decomposition products of **2**.

49. Dervan, P.B.; Squillacote, M.E.; Lahti, P.M.; Sylwester, A.P.; Roberts, J.D. *J. Am. Chem. Soc.* **1981**, *103*, 1120-1122. Duan, D.C.; Dervan, P.B. *J. Org. Chem.* **1983**, *48*, 970-976.

50. The reaction requires less than 15 min if the nickel peroxide is sufficiently active (see **Experimental**).

51. Photolysis of these dimers produces neither the EPR nor the optical spectra to be discussed below.

52. The oxidation of similar semicarbazides at -50°C **3a** works with nickel peroxide that seems insufficiently active for the oxidation of **66** at -78°C .

53. George, M.V.; Balachandran, K.S. *Chem. Rev.* **1975**, *75*, 491-519, and references therein. Terabe, S.; Konaka, R. *J. Am. Chem. Soc.* **1969**, *91*, 5655-5657. Konaka, R.; Terabe, S.; Kuruma, K. *J. Org. Chem.* **1969**, *34*, 1334-1337.

54. Burger, U.; Mentha, Y.; Thorel, J.P. *Helv. Chim. Acta* **1986**, *69*, 670-675. Gleiter, R.; Zimmermann, H.; Sander, W.; Hanck, M. *J. Org. Chem.* **1987**, *52*, 2644-2653.

55. Kaisaki, D.A.; Dougherty, D.A. *Tet. Lett.* **1987**, *28*, 5263-5266.

56. Closs, G.L.; Closs, L.E. *J. Am. Chem. Soc.* **1963**, *85*, 2022-2023.

57. Olsen, H.; Oth, J.F.M. *Angew. Chem., Int. Ed. Engl.* **1981**, *20*, 983-984.

58. (a) Oth, J.F.M.; Olsen, H.; Snyder, J.P. *J. Am. Chem. Soc.* **1977**, *99*, 8505-8506. (b) Olsen, H.; Snyder, J.P. *J. Am. Chem. Soc.* **1977**, *99*, 1524-1536.

59. Snyder, J.P.; Bandurco, V.T.; Darack, F.; Olsen, H. *J. Am. Chem. Soc.* **1974**, *96*, 5158-5166.

60. Both the chemical shifts and the splitting observed are consistent with the allene moiety. Gordon, A.J.; Ford, R.A. *The Chemist's Companion*; Wiley: New York, 1972; pp. 260, 279. For a related vinyl allene system, see Delbecq, F.; Baudouy, R.; Goré, J. *Nouv. J. Chim.* **1979**, *3*, 321-327.

61. Ring opening of **69** could conceivably be facilitated relative to cyclobutene by a combination of strain and substituent effects. See, for example, the activation parameters for substituted cyclobutenes in Gajewski, J.J. *Hydrocarbon Thermal Isomerizations*; Academic: New York, 1981; pp. 47-51.

62. The error in each of these values is estimated as ± 0.0003 , by spectral simulation: see ref. 63.

63. Simulations were performed on an IBM PC/AT with a FORTRAN program obtained from E.F. Hilinski, which was originally written by J.M. McBride. The simulation uses the method of Kottis, P.; Lefebvre, R. *J. Chem. Phys.* **1963**, *39*, 393-403; **1964**, *41*, 379-393 (see also ref. 64a). The program was adapted for use on the PC/AT by R. Jain (see Jain, R. Ph.D. thesis, California Institute of Technology, 1987) and modified to incorporate isotropic hyperfine splitting.

64. (a) Wasserman, E.; Snyder, L.C.; Yager, W.A. *J. Chem. Phys.* **1964**, *41*, 1763-1772. (b) deGroot, M.S.; van der Waals, J.H. *Physica* **1963**, *29*, 1128-1132. The intensity of the double-quantum line is much more power-dependent than the surrounding $\Delta m_s = 1$ lines. In addition, this central line vanishes reversibly at very low power and at higher temperature, and irreversibly upon photochemical destruction of the biradical (see below).

65. Wertz, J.E.; Bolton, J.R. *Electron Spin Resonance: Elementary Theory and Practical Applications*; McGraw-Hill: New York, 1972; Ch. 10, pp. 223-257.

66. (a) Dowd, P. *J. Am. Chem. Soc.* **1966**, *88*, 2587-2589. (b) Claesson, O.; Lund, A.; Gillbro, T.; Ichikawa, T.; Edlund, O.; Yoshida, H. *J. Chem. Phys.* **1980**, *72*, 1463-1470.
67. Platz, M.S.; McBride, J.M.; Little, R.D. Harrison, J.J.; Shaw, A.; Potter, S.E.; Berson, J.A. *J. Am. Chem. Soc.* **1976**, *98*, 5725-5726.
68. Wright, B.B.; Platz, M.S. *J. Am. Chem. Soc.* **1983**, *105*, 628-630. Goodman, J.L.; Berson, J.A. *J. Am. Chem. Soc.* **1985**, *107*, 5409-5424; **1984**, *106*, 1867-1868.
69. de Groot, M.S.; Hesselmann, I.A.M.; van der Waals, J.H. *Mol. Phys.* **1969**, *16*, 45-60.
70. Brandon, R.W.; Closs, G.L.; Davoust, C.E.; Hutchison, C.A., Jr.; Kohler, B.E.; Silbey, R. *J. Chem. Phys.* **1965**, *43*, 2006-2016. Wasserman, E.; Trozzolo, A.M.; Yager, W.A.; Murray, R.W. *J. Chem. Phys.* **1964**, *40*, 2408-2410.
71. Hilinski, E.F.; Dougherty, D.A.; Berson, J.A., unpublished results.
72. (a) Feller, D.; Davidson, E.R.; Borden, W.T. *J. Am. Chem. Soc.* **1982**, *104*, 1216-1218. (b) Davidson, E.R.; Borden, W.T.; Smith, J. *J. Am. Chem. Soc.* **1978**, *100*, 3299-3302. (c) Borden, W.T.; Davidson, E.R. *J. Am. Chem. Soc.* **1977**, *99*, 4587-4594.
73. Borden, W.T.; Davidson, E.R.; Feller, D. *Tetrahedron* **1982**, *38*, 737-739.
74. Rule, M.; Matlin, A.R.; Seeger, D.E.; Hilinski, E.F.; Dougherty, D.A.; Berson, J.A. *Tetrahedron* **1982**, *38*, 787-798.

75. We use the term "localized" to describe those biradicals whose unpaired electrons are conjugatively insulated from one another by saturated carbon atoms.

76. Feller, D.; Borden, W.T.; Davidson, E.R. *J. Chem. Phys.* **1981**, *74*, 2256-2259. See also ref. 77, pp 25-27.

77. Borden, W.T. In ref. 10; Ch. 1, pp. 1-72.

78. Dowd, P.; Paik, Y.H. *J. Am. Chem. Soc.* **1986**, *108*, 2788-2790.

79. For a general discussion of $\Delta m_s = 2$ hyperfine, see Grivet, J.-Ph. *Mol. Phys.* **1970**, *19*, 389-398. See also ref. 64a.

80. (a) Constant a_2 was determined from simulations of both 1 and 1- d_2 spectra, and we estimate its accuracy to be (conservatively) ± 0.4 G. Because our primary concern is the ratio of spin densities at the ring and methylene positions, we fixed a_2 and systematically varied a_1 from 5.90 to 9.56 G (Figure 2-13). Simulations with $a_1 = 7.03, 7.31$, and 7.59 G are clearly acceptable, while those with $a_2 = 6.47$ and 8.15 G are not. (The use of a slightly different value for a_2 does not increase the range of values for a_1 .) We therefore place a conservative error limit of ± 0.6 G on a_1 . (The ratio of the coupling constants, $a_1/a_2 = 1.24 \pm 0.1$.) (b) The absolute error limits on the spin densities are thus ± 0.05 on ρ_1 and ± 0.03 on ρ_2 , and the ratio of spin densities is 1.15 ± 0.1 . Inspection of Figure 2-13 reveals that this ratio is significantly different from 1.0 ($a_1 = 6.47$ G, $\rho_1/\rho_2 = 1.02$, provides an unsatisfactory simulation) and substantially different from the Hückel ratio of 1.5, corresponding to $a_1 = 9.56$ G.

81. Kottis, P.; Lefebvre, R. *J. Chem. Phys.* **1963**, *39*, 393-403. See also ref. 65.

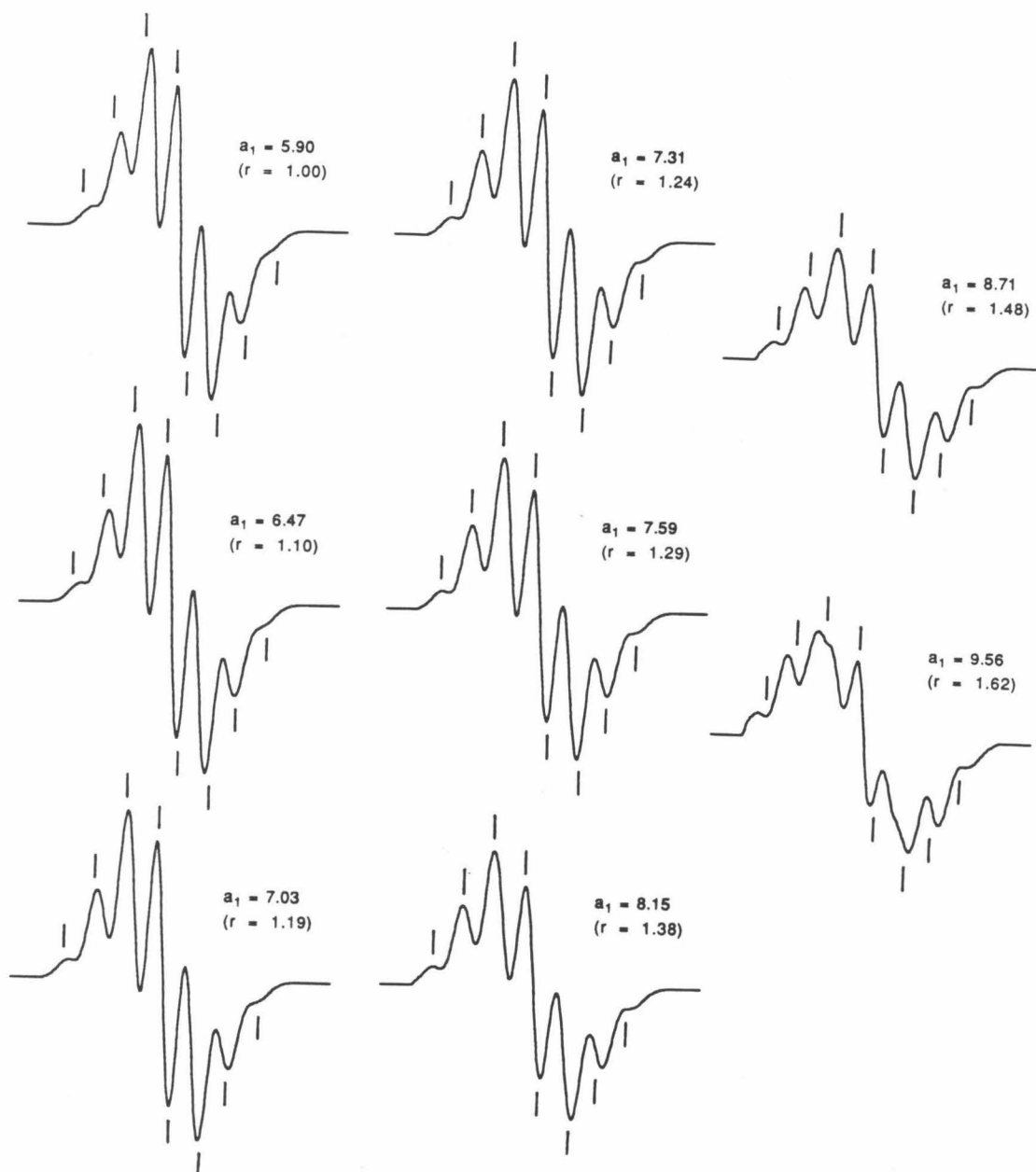


Figure 2-13. Computer-simulated $^{63}\Delta m_s=2$ hyperfine splitting for 1. The simulations were performed with $a_2 = 5.90$ G (established in part by the spectrum of 1- d_2 — see Figure 2-2) and $a_1 = 9.56$ G (the value corresponding to the Hückel spin densities) to 5.90 G (correspond to $\rho_1 < \rho_2^{113}$). A linewidth of 5.5 G was used for each spectrum. The marks designate the peak positions in the experimental spectrum (Figure 2-2a).

82. Morton, J.R. *Chem. Rev.* 1964, 64, 453-471. See also ref. 65, Ch 6-8, pp. 112-191.

83. This has been demonstrated computationally for π -electron free radicals. For unit spin density the principal components of the α -proton hyperfine interaction tensor are approximately -30 , -90 , and -60 MHz,⁸² the z (third) axis being chosen as that perpendicular to the molecular plane and the x (first) axis defined to lie along to the C-H bond. This tensor can be separated into isotropic (-60 MHz) and traceless anisotropic ($+30$, -30 , 0 MHz) parts. It has been demonstrated that, for planar carbon radical centers, the separation between the peaks of maximum amplitude will be the median absolute value of the principal elements of the total tensor, i.e., -60 MHz, which is the isotropic value. Smaller lines should appear at separations of 30 and 90 MHz. These peaks would, in principle, be visible beyond the outer edges of the Figure 2-2 spectra, but they are apparently too small to be seen under the conditions used. Sternlicht, H. *J. Chem. Phys.* 1960, 33, 1128-1132. See also Lefebvre, R. *J. Chem. Phys.* 1960, 33, 1826-1829. The spectra of several free radicals have been found to display isotropic α -proton splittings. Cochran, E.L.; Adrian, F.J.; Bowers, V.A. *J. Chem. Phys.* 1961, 34, 1161-1175. Agscough, P.B.; Thompson, C. *Trans. Faraday Soc.* 1962, 59, 1477-1494.

84. Yoshida, H.; Edlund, O. *Chem. Phys. Lett.* 1976, 42, 107-110. Yamaguchi, T.; Irie, M.; Yoshida, H. *Chem. Lett.* 1973, 975-978.

85. This is evident from a simple PMO analysis.

86. If the singlet state is populated in competition with the triplet the temperature dependence of the EPR signal intensity is given by $I = 3C/T(3 + e^{-\Delta E/RT})$, where $\Delta E = E_S - E_T$. Including a data point obtained near 8

K in the data set of Figure 2-4 (and allowing flexibility in the intercept as an approximation to the more general Curie-Weiss Law), a reasonable fit to the curve can be obtained by using $\Delta E = -15$ to -20 cal mol⁻¹ (see Figure 2-14). Because we have found the signal to be saturated in the temperature range that shows the detectable curvature, this value represents a (conservative) lower limit on ΔE , *i.e.* either $\Delta E \approx 0$ or the triplet is the ground state of 1.⁸⁷ We also note that any thermal population of the singlet state would be virtually undetectable in the present case. As a result of the statistical factor favoring the triplet, at most 25% of its population can be lost to a higher-lying singlet at infinite temperature. The Curie effect serves to overwhelm any small loss in signal intensity caused by population of a singlet state. Thus, any deviation from linearity caused by this effect would be well within the experimental error of the data of Figure 2-4. Curves calculated ("CURIE" – Appendix 3) for various singlet-triplet gaps are presented in Figure 2-14 along with the experimental I vs T^{-1} data (the 8 K point is included).

87. For a similar analysis, see: Seeger, D.E.; Lahti, P.M.; Rossi, A.R.; Berson, J.A. *J. Am. Chem. Soc.* **1986**, *108*, 1251-1265. See also: Breslow, R.; Chang, H.W.; Hill, R.; Wasserman, E. *J. Am. Chem. Soc.* **1967**, *89*, 1112-1119.

88. Slow decay is observed in a variety of solvents, but, interestingly, the EPR signal intensity does not decrease perceptibly at 77 K in 1:1 EtOH/MeOH.

89. The most probable rate constant in the distribution, k_0 , is given by $k_0 = c^2/6$, where c is the slope of the plot. Doba, T.; Ingold, K.U.; Siebrand, W. *Chem. Phys. Lett.* **1984**, 339-342. Doba, T.; Ingold, K.U.; Siebrand, W.;

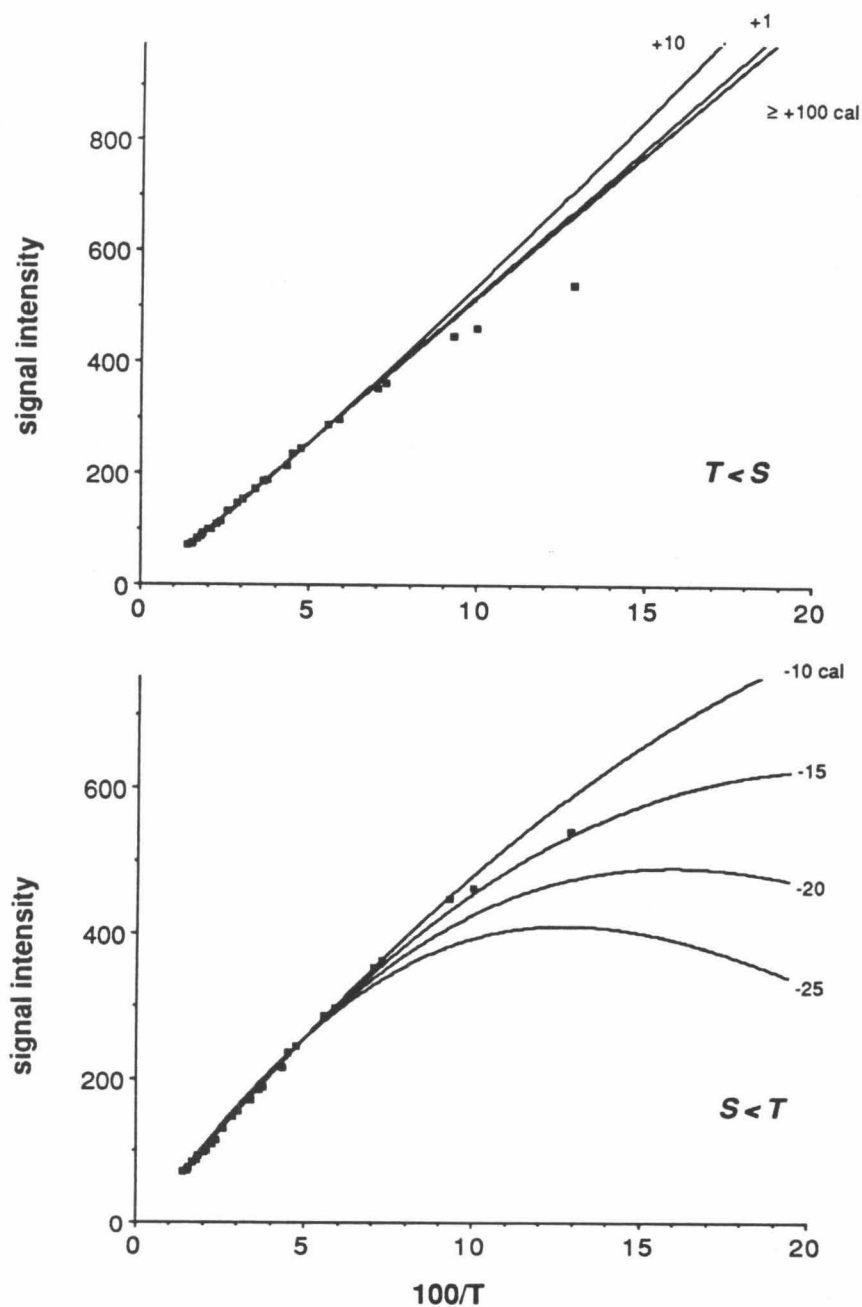


Figure 2-14. Curie law plots of the Figure 2-4 data points along with the curves calculated ("CURIE" - Appendix 3) according to the equation $I = 3C/T(3 + e^{-\Delta E/RT})$, where $\Delta E = E_S - E_T$ (ΔE is given next to each curve). The curves were fitted to the data so that they intersect the least-squares line of Figure 2-4 at 20 and 80 K.

Wildman, T.A. *J. Phys. Chem.* 1984, 88, 3165-3167. The half-life is then given by $t_{\frac{1}{2}} = (\ln 2) / 6k_0$.

90. In the limit that every singlet biradical present is instantly converted to photoproduct(s), the maximum photochemical destruction rate of the triplet, $-dT/dt$, is $k_{TS}[T]$, the rate of intersystem crossing to the singlet. If we estimate $-dT/dt$ from the maximum slope of the EPR signal intensity function of Figure 2-6a as 10^{-3} s^{-1} , and the concentration of triplet 1 as 10^{-4} M (see below), k_{TS} would be 10 s^{-1} . (This value is low by at least 2-3 orders of magnitude, since the rate used is much less than the maximum photochemical destruction rate we have observed at 4 K; $k_{TS} = 10^4 \text{ s}^{-1}$ would be more realistic.) If $\log A$ for isc is assumed to be 10, as an upper limit,⁹¹ E_a for T→S, or ΔE , is $\leq 150 \text{ cal mol}^{-1}$ (using $k_{TS} = 10^4 \text{ s}^{-1}$, and $\log A = 8$, $\Delta E = 70 \text{ cal mol}^{-1}$).

91. Turro, N.J. *Modern Molecular Photochemistry*; Benjamin/Cummings: Menlo Park, CA, 1978; pp 185-187.

92. Ref. 91, p. 87.

93. For example, see ref. 91, Ch. 5, pp. 76-152.

94. (a) Chisholm, W.P.; Yu, H.L.; Murugesan, R.; Weissman, S.I.; Hilinski, E.F.; Berson, J.A. *J. Am. Chem. Soc.* 1984, 106, 4419-4423. (b) Chisholm, W.P.; Weissman, S.I.; Burnett, M.N.; Pagni, R.M. *J. Am. Chem. Soc.* 1980, 102, 7103-7104. (c) Kottis, P.; Lefebvre, R. *J. Chem. Phys.* 1964, 41, 3660-3661. Lhoste, J.-M.; Haug, A.; Ptak, M. *J. Chem. Phys.* 1966, 44, 648-654; 654-657. (d) El-Sayed, M.A.; Siegel, S. *J. Chem. Phys.* 1966, 44, 1416-1423.

95. (a) Suzuki, H. *Electronic Absorption Spectra and Geometry of Organic Molecules*; Academic: New York, 1967; pp. 499-501. (b) Rau, H.

Angew. Chem., Int. Ed. Engl. **1973**, *12*, 224-235. Mirbach, M.J.; Liu, K.C.; Mirbach, M.F. Cherry, W.R.; Turro, N.J.; Engel, P.S. *J. Am. Chem. Soc.* **1978**, *100*, 5122-5129.

96. Albrecht, A.C. *J. Molec. Spectroscopy* **1961**, *6*, 84-108.

97. See the discussion in ref. 83.

98. In contrast, the splitting in the x and y directions should be quite different from the isotropic splitting. We can estimate the expected splittings from the angles of the C-H bonds with the molecular axes and the known form of the hyperfine coupling tensor.⁹⁷ The magnitude of the coupling is given by

$$(A^2 \cos^2 \theta_a + B^2 \cos^2 \theta_b + C^2 \cos^2 \theta_c)^{\frac{1}{2}},$$

where A , B , and C are the hyperfine tensor elements of the C-H bond,⁸³ and the θ s are the angles between these tensor elements and the molecular axis of interest. The methylene protons should produce a splitting in the x direction of approximately $((30 \text{ MHz})^2 \cos^2 60^\circ + (90 \text{ MHz})^2 \cos^2 30^\circ)^{\frac{1}{2}} = 79.4 \text{ MHz}$ for unit spin density, 1.32 times the isotropic value of 60 MHz.⁸³ Thus, the splitting should be $1.32 \times 5.9 \text{ G} = 7.8 \text{ G}$. The methine protons should produce a splitting of $(90/60) \times 7.3 \text{ G} = 11.0 \text{ G}$ in this direction. In the y direction, the methylene splitting should be approximately $((30 \text{ MHz})^2 \cos^2 30^\circ + (90 \text{ MHz})^2 \cos^2 60^\circ)^{\frac{1}{2}} = 52.0 \text{ MHz}$ for unit spin density, or 0.87 times the isotropic value. The splitting should then be $0.87 \times 5.9 \text{ G} = 5.1 \text{ G}$. For the methine protons, the splitting should be $(30/60) \times 7.3 \text{ G} = 3.7 \text{ G}$. See ref. 65, pp 135, 145. For a similar treatment of the splitting in the naphthalene spectrum, see Hutchison, C.A., Jr.; Magnum, B.W. *J. Chem. Phys.* **1961**, *34*, 908-922.

99. Horning, A.W.; Hyde, J.S. *Mol. Phys.* **1963**, *6*, 33-41.

100. Rotation of the sample tube by 90° transforms the X-depleted assembly (see Figure 2-7c) into one with primary orientations X_z , X_y , Y_z , and Z_y . As expected, such a rotation then transforms the spectrum of Figure 2-9b into one whose X-transitions are roughly twice as intense as their neighbors.

101. Each vibronic peak has been found to carry the same transition moment (see **Experimental**).

102. The intensity of the scattered light depends on λ^{-4} . Berne, B.J.; Pecora, R. *Dynamic Light Scattering*; Wiley: New York, 1976; p. 37.

103. Ideally, before such a photolysis, X, Y, and Z orientations should be present in a 2:3:3 ratio.

104. Orchin, M.; Jaffé, H.H. *Symmetry, Orbitals, and Spectra*; Wiley: New York, 1971; Ch. 8, pp. 204-230.

105. Cotton, F.A. *Chemical Applications of Group Theory*; Wiley: New York, 1971; pp. 316-320.

106. A symmetric product $\chi_{1k} \chi_{2e}$ could, of course, arise if χ_{1k} and χ_{2e} were both of the same symmetry but other than A_g . However, the vibronic series would then be $k, l = 0,0; 0,2; 0,4; 1,1; 1,3; 1,5; 2,0; 2,2$; etc. The 1,0 band would then be absent (*i.e.*, the second progression would be displaced), inconsistent with the observed spectra.

107. For a general discussion of spin polarization, see ref. 77, pp 15-17.

108. Borden, W.T.; Davidson, E.R.; Feller, D. *Tetrahedron* **1982**, *38*, 737-739.

109. See ref. 77, pp 25-27.

110. The factor of $\frac{1}{2}$ is included for triplets when the exchange interaction is much larger than $|A_0|$. ($a = hA_0/g\beta$) Reitz, D.C.; Weissman, S.I. *J. Chem. Phys.* **1960**, *33*, 700-704. See also ref. 65, pp. 250-255.

111. Use of the more accurate relationship^{77,112a}

$$a_i = \frac{1}{2}(Q_i p_i + Q_j p_j)$$

where the second term refers to the negative spin density on the adjacent carbon (j) with $Q_j = -1.9$ G,^{77,112a} does not significantly change the calculated spin densities. Its application to the data presented involves solving three equations, the third describing normalization of the total spin density.^{77,112a}

112. (a) Gold, A. *J. Am. Chem. Soc.* **1969**, *91*, 4961-4963. (b) Gondo, Y.; Maki, A.H. *J. Chem. Phys.* **1969**, *50*, 3638-3639.

113. We use $Q = 24.4$ and 26.2 G for CH_2 and CH centers, respectively. See ref 65, pp. 121.

114. Dowd, P.; Gold, A.; Sachdev, K. *J. Am. Chem. Soc.* **1968**, *90*, 2715-1716.

115. Note, however, that correlation of the $1b_{1u}$ electrons should increase the spin density at the ring methine positions more than at the exocyclic methylenes because the methine carbons bear the larger AO coefficients (Figure 2-10).

116. Hashimoto, K.; Fukutome, H. *Bull. Chem. Soc. Japan* **1981**, *54*, 3651-3658.

117. Because $2b_{1u}$ is free to adjust its ring and exocyclic NBMO coefficients in response to electron correlation demands, the RHF spin densities on the methylene carbons are artificially low.^{72c}

118. This problem has been addressed most recently by ab initio CI calculations,⁷⁶ and earlier with UHF^{112a} and PPP^{112b} wavefunctions.

119. The calculations were performed by using the previously mentioned point-charge method⁷⁴ and Hückel wavefunctions. To compensate for an apparent error in the program used, the signs of the energy levels have been reversed. (The calculated levels for **4** are then quite close to those calculated with an RHF wavefunction.⁷⁶)

120. The D value for TMM (Table 2-1) has been shown to be positive^{66b} in accord with the theoretical results.^{76,112}

121. The authors^{94a} assigned the outer pair of $\Delta m_s = 1$ transitions to the z -axis (perpendicular to the molecular plane) of **9**, by analogy with TMM (**4**). This is intuitively reasonable and is also consistent with the observation of similar D values for the two (Table 2-1), both of which are positive.^{94a,66b} Photolysis of diazene **10** with light of $E // H_0$ causes enhancement of the inner pair of $\Delta m_s = 1$ lines of **9**.^{94a} The known transition dipole moment of the azo chromophore⁹⁵ requires that these EPR lines be assigned to the biradical x -axis.¹²² (As defined in text, the x -axis lies along the exocyclic double bond.) This assignment is entirely consistent with structural considerations. On going from TMM (**4**) to **9** two radical centers are moved closer together, and the dipolar coupling in the y direction should become larger than that in the x . The energy level pattern calculated (method of ref. 74; Hückel wavefunction) for **9** supports this idea (i.e., $|y| > |x|$). Accordingly, we assign the $\Delta m_s = 1$ transitions of **9** as $z, y, x; x, y, z$. This appears to be at variance with the assignment made in ref. 94a.

122. Because diazene 10 has C_s symmetry, a transition between A'' orbitals, such as the azo n_- and π^* , must be polarized in the mirror plane. Rigorously, therefore, photolysis of 10 could produce biradicals 9 with their x - or z -axes aligned with the E vector of the photolysis beam. However, the local symmetry of the azo group (C_{2v}) provides for the formation only of the x -orientation, in accord with the observed spectra.

123. The azo π, π^* excitation is $b_2 \rightarrow a_2$, and therefore carries b_1 polarization ($a_2 \times b_1 \times b_2 = a_1$).

124. Specifically, viable excitations are: (1) from the in-phase combination of C—C double bonds, π_+ , and/or the in-phase combination of nitrogen lone pair MOs, n_+ , to the in-phase combination of antibonding π -orbitals, π^*_+ , all of a_1 symmetry; or (2) from π_- and/or the azo π -orbital to π^*_- , all of b_1 symmetry. However, none of the resulting states would appear to overlap strongly with the n_-, π^* , so the matrix element for mixing should be small. See ref. 91, pp. 96-97.

125. Turro, N.J.; Mirbach, M.H.; Harrit, N.; Berson, J.A.; Platz, M.S. *J. Am. Chem. Soc.* **1978**, *100*, 7653-7568. The source of the extremely weak 428-nm band is uncertain: see, for example, ref. 126.

126. Gisin, M.; Wirz, J. *Helv. Chem. Acta* **1983**, *66*, 1556-1568.

127. Roth, W.R.; Biermann, M.; Erker, G.; Jelich, K.; Gerhartz, W.; Görner, H. *Chem. Ber.* **1980**, *113*, 588-597.

128. Roth, W.R.; Langer, R.; Bartmann, M.; Stevermann, B.; Maier, G.; Reisenauer, H.P.; Sustmann, R.; Müller, W. *Angew. Chem., Int. Ed. Engl.* **1987**, *26*, 256-258.

129. Migirdicyan, E.; Baudet, J. *J. Am. Chem. Soc.* **1975**, *97*, 7400-7404.

130. Hasler, E.; Gassmann, E.; Wirz, J. *Helv. Chim. Acta* **1985**, *68*, 777-788. See also: Muller, J.-F.; Muller, D.; Dewey, H.J.; Michl, J. *J. Am. Chem. Soc.* **1978**, *100*, 1629-1630. Gisin, M.; Rommel, E.; Wirz, J.; Burnett, M.N.; Pagni, R.M. *J. Am. Chem. Soc.* **1979**, *101*, 2216-2218.

131. Callomon, J.H.; Dunn, T.M.; Mills, I.M. *Phil. Trans. Roy. Soc.* **1966**, A259, 499-532.

132. Menche, D. *Helv. Chim. Acta* **1966**, *49*, 1278-1283.

133. Blomquist, A.T.; Maitlis, P.M. *Proc. Chem. Soc. London*, **1961**, 332.

134. Maier, G.; Reisenauer, H.P.; Rohde, B.; Dehnicke, K. *Chem. Ber.* **1983**, *116*, 732-740.

135. Bodily, D.M.; Dole, M. *J. Chem. Phys.* **1966**, *45*, 1428-1432.

136. Pranata, J.; Dougherty, D.A. *J. Am. Chem. Soc.* **1987**, *109*, 1621.

See also ref. 126.

137. Ref. 91, pp. 92-93; ref. 104, p. 227; ref. 95a, p. 86.

138. Still, W.C.; Kahn, M.; Mitra, A. *J. Org. Chem.* **1978**, *43*, 2923-2925.

139. The analysis employed the FORTRAN program "QEPR", written by Jeff Gelles at Caltech (1984).

140. Katz, T.J.; Wang, E.J.; Acton, N. *J. Am. Chem. Soc.* **1971**, *93*, 3782-3783. Katz, T.J.; Roth, R.J.; Acton, N.; Carnahan, E.J. *Org. Synth.* **1973**, *53*, 157. The concentration of benzvalene was determined by NMR by using an internal standard.

141. Christl, M.; Brüntrup, G. *Chem. Ber.* **1974**, *107*, 3908-3914.

142. Fieser, L.F.; Fieser, M. *Reagents for Organic Synthesis*, Vol. 1; Wiley: New York, 1967; p. 584.

143. Corey, E.J.; Venkateswarlu, A. *J. Am. Chem. Soc.* **1972**, *94*, 6190-6191.
144. This assignment is made tentatively on the basis of the chemical shifts¹⁸ and coupling constants of protons in similar systems. Griesbaum, K.; Mach, H.; Hittich, R. *Chem. Ber.* **1982**, *115*, 1911-1921. Lasne, M.-C.; Thuillier, A. *J. Chim. Phys.-Phys. Chim. Biol.* **1977**, *74*, 799-808.
145. Cookson, R.C.; Gupte, S.S.; Stevens, I.D.R.; Watts, C.T. *Org. Synth.* **1971**, *51*, 121-127.
146. Stickler, J.C.; Pirkle, W.H. *J. Org. Chem.* **1966**, *31*, 3444-3445.
147. Crossland, R.K.; Servis, K.L. *J. Org. Chem.* **1970**, *35*, 3195-3196.
148. Schaefer, J.P.; Higgins, J.G.; Shenoy, P.K. *Org. Synth.*, coll. vol. 5; Wiley: New York, 1973; pp. 249-251.
149. Bauer, H. *Chem. Ber.* **1913**, *46*, 92-98.
150. Reich, H.J.; Renga, J.M.; Reich, I.L. *J. Am. Chem. Soc.* **1975**, *97*, 5434-5447.
151. Nakagawa, K.; Konaka, R.; Nakata, T. *J. Org. Chem.* **1962**, *27*, 1597-1601.
152. Rice, S.F.; Gray, H.B. *J. Am. Chem. Soc.* **1983**, *105*, 4571-4575.
153. Savitzky, A.; Golay, M.J.E. *Anal. Chem.* **1964**, *36*, 1627-1639.
154. Platz, M.S.; Berson, J.A. *J. Am. Chem. Soc.* **1980**, *102*, 2358-2364.
155. Nocera, D.G.; Winkler, J.R.; Yocom, K.M.; Bordignon, E.; Gray, H.B. *J. Am. Chem. Soc.* **1984**, *106*, 5145-5150.

Chapter 3

2,4-Dimethylenebicyclo[1.1.0]butane:

**Preparation, Spectroscopic and Chemical Characterization.
Thermal and Photochemical Interconversion of Triplet 2,4-
Dimethylene-1,3-cyclobutanediyl and Its Covalent Isomer.**

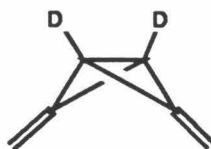
Our studies of the solution-phase thermal chemistry and photochemistry of diazene **2** were motivated in part by the prospect of generating dimethylenebicyclobutane (**3**) and studying the chemistry of this novel species. In addition, we had hoped to chemically intercept the singlet biradical, thereby demonstrating its existence as a stable structure. Such studies could eventually lead to a determination of the singlet-triplet splitting for **1**.

Although the work described herein has provided no direct information concerning the singlet biradical, we have succeeded in generating **3** and characterizing it by ^1H NMR spectroscopy. Dimethylenebicyclobutane (**3**) undergoes a novel, direct dimerization at low temperature. The facility of this reaction attests to the high strain energy of **3** and perhaps its unusual structure as well. In contrast to this singlet-manifold dimerization, which ultimately leads to a mixture of two dimers, triplet-manifold dimerization, which involves biradical **1**, provides a total of five dimers.

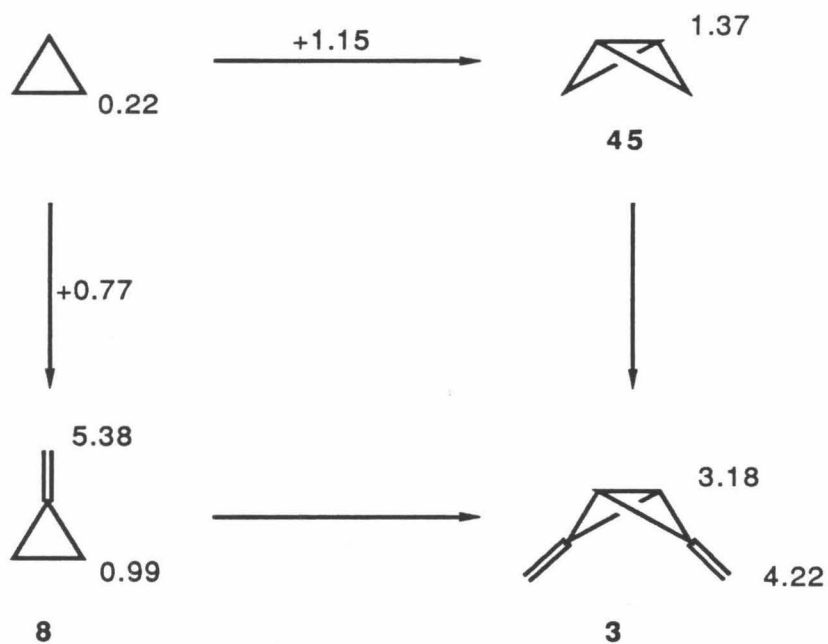
In addition, we address the photochemical ring closure of triplet **1** and ring opening of **3**. Triplet biradical **1** also undergoes surprisingly facile ring closure at $\geq 77\text{ K}$, while **3** appears to open thermally to triplet **1** near room temperature. The implications of these thermal reactions and of the dimerization of **3** for the energetics of this system are discussed.

Preparation of dimethylenebicyclobutane (3) and characterization of dimers.

^1H NMR spectroscopy of 3. Upon direct photolysis or thermolysis of diazene 2 in CD_2Cl_2 several ^1H NMR signals are observed that are attributed to stable dimeric ($\text{C}_{12}\text{H}_{12}$) products (see below). In addition, a thermally labile species is observed. This compound displays singlets at δ 4.22 and 3.18 in a 2:1 ratio; upon photolysis of 2- d_2 , only the δ 4.22 singlet is observed. These signals are assigned to 2,4-dimethylenebicyclo[1.1.0]butane (3) and its deuterated analog, 3- d_2 . These species are, in fact, the only reasonable sources of these NMR signals, given their method of generation and the chemistry to be described.¹

2- d_2 3- d_2

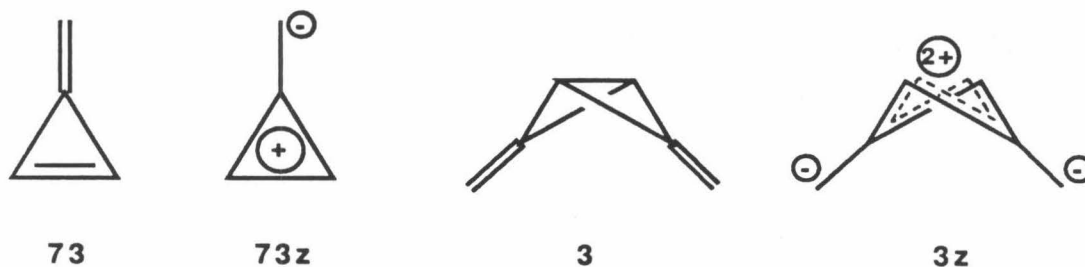
The ^1H NMR data for 3 attest to its unusual structure. In particular, its bridgehead protons appear farther downfield, and its olefinic methylenes further upfield than expected. This is illustrated by a comparison to the related compounds presented in Scheme 3-1. By analogy to the cyclopropane-methylenecyclopropane (8) transformation, one would expect the bridgehead protons of 3 to appear 2×0.77 ppm downfield of those of bicyclobutane (45), or at δ 2.91. Similarly, comparing cyclopropane and bicyclobutane leads to the (probably more reasonable) estimate that these protons should appear 1.15 ppm downfield of the ring protons of 8, at δ 2.14.⁴ In addition to the

Scheme 3-1.^a

^aRelevant ¹H NMR chemical shifts (δ) for cyclopropane,² **8**,² **45**,^{3a} and **3**.

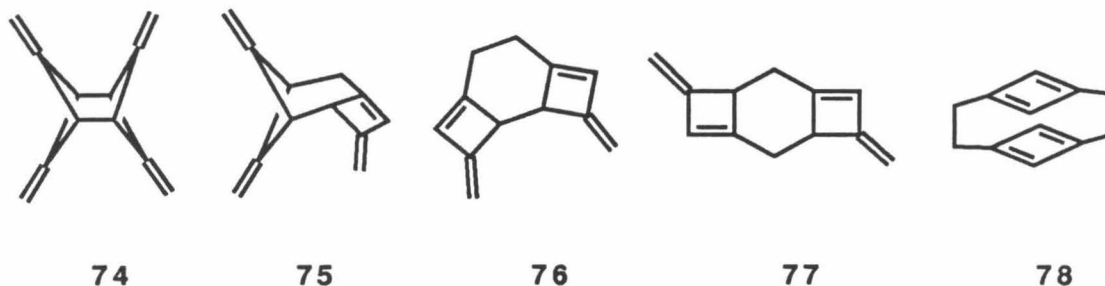
anomalous downfield shift observed for the bridgehead protons, the methylene protons of **3** are found to be about 1 ppm upfield of their expected position (Scheme 3-1).

This pattern of chemical shifts immediately brings to mind the ^1H NMR spectrum of methylenecyclopropene⁸ (**73**). The methylene protons of **73** are found upfield, and the ring protons downfield of their expected positions, implying a substantial contribution from the zwitterionic resonance form **73z**.⁸ Analogously for **3**, one would invoke resonance structure **3z** to depict electron donation from the central bond into the π^* orbitals.⁹ Because **3z** contains a cyclic 2- π -electron system, it would be expected to prefer a planar geometry. That calculations^{9,10} find **3** to be flattened relative to bicyclobutane (**45**) (see Chapter 1) is therefore consistent with a contribution from such a structure.⁹ Also consistent with this idea is a calculated lengthening of the double bonds of **3** by 0.005 Å relative to methylenecyclopropane (**8**).⁹



Potential dimers. Early in our studies we observed products from the decomposition of diazene **2** that we suspected were dimers of biradical **1**. We considered the five structures **74-78** to be the only reasonable candidates for these dimers. These structures are formally derived by simply making every

reasonable union of two biradicals **1** at their centers of unpaired electron density. The involvement of **3** (or for that matter **44**) in the dimerization should not introduce additional structures, and we have found no evidence to suggest that more structures need be considered (see below).



In order to determine their geometries and relative energies, we have carried out empirical force field (MM2¹¹) calculations on **74-77**. Dimers **76** and **77** can, of course, exist as cis or trans stereoisomers, and thus, in all, six potential dimers were considered. Figure 3-1 shows the calculated geometries of **74-77** and lists their MM2 strain energies and point group symmetries. While it is evident that all six species are energetically reasonable, several are of relatively higher energy due to the presence of boat cyclohexane moieties and the attendant eclipsing interactions. Most notably, the cis isomers, **76c** and **77c** are of significantly higher energies than their trans counterparts, whose cyclohexane rings are locked into chair conformations. Compound **74** has the highest strain energy for this reason.

The key to the potential existence of cyclobutadienophane **78**¹² is the notion that it might experience a stabilizing electronic interaction of the nominal NBMOs of the cyclobutadiene units. Such an interaction could then make **78** "three-dimensionally aromatic." Unfortunately, we have found no hint that **78** is among the dimeric products formed from **2**.

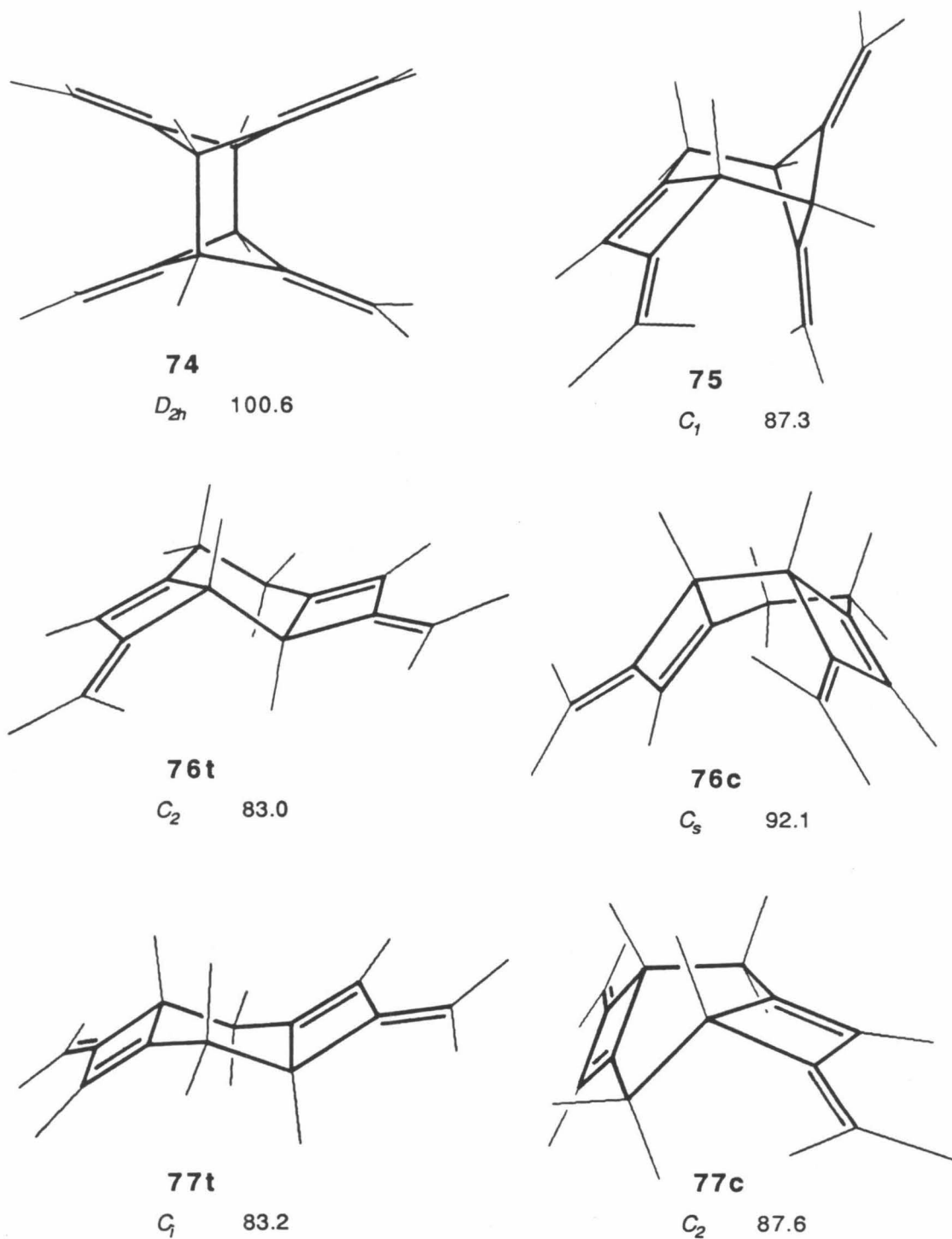


Figure 3-1. MM2 geometries and strain energies of dimers (kcal mol⁻¹).

The solution-phase thermal chemistry and photochemistry of diazene **2** afford primarily three of the seven possible dimers, which we have identified by NMR spectroscopy (see below) as **75**, **76**, and **77**. Because of their bilateral symmetries, we have not been able to conclusively assign **76** and **77** the cis or trans stereochemistry. However, we favor the trans for each on the basis of the calculated strain energies (Figure 3-1) and the mechanistic analysis to follow. Because three-dimensional structures are more aesthetically pleasing than flat, generic ones, we will anticipate the mechanistic arguments and present dimers **76** and **77** as the trans stereoisomers, but with the caveat that they have not been firmly established as such.

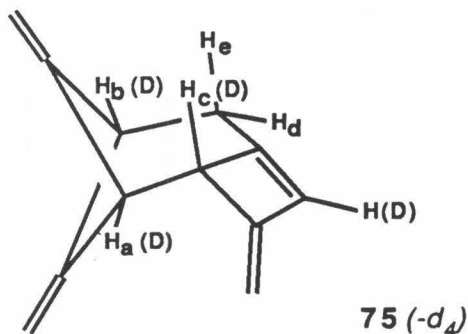
Dimerization in the singlet and triplet manifolds. Spectroscopic assignment of dimers. Direct photolysis ($\leq -78\text{ }^{\circ}\text{C}$) or thermolysis ($\geq -78\text{ }^{\circ}\text{C}$) of diazene **2** in CD_2Cl_2 ultimately provides a quantitative yield of dimers **75** and **76t** (Table 3-1) in ratios varying from 9:1 to 4:1 depending on temperature (Table 3-1). (Very small amounts of three other dimers are also detected by GC; these are assigned below, and the mechanistic implications of their formation are addressed in **Discussion**.) These compounds are thermally stable to approximately $100\text{ }^{\circ}\text{C}$ but both are air sensitive – **75** especially so. That these species are, in fact, $\text{C}_{12}\text{H}_{12}$ hydrocarbons is confirmed by GC-MS analysis of the products from **2** (M^+ , m/e 156) and from **2-*d*₂** (M^+ , m/e 160). The structural assignments are unambiguous from the 400 MHz ^1H NMR spectra of the protiated and deuterated species. (These spectra are presented as Figure 3-11 in **Experimental**.)

Table 3-1. Product mixtures from thermal and photochemical decompositions of **2**.

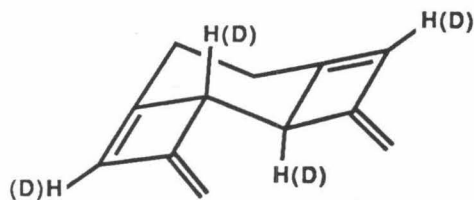
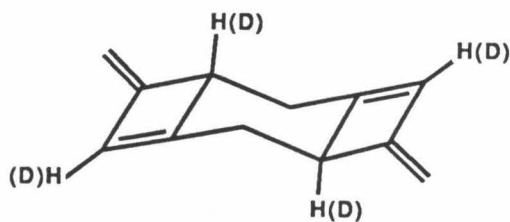
	75 ^a	76 ^{ta}	77 ^{ta}	D ₁ ^b	D ₂ ^b
Δ: -78°C	90 %	10 %	0 ^c	0 ^c	0 ^c
+40°C ^d	80 % ^b	20 % ^b	ca. 0.2 % ^b	ca. 0.1 %	trace
hν: -95°C	90 %	10 %	ca. 0.1 % ^b	ca. 0.05 %	trace
3hν: -78°C					
(0.01 M Ph ₂ CO)	40 %	10 %	50 %	ca. 1 %	ca. 1 %
(0.10 M Ph ₂ CO) ^e	60 %	10 %	30 %	ca. 1 %	ca. 1 %

^aby ¹H NMR unless otherwise noted. ^bby GC. ^cestimated as <0.005 % by GC. ^dthe experiment was conducted by dropwise addition of a cold (-78°C) solution of **2** to a 40°C flask. ^ethe composition of the initial product mixture is reported.

The major product displays five aliphatic and seven olefinic signals, one of which is attributable to a cyclobutene proton. It is therefore assigned as the only asymmetric dimer, **75**. Bridgehead protons H_a and H_b couple, while H_c appears as a slightly broadened singlet. The aliphatic methylene protons, H_d and H_e , give rise to an AB-quartet, one member of which is split further by a 4-Hz coupling to H_b . That this is the only 3-bond coupling observed is entirely consistent with the calculated dihedral angles. The H_a-H_c and H_b-H_e dihedral angles are 73° , while that between H_b and H_d is 50° . Accordingly, only the latter pair should couple significantly. This assignment is confirmed by the spectrum of **75-d₄** and is additionally supported by ^{13}C NMR data (see Experimental).



The spectrum of the minor isomer comprises six signals — three aliphatic and three olefinic — establishing it as either **76** or **77** by symmetry considerations. The key to its assignment as **76** is the observation that the bridgehead methines appear as a singlet, whereas those of **77** must couple with the neighboring methylene protons. Again, although we cannot distinguish **76t** from **76c**, we will refer to this product as **76t** for reasons to be discussed later.

**76t(-d₄)****77t(-d₄)**

Triplet sensitized photolysis of diazene **2** in CD_2Cl_2 affords three dimers that are easily observed by ^1H NMR and two others, **D₁** and **D₂**, each in approximately 1% yield (Table 3-1), which are seen by GC only. The three major products are **75**, **76t**, and a new dimer whose six-signal ^1H NMR spectrum, GC retention time, and GC/MS fragmentation pattern are very similar to those of **76t**. The distinguishing characteristic of the new dimer, however, is that the ^1H NMR signal of its bridgehead methines is split by coupling to the neighboring methylenes, and it must therefore be **77** (we will refer to it as **77t**). Consistent with this assignment is the ^1H NMR spectrum of **77t-d₄**, in which the methylene proton multiplets have collapsed to doublets. With regard to the minor (1%) dimers, **D₁** and **D₂**, we currently have no structural information except that the mass spectrum of **D₁** is almost identical to that of **77t**, while **D₂** displays a unique MS fragmentation pattern, but one more like that of **75** than **76t** or **77t** (see **Experimental**). Control experiments have demonstrated that neither **77t** nor the minor dimers **D₁** and **D₂** are produced upon sensitized photolysis of **75** and **76t**.

The addition of 0.8 atm of O_2 completely shuts down dimer formation (although **2** is still destroyed) in the sensitized photolysis,¹⁴ while it has no effect on the thermal dimerization.^{15,17} Oxygen is an excellent trap for triplet

biradicals,¹⁸ and these observations indicate that triplet 1 is an intermediate in the formation of dimers upon sensitized photolysis, but not upon thermolysis or direct photolysis of 2. In addition, because 77t is indigenous only to the product mixtures produced by the triplet photochemistry and is formed in substantial quantities, it is an excellent indicator of bimolecular triplet 1 chemistry. The (virtual) absence of 77t among the products of thermolysis or direct photolysis of 2, combined with oxygen's inability to perturb the reaction, demonstrates that triplet 1 is not involved. Thermolysis and direct photolysis of 2 therefore provide dimers 75 and 76t by a mechanism *confined exclusively to the singlet manifold*.

Thermal decomposition of diazene 2.

Diazene 2 loses nitrogen with strict first-order kinetics, as monitored by ^1H NMR between -45 and -65°C , with activation parameters $E_a = 18.2 (\pm 0.1)$ kcal mol $^{-1}$ and $\log A = 14.9 (\pm 0.1)$ (Figure 3-2) ($\Delta H^\ddagger = 17.8 (\pm 0.1)$ kcal mol $^{-1}$, $\Delta S^\ddagger = 8.3 (\pm 0.3)$ eu). These activation parameters are readily interpretable on the basis of structural considerations. Table 3-2 lists corresponding values for a series of monocyclic and bicyclic pyrozolines. A simple comparison of the E_a values for the three pairs of diazenes reveals that introduction of an exocyclic double bond so as to stabilize the incipient radical centers lowers E_a by 8-9 kcal mol $^{-1}$. This is consistent with a one-bond cleavage mechanism for deazetation of 2, a point that is best illustrated by the last two pairs of diazenes in Table 3-2.

The deazetations of 79,²⁴ 10,²⁰ and 46^{21a,25} have been established to proceed by one-bond scission. The decrease in E_a on going from 79 to 10 can therefore be attributed to the developing allylic resonance of 80. If 2 also cleaves to a diazenyl biradical (81),²⁶ then its E_a should be lowered relative to



46 in accord with the developing pentadienyl resonance energy. Since the ratio of the pentadienyl and allyl resonance energies is 19²⁸/12³⁰, one would expect — all other things being equal — that this factor would lead to a ratio $\Delta E_a(2-46)/\Delta E_a(10-79)$ of 1.6.

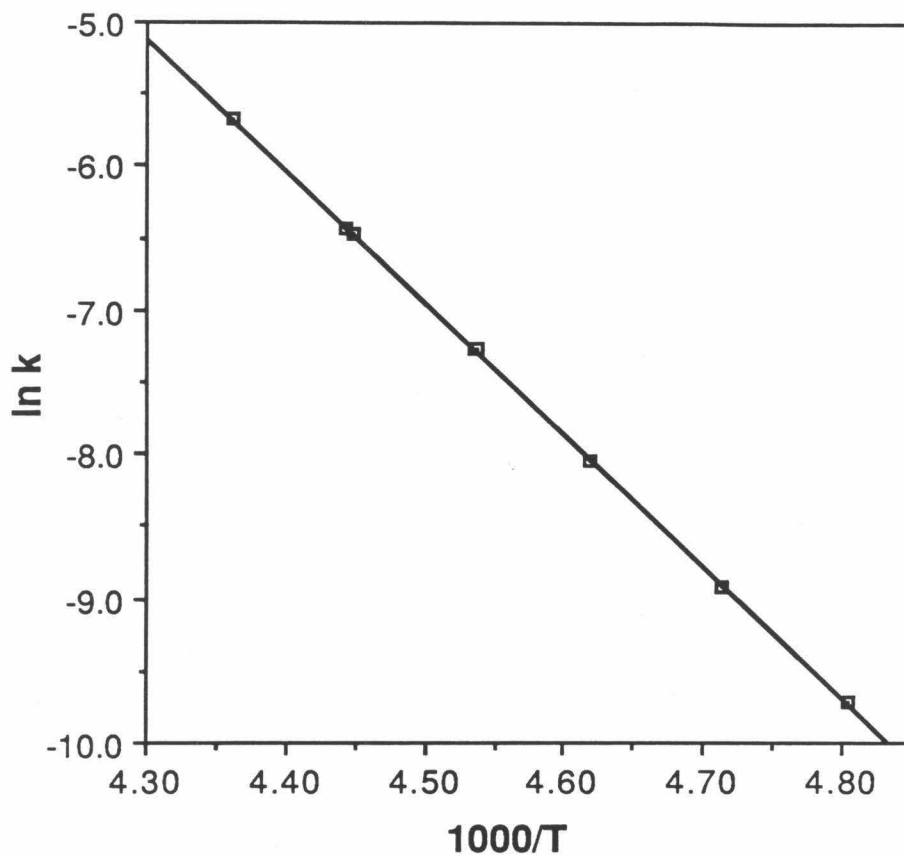

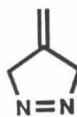
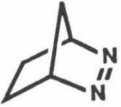





Figure 3-2. Arrhenius plot of the thermal decomposition kinetics of diazene **2** between -45 and -65 $^{\circ}\text{C}$ in CD_2Cl_2 . The activation parameters are $E_a = 18.2 (\pm 0.1)$ kcal mol^{-1} and $\log A = 14.9 (\pm 0.1)$.

Table 3-2. Activation parameters for diazene thermolyses.

			E_a	ΔE_a	$\log A$	ΔS	ref.
		(g)	42.4 kcal mol ⁻¹	8.8	15.9	11.2 eu	19a
	6	(g)	33.6		13.8	1.3	19b
	79	(g)	36.9	9.3	14.7	5.8	19a
	10	(C ₆ H ₆) ^a	27.6		14.7	6.5	20
	46	(C ₆ D ₆)	34.4	16.2	15.5	10.0	21
	2	(CD ₂ Cl ₂) ^b	18.2		14.9	8.3	This work

^ain CH₃CN E_a = 28.8 kcal mol⁻¹ and $\log A$ = 15.1.²⁰ ^bsee ref. 22.

Of course, changes in strain energy must also be considered. The two five- and the two four-membered ring diazenyl biradicals have roughly the same strain energies. However, our force field calculations indicate that adding two exocyclic olefins to **46** raises the strain energy about twice as much as adding one to **79**.³¹ This factor alone should therefore lead to a ratio $\Delta E_a(2-46)/\Delta E_a(10-79)$ of 2. The actual ratio of ΔE_a s (Table 3-2), 1.7, is quite reasonably interpreted as a combination of the delocalization and strain effects.

Similar deazetation mechanisms for **2** and **10** are also consistent with the nominal NBMOs of both biradicals **1** and **9** being S < A in energy.³² Such an ordering for **1** (more specifically, $2b_{1u} < b_{3g}$ — see Figure 2-10) has been predicted by ab initio calculations.^{10,38}

Dimerization in the singlet manifold.

Dimethylenebicyclobutane dimerization kinetics. When a sample of **2** in CD_2Cl_2 is irradiated at -95°C until no diazene remains, **3** is produced with a typical initial concentration of $1\text{--}3 \times 10^{-3}$ M, along with **75** and **76t**. Bicyclobutane **3** is unstable at this temperature, and its decay can be monitored by ^1H NMR between -80 and -25°C . The decay is cleanly *second-order*, as illustrated in Figure 3-3, which shows plots of the -39 and -79°C data according to the integrated first- and second-order rate laws. The Eyring plot of Figure 3-4 furnishes activation parameters $\Delta H^\ddagger = 6.8 (\pm 0.7)$ kcal mol $^{-1}$ and $\Delta S^\ddagger = -28 (\pm 3)$ eu³⁹ ($E_a = 7.3$ kcal mol $^{-1}$, $\log A = 7.0$). Because bicyclobutanes are especially susceptible to electrophilic attack at the bridgehead positions,^{3,40} we were concerned that the observed decay of **3** might incorporate some component of acid-catalysis. We therefore checked these activation parameters by using samples containing 0.02 M 2,6-lutidine to scavenge any adventitious acid and obtained values within the error limits specified above.¹⁷

We have also measured the secondary deuterium kinetic isotope effect (KIE) on the dimerization rate by using samples of **3** and **3-*d*₂**. In the range -40 to -75°C , $k_{\text{H}}/k_{\text{D}}$ was found to be $1.3 (\pm 0.1)$, corresponding to a $k_{\text{H}}/k_{\text{D}}$ of 1.2 at room temperature.⁴¹

Intermediacy of **3 in formation of dimers from **2**.** Several pieces of evidence indicate the intermediacy of **3** in the formation of dimers **75** and **76t** and lead us to conclude that it is produced quantitatively⁴² upon both thermolysis and direct photolysis of **2**. The observation of approximately the

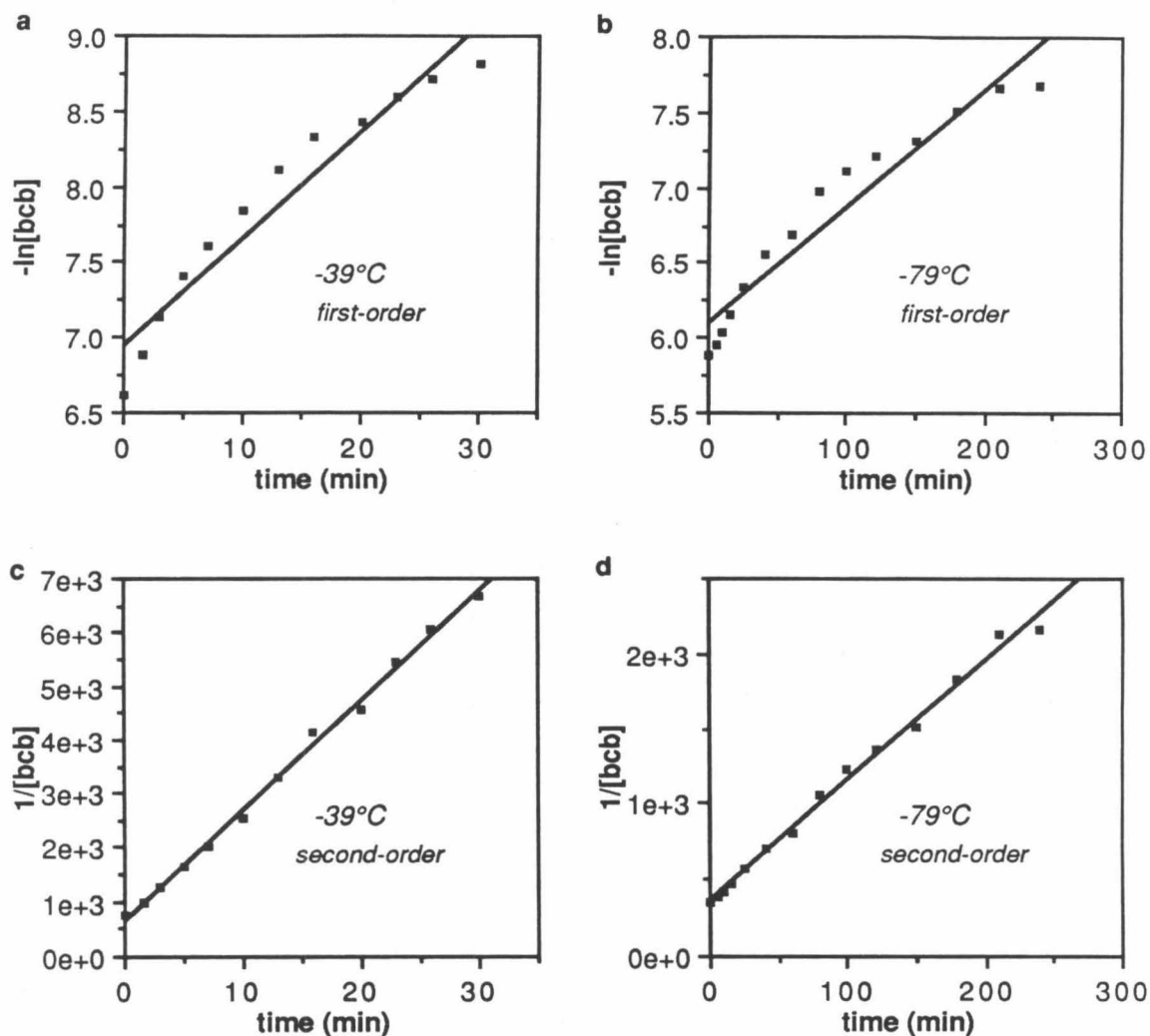


Figure 3-3. Concentration *vs* time data for the dimerization of dimethylenebicyclobutane (3). Analysis of the data according to the first-order rate law provides the plots shown for (a) the -39°C and (b) the -79°C decay of 3. These data are recast in second-order form to provide the $1/[3]$ *vs* t plots (c and d).

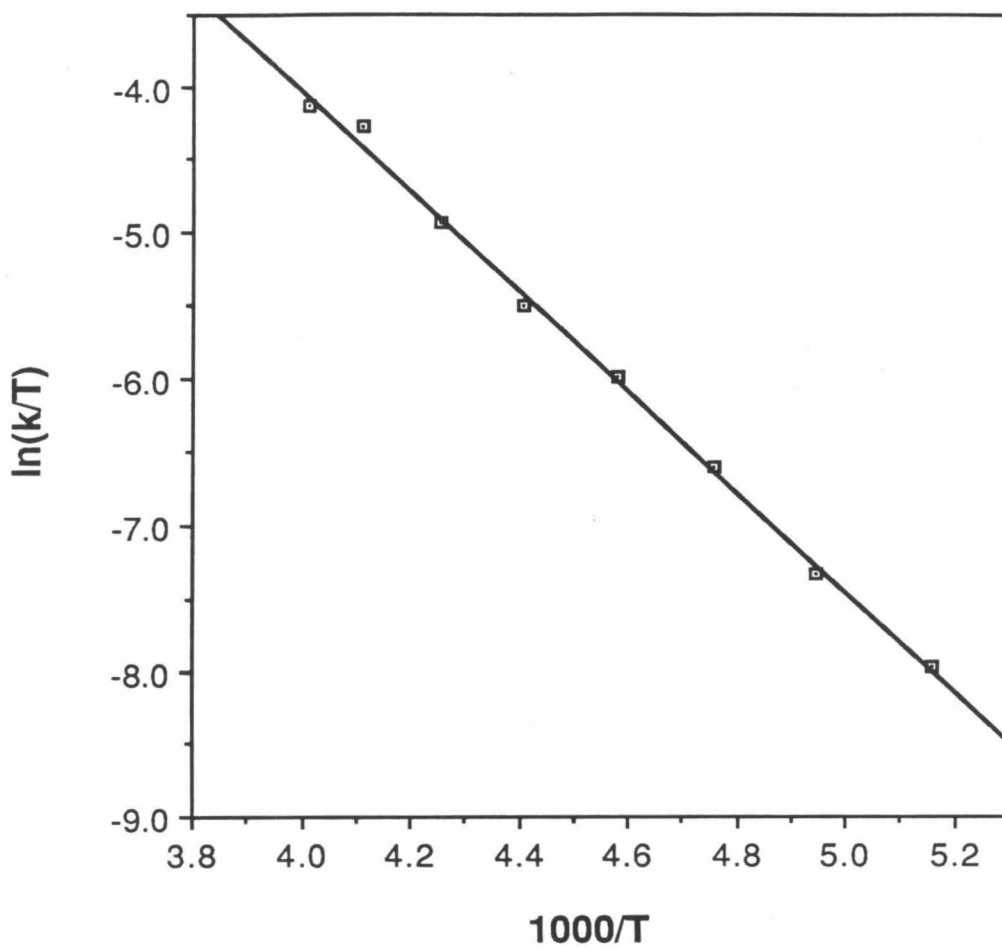
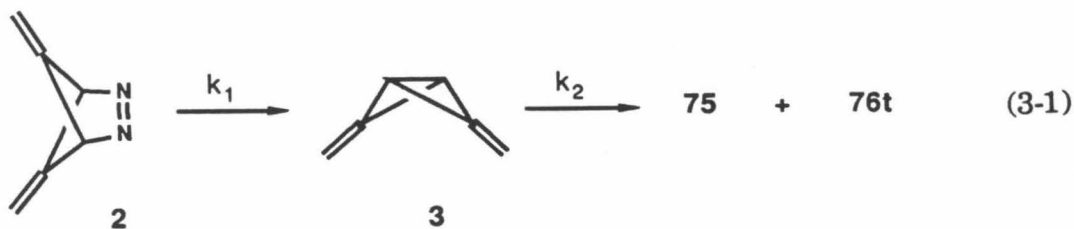


Figure 3-4. Eyring plot for the thermal dimerization kinetics of dimethylenebicyclobutane (**3**) between -25 and -80 $^{\circ}\text{C}$ in CD_2Cl_2 . The activation parameters are $\Delta H^{\ddagger} = 6.8 (\pm 0.6)$ kcal mol $^{-1}$ and $\Delta S^{\ddagger} = -28 (\pm 3)$ eu.³⁹

same ratio of **75** to **76t** in the thermal and photochemical decompositions of **2** at -78°C (Table 3-1) is consistent with the intervention of a common intermediate. Ideally, one would like to establish that **3** independently forms the same product mixture; however, the thermal lability of **3** makes such an experiment quite difficult. For example, when a typical (*ca.* 10^{-2} M) sample of diazene **2** in CD_2Cl_2 is irradiated at $\geq -95^{\circ}\text{C}$, ^1H NMR spectroscopy reveals a large amount of **75** and **76t** and a small amount of **3** (*ca.* 10%). Dimerization of **3** is known to occur at the photolysis temperature,⁴³ consistent with its being the source of the large amount of dimers produced during the photolysis. Although we cannot accurately measure the ratio of **75** to **76t** formed from decay of the small amount of **3** observed, it is roughly the same as that present at the end of the photolysis. These observations are consistent with the postulate that photoexcited **2** produces dimers exclusively via dimethylenebicyclobutane (**3**).

More compelling evidence that dimers **75** and **76t** originate entirely from **3** is provided by the course of the thermal decomposition of **2**. As diazene **2** decays, the concentration of **3** first increases rapidly then decreases, while the concentrations of **75** and **76t** increase steadily, as illustrated in Figure 3-5 at -48 and -61°C . Given the thermal lability of **3** at these temperatures, this behavior is what one would expect if the reaction proceeds via eqn 3-1.



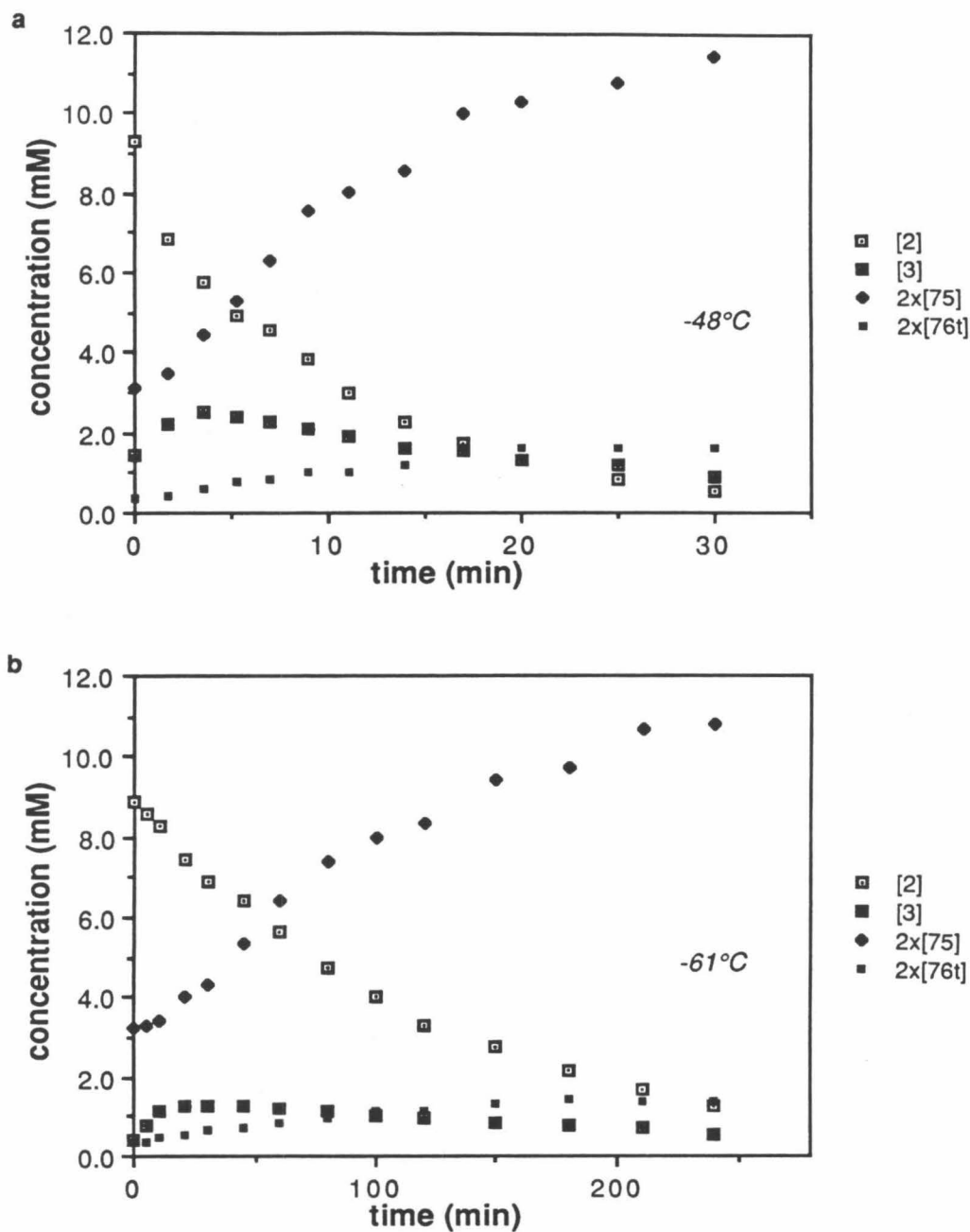


Figure 3-5. The concentrations of diazene **2**, dimethylenebicyclobutane (**3**), and dimers during the course of the thermolysis of **2** in CD_2Cl_2 (a) at -48°C and (b) at -61°C .

Moreover, if this mechanism represents the only pathway from **2** to **75** and **76t**, the time evolution of the concentration of **3** is quantitatively predictable, since k_2 is known, and k_1 is simply the rate of loss of diazene **2**.

Figure 3-6 shows the calculated $[3]$ vs time curves. Given the uncertainty in both k_2 and the measured concentrations, the experimental data follow the calculated curve quite well. We estimate that a 20 to 30% diversion of **2** from the route of eqn 3-1 would produce a meaningful disparity between the calculated curves of Figure 3-6 and the experimental data points. Such a diversion would make the rate of formation of **3** lower than the rate of decay of **2**, and the experimental points would fall substantially below the calculated curves. Rigorously, therefore, at least 70 to 80% of the diazene **2** that decays thermally produces **3**. However, we have no evidence to suggest that a second dimerization pathway bypassing **3** is involved, and so, in keeping with Occam's razor,⁴⁴ we conclude that both thermally and photochemically, **3** is the exclusive source of **75** and **76t** in the singlet manifold.

Dimerization mechanism. One can imagine three reasonable mechanisms for the dimerization of dimethylenebicyclobutane (**3**). These are presented in Scheme 3-2. Of course, direct dimerization (mechanism *a*) produces second-order kinetics. In addition, if singlet **1** has a finite lifetime and is thermally accessible from **3**, it could also participate. The dimerization step could then involve either trapping of singlet **1** by **3** (mechanism *b*) or the reaction of two singlet biradicals (mechanism *c*). The rate laws presented in Scheme 3-2 for these mechanisms were derived under the assumption that the steady-state approximation is applicable to the concentration of singlet **1**.

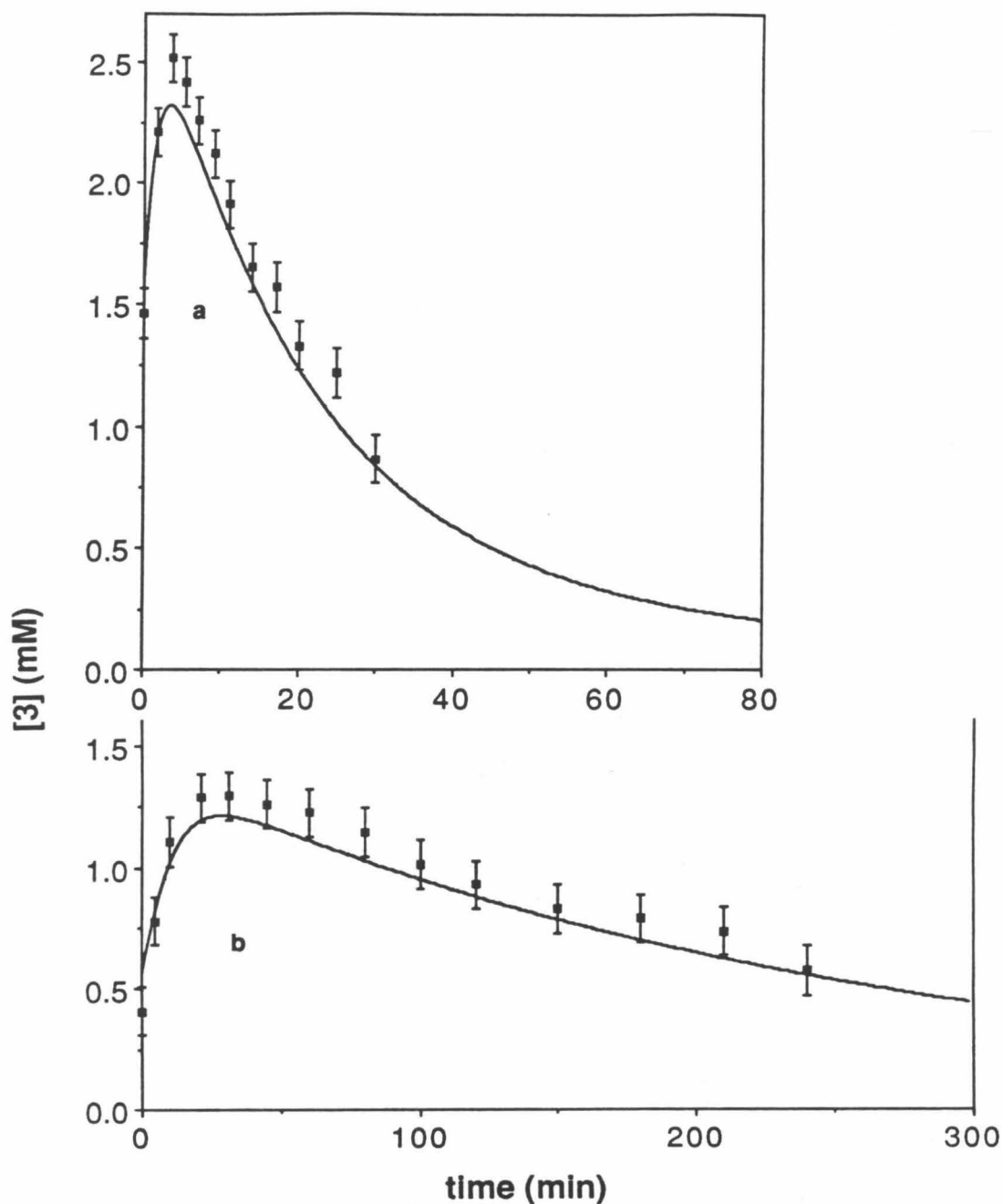
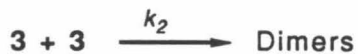


Figure 3-6. Time evolution of [3] during thermolysis of 2 (a) at $-48\text{ }^{\circ}\text{C}$ and (b) at $-61\text{ }^{\circ}\text{C}$. The data points were obtained by ^1H NMR. The curves were calculated numerically according to the equation $d[3] = (k_1[2] - 2k_2[3]^2)dt$, where k_2 is the second-order rate constant for dimerization of 3 and k_1 , the first-order rate constant for decomposition of 2, is assumed also to be the rate constant for formation of 3.

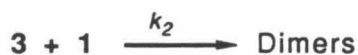
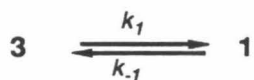
Scheme 3-2.

a.



$$-d[3]/dt = 2k_2[3]^2$$

b.



$$-d[3]/dt = \frac{2k_1k_2[3]^2}{k_{-1} + k_2[3]}$$

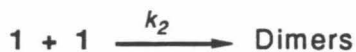
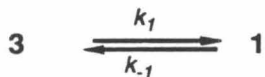
rapid equil.

*rapid
dimerization*

$$= \frac{2k_1k_2[3]^2}{k_{-1}}$$

$$= 2k_1[3]$$

c.



$$-d[3]/dt = \frac{k_1k_2[3][1]}{k_{-1} + k_2[1]}$$

rapid equil.⁴⁵

*rapid
dimerization*

$$= \frac{k_1^2k_2[3]^2}{k_{-1}^2}$$

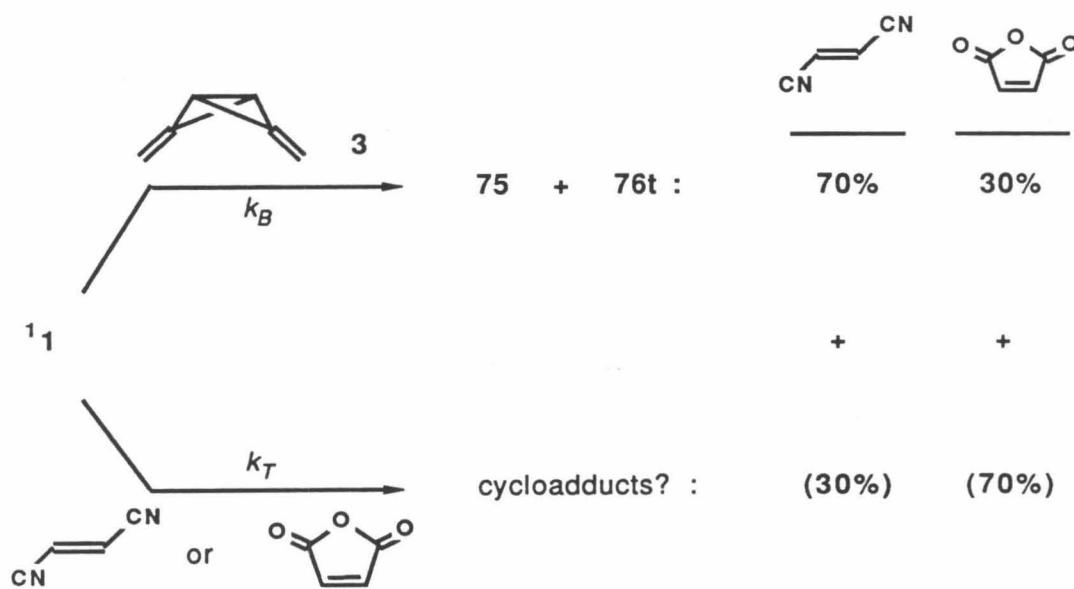
$$= \frac{k_1[3]}{k_{-1}}$$

Mechanism *b* could lead to second-order decay of **3** if the pre-equilibrium step were rapid compared to the dimerization step — that is to say, $k_{-1} \gg k_2[\mathbf{3}]$. The rate law for mechanism *c* is more complex; however, if the condition of rapid pre-equilibrium can be imposed in addition to the steady-state approximation,⁴⁵ then $k_{-1} \gg k_2[\mathbf{1}]$, and since $[\mathbf{1}]$ is proportional to $[\mathbf{3}]$, the rate depends on $[\mathbf{3}]^2$.

If singlet **1** is a participant in the dimerization mechanism, it should be possible to chemically intercept it, thereby shutting down the formation of the dimers. We therefore decided to test the effect of a large concentration of two electron-deficient olefins, fumaronitrile and maleic anhydride, which have been found to be excellent traps for singlet **9**.^{16b} When an 8.5×10^{-3} M solution of diazene **2** in acetone-*d*₆ is allowed to decompose thermally at -50 °C in the presence of 0.9 M fumaronitrile, dimers **75** and **76t** are formed in 70% yield. In the presence of 1.0 M maleic anhydride a 30% yield of dimers is obtained. Although we have not been able to determine the fate of the rest of the material, the mechanistic analysis relies only on the yield of **75** and **76t**.

We will first analyze these results in terms of mechanism *b* (Scheme 3-2). Because the rate constants for the formation and loss of **3** at -50 °C are known, we can calculate that during the thermolysis of 8.5×10^{-3} M **2** the maximum concentration of **3** present at any one time is 2×10^{-3} M. We will assume, for the sake of argument, that **3** is produced quantitatively under these conditions and all the **3** that does not appear in the form of dimers has been trapped as singlet **1**. Then, if mechanism *b* is operative, singlet **1** is trapped competitively by **3** and the olefin with rate constants k_B and k_T , respectively (Scheme 3-3). For 30% dimer formation in the presence of 1.0 M

Scheme 3-3.



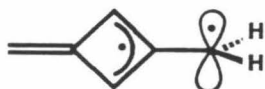
maleic anhydride, $k_B(2 \times 10^{-3} \text{ M}) > (3/7)k_T(1.0 \text{ M})$, or $k_B > 200k_T$; similarly, for 70% dimers with 0.9 M fumaronitrile, $k_B > 1000k_T$.

We note that the less-than-quantitative yields of dimers formed in the presence of these olefins is not necessarily inconsistent with the dimerization proceeding entirely by mechanism *a*. Electron-deficient olefins are known to attack bicyclobutanes,⁴⁰ and **3** might be exceptionally reactive toward the olefins used. Furthermore, thermal deazetation of **2** could produce **3** via singlet **1**, which may be intercepted before it undergoes ring closure. Either of these reactions would be interesting; however, additional experiments are required to determine the fate of the missing material and its mechanistic implications.

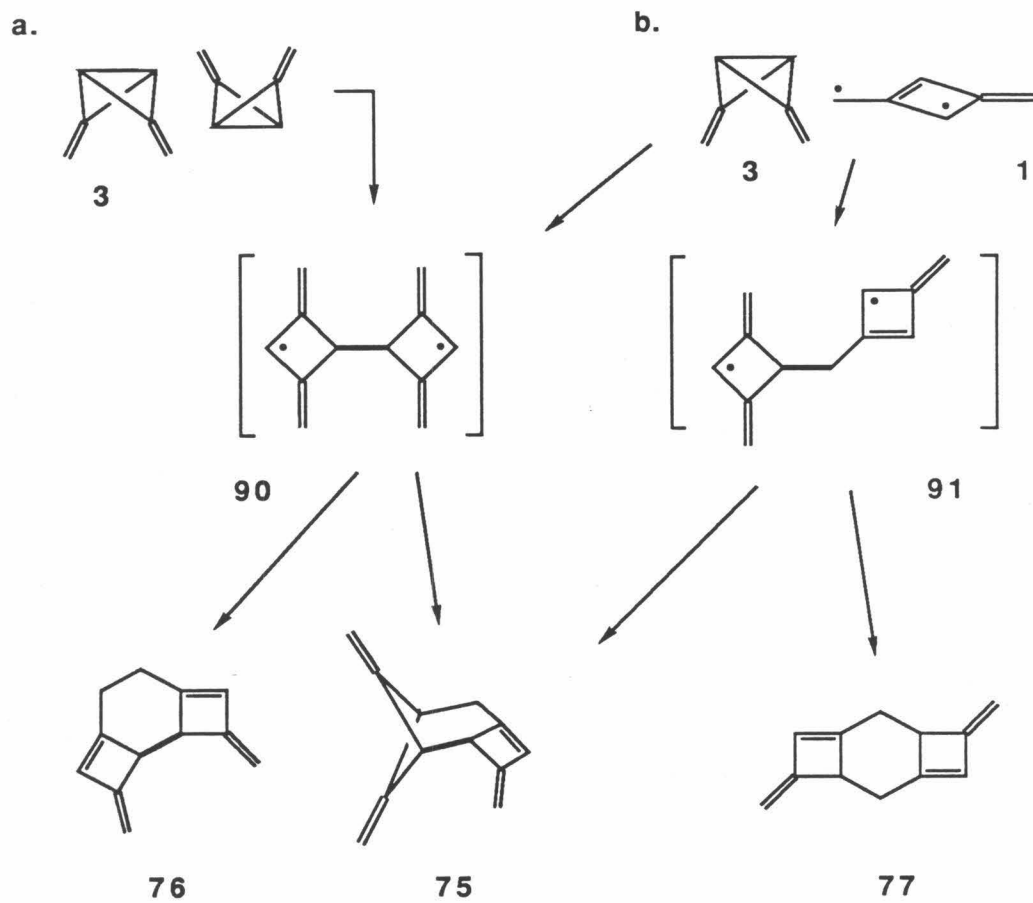
Our best estimates of the olefin trapping rates come from a comparison to the extensively investigated chemistry of biradical **9**. Both maleic anhydride and fumaronitrile trap singlet **9** at or near the diffusion rate, k_d .⁴⁶ If singlet **1** were also trapped at the diffusion rate, this mechanism would require that **3** react significantly faster than k_d and would consequently be eliminated. (Mechanism *c* of Scheme 3-2 is obviously even more untenable in light of this result and will not be considered further.) Of course, one could question the extent to which **9** is a good model for **1**. However, we see no reason that the reactivity of singlet **1** toward the trapping olefin used should be significantly lower than that of singlet **9**. (In particular, there is no indication of an inverse electron demand for singlet **1**,⁵⁰ trapping should be quite exothermic, as it is for singlet **9**,⁵¹ and a geometry change, such as rotation of a CH₂ group, is ruled out by the third argument presented below.)

A second argument against the involvement of singlet **1** in the dimerization of **3** is based on its expected lifetime. Taking $10^{10} \text{ M}^{-1} \text{ s}^{-1}$ as an upper limit on the diffusion rate in CH_2Cl_2 at -78°C , reaction of singlet **1** with 10^{-3} M **3** (the maximum feasible concentration) would occur no faster than 10^7 s^{-1} ; intersystem crossing (isc) to the triplet ground state of **1** would have to be at least two orders of magnitude slower than this to account for the lack of characteristic triplet-derived dimer **77t** in the -78°C thermolysis of **2** (Table 3-1).⁵⁸ Based on precedent from a variety of systems,⁶⁰ an isc rate constant of $\leq 10^5 \text{ s}^{-1}$ would be unusually small.

The final point that argues against participation of singlet **1** in the dimerization is the product mixture, which consists of **75** and **76t**, but lacks **77t** (Table 3-1). Singlet **1** certainly has unpaired electron density at its methylene as well as its methine positions. Attack of the biradical upon **3** is a very exothermic reaction (see below) and cannot have a large E_a ; the reaction should therefore be regiochemically indiscriminant with respect to singlet **1**. That is, both intermediates **90** and **91** (Scheme 3-4) should be produced, and **91** must close to form some amount of **77t**. This is especially so given the course of the triplet dimerization discussed below. Accordingly, participation of the bisected singlet, **1p**, is even more unreasonable, as this species must have unit spin density at the perpendicular methylene group.

**1p**

Scheme 3-4.



We conclude that the dimerization must involve *direct combination of two molecules of dimethylenebicyclobutane (3) as the rate-determining step*. We propose that the dimerization proceeds as shown in Scheme 3-4a. Concerted routes that produce **75** and **76t** but not **77t** are difficult to envision. We favor a stepwise process involving initial bond formation at the bridgehead positions to produce biradical intermediate **90** (Scheme 3-4).¹³⁰ This step provides a pathway to **75** and **76t**, both of which contain a methine-methine connection, and excludes **77t**, which does not.

Stepwise, back-side attacks on the transannular bonds of bicyclobutanes are well precedented.^{40,61} The orbital topology of this "bent" bond⁶² requires that the direction of attack be substantially below the line of the bridgehead carbons. With the alignment of bond-forming orbitals in mind, steric considerations suggest the geometrically specific approach shown in Scheme 3-4a. The observed activation entropy, -28 eu, is quite consistent with a mechanism involving a rate-determining bimolecular reaction of **3**, especially one requiring such a specific alignment of reacting partners.

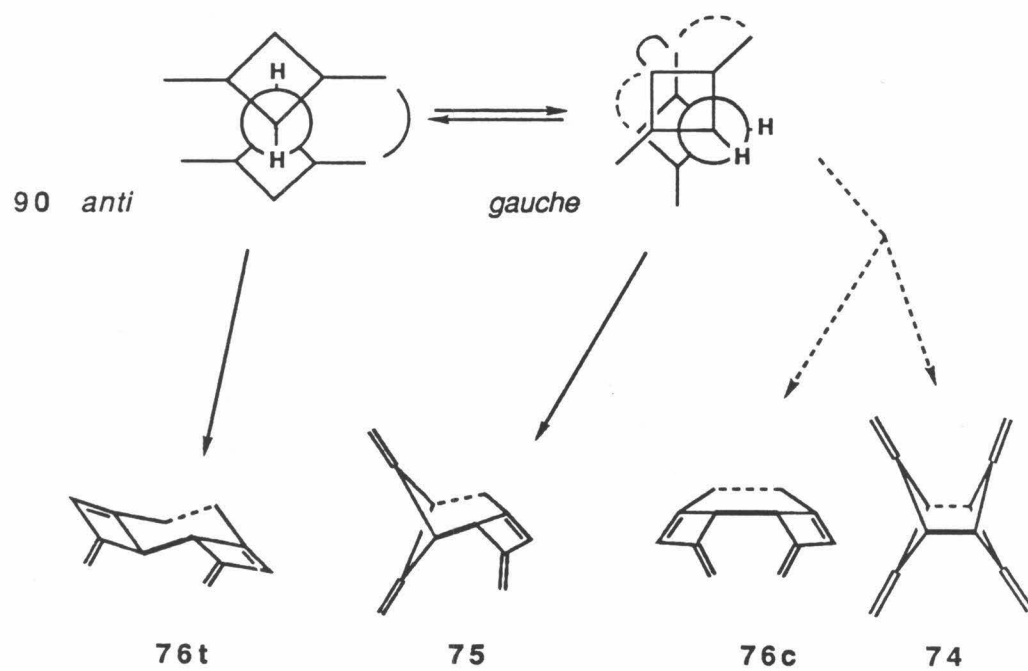
The activation enthalpy, 7 kcal mol⁻¹, would appear inordinately low for a reaction that involves cleavage of two σ -bonds to form a biradical in the rate-determining step. However, thermochemical estimates indicate that this reaction should be quite exothermic. Thus, the net loss of one C—C σ -bond, worth 80 kcal mol⁻¹,⁶³ is offset by the delocalization energy of the two pentadienyl systems of **90**, estimated as 19 kcal mol⁻¹ ²⁸ each, and a release of about 98 kcal mol⁻¹ of strain. The difference in strain energies is determined by subtracting 60 kcal mol⁻¹ for biradical **90**⁵⁶ from 2×79 for the strain of two dimethylenebicyclobutanes (**3**).⁵⁵ Thus, the enthalpy change for the first step

of the dimerization (Scheme 3-4a) is $80 - 38 - 98 = -56$ kcal mol⁻¹. The transition state must surely feel some of this energy release, and an unusually low activation enthalpy, 7 kcal mol⁻¹, is therefore not unreasonable.

The secondary deuterium KIE observed, $k_H/k_D \approx 1.2$ (298 K), is also consistent with this direct dimerization mechanism. On going from two molecules of **3** to biradical **90** (Scheme 3-4a) two nominal sp³ centers are converted to sp², leading to the expectation that $k_H/k_D > 1.64$. Of course, the bridgehead carbons of **3** participate in rather unusual bonding.^{9,10} Nevertheless, the factor governing the magnitude of k_H/k_D is the reduction in the frequency of the vibrational mode that becomes the out-of-plane C–H bend at the radical centers of **90**.⁶⁴ Regardless of what type of hybridization best describes the bridgehead carbons of **3**, the corresponding frequency – that of the C–H bend in the direction of the central bond – should be significantly higher than that of the out-of-plane sp² C–H bend.

There are four dimers with methine-methine bonds, **74**, **75**, **76t**, and **76c**, that could potentially be formed upon closure of intermediate **90**, but only two of these are observed. We analyze the product-determining step as illustrated in Scheme 3-5. If the dimerization step occurs exactly as shown in Scheme 3-4, biradical **90** is born in the anti-conformation (Scheme 3-5). Formation of the second bond can then occur between neighboring methylene groups to produce either enantiomer of **76t**. Rotation of **90** to either C₂-symmetric gauche conformer followed by ring closure at the proximate radical centers provides enantiomeric forms of **75** (Scheme 3-5). On the other hand, the pathway to **74** and **76c** involves rotation of **90** toward the eclipsed conformation. Because the eclipsing interactions that destabilize **74** and **76c** (Figure 3-1) develop

Scheme 3-5.



relatively early along the reaction coordinate for closure, the transition states leading to these products should be destabilized relative to those leading to **75** and **76t**. It is worth emphasizing that this argument does not exclude **74** and **76c** from the product mixture; it merely predicts that two of the four possible dimers, **75** and **76t**, should be formed preferentially. The finding that, in fact, only⁴² **75** and one stereoisomer of **76** are formed strongly supports this analysis. On this basis we assign the observed isomer of **76** the *trans* stereochemistry.

The predominance of **75** over **76t** implies that — if steric approach control in the dimerization step indeed leads to initial formation of the anti conformer — rotation of biradical **90** about its central bond must be rapid compared to ring closure. That rotation could be significantly faster than ring closure for singlet **90** is quite reasonable, especially considering that **90** is stabilized by delocalization of its unpaired electrons and also "strain-protected"³⁴ to some extent. Applying our usual thermochemical analysis, **90** suffers energetically from a missing C—C bond (80 kcal mol^{-1} ⁶³) and the strain present in the cyclobutyl rings ($2 \times 30 \text{ kcal mol}^{-1}$ ⁵⁶), but some of this is offset by the pentadienyl delocalization energy ($2 \times -19 \text{ kcal mol}^{-1}$ ²⁸). Ring closure produces dimers with approximately 85 kcal mol^{-1} of strain energy (Figure 3-1), making formation of the second bond exothermic by only about $(80 + 60 - 38) - 85 = 17 \text{ kcal mol}^{-1}$. The 1,4-biradical tetramethylene provides a useful comparison to **90** in terms of conformational mobility. Its rotation is an order of magnitude faster than ring closure to cyclobutane,⁶⁵ although this reaction is exothermic by approximately $80 - 27^{54} = 53 \text{ kcal mol}^{-1}$. Rotation of **90** should be even more favorable because its ring closure is much less

exothermic. The alternative explanation for the predominance of **75** over **76t** — that rotation of **90** is slow and the first formed conformer is the gauche (Scheme 3-5) — is therefore unreasonable.

In keeping with this analysis, the **75/76t** ratio depends only on the relative activation parameters for the closure reactions (the Curtin-Hammett principle⁶⁶). The temperature dependence of the **75/76t** ratio, r , can be expressed as

$$\ln(r) = \ln\left(\frac{A_{75}}{A_{76t}}\right) + \frac{\Delta E_a}{RT} \quad (3-2)$$

where $\Delta E_a = E_a(\mathbf{76t}) - E_a(\mathbf{75})$. A plot of $\ln(r)$ vs. $1/T$ (Figure 3-7) yields $A_{75}/A_{76t} = 0.8 (\pm 0.3)$ and $\Delta E_a = 0.9 (\pm 0.2)$ kcal mol⁻¹. Since, there are two gauche conformers of **90** and thus four ways to make **75**, A_{75}/A_{76t} includes a statistical factor of 2. The intrinsic ratio A_{75}/A_{76t} for the closure processes is therefore 0.4.

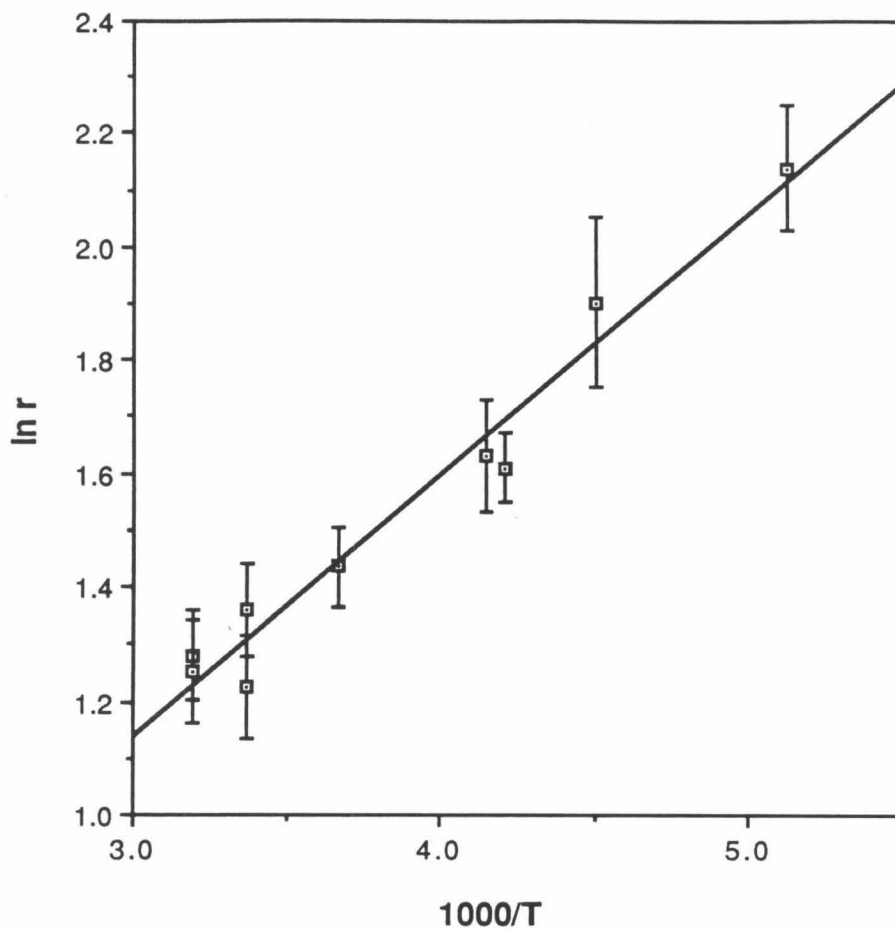


Figure 3-7. Ratios of dimers, $r=[75]/[76t]$, formed upon thermolysis of **2**, vs temperature from -78 to $+40$ °C. The data are plotted according to eqn 3-2 to provide activation parameters $E_a(76t) - E_a(75) = 0.9 (\pm 0.2)$ kcal mol $^{-1}$ and $A_{75}/A_{76t} = 0.8 (\pm 0.3)$.

Dimerization in the triplet manifold.

As noted above, sensitized photolysis of diazene **2** at -78°C produces primarily **77t**, **75**, and **76t**, along with small amounts of two unidentified dimers, **D**₁ and **D**₂ (Table 3-1). This reaction must involve biradical **1** in its triplet ground state. Interestingly, the relative amounts of **75** and **77t** produced are dependent on the reaction conditions (Table 3-1). Figure 3-8 shows the relative amounts of **75**, **76t**, and **77t** formed upon photosensitization of diazene **2** by 0.10 M and 0.01 M Ph₂CO (Figure 3-8a and b, respectively), as monitored by ¹H NMR spectroscopy. While there is quite a bit of uncertainty in the data, it is clear that the initial ratio **77t**/**75** in the Figure 3-8a photolysis is significantly different from the final ratio or that in the Figure 3-8b photolysis.

There are two likely mechanisms for the triplet-manifold dimerization: (1) combination of two triplet biradicals,⁶⁷ which would probably (but not necessarily) occur via a stepwise mechanism, and (2) closure of the triplet biradical (either thermally or by adventitious photolysis — see below) to **3**, followed by attack of triplet **1** upon **3** at its bridgehead position. In light of the ease with which triplet **1** undergoes both photochemical ring closure and thermal ring closure at $\geq 77\text{ K}$ (see below and Chapter 2), formation of some **3** in the sensitized photolysis appears quite reasonable. Moreover, given the facility of the direct dimerization of **3** (see above), reaction of triplet **1** and **3** must be feasible. This mode of dimerization therefore almost certainly occurs to some extent.

Scheme 3-6 shows all the viable dimerization pathways for this system. The only substantive difference from the previous dimerization scheme (3-4) is

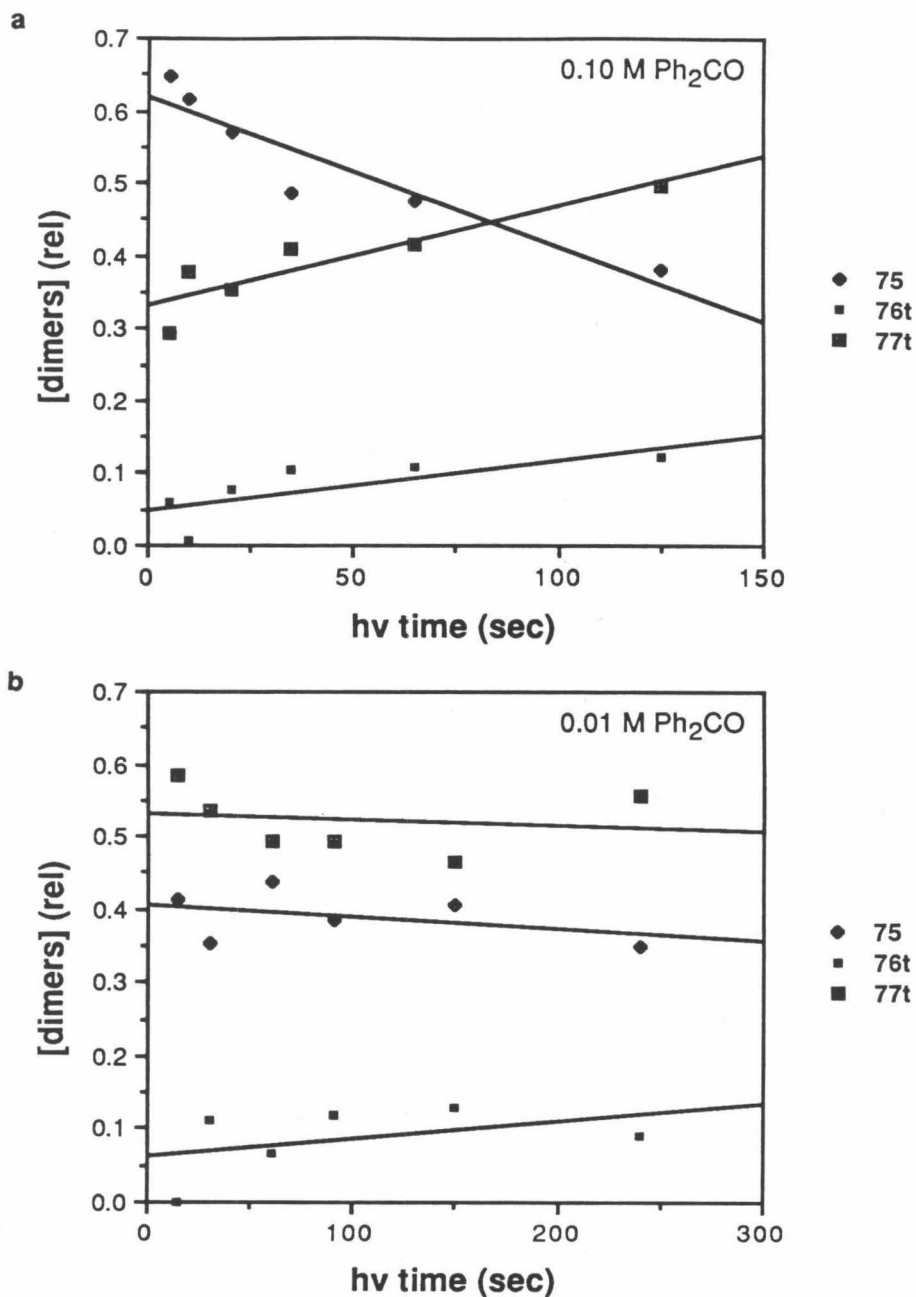
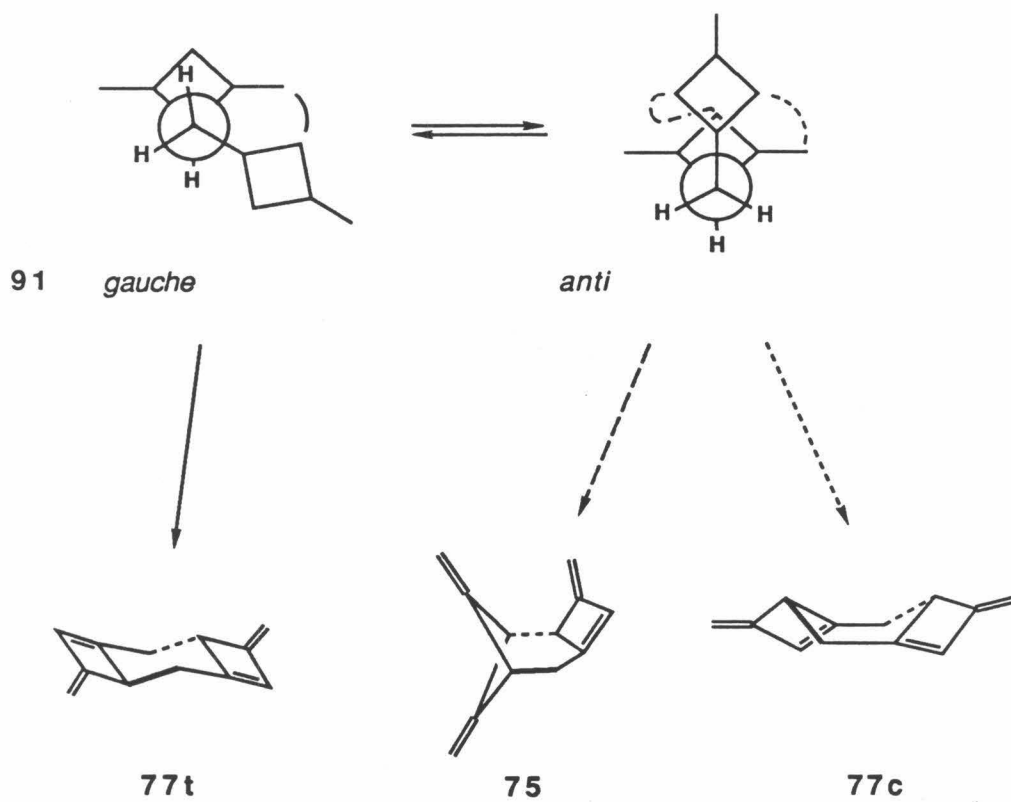


Figure 3-8. Relative amounts of dimers formed during the course of the sensitized photolysis of **2**. (a) 0.10 M Ph_2CO . The mass balance was 70-80% throughout the photolysis, and 85% of the diazene was consumed. (b) 0.01 M Ph_2CO . The mass balance was *ca.* 90% throughout the photolysis and 90% of the diazene was consumed. The diazene concentration was *ca.* half that in the sample of experiment a.

the addition of the triplet-triplet dimerization (Scheme 3-6c), which can produce intermediate **90**, **91**, or **92**. Since **92** can close only to **76** (conformational considerations again suggest **76t** should be preferred) or the mythical dimer **78**, its branch of the scheme is uninteresting in terms of the present mechanistic analysis. Scheme 3-6 also reveals that the only stepwise route to dimer **77** is via **91**. While **91** can, in principle, close to **75**, **77t**, or **77c**, it should prefer to form **77t**, as illustrated in Scheme 3-7. The *gauche* conformer can close to **77t** without incurring eclipsing interactions; however, the *anti* conformer must rotate somewhat toward an eclipsed conformation in order to form **75** or **77c**. Although the eclipsing appears to be less severe than that presumably responsible for preventing closure of **90** to **74** or **76c** (Scheme 3-5), one would expect **91** to show some preference for cyclization to **77t**. This argument leads us to tentatively assign the *trans* stereochemistry to the isomer of **77** observed by ^1H NMR (see above). (In view of this analysis it is interesting that, as mentioned above, one of the minor dimers, **D**₁, produced via sensitized photolysis of **2** (Table 3-1) has a mass spectrum almost identical to that of **77t**.)

The $3 + ^31$ (Scheme 3-6b) and $^31 + ^31$ (Scheme 3-6c) mechanisms must produce different ratios of intermediates **90** and **91**. Because **90** has been established to close primarily to **75** in the singlet-manifold dimerization and **91** is postulated to prefer closure to **77t**, a shift in mechanism might reasonably be reflected in a shift in the **77t/75** ratio. The observed change in this product ratio upon going from conditions presumed to generate a relatively high concentration of triplet biradical (Figure 3-8a) to conditions that could allow more formation of **3** (Figure 3-8a,b)⁶⁸ is therefore consistent

Scheme 3-7.



with such a shift in mechanism. If this is the case, the Figure 3-8 results indicate that the $3 + {}^31$ reaction produces a higher **91/90** ratio than the $31 + 31$ dimerization. That the **77t/75** ratio > 1 when the $3 + {}^31$ mechanism is presumed to operate (Figure 3-8b) indicates that triplet **1** prefers to attack **3** with its methylene carbons, so that more **91** than **90** is formed.

Interconversion of triplet 1 and 3.

Photochemistry of triplet 1 at 77 K. Triplet 1 displays a strong, spin-allowed electronic transition at 506 nm (with vibronic structure extending to near 400 nm) (Chapter 2; Figure 2-5). Excitation of this transition causes rapid, irreversible destruction of the triplet biradical in addition to a strong fluorescence. We also noted that upon photolysis (at 4 or 77 K) the loss of the triplet EPR signal of 1 is accompanied by the appearance of no free-radical (or other) signal (Chapter 2). This demonstrates that the photochemistry does not involve H-atom abstraction from the matrix material.⁶⁹ Because the biradicals are immobilized in distinct matrix sites, the photochemical reaction must therefore be a unimolecular process. Ring closures to 3 or 44 come to mind immediately, at least as the initial step in the mechanism. Although closure to 44 appears less favorable, it cannot be ruled out a priori. The more likely potential photoproduct, 3, is also formed upon adventitious thermolysis and direct photolysis of diazene 2 (and also upon thermal decay of triplet 1; see below). Consequently, simple product analysis is not sufficient to unambiguously assign the photoproduct. The first step in identifying the photoproduct is therefore photolyzing enough triplet 1 that either (1) a product other than 3 and its dimers can be detected, or (2) by the absence of such a new species, 3 can be established as the photoproduct.

We elected to measure the amount of triplet 1 photolyzed by EPR and to analyze the sample by low-temperature ¹H NMR. Accordingly, a sample consisting of 2 and 0.24 M acetophenone as a photosensitizer in 8:1 toluene-*d*₈/3-methylpentane was irradiated at 77 K in the EPR cavity with light of

340-390 nm — a region in which only the sensitizer absorbs. Under these conditions the signal intensity of triplet 1 was found to level off considerably after about 30 sec of photolysis, presumably as a result of competitive secondary photolysis of 1 by scattered⁷² and emitted light. This effect made it possible to generate only about 3.5×10^{-5} M triplet 1 from a given photolysis, as determined by spin-counting. Consequently, it was necessary to repeatedly generate and destroy in order to accumulate a detectable amount of photoproduct. The sample was therefore subjected to 150 cycles of a 30-sec sensitized photolysis of 2 followed by a 10-sec direct photolysis of triplet 1 at $\lambda > 450$ nm. Constant monitoring of the EPR signal intensity and intermittent spin-counting provided an estimate of the total biradical photolyzed, in terms of an effective concentration at -80°C , as 2.7 mM. Because the (presumably significant) quantity of biradical photolyzed adventitiously during generation of the EPR signal is not included in this estimate, the stated concentration represents a lower limit on the amount of photoproduct produced.

^1H NMR spectroscopy at -80°C revealed that the initial mixture, 12.1 mM 2, 1.8 mM 3, and 3.3 mM dimers had been converted to a mixture of 5.2 mM 2, 3.3 mM 3, and 6.6 mM dimers 75 and 76t. That all the material present before the photolysis was thus accounted for (within experimental error) among the compounds 2, 3, and the dimers provides good evidence that the photoproduct is 3 (which dimerized to some extent upon thawing the sample for NMR analysis). Moreover, the sample displayed no new ^1H NMR signals in the solvent "window" between δ 2.3 and 6.8, although a photoproduct

present in a concentration of 2.7 mM would have been easily observable.^{73,74} We thus conclude that photolysis of triplet **1** cleanly produces **3**.

Photochemistry of dimethylenebicyclobutane (3). Compound **3** is a hydrocarbon that lacks a long-wavelength chromophore in the traditional sense. Nevertheless, its potentially unusual structure and the possibility of electronic interactions between the olefinic groups and the strained, transannular bond led us to wonder if **3** could be induced to ring-open to triplet (or singlet) **1** photochemically, either in solution or in a glass. Indeed, we have found evidence that triplet photosensitization converts **3** to triplet biradical **1**.

Samples of **3** in CH₂Cl₂ containing various triplet sensitizers were irradiated at -78 °C, warmed to room temperature, and analyzed by GC. Substantial amounts of **77t**, a clear indicator for the intervention of triplet **1**, were produced when benzophenone (triplet energy, E_T = 68.5 kcal mol⁻¹⁷⁵), benzil (E_T = 53.7⁷⁵), or fluorenone (E_T = 53.3⁷⁵) were used as sensitizers. Smaller but still significant quantities of **77t** were found in samples containing the photosensitizers 9-methylanthracene, acridine, and phenazene, which have triplet energies, E_T , of 41-45 kcal mol⁻¹,⁷⁶ as well as methylene blue, whose E_T is about 32 kcal mol⁻¹.⁷⁷ Control experiments demonstrated that, except, of course, in the case of Ph₂CO, **77t** is not formed upon photolysis of **2**, **75**, or **76t**. We, therefore, conclude that the **77t** observed originates via photosensitized ring opening of **3**.⁷⁸

Given this result it should, in principle, be possible to generate and directly observe the triplet biradical by sensitized photolysis of **3** in a glass at 77 K. Unfortunately, in practice, such an experiment presents technical

obstacles that we have not yet been able to overcome. Specifically, we have been unable to find a low-energy ($E_T < E_T$ of **2**), non-emissive sensitizer that is sufficiently soluble at $-78\text{ }^\circ\text{C}$ in a suitable glass-forming solvent. If successful, this process, coupled with the photochemical conversion **31**→**3**, would constitute a novel photochemical "switch" involving the interconversion of colored paramagnetic and colorless diamagnetic materials.

We have also attempted to photolyze **3** directly. Irradiation of a sample of **3** in MTHF at 77 K with 254-nm light failed to produce the absorption spectrum of triplet **1**. We suspect that the visible light scattered by the MTHF matrix rendered this experiment impractical;⁷² the photochemical opening of **3** may have occurred under these conditions, but not efficiently enough to compete with the adventitious photolysis of triplet **1**. This experiment also may be viable under different conditions.

Thermal decay of triplet 1 in rigid media. In Chapter 2 it was noted that triplet **1** decays slowly and non-exponentially at 77 K in MTHF to produce an EPR-silent species. We now describe a preliminary investigation of the temperature dependence of the decay rate in CH_2Cl_2 between 90 and 130 K. While methylene chloride is not a standard solvent for such studies, our choices are again limited by technical considerations. The experiment demands a solvent capable of dissolving **2** (and therefore remaining non-viscous at $-78\text{ }^\circ\text{C}$) as well as a photosensitizer (to improve EPR signal intensity), yet not allowing diffusion up to (ideally) 150 K. Glass-forming solvents in general solidify too slowly to meet both these viscosity criteria.⁷⁹

Of the polycrystalline solvents that freeze in the required range, CH_2Cl_2 was particularly attractive in terms of solubility.⁸⁰

We have not attempted to determine directly the solid-state thermolysis product of triplet 1. A biradical isolated in a single matrix site can decay either by a unimolecular reaction or by interaction with the matrix. The only reasonable reaction triplet 1 might undergo with the matrix is H-atom abstraction⁸¹; however, we have never observed the appearance of a free radical EPR signal accompanying the decay of the biradical. In particular, no free radical signal was observed at 90 K after partial decay or at 130 K after nearly complete decay of 1 in CH_2Cl_2 . The decay process must therefore be a unimolecular reaction. Given the chemistry discussed above (and especially the photochemistry of 1) we feel quite certain that this reaction can only be ring closure to 3.

When samples of 2 and Ph_2CO in CH_2Cl_2 are irradiated at 90-130 K with light of λ 305-390 nm for 10 sec the triplet EPR signal of 1 grows in rapidly during the photolysis then decays non-exponentially. Such behavior is common for species immobilized in various sites of a host matrix. In the present case $-\ln I$ vs $t^{1/2}$ plots⁸³ for the decay data obtained below 130 K were linear, implying a distribution of rate constants whose maximum value can be extracted from the slope of the plots.⁸³ Such an analysis provides "most probable" rate constants, which are presented in the form of an Arrhenius plot in Figure 3-9. Several additional decays were monitored at temperatures up to 145 K, but these were rejected because the $-\ln I$ vs $t^{1/2}$ plots displayed considerable curvature, perhaps because of the onset of diffusion or some other complication.⁸⁴ The highest temperature data point of Figure 3-9 is

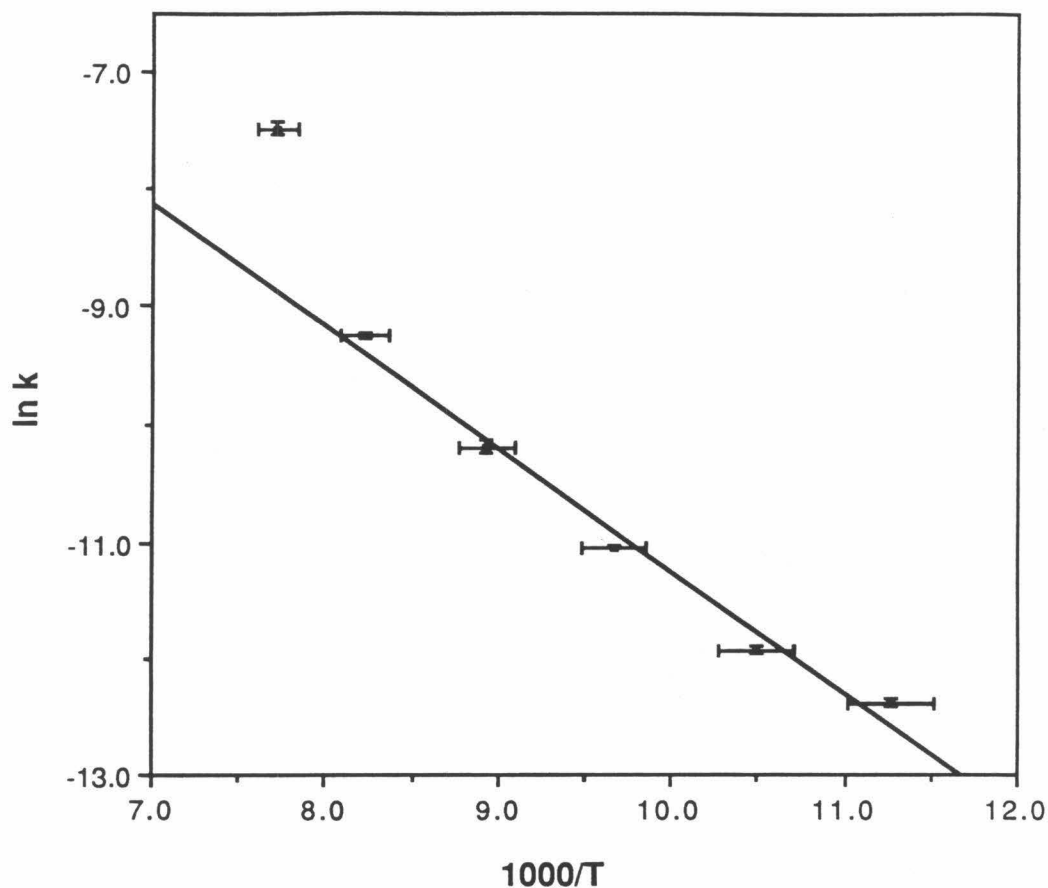
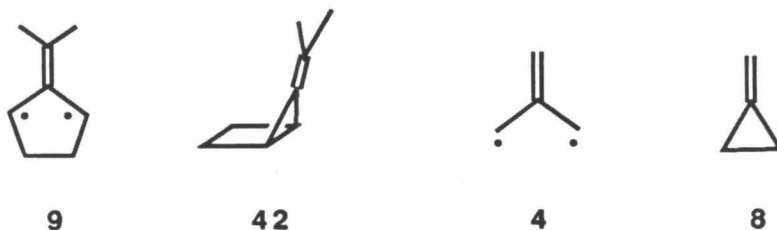


Figure 3-9. Kinetics of ring-closure of triplet 1 to form 3 in CH_2Cl_2 between 90 and 130 K, plotted according to the Arrhenius equation. The line shown was obtained by a least-squares analysis of the five data points that it intersects to provide Arrhenius parameters $E_a = 2.1 (\pm 0.2)$ kcal mol⁻¹ and $\log A = -0.3 (\pm 0.3)$. The final point may be spurious (see **Experimental**).

considered questionable for this reason. In contrast, the other points shown include no such complicating factors,⁸⁴ and they represent unimolecular decay of triplet 1. A least-squares analysis of these five points (Figure 3-9) — although admittedly questionable to begin with because the points appear to lie on a curve — provides Arrhenius “activation parameters” of $E_a = 2.1$ kcal mol⁻¹ and $\log A = -0.3$.

Discussion.

For most biradicals ring closure to a fully covalent structure is a very exothermic process. Ring closure is therefore normally quite facile from the triplet state and even more so from the singlet. However, in some cases the combined effects of resonance stabilization of the biradical and strain-induced destabilization of the covalent isomer can offset the energetic advantage of bond formation. This is the case for Berson's biradical, **9**. Experimentally hydrocarbon **42** is found to be less stable than triplet **9**,^{48,5,34} and ring closure of the triplet biradical is therefore not observed.^{85,34} In addition, singlet **9** encounters a finite barrier to ring closure, and this is also believed to be a consequence of the high strain energy of **42**.³⁴ Recall that, in contrast, triplet TMM (**4**), which lies about 15 kcal mol⁻¹ higher in energy than **8**,⁸⁶ ring closes with only a 7 kcal mol⁻¹ activation energy,⁵⁹ and singlet **4** has not been demonstrated to be a stable structure. Because our system was a priori expected to resemble Berson's energetically (see Chapter 1), much of the following discussion addresses similarities and dissimilarities in the behaviors of the two systems.



The Berson cascade mechanism. Partly as a consequence of the barrier to closure of singlet **9**, the chemistry of Berson's system is characterized by the

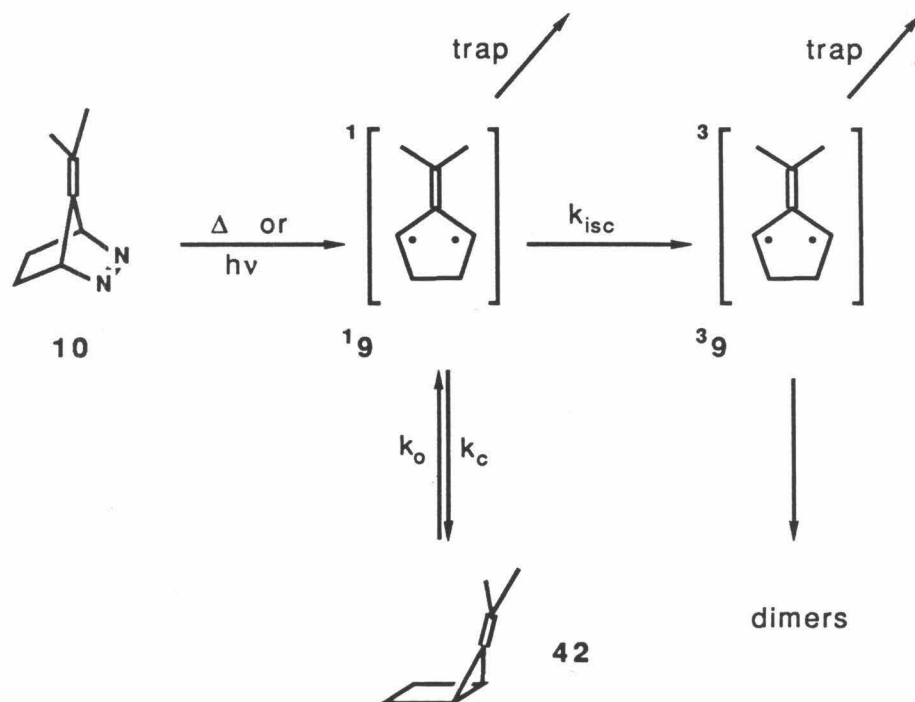
sequential formation of the singlet and triplet biradicals upon photolysis or thermolysis of diazene 10. This "cascade mechanism"^{34,47} is summarized in Scheme 3-8a. Both singlet and triplet 9 are trapped by dienes and electron-deficient olefins. Trapping of the singlet occurs in competition with isc to the ground triplet state, and in the absence of traps dimerization occurs exclusively via triplet 9.^{34,47} In addition, singlet 9 closes to 42 in competition with isc to the triplet. Because of its relatively high energy, 42 reopens to singlet 9 at temperatures above $-50\text{ }^{\circ}\text{C}$.^{5,48,34} Mazur and Berson⁴⁸ have determined the activation energies for disappearance of 42 in the absence of trapping olefin — conditions under which a pre-equilibrium is established and isc to the triplet is rate-determining — and in the presence of a large amount of an efficient trap — in which case opening of 42 is rate-determining. The difference between these two values, which were found to be 13.3 and 15.6 kcal mol⁻¹, respectively, was taken as an approximation to the ring closure barrier.^{48,34}

The energy profile for the system is shown in Scheme 3-8b. The energetics of the system establishes three distinct behaviors in various temperature regimes.³⁴ At very low temperatures, e.g. 77 K, isc dominates activated ring closure of singlet 9, and the triplet biradical is the major product.^{5,34} At intermediate temperatures, passage over the 2.3 kcal mol⁻¹ barrier occurs to the exclusion of isc, and 42 is formed in quantitative yield.^{5,34} At high temperatures ($\geq -50\text{ }^{\circ}\text{C}$), 42 can open to regenerate singlet 9, and the system eventually finds its thermodynamic sink — triplet 9.³⁴

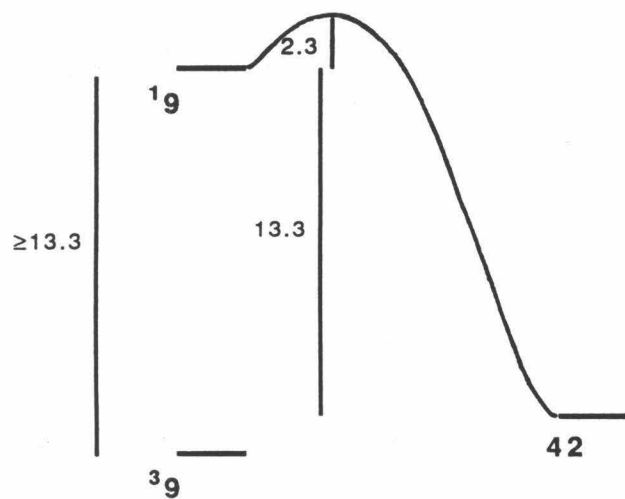
It is important to appreciate that in the high temperature regime ring closure dominates both isc and trapping. For instance, at 60 $^{\circ}\text{C}$ (the thermal

Scheme 3-8.³⁴

a.



b.



decomposition temperature for diazene 10^{16}), and assuming a lower limit of 12 on $\log A$ for closure of singlet **9**,⁸⁷ closure is at least 10 times faster than isc (assuming $k_{isc} \approx 10^{9.5} \text{ s}^{-1}$ ⁸⁸) and 3 times faster than diffusion-controlled trapping with 1 M olefin. (If one instead assumes a more reasonable $\log A$ of 15,⁸⁷ closure is found to be respectively 10^4 and 3×10^3 times the rates for these processes.) Thus, although the high temperature reactivity of this system is characterized by the singlet-triplet cascade, entry onto the singlet surface is followed instantly by ring closure just as it is for "ordinary" biradicals.³⁵ In Berson's system the cascade is then established by reopening of **42**. This leads us to a conclusion that is perhaps not widely appreciated: *The Berson cascade mechanism depends not on the height of the barrier for closure of singlet 9 (as long as this barrier is finite) but on the height of the barrier for opening of 42.* The key is that the ring opening barrier is low enough that **42** and singlet **9** can establish an equilibrium.

Concerning the possibility of a cascade mechanism for 1. With this point in mind, we note that the absence of a singlet-triplet cascade for **1** does not necessarily mean that singlet **1** closes more easily than singlet **9**. Rather, it could signify that **3** is just unable to return to the singlet biradical. Of course, if this is the case, the failure of **3** to reopen could well be a result of its facile dimerization rather than an inordinately large E_a for its ring opening.

We have described two experiments that can provide an estimate of the upper limit on the ring closure barrier for singlet **1**. However, it is worth emphasizing that neither experiment conclusively establishes the existence of the singlet biradical.

First, as shown in Table 3-1, photolysis of **2** at $-95\text{ }^{\circ}\text{C}$ produces a small amount (0.1-0.2%) of triplet-derived dimers. If we assume that the photolysis generates exclusively singlet **189** and this undergoes isc in competition with closure to **3**, then $k_{\text{isc}} = (0.002)k_{\text{c}}$. By using a lower limit of $k_{\text{isc}} = 10^7\text{ s}^{-1}$ ⁹⁰ and an upper limit of $\log A = 15$ for closure of singlet **1**, we find that $E_{\text{a}} \leq 4.3\text{ kcal mol}^{-1}$.

On the other hand, entry into the triplet manifold could very well be gained by isc from S_1 to T_1 of the diazene (**2**) followed by spin-conservative nitrogen loss to form triplet **1** directly. The latter mechanism is quite feasible considering the finding that diazenes commonly encounter a barrier to nitrogen loss from S_1 ,⁹¹ and such a barrier is suggested by the temperature-dependent photochemistry of the parent bicyclo[2.1.1] diazene **46**.⁹² Intersystem crossing to T_1 therefore competes more effectively with singlet-manifold deazetation at lower temperatures. (This mechanism therefore also accounts for the generation of a strong triplet EPR signal upon direct photolysis of **2** at cryogenic temperatures (see Chapter 2)).

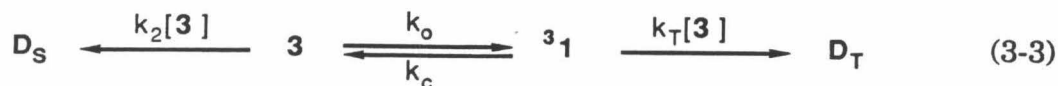
Second, thermolysis of **2** at $-50\text{ }^{\circ}\text{C}$ in the presence of maleic anhydride or fumaronitrile produces less than a quantitative yield of dimers **75** and **76t** (Scheme 3-3). Assuming that the "missing" material was intercepted as singlet **1** before it could ring-close and ultimately dimerize, then for 1 M maleic anhydride, $k_{\text{c}} = (3/7)k_{\text{T}}(1\text{ M})$. Since the trapping rate constant, $k_{\text{T}} = k_{\text{d}} = 5 \times 10^9\text{ M}^{-1}\text{ s}^{-1}$;⁴⁶ $k_{\text{c}} = 2 \times 10^9\text{ s}^{-1}$. Again using an upper limit of 15 on $\log A$ for ring closure of the singlet, we find $E_{\text{a}} \leq 5.8\text{ kcal mol}^{-1}$. The fumaronitrile trapping results similarly provide $E_{\text{a}} \leq 5.1\text{ kcal mol}^{-1}$. However, as mentioned above, **3** might be especially susceptible to attack by the olefins

used, and all or some of the missing material might be accounted for in this way.

These two experiments thus effectively limit E_a for closure of the singlet biradical to between 0 and about 5 kcal mol⁻¹. Given the chemistry of TMM (4) and 9, this is probably what one would have conservatively predicted for 1, and this result therefore is of no great quantitative value. It does, however, serve to illustrate that the apparent ease with which singlet 1 ring closes to 3 is not inconsistent with a significant closure barrier. This point might initially have been somewhat counter-intuitive considering the widely different behaviors of our system and Berson's in terms of the singlet-triplet cascade mechanism.

Good evidence that our system does cross from the singlet to the triplet surface — whether via the singlet biradical or some other route — comes from the high temperature thermolysis of 2. A small but significant amount of triplet-derived dimers is formed upon thermolysis of 2 at 40 °C but not at -78 °C (Table 3-1). Dimethylenebicyclobutane (3) is almost certainly formed quantitatively from 2, and these results suggest that ring opening of 3 can begin to compete with its dimerization at higher temperatures. This is intuitively reasonable, since $\log A$ for dimerization of 3, 7.0 (see above) could easily be lower than $\log A$ for its ring opening to triplet 1, thereby making the latter process increasingly important at higher temperatures. Due to the nature of the experiment it is very difficult to determine quantitatively meaningful activation parameters for opening at 3 to triplet 1; however, we can roughly estimate the size of the barrier required to allow the observed amount of triplet-manifold dimerization.

We will analyze the observed product composition in terms of eqn 3-3. The



ratio of triplet-manifold dimers, D_T (assumed to originate via a ${}^31+3$ mechanism), to singlet-manifold dimers, D_S , is given by the ratio of their formation rates. These rates are

$$\frac{d[D_S]}{dt} = 2 k_2 [3]^2$$

and

$$\frac{d[D_T]}{dt} = k_T [3] [{}^31].$$

Applying the steady state approximation to $[{}^31]$, we have

$$\frac{d[D_T]}{dt} = \frac{k_o k_T [3]^2}{k_c + k_T [3]}. \quad (3-4)$$

Trapping of the triplet biradical by 3 is probably faster than its ring closure.⁹³

Thus eqn 3-4 becomes

$$\frac{d[D_T]}{dt} = k_o [3].$$

Formation of approximately 0.4%⁹⁴ triplet-manifold dimers at 40° C requires that

$$\frac{d[D_T]}{dt} = (0.004) \frac{d[D_S]}{dt},$$

or

$$k_o = (0.004) 2 k_2 [3].$$

Rate constant k_2 can be obtained by extrapolation of the Eyring plot of Figure

3-4 to 40 °C, whereby one obtains $k_2 = 90 \text{ M}^{-1} \text{ s}^{-1}$. The concentration of **3** is unknown, but if we assume a value of 10^{-4} M , $k_0 = 7 \times 10^{-5} \text{ s}^{-1}$. Using $\log A = 9.6$ (the value for the reaction $42 \rightarrow 39^{48}$), we find that E_a for opening of **3** to triplet **1** is about 20 kcal mol⁻¹.

It is difficult to attach a meaningful error to this value, given the various assumptions used and the intrinsic uncertainty in the experiment. However, it is worth noting that if $\log A$ and E_a for opening of **3** were the same as those for opening of **42**, namely $\log A = 9.6$ and $E_a = 13.7 \text{ kcal mol}^{-1}$,⁴⁸ we would predict that at 40 °C triplet-manifold dimerization would dominate the singlet manifold reaction by a factor of 60. Additionally, such activation parameters provide for a measurable amount of triplet-manifold dimerization at -78 °C,⁹⁵ whereas none is observed (Table 3-1). In other words, it would appear that E_a for opening at **3** must be significantly larger than that for opening at **42** in order for dimerization of **3** to predominate at this temperature. (Alternatively, $E_a = 13.7$ and $\log A = 5.2$ would provide the above value for k_0 at 40 °C.)

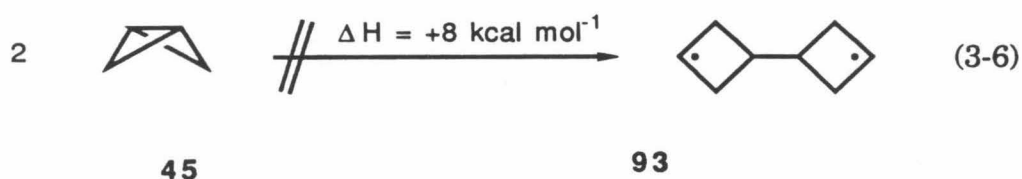
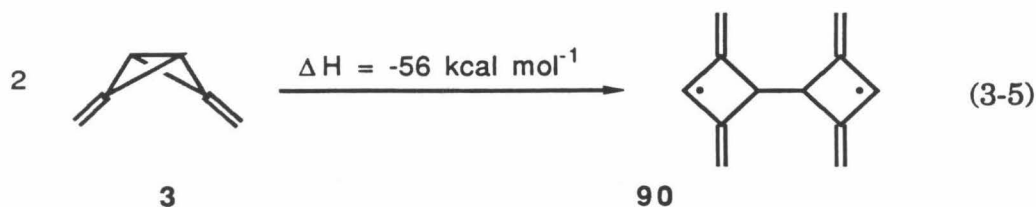
We have found that triplet **1** ring closes irreversibly to **3** in rigid media at $\geq 77 \text{ K}$ (see above). This clearly indicates that **3** must lie lower in free energy than triplet **1**, at least at the temperatures of the EPR kinetic studies. The entropy term favoring the triplet biradical would, of course, be more important at higher temperatures and could place triplet **1** slightly below **3** near room temperature if the enthalpy of triplet **1** were no more than 1 kcal mol⁻¹ higher than that of **3**.⁹⁶

Because the enthalpy of **3** is less than or about equal to that of triplet **1**, and if the conversion of **3** to triplet **1** at 40 °C occurs via singlet **1**, 20 kcal mol⁻¹

represents an approximate upper limit on the S-T gap for biradical 1. Since one would probably not expect an S-T splitting larger than this value, such an estimate again provides little new information.

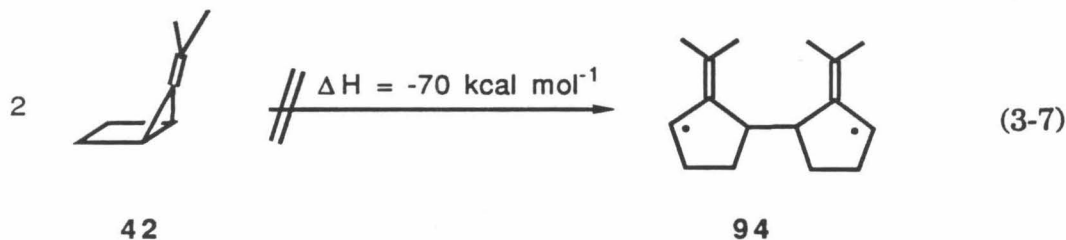
We must emphasize that we have no direct evidence for a cascade mechanism such as that observed in Berson's system. However, all the data we do have can be interpreted in terms of such a mechanism. The vast difference in the behaviors of the two systems may simply result from 3 being removed from the picture via its facile dimerization faster than it can return to singlet 1 and thereby establish the cascade. In addition, we must emphasize that there is no direct evidence for a barrier to closure of singlet 1, and such a structure might be only a transition state for inversion of 3. The paucity of intersystem crossing in the chemistry of 3 could therefore indicate only that 3 has no good way to enter the triplet surface.

The dimerization of 3. We have established that dimethylene-bicyclobutane (3) undergoes an extremely facile and novel direct dimerization that involves rate-determining scission of two σ -bonds to form a biradical intermediate. Such a process is to our knowledge completely without precedent in bicyclobutane chemistry and virtually unprecedented in general. We cited the large exothermicity of the reaction (eqn 3-5), estimated as $\Delta H = -56 \text{ kcal mol}^{-1}$, to rationalize the unusually small activation enthalpy of 7 kcal mol^{-1} . It is instructive to compare ΔH for the dimerization of 3 to the analogous dimerization of the parent bicyclobutane (45) (eqn 3-6), which is not observed.³ We estimate ΔH for this reaction to be $+8 \text{ kcal mol}^{-1}$.⁹⁸ It is quite evident that the large exothermicity of the eqn 3-5 dimerization



results from a combination of the strain energy of **3**, which is 15 kcal mol⁻¹ higher than that of **45**, and the delocalization of the unpaired electrons of **90**, which contributes 19 kcal mol⁻¹ ²⁸ for each of the pentadienyl systems.

However, the exothermicity of the reaction cannot be the only reason that **3** dimerizes so easily, and the (presumably) unusual structure of this species (see Chapter 1) must be a contributing factor. This point is nicely illustrated by the fact that an analogous dimerization of **42** (eqn 3-7) should also be quite



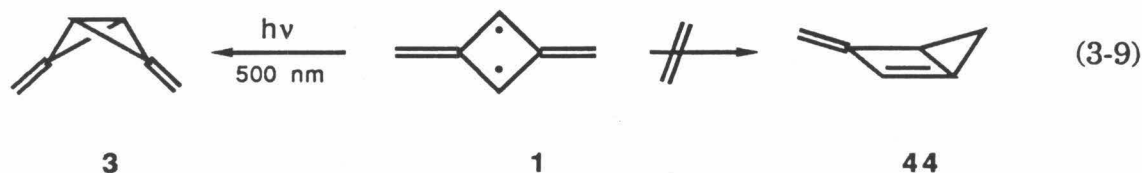
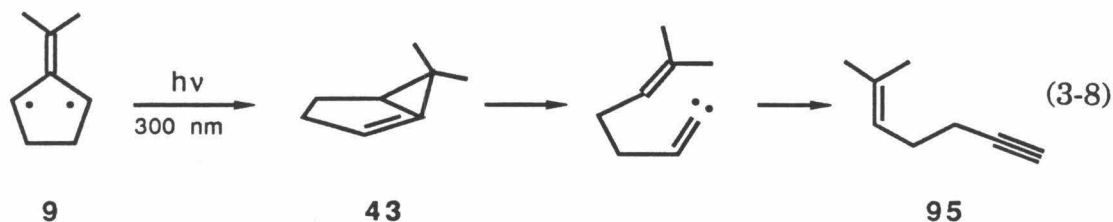
exothermic, with $\Delta H = -70 \text{ kcal mol}^{-1}$!⁹⁹ However, such a reaction is not observed for **42**, even at -78°C , where its ring opening is extremely slow.^{48,5,34} If such a dimerization had activation parameters comparable to ours, it should have been readily observable at this temperature. However, if E_a were just a few kcal mol⁻¹ higher than that for the dimerization of **3**,

dimerization of 42 would be unable to compete with its facile ring opening.¹⁰⁰ That such a dimerization may be lurking just over the energetic horizon for 42 remains an intriguing possibility.

It would appear that structural features of 3 are partially responsible for its propensity to dimerize. Recall that calculations find 3 to be flattened relative to normal bicyclobutanes,^{9,10} and our NMR data (see above) support this idea. Additionally, the bridgehead carbons of 3 are predicted to be substantially inverted.^{10,9} One could easily envision such features as contributing to the ease of the dimerization.

Photochemistry of triplet 1 and 3. Photolysis of the triplet biradical with light of 400-510 nm excites a $^3B_{2u} \rightarrow ^3B_{1g}$ transition of 1.^{101,102} Ring closure to 3 could then occur, with isc to the singlet surface either preceding or concomitant with puckering of the biradical. It is worth noting that in the first case the spin flip could presumably be aided by torsion of an exocyclic methylene group.¹⁰³ Such a rotation is apparently involved in the photochemistry of biradical 9,¹⁰⁴ which provides, to our knowledge, the only reported example of the photochemistry of a simple TMM derivative. Upon irradiation of triplet 9 at 77 K with 300-nm light, the predominant photoproduct was found to be enyne 95.¹⁰⁴ The reaction is initiated by a spin-allowed transition of 9¹⁰⁵ and is proposed to occur as shown in eqn 3-8.¹⁰⁴ In the case of triplet 1 there is no indication that the analogous ring closure to 44 (eqn 3-9) plays any part in the photochemistry.¹⁰⁶ Closure to 3 is certainly expected to be the preferred route in the ground state because of the enormous

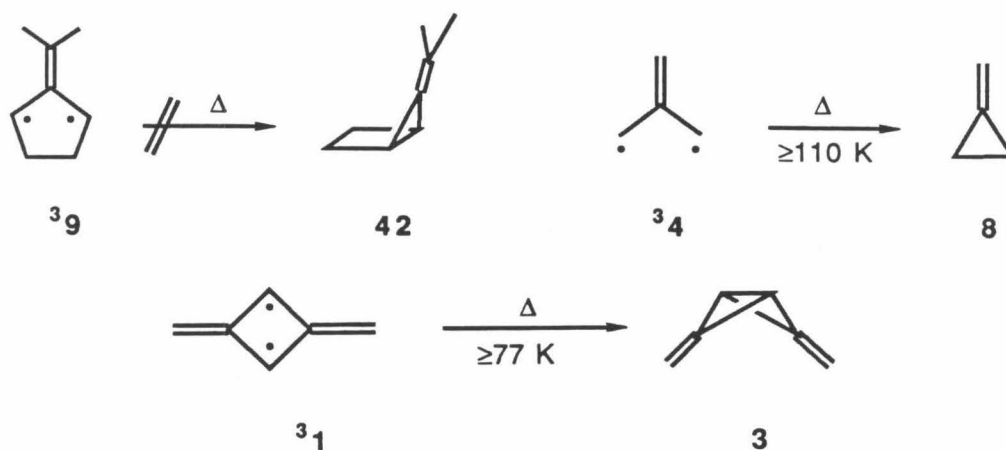
strain energy of 44, and this should influence the excited state energetics to some extent.



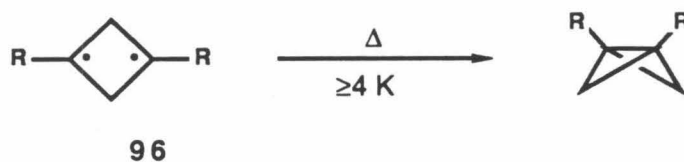
With regard to the mechanism of the photosensitization of **3** to form triplet **1** in solution, we can only speculate. Because opening of **3** to **1** is promoted by sensitizers having extremely low triplet energies, an excited state of **3** is probably not involved. Specific chemical interactions between **3** and the sensitizer, such as reversible attack at a bridgehead carbon, appear unlikely, given that the reaction is promoted by a variety of aromatic ketones, hydrocarbons, and heterocycles. Another possibility is electron transfer from the relatively high-lying σ -orbital of the central bond of **3**. Since **3** and triplet **1** are predicted to be of comparable energies,¹⁰ and **3** may also be significantly flattened relative to a "normal" bicyclobutane, the energy of the S-T surface crossing may be quite low. It is perhaps intuitively reasonable, therefore, that **3** is opened to triplet **1** by very low energy sensitizers. In addition, the gradual fall-off in photosensitization efficiency appears to fit the Balzani model for energy transfer processes,¹²⁹ although a firm conclusion with regard to this point requires more quantitative experimental results.

Thermal ring closure of triplet 1. Because technical limitations have prevented us from investigating the ring closure kinetics of triplet 1 under a variety of conditions, we hesitate to place too much emphasis on the results we have obtained. Several factors complicate the kinetic analysis. The decay of the triplet EPR signal is non-exponential, indicating that matrix site effects influence the decay rates; however, the extraction of rate constants from such decay data is well understood¹⁰⁷ and straightforward in the present case. Of particular concern is the variation of activation parameters observed for the ring closure of TMM (4) with the identity of the matrix and the method by which the biradical had been generated.⁵⁹ Specifically, $\log A$ for this process was found to vary from 2 to 10, although its value ranged only from 6 to 10 under most of the experimental conditions employed.⁵⁹ We are therefore reluctant to attribute the anomalously weak temperature dependence of the biradical decay rates (Figure 3-9) to quantum-mechanical tunnelling.

On the other hand, we note that the EPR signal of triplet 1 does decay at 77 K in a variety of solvents¹⁰¹ (although these were unsuitable for higher temperature work). For comparison, triplet 9 is indefinitely stable with respect to unimolecular reaction to near room temperature,⁸⁵ while triplet 4 closes to 8 at about 110 K and above.⁵⁹ Since ring closure of 9 is endothermic,^{48,5} and closure of triplet 1 is exothermic (see above), it is not surprising that triplet 1 is less stable than triplet 9. However, the finding that triplet 1 ring closes more easily than the parent TMM (4) is quite surprising. Certainly, the closure of 1 is not nearly as exothermic as the closure of 4 and other factors must then make 1 exceptionally prone to ring closure.



We do note that heavy-atom tunnelling has been observed in the ring closures of alkyl-substituted cyclobutanediyls, $\mathbf{96}$,^{108,109} although it is, to the



best of our knowledge, unprecedented in the ring closure of a delocalized (non-Kekulé) biradical. One might speculate that the flattened geometry of $\mathbf{3}$ would place the energy surfaces of $\mathbf{3}$ and triplet $\mathbf{1}$ unusually close to one another, thereby enhancing a tunnelling mechanism. Further experiments concerning this ring closure reaction are underway.

Conclusion.

The ^1H NMR spectrum of **3**, combined with its novel and surprisingly facile direct dimerization, indicate that this species may have quite an unusual structure, as suggested by *ab initio* calculations.^{9,10} In addition, we have found that **3** is close to or below triplet **1** in energy. This is in reasonable agreement with the *ab initio* prediction that these two species are of comparable energies.¹⁰ However, it demonstrates that our thermochemical estimate that triplet **1** should be 7 kcal mol⁻¹ more stable than **3** (Chapter 1) was in error, most likely due to the difficulty in estimating the π -energy of triplet **1**.

The prediction that **3** should be nearly equienergetic with triplet **1**¹⁰ suggests that, as in Berson's system,³⁴ singlet **1** might encounter a barrier to ring closure, thereby making possible a singlet-triplet cascade. Although our system exhibits behavior very different from Berson's, the chemistry we observe in no way rules out the possibility of similar energy surfaces for the two systems. The absence of a similar cascade mechanism for our system might simply result from **3** dimerizing faster than it can establish the necessary equilibrium with singlet **1**. However, we have unfortunately found no direct evidence for the existence of the singlet biradical. Further experiments are necessary to establish this point as well as the more quantitative aspects of the energy surface.

Experimental.

Solvents and reagents. CD_2Cl_2 was obtained from Aldrich or MSD Isotopes and used without further purification unless otherwise noted. The CH_2Cl_2 used to make diazene solutions was "spectro"-grade solvent that had been distilled from CaH_2 or P_2O_5 and stored under N_2 . Mesitylene was distilled from Na. Benzophenone was recrystallized from CH_2Cl_2 /hexane, and acetophenone was distilled prior to use. 2-Methoxynaphthalene was recrystallized from CH_2Cl_2 /MeOH, 2,6-dimethylpyridine (lutidine) was distilled from BaO, and fumaronitrile was recrystallized from CH_2Cl_2 . Other reagents and solvents were used as obtained commercially unless otherwise noted.

Sample preparation. Freshly-made samples of diazene 2^{101} at $-78\text{ }^\circ\text{C}$ were dissolved in the appropriate solvent, and the solution was transferred via 30-gauge teflon tubing to a sample tube. Alternatively, the solution was transferred to a graduated storage tube, from which it could be apportioned to several sample tubes. Typically, CD_2Cl_2 (1-3 ml) containing a known volume of mesitylene (*ca.* 2 μl) as an internal standard was used, and the mesitylene concentration at *ca.* $-80\text{ }^\circ\text{C}$ was calculated as the room temperature concentration/0.9 to account for the *ca.* 10% volume contraction (see below) accompanying the temperature change. The sample tubes were Wilmad Glass 701-PQ 5-mm o.d., 3.5-mm i.d. quartz tubes, which had been base-washed, rinsed thoroughly with water and organic solvents, and dried.¹⁰¹ The samples were typically degassed by three freeze-pump-thaw cycles (liq. N_2 — CO_2 /Me₂CO),¹⁰¹ frozen, and sealed with an oxygen-gas flame. When

oxygen was to be introduced, the sample was warmed to $-95\text{ }^{\circ}\text{C}$ (liq. N_2/MeOH) or $-78\text{ }^{\circ}\text{C}$ (CO_2/iPrOH), the appropriate amount of gas ($<1\text{ atm}$) was admitted to the manifold and to the sample tube, and (after a few minutes) the tube was sealed carefully with a flame.¹¹⁰ Samples were stored at $-100\text{ }^{\circ}\text{C}$ or at 77 K before use.

Photolysis. Samples were irradiated with light from an Oriel 1000-Watt "ozone-free" Hg(Xe) arc lamp (operated at 950-980 Watts) mounted in a housing equipped with an $f/0.7$ quartz lens assembly and a water filter. The light was directed through a series of filter glasses resting in a water-filled

Table 3-3. Transmittance data for filter combinations.

No.	Filters ^a	Transmittance range ^b	λ_{max} (Trans)
1	WG-305/KG-5/UG-11	$306 < \lambda < 386\text{ nm}$	355 nm (0.35)
2	# 1 + 334 int ^c	$326 < \lambda < 342\text{ nm}$	335 nm (0.08)
3	WG-305 or -345, GG-375 ^d , KG-5, UG-11	$352 < \lambda < 386\text{ nm}$	368 nm (0.16)
4	(WG-305), WG-360, KG-5, UG-11	$342 < \lambda < 386\text{ nm}$	365 nm (0.25)
5	WG-360, GG-455, KG-5	$446 < \lambda < 806\text{ nm}$	490-600 nm (0.6)
6	WG-305, OG-570, KG-5	$557 < \lambda < 807\text{ nm}$	594 nm (0.57)
7	WG-360, KG-5	$341 < \lambda < 809\text{ nm}$	380-600 nm (0.6)
8	UG-5	$223 < \lambda < 417; \lambda > 653\text{ nm}$	330 nm (0.92)

^a obtained from Schott (3mm thickness). ^b cutoff values are defined as 1% transmittance.

^c 334 nm interference filter obtained from Oriel. ^d 1 mm thickness.

chamber. The filter combinations used and their transmittance data are listed in Table 3-3.

NMR experiments. Unless otherwise noted ^1H NMR experiments were performed on a JEOL GX-400 FT NMR spectrometer. Because of an uncorrectable software error, ejecting the sample from the probe at low temperature causes the VT system to shut off; near $-80\text{ }^\circ\text{C}$ the fastest possible sample change causes the probe to warm *ca.* $10\text{ }^\circ\text{C}$ (recooling requires *ca.* 30 sec). To compensate for this, samples were placed in the probe partially frozen, and for experiments in which it was especially important to avoid thermal decomposition of diazene **2** (*e.g.*, monitoring the progress of the sensitized photolysis — see below) the probe was cooled to $-90\text{ }^\circ\text{C}$ before the sample was inserted or removed. Control experiments demonstrated that this procedure prevented sample decomposition. Spectra were typically recorded at $-80\text{ }^\circ\text{C}$ with 64 scans and sufficient time between pulses (*ca.* 9 sec) to ensure complete relaxation of all the protons in the species present (as determined by simply varying the pulse delay). For convenience, dimer concentrations are reported in terms of (monomer units)/2. Before each kinetics experiment the probe temperature was measured at a series of predetermined settings with a standard methanol sample¹¹¹ and was monitored continuously by a permanent thermocouple mounted just below the probe, whose temperature generally fluxuated by $\pm 0.1\text{ }^\circ\text{C}$ at most. The sample temperatures were measured several times and found to be reproducible at a given thermocouple reading.

Spectroscopic characterization of 2,4-dimethylenebicyclo[1.1.0]-butane (3). Direct photolysis of solutions of diazene **2** in various solvents at ≤ -78 °C produces the characteristic singlets of **3**, identified by their thermal lability. ^1H NMR (400 MHz, CD_2Cl_2 , -80 °C) δ 4.22 (s, 4 H, olefinic methylenes), 3.18 (s, 2 H, bridgehead methines). ^1H NMR (400 MHz, C_7D_8 , -80 °C) δ 4.34 (s, 4 H), 2.37 (s, 2 H).

The facility with which **3** dimerizes in solution demanded the use of special techniques at very low temperature to attempt to acquire natural abundance ^{13}C NMR spectra. Thus, a crystalline sample of diazene **2** at -78 °C was dissolved in *ca.* 120 μl of cold CD_2Cl_2 ,¹¹² and this solution was diluted with a cold solution of 600 μl of $\text{Et}_2\text{O}-d_{10}$ (MSD Isotopes) in 2.0-2.5 ml of CF_2Cl_2 (Aldrich; freshly vacuum-transferred from CaH_2). The sample was transferred to a cold 10-mm o.d. NMR tube, evacuated at -78 °C for several minutes until the solvent volume reached *ca.* 2.5 ml, frozen in liq. N_2 , evacuated to <0.01 mm, and sealed with an oxygen-gas flame. Because other samples had demonstrated a propensity for stress-fracturing and breaking their NMR tubes, the sample was thawed slowly by placing its 77 K dewar in a -100 °C freezer overnight. A UV spectrum of the sample had a 331-nm absorbance of 1.8 (out of the linear range of the spectrophotometer), implying a concentration of **2** ($\epsilon = 240 \text{ M}^{-1} \text{ cm}^{-1}$ 101) of $\geq 7.5 \times 10^{-3} \text{ M}$.

A ^{13}C NMR spectrum of diazene **2** was obtained at -120 °C by using the DEPT⁺⁺ 113 pulse sequence. Unfortunately, because of technical problems (which included difficulty in spinning the sample tube, inability to tune the probe or measure an accurate 90° ^1H pulse at -120 °C, and the fact that the accumulation time was limited by the capacity of the liq. N_2 dewar of the VT

system) 2-3 hrs of accumulation provided a spectrum whose methine peaks had S/N of only about 2-3. The methylene signal was even smaller. It was decided that the chances of obtaining a spectrum of **3** and unambiguously assigning its peak positions and coupling constants under these conditions were so small that further experimental effort was not warranted.

Empirical Force Field (EFF) Calculations. MM2¹¹ calculations employed a version of N.L. Allinger's (QCPE 395) FORTRAN program that had been adapted for use on the IBM-PC by Serena Software. This company also supplied a version of M. Saunders' "STR" program for generating MM2 input structures. The optimized structures of Figure 3-1 were obtained by using a simple graphics program for the IBM-PC/XT.

This version of MM2 does not include parameters for the central bond of conjugated diene units; however, we did not feel that treatment of the planar 1,3-diene units of the dimers (**10-13**) required the use of a more sophisticated force field.¹¹⁴ Consequently, parameters were chosen that roughly reproduced the relative energies and geometries of *s-cis* and *s-trans* rotomers of a few butadienes as well as the E_a 's for their interconversion, as determined by more sophisticated EFF calculations.¹¹⁵ Thus, for the diene sp^2 - sp^2 single bond stretching constants we used $k=5.0$, $r_0=1.46$ Å; for the torsional constants (defined in terms of the C-C-C-C dihedral angle), $V_1=1.7$, $V_2=7.0$, $V_3=0$ kcal mol⁻¹.

For *s-trans*- and *s-cis*-butadiene and for *s-trans*-2-methylbutadiene and *s-trans*-2,3-dimethylbutadiene we calculated central bond lengths within 0.001 Å of those calculated by Tai and Allinger.¹¹⁵ Our calculated energy difference

between *s-cis*- and *s-trans*-butadiene, 2.57 kcal mol⁻¹ and the E_a for rotation of the *s-trans* (the transition structure being approximated by enforcing a 90° central dihedral angle), 6.92 kcal mol⁻¹, compare well with the reported values of 2.62 and 7.31 kcal mol⁻¹.¹¹⁵ The analogous values we obtain for 2-methylbutadiene, 2.03 and 5.79 kcal mol⁻¹ are also in reasonable agreement with Tai and Allinger's values, 2.26 and 6.0 kcal mol⁻¹,¹¹⁵ although they report the *s-cis* conformer to be twisted by 37°, while our calculations find a planar minimum. Comparison of the known heats of formation of the three butadienes¹¹⁶ with the values calculated by using the MM2 "bond enthalpy constants" furnished the missing value for the sp²-sp² single bond as -4.34 (±0.14) kcal mol⁻¹. Because an adequate treatment of the methylenecyclobutene system was critical to the present study, we also calculated the heat of hydrogenation of 1-methyl-3-methylenecyclobutene. Our value of -58 kcal mol⁻¹¹¹⁷ is in reasonable agreement with the reported value of -55 kcal mol⁻¹.¹¹⁸

The calculated geometries and strain energies for dimers 74-77 are presented in Figure 3-1. The strain energies were obtained by subtracting the MM2 "strainless bond enthalpy" from the calculated heats of formation. Calculated ΔH_f° values are as follows: 74, 151.6; 75, 134.1; 76t, 125.7; 76c, 134.8; 77t, 126.0; 77c, 130.3 kcal mol⁻¹. The calculated bond lengths and angles are presented in Figure 3-10.

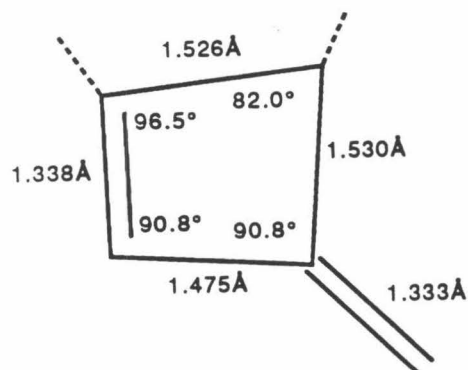
Whereas the chair conformations of the cyclohexane rings of 76t and 77t are unique, several possibilities exist for the boat conformations of 76c and 77c. For 76c a conformation with one methylene and one methine at the apical positions (*i.e.*, the bow and stern) of the boat rather than the two olefinic

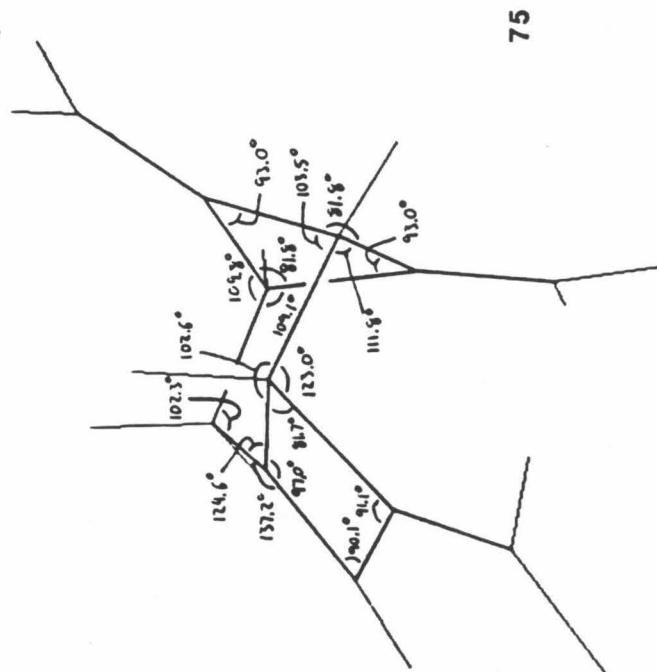
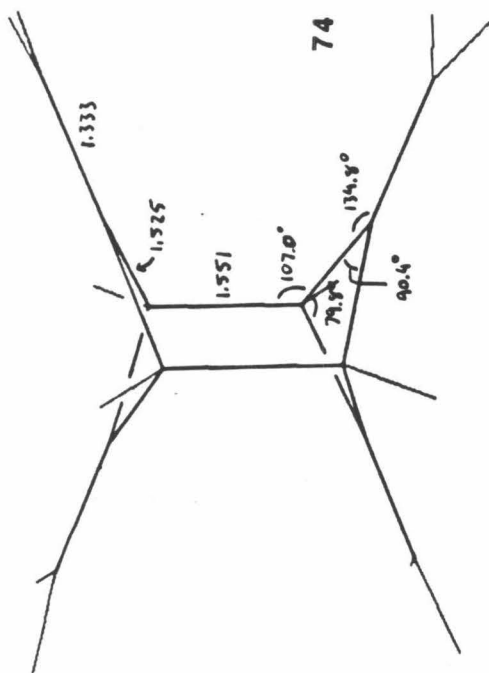
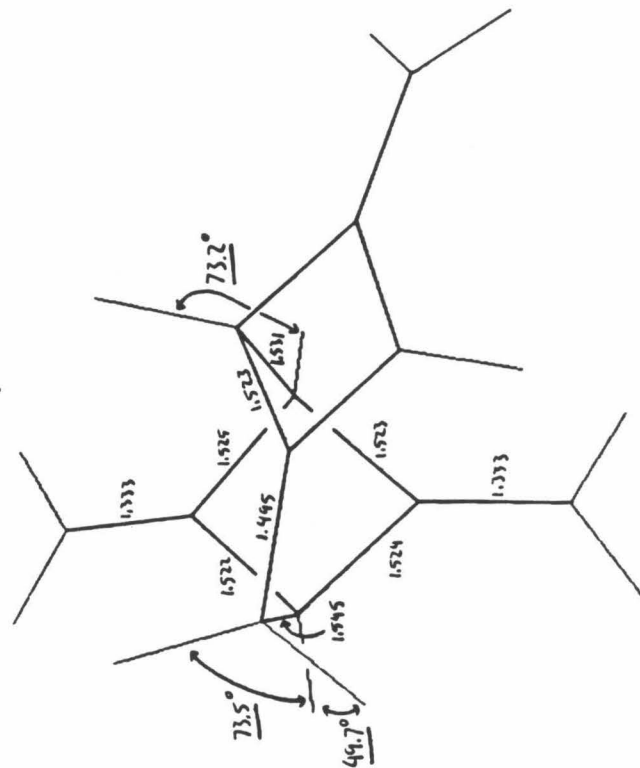
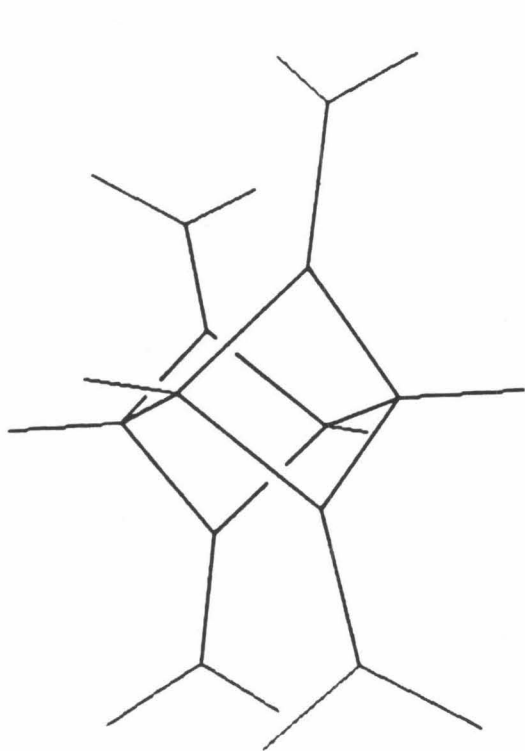
carbons was found to be an energy minimum, but its strain energy was 201 kcal mol⁻¹ – 109 kcal mol⁻¹ higher than that of the structure shown in Figure 3-1. The input structure **77c** had the olefinic carbons at the apexes, but the optimization instead placed the methines at the apical positions (Figure 3-1, 3-10). The alternative structure with the methylenes at those positions is seen to be quite unreasonable by the use of simple molecular models and was not considered.

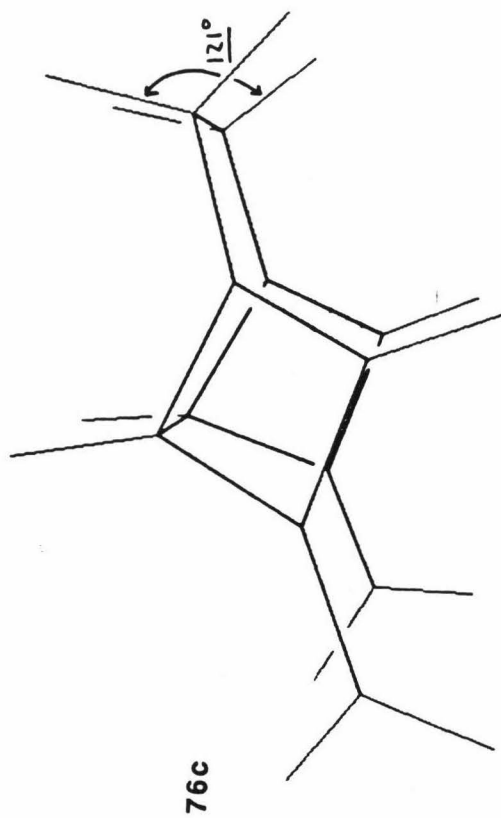
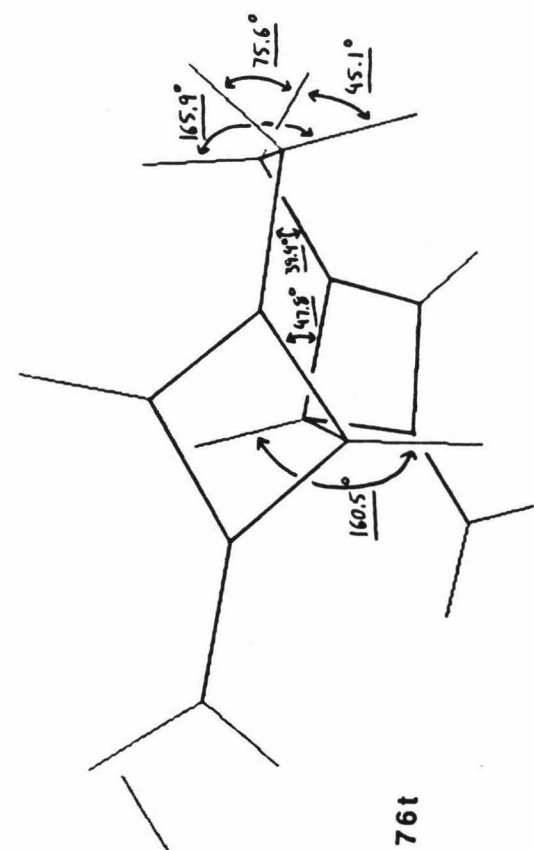
Characterization of dimers. Because we have obtained the dimers only in relatively small quantities and have found them to be quite air sensitive (and seemingly more labile in the absence of solvent), we have made no serious attempt to separate them on a preparative scale. The ¹H NMR spectra reported here were obtained at –80 °C because the aliphatic methine and especially the cyclobutene protons of **75** and **76t** have severe relaxation problems at room temperature in both CD₂Cl₂ and C₇D₈ solutions (T₁ for the cyclobutane protons is *ca.* 0.5 min). Spectra of dimers **75**, **76t**, and **77t** and their deuterated analogs are presented as Figure 3-11.

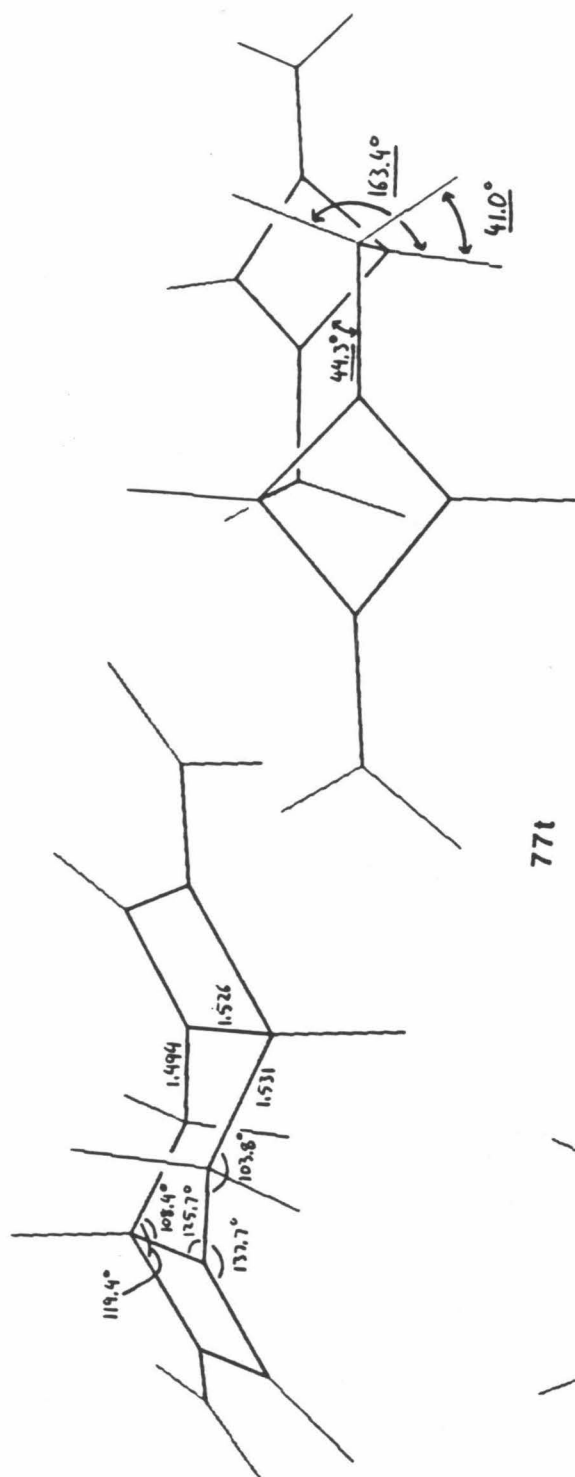
3,8,9-Trimethylenetricyclo[5.1.1.0^{2,5}]non-4-ene (75**).** ¹H NMR (400 MHz, CD₂Cl₂, –80 °C; Figure 3-11a) δ 6.11 (d, *J* = 1-2 Hz, 1 H, cyclobutene), 4.815, 4.813, 4.78, 4.72, 4.48, 4.35 (6s, 1 H each, olefinic methylenes¹¹⁹), 3.46 (d, *J*_{1,7} = 5.9 Hz, 1 H, H-1), 3.38 (s, 1 H, H-2), 3.30 (pseudo-t, 1 H, H-7), 2.84 (dd, *J*_{6,6} = 13.4 Hz, *J*_{6,7} = 4.4 Hz, 1 H, H-6, *cis* to the cyclobutene ring), 2.77 (d, *J*_{6,6} = 13.2 Hz, 1 H, H-6, *trans* to the cyclobutene ring).¹²⁰ A decoupling experiment along with the spectrum of **75-d₄** (see below) confirmed the

Figure 3-10. MM2¹¹ geometries for dimers 74-77. Two views of each are shown. Bond lengths are in Å, and dihedral angles are underlined. The geometrical parameters for the methylenecyclobutane groups were roughly constant from structure to structure (unless otherwise noted) and are shown below.

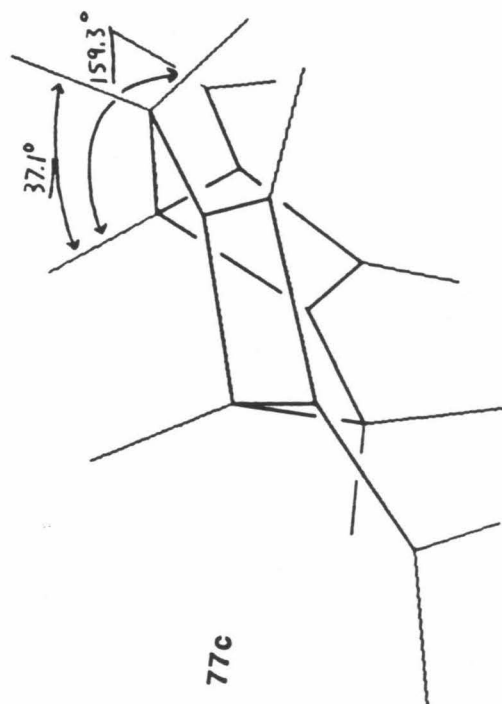








77f



77c

Figure 3-11. ^1H NMR spectra of dimers obtained at -80°C in CD_2Cl_2 . (Impurity peaks are marked "x"; peaks of **2** and **3** are designated by their numbers.) Included are spectra of (a) **75** + **76t** from -40°C thermolysis of diazene **2**; (b) **75-d₄** + **76t-d₄** from -95°C photolysis of diazene **2**; (c) a sample of **2** (+ **75** + **76t**) and Ph_2CO before and after sensitized photolysis. The final sample composition is **75** + **76t** + **77t**; (d) **77t** obtained by subtraction of the two spectra in c (lower spectrum $-2.0 \times$ upper); (e) a sample of **2-d₂** (**75-d₄** + **76t-d₄**) and Ph_2CO before and after sensitized photolysis. The final sample composition is **75-d₄** + **76t-d₄** + **77t-d₄**; (f) **77t-d₄** obtained by subtraction of the two spectra in e (lower $-2.3 \times$ upper).

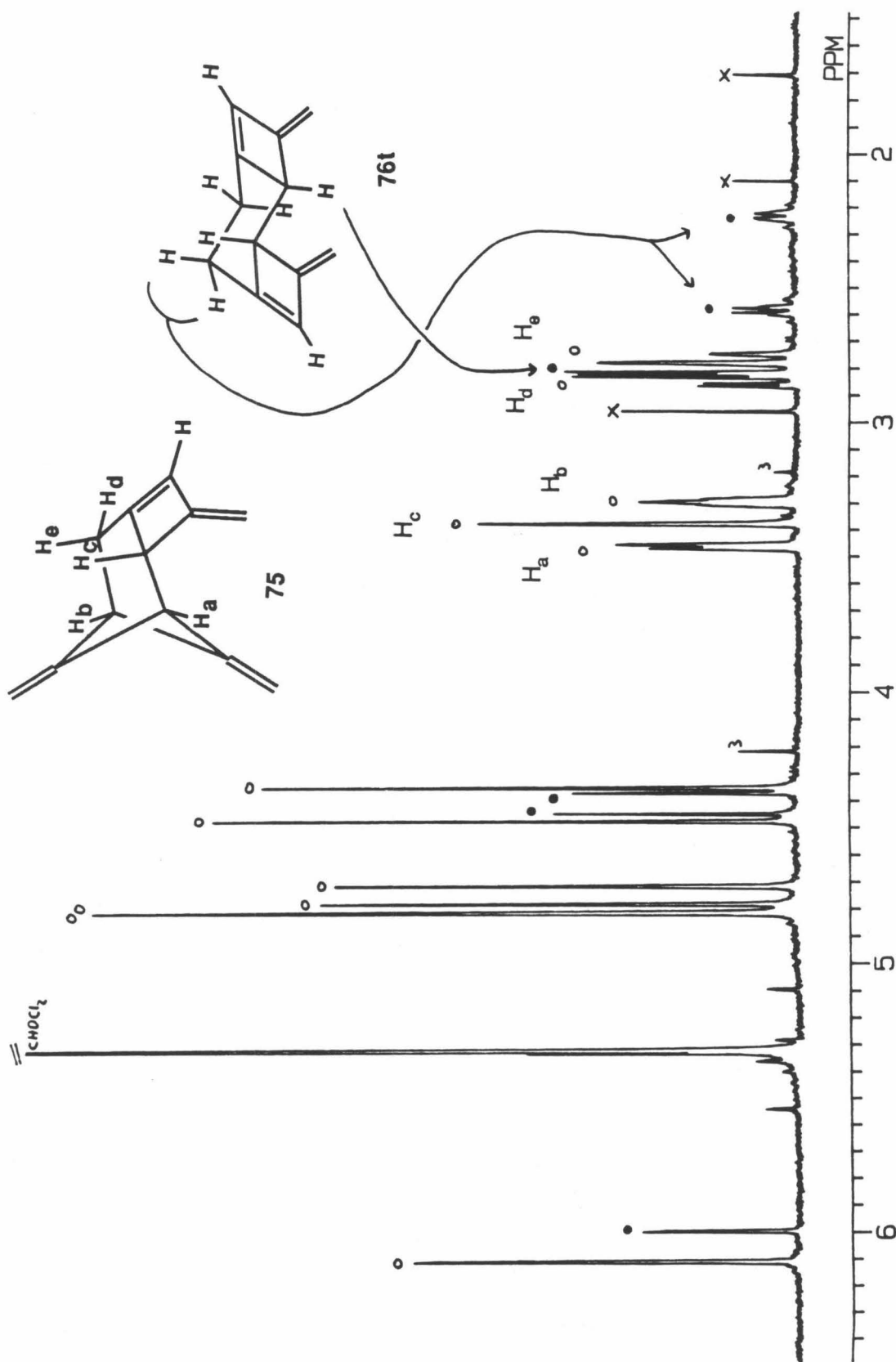
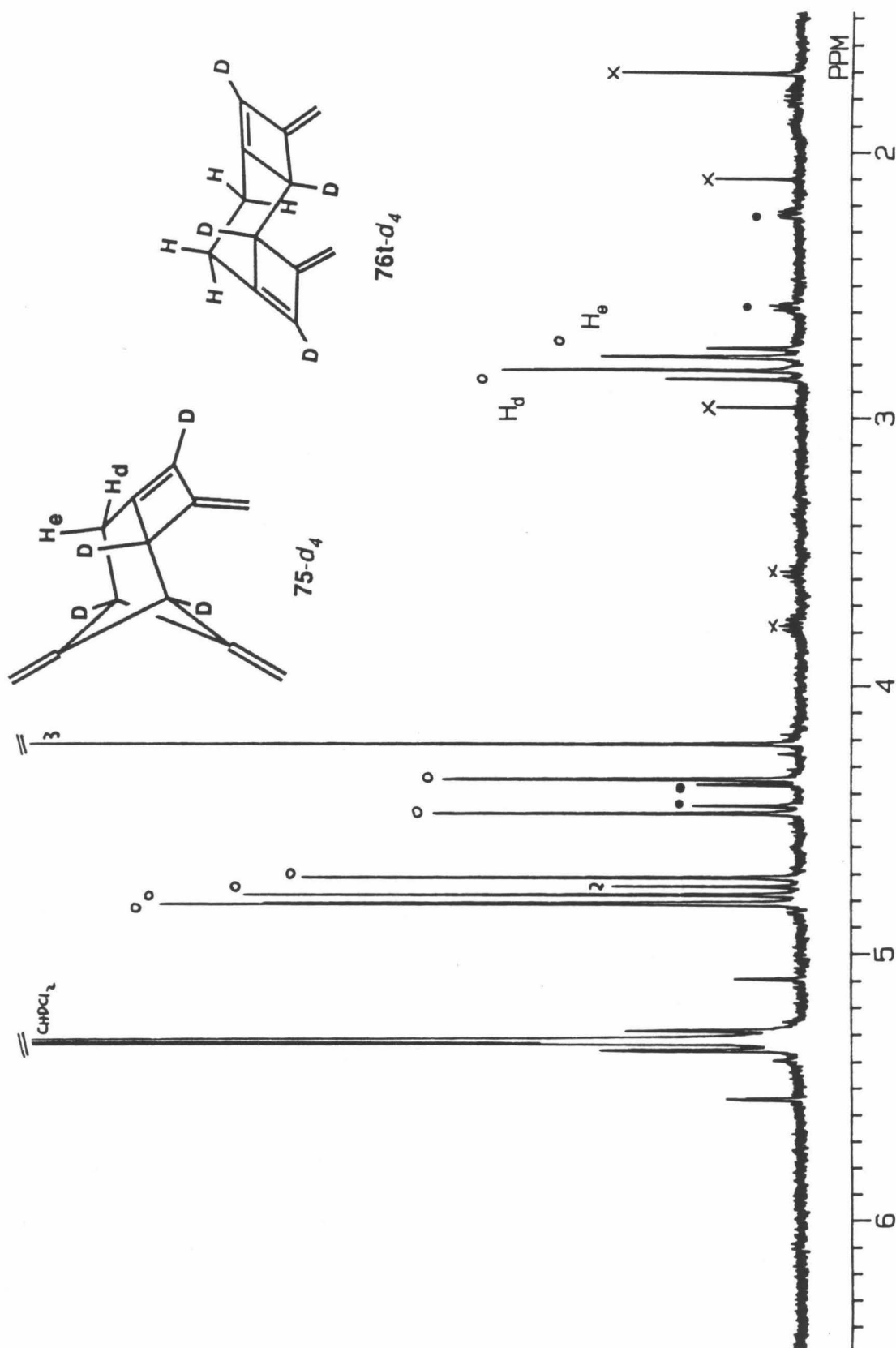


Figure 3-11a. 75, o; 76t, •.

Figure 3-11b. 75-d₄, o; 76t-d₄, ●.

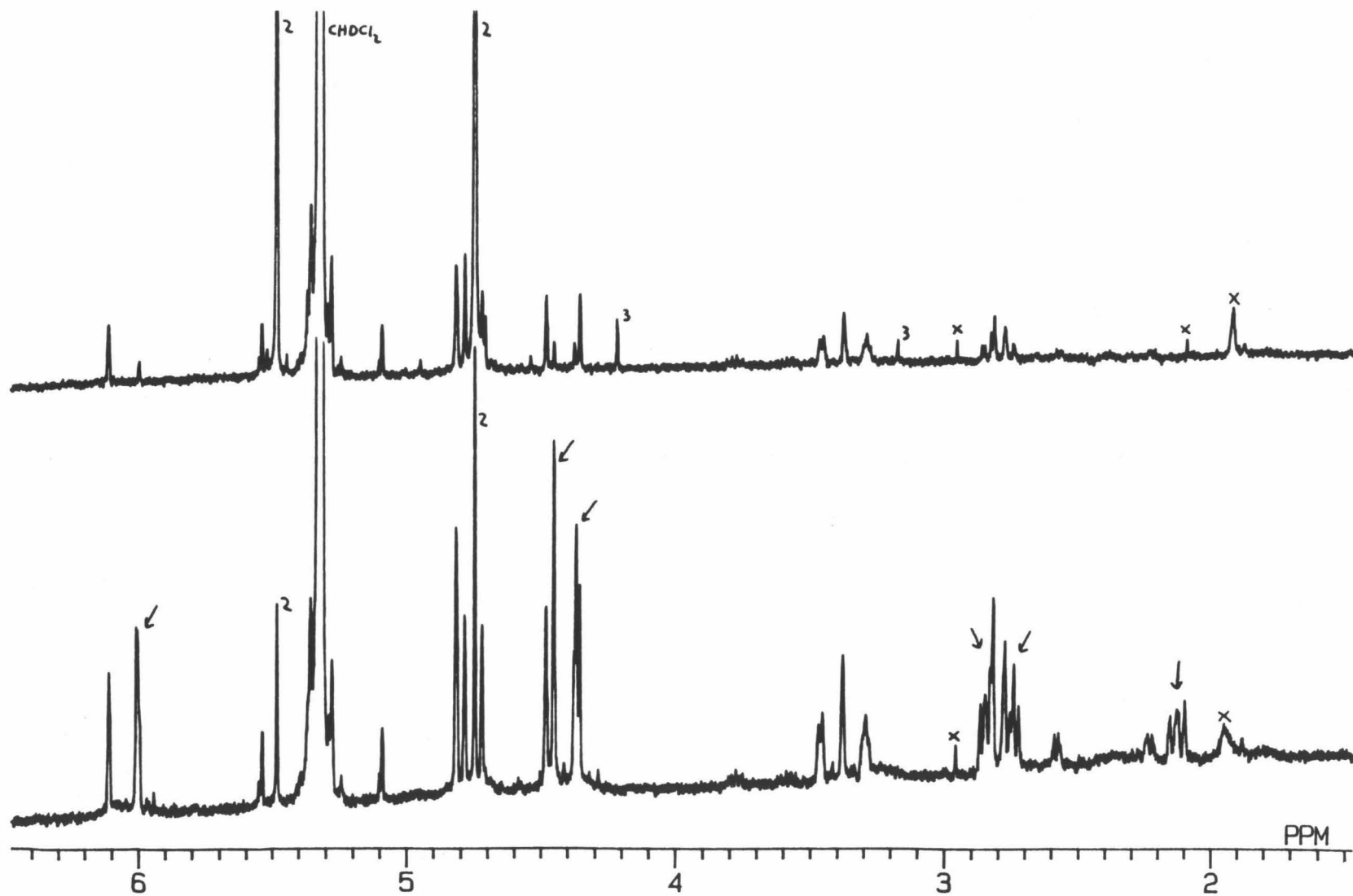


Figure 3-11c. Top: Before $3h\nu$. Bottom: after $3h\nu$; signals of 77t are marked with arrows.

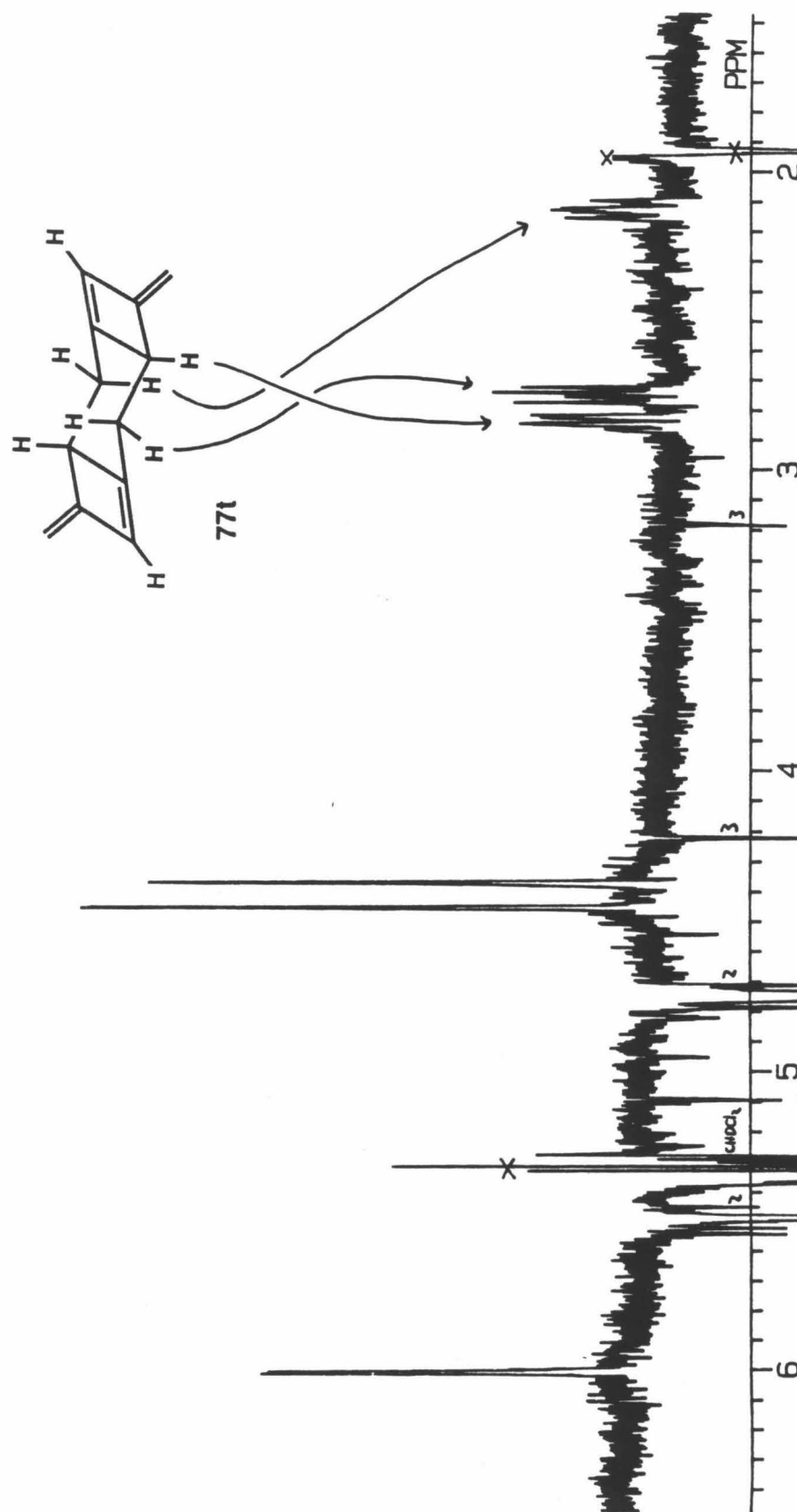


Figure 3-11d. 77t, by subtraction of the 3-11c spectra.

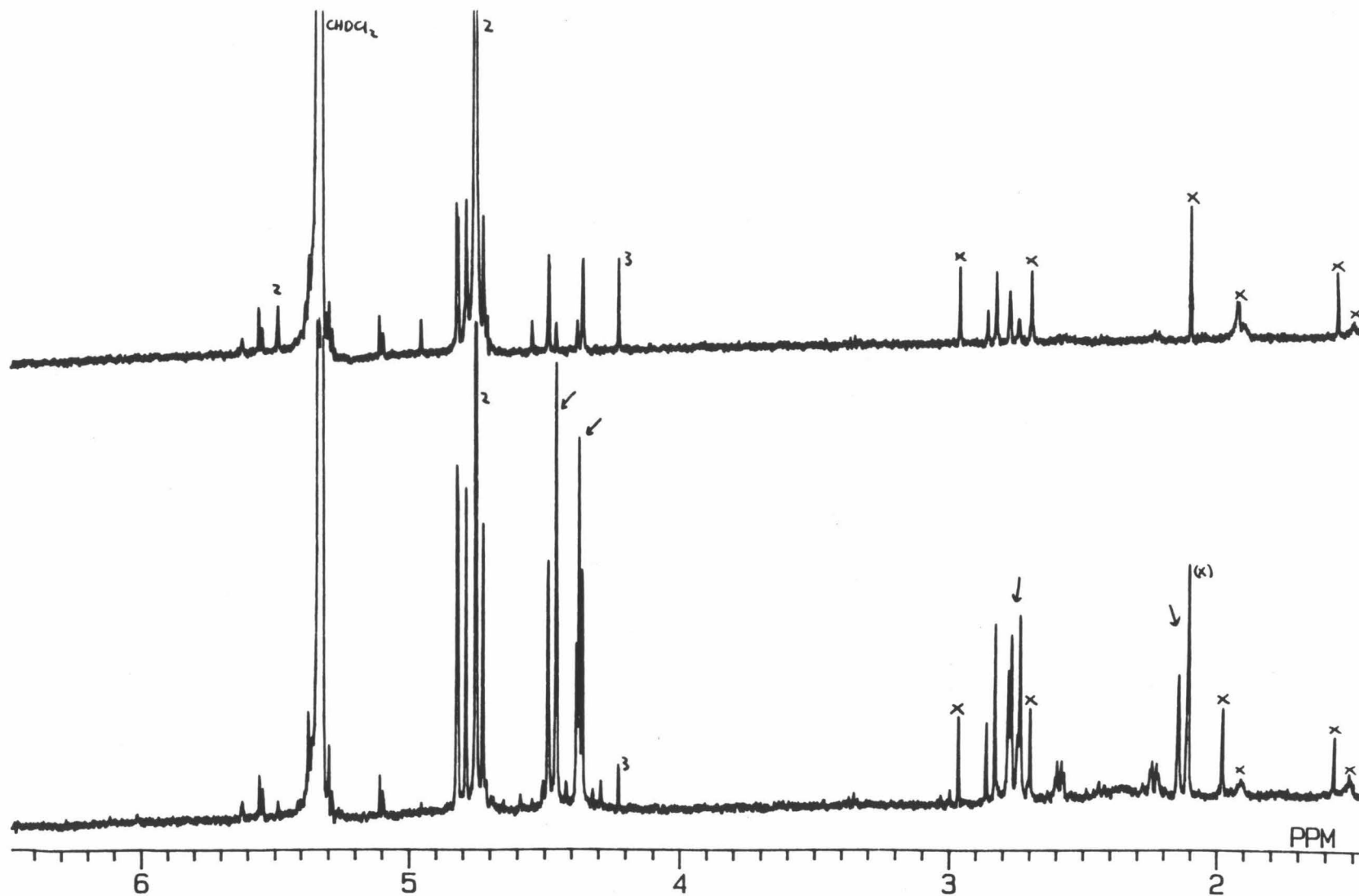


Figure 3-11e. Top: before $^3\text{h}\nu$. Bottom: after $^3\text{h}\nu$; signals of $^{77}\text{t-d}_4$ are marked with arrows.

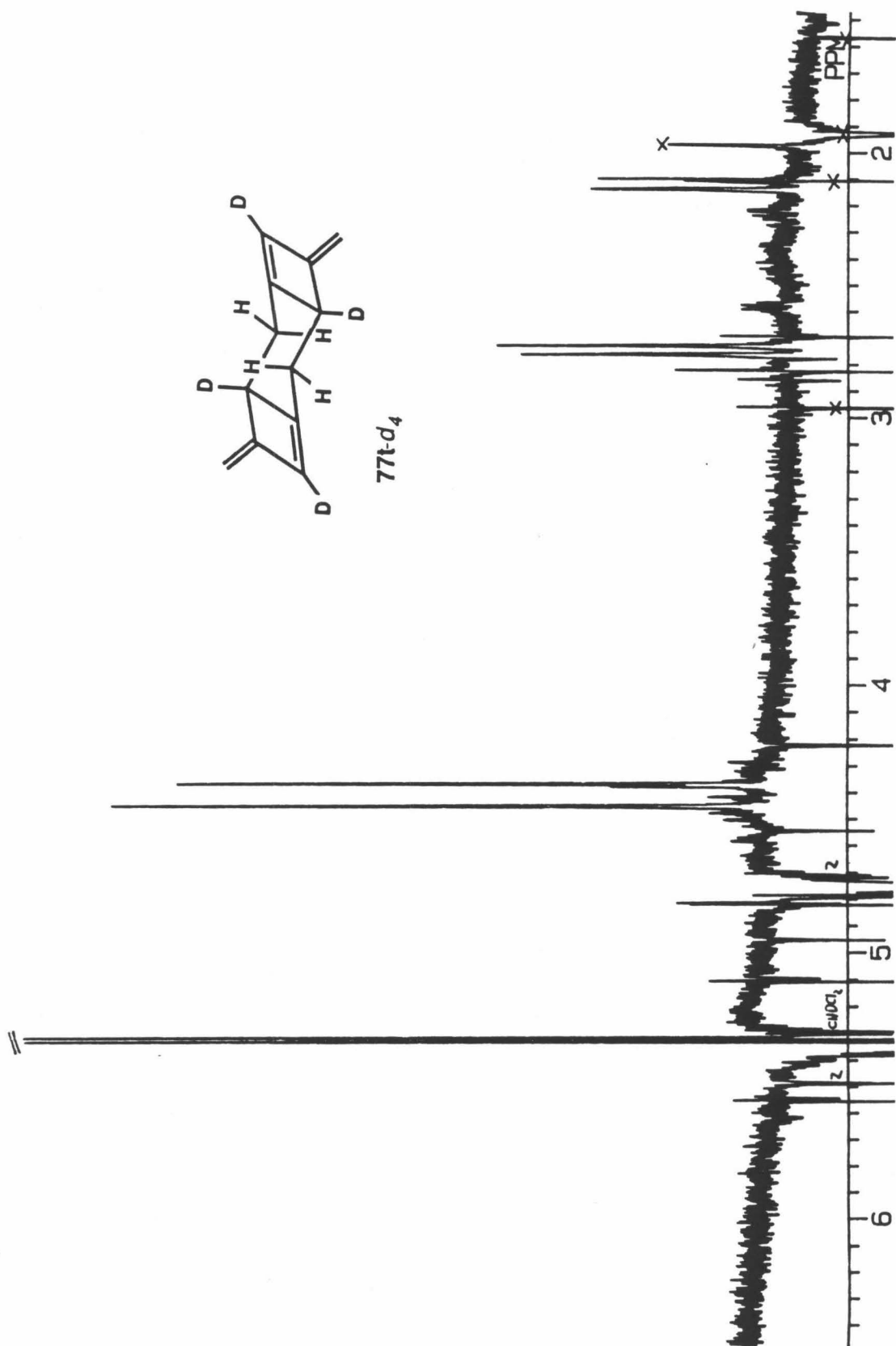


Figure 3-11f. ${}^{77}\text{Tl}$ - d_4 , by subtraction of the 3-11e spectra.

assignments. ^{13}C NMR (125 MHz, CD_2Cl_2) 123 δ 155.4, 151.0, 147.6, 146.8 (quaternary olefinic, C-3,5,8,9), 131.9 (cyclobutene, C-4), 102.9, 100.0, 94.9 (olefinic methylenes), 59.8, 55.7, 52.6 (aliphatic methine, C-1,2,7), 40.0 (aliphatic methylene, C-6). An INEPT pulse sequence confirmed the assignments of the methylene carbons and provided coupling constants of $J_{\text{CH}} = 157$ Hz for the olefinic and $J_{\text{CH}} = 134$ Hz for the aliphatic methylenes.

***trans*-3,10-Dimethylenetricyclo[6.2.0.0 2,5]deca-4,8-diene (76t).** ^1H NMR (400 MHz, CD_2Cl_2 , -80°C ; Figure 3-11a) δ 6.00 (d, $J = 1$ Hz, 2 H, cyclobutene), 4.45, 4.37 (2s, 2 H each, olefinic methylenes), 2.81 (s, 2 H, H-1,2), 2.58 (m, major line separations *ca.* 7 and 3 Hz, 2 H, H-6,7 124), 2.23 (m, major line separation *ca.* 7 Hz, 2 H, H-6,7 124). (A decoupling experiment confirmed that the protons responsible for the last two signals are coupled to each other.) ^{13}C NMR (125 MHz, CD_2Cl_2) 123 δ 128.2 (cyclobutene, C-4,9), 94.4 (olefinic methylenes), 52.4 (aliphatic methines, C-1,2), 26.5 (aliphatic methylenes, C-6,7), the quaternary carbons, C-3,5,8,10, were not visible.

***trans*-5,10-Dimethylenetricyclo[6.2.0.0 3,6]deca-3,8-diene (77t).** ^1H NMR (400 MHz, CD_2Cl_2 , -80°C ; obtained by spectral subtraction of the signals of 75 and 76t; Figure 3-11c,d) δ 6.01 (d, $J = 1\text{--}2$ Hz, 2 H, cyclobutene), 4.45, 4.37 (2s, 2 H each, olefinic methylenes), 2.83 (pseudo-t, line separation *ca.* 8 Hz, 2 H, H-1,6), 2.76 (dd, $J_{2,2} = 13$ Hz, $J_{1,2\text{eq}} = 7$ Hz, 2 H, H-2,7-equatorial), 2.13 (pseudo-t, line separation *ca.* 10 Hz, 2 H, H-2,7-axial). 124

1,2,4,7-Tetradeuterio-75 (75-*d*₄). ¹H NMR (400 MHz, CD₂Cl₂, -80 °C; Figure 3-11b) δ 4.814, 4.809, 4.78, 4.71 (4s, 1 H each, olefinic methylenes), 4.47, 4.35 (2d, *J* = 1 Hz, 1 H each, olefinic methylenes¹¹⁹), 2.83 (d, *J*_{6,6} = 13.4 Hz, 1 H, H-6, cis to the cyclobutene ring), 2.76 (d, *J*_{6,6} = 13.4 Hz, 1 H, H-6, trans to the cyclobutene ring).

1,2,4,9-Tetradeuterio-76t (76t-*d*₄). ¹H NMR (400 MHz, CD₂Cl₂, -80 °C; Figure 3-11b) δ 4.45, 4.37 (2s, 2 H each, olefinic methylenes), 2.59 (m, 2 H, H-6,7), 2.23 (m, 2 H, H-6,7).¹²⁴

1,4,6,9-Tetradeuterio-77t (77t-*d*₄). ¹H NMR (400 MHz, CD₂Cl₂, -80 °C; obtained by spectral subtraction of the signals of 75-*d*₄ and 76t-*d*₄; Figure 3-11e,f) δ 4.45, 4.37 (2s, 2 H each, olefinic methylenes), 2.74 (d, *J*_{2,2} = 13 Hz, 2 H, H-2,7-equatorial), 2.12 (d, *J*_{2,2} = 13 Hz, 2 H, H-2,7-axial).¹²⁴

GC and GC-MS analysis of dimers. GC analyses were performed on a Hewlett-Packard 5840A gas chromatograph equipped with a flame-ionization detector. The instrument had been modified for capillary capability and a J & W scientific 30-m, 0.25-μm Durabond-17 (bonded phenyl methyl silicone – OV-17) was used with H₂ as the carrier. Although retention times varied somewhat depending on flow rate and column age, typical retention times at 100° C were as follows: 75, 3.85; 76t, 6.82; 77t, 6.15; D₁, 8.37; D₂, 10.87 min. GC-MS analyses were performed by the U.C. Riverside Mass Spectrometry Lab with an equivalent column. The intensities of the prominent peaks are listed in Table 3-4 and are normalized to M⁺. Aside from the M⁺ – 1 peaks,

Table 3-4. Mass spectral data for dimers and d_4 -dimers ^a —
relative intensities.^b

<i>m/e</i>	75	76t	77t	D ₁	D ₂
157	13	14	13	14	10
156 (M ⁺)	100	100	100	100	100
155	91	28	51	53	110
154	21	11	10	12	21
153	33	17	19	21	39
152	17	10	10	12	21
141	113	34	61	63	125
129	40	17	24	23	39
128	64	27	32	31	58
127	28	14	15	16	29
117	55	36	48	38	45
116	35	17	27	26	29
115	133	72	89	79	123
102	11	5	6	5	8
91	41	21	34	27	26
89	11	6	7	6	9
78	13	8	11	8	8
77	21	12	14	12	14
76	11	7	8	6	9

Table 3-4. Mass spectral data for dimers and d_4 -dimers ^a —
relative intensities.^b (continued)

<i>m/e</i>	75	76t	77t	D ₁	D ₂
65	21	11	14	9	10
64	11	7	7	5	5
63	25	15	17	10	16
52	12	7	10	5	5
51	36	19	23	13	16
<i>m/e</i>	75- d_4	76t- d_4	77t- d_4	D ₁ - d_4	D ₂ - d_4
161	12	12	13	14	11
160 (M ⁺)	100	100	100	100	100
159	84	28	49	48	84
158	38	13	23	21	43
157	22	9	12	14	18
156	22	10	12	14	18
145	62	17	34	33	64
144	62	16	35	32	64
143	25	7	12	11	27
133	16	7	9	9	18
132	43	15	23	23	45
131	45	16	25	25	52
130	33	12	17	18	36
129	16	6	9	9	18

Table 3-4. Mass spectral data for dimers and d_4 -dimers ^a – relative intensities.^b (continued)

m/e	75- d_4	76t- d_4	77t- d_4	D ₁ - d_4	D ₂ - d_4
120	65	36	53	47	64
119	40	17	28	27	36
118	79	34	56	54	84
117	57	27	42	39	64
116	15	7	9	9	18
105	8	3	4	5	9
94	24	10	17	16	18
93	22	9	19	18	27
80	12	6	11	9	9
79	14	6	9	10	16
78	13	5	8	9	11
52	26	10	14	14	18

^a GC-MS (EI). See text for details. Intensity data are normalized to the M⁺ peak. ^b The prominent peaks - i.e., those consistently \geq ca.10% in the spectra of all the dimers and those that dominate the smaller clusters of peaks - with $m/e \geq 51$ are listed for the protio dimers. For the d_4 -dimers, most of the peaks of $\geq 15\%$ above m/e 116 are listed, along with selected peaks from m/e 51-115 (specifically, moderately intense peaks at m/e 63-67 and 51,53, and 54 have been omitted).

which varied slightly from spectrum to spectrum, the relative intensities were quite reproducible. Because dimers **76t** and **77t** were not completely resolved under the conditions of the GC-MS experiments, spectra of **76t** and **76t-d₄** were obtained from a sample free of **77t**, while the spectra of **77t** and **77t-d₄** were acquired by using samples in which **77t** dominated **76t** by *ca.* 3:1.

Thermal stability and air sensitivity of dimers. Heating a sample of **75** and **76t** in CD₂Cl₂ in a sealed (thick-walled) tube for *ca.* 1 day caused loss of about half of the dimers, with **75** decomposing slightly more rapidly than **76t**. The decomposition products have not been identified, however the thermolysis initially produced several new ¹H NMR signals at δ 6.0 (s), 5.1 (s), 5.0 (s), 4.8 (s), 4.7 (s), 4.6 (d), 4.2 (br s), 3.2 (br t). Continued heating for several days afforded a product mixture with an extremely complex ¹H NMR spectrum, including both sharp and broad signals. A similar sample was exposed to air at room temperature. Most of the **75** was gone after *ca.* 1 day; a small amount of **76t** persisted for several days. (Injudicious sample manipulation or concentration of the solution causes more rapid degradation.) The decomposition products are characterized by sharp singlets near δ 6.2 in addition to other less prominent signals and numerous broad peaks. GC analysis under the conditions described above reveals that upon exposure to air the loss of **75** is accompanied by an increase in a new peak at retention time 9.75 min (corresponding to 20 (\pm 10)% of the **75** lost if the response factors are similar), in addition to several other peaks at longer retention times. GC-MS analysis of the new species revealed incorporation of one oxygen atom: *m/e* (relative intensity) 172 (4, M⁺), 171 (6), 157 (5), 153 (4), 144

(18), 143 (33), 142 (6), 141 (12), 130 (25), 129 (100), 128 (93), 127 (26), 117 (13), 116 (33), 115 (51), 105 (13), 104 (8), 103 (14), 102 (6), 91 (33), 79 (9), 78 (14), 77 (23), 65 (20), 63 (14), 51 (23). For the deuterated analog: m/e (rel. int.)¹²⁵ 176 (7, M^+), 175 (7), 174 (4), 161 (4), 160 (4), 157 (4), 156 (4), 148 (24), 147 (32), 146 (24), 145 (8), 144 (11), 134 (33), 133 (78), 132 (100), 131 (92), 130 (54), 129 (21), 120 (19), 119 (43), 118 (52), 117 (30); 108 (18), 94 (29), 93 (20), 80 (20), 79 (23), 67 (16), 52 (27). Under the conditions of the GC-MS experiment another prominent peak was found at r.t. 13-14 min, apparently containing two oxygens: (from the protio-dimer sample) m/e (rel. int.)¹²⁵ 188 (6, M^+), 173 (3), 160 (31), 159 (23), 146 (19), 145 (22), 132 (18), 131 (44), 129 (13), 118 (18), 117 (56), 116 (24), 115 (33), 105 (14), 104 (14), 103 (13), 92 (13), 91 (100); 77 (22), 65 (18), 53 (22), 51 (25).

Thermal and photochemical reactions of diazene 2. (a) **Thermolysis and direct photolysis.** A sample of diazene 2 in CD_2Cl_2 containing mesitylene as an internal standard was found by 1H NMR to contain 22.8 mM 2, 1.1 mM 3, 5.9/2 mM 75, and 0.7/2 mM 76t, for a total of 30.5 mM monomer (C_6H_6) equivalents. After thermal decomposition at $-78\text{ }^\circ C$, the sample was found to contain 30.6/2 mM 75 and 3.6/2 mM 76t, for a total of 34.2 monomer equivalents (no insoluble material was observed after any thermal or photochemical decomposition), indicating quantitative formation of dimers from 2, within experimental error. The decomposition of two additional diazene samples at $-51\text{ }^\circ C$ and $-32\text{ }^\circ C$ was analyzed in a similar fashion. At $-51\text{ }^\circ C$, 31.4 mM 2, 1.1 mM 3, 16.7/2 mM 75, and 2.4/2 mM 76t, totaling 51.6 mM monomer equivalents, formed 43.9/2 mM 75 and 6.6/2 mM 76t, or 50.5

mM monomer equivalents. At $-32\text{ }^{\circ}\text{C}$, 36.7 mM **2**, 0.4 mM **3**, 9.8/2 mM **75**, and 1.2/2 mM **76t**, totaling 48.1 mM, produced 41.8/2 mM **75** and 7.5 mM **76t**, or 49.3 mM monomer equivalents.

The statement that **3** produces approximately the same ratio of **75** to **76t** as that resulting from thermolysis or photolysis of **2** derives primarily from qualitative observations. The best quantification we have obtained is the finding that a freshly-photolyzed ($-95\text{ }^{\circ}\text{C}$) diazene sample containing *ca.* 3.5 mM **3** (at $-80\text{ }^{\circ}\text{C}$), 7.7/2 mM **75**, and 0.9/2 mM **76t** provided, upon thermolysis at $-63\text{ }^{\circ}\text{C}$ for 2 hrs, 0.2 mM **3**, 10.1/2 mM **75**, and 1.5/2 mM **76t**. Thus, the ratio of **75/76t** formed from **3** is *ca.* 4. Although it is difficult to ascribe a quantitatively meaningful error to this value, its significance might be conservatively delimited by the statement that **75** is by far the primary decomposition product and that some **76t** is definitely formed in addition.

Samples of diazene **2** and **2-*d*₂** were photolyzed (using filter combination #1, Table 3-3) at $-95\text{ }^{\circ}\text{C}$, then thermolyzed at $-75\text{ }^{\circ}\text{C}$. GC analysis of the product mixture (DB-17 capillary, $100\text{ }^{\circ}\text{C}$; see above) revealed the presence of *ca.* 0.1% of **77t**, *ca.* 0.05% of **D₁**, and a trace ($<0.01\%$) of **D₂**, identified by their retention times. In contrast, analysis of several diazene samples that had undergone thermal decomposition at $-78\text{ }^{\circ}\text{C}$ showed no sign of these products ($<0.005\%$). A cold ($-78\text{ }^{\circ}\text{C}$) solution of **2** in CH_2Cl_2 was added via cannula (30-gauge teflon tubing) to an N_2 -filled flask at $40\text{ }^{\circ}\text{C}$. GC analysis of the product mixture revealed *ca.* 0.1-0.3% of **77t**, *ca.* 0.1% of **D₁** a smaller amount of **D₂**. As a control experiment, a sample of **75** and **76t** (containing a trace of **77t**, **D₁** and **D₂**) was heated at $60\text{ }^{\circ}\text{C}$ for *ca.* 15 min. GC analysis revealed no increase (or decrease) in the amounts of **77t**, **D₁** and **D₂** present. While we

have not attempted to quantify the temperature dependence of the thermal formation of these products, we have found that when **2** is thermolyzed in a similar manner at 0 °C, *ca.* 0.1% of **77t** is formed, and at -30 °C only a trace is observed.

To test for CIDNP in the thermal dimerization, a sample of **2** in CD₂Cl₂ at *ca.* -95 °C was placed in the probe of a Varian EM-390 CW NMR spectrometer, which was at ambient temperature. The first scan showed the peaks of **2**, and these were replaced by the signals of **75** and **76t** as the sample warmed, but no unusual intensity effects were observed.

(b) Sensitized photolysis. A sample of diazene **2** (*ca.* 8 mM) in CD₂Cl₂ containing 0.1 M benzophenone (Ph₂CO) and mesitylene as an internal standard was irradiated at -78 °C using filter combination #3 (Table 3-3, λ 352-386 nm). The progress of the photolysis was monitored by ¹H NMR, initially at 5-15 sec intervals and later less frequently, for a total of seven measurements spanning a photolysis time of 2 min. The spectra were recorded at -80 °C. The sample was placed in the probe partially frozen and cooled to -90 °C before it was removed in order to avoid thermal decomposition of **2**. As a control, a sample of **2** was carried through the same manipulations and underwent at most, 2-3% thermal decomposition. In addition, irradiation of **2** under these conditions (filter combination #3 or 4, Table 3-3) in the absence of Ph₂CO causes no decomposition. The relative amounts of dimers **75**, **76t**, and **77t** present during the course of the photolysis (corrected for the amounts of **75** and **76t** initially present) are presented as Figure 3-8a.

A sample containing 0.01 M Ph₂CO and *ca.* 4 mM diazene **2** was photolyzed as described above (with the same light intensity), but spectra were recorded at longer time intervals, and the photolysis was monitored for 4 min to provide the plot of Figure 3-8b. A third sample containing 0.10 Ph₂CO (similar to the first) was irradiated using filter combination #4 (Table 3-3, λ 342-386 nm) to provide higher UV light intensity (but also more emitted light from the Ph₂CO). The photolysis was monitored at 5-10 sec intervals for *ca.* 1 min. Again, the product distribution remained fairly constant, with **75** at *ca.* 30%, **76t** at 10-15%, and **77t** at 50-60%. The mass balance was *ca.* 70% throughout the reaction, and >90% of the diazene was photolyzed.

A control experiment was conducted to demonstrate that dimers **77t**, **D**₁, and **D**₂ do not result from secondary photolysis of **75** and **76t**. Thus, Ph₂CO was added to a sample at **75** and **76t** (which contained a trace of **77t**, **D**₁ and **D**₂) and the sample was degassed, sealed, and irradiated at -78 °C using filter combination #4 (Table 3-3) for 30 sec. GC analysis revealed no increase (or decrease) in the amounts of **77t**, **D**₁, and **D**₂ present.

(c) **Effect of oxygen.** A sample of diazene **2** in CD₂Cl₂ under 0.8 atm of O₂ was thermolyzed at -50 °C for 1.5 hrs. By ¹H NMR the thermolysis converted a mixture of 8.1 mM **2**, 2.5/2 mM **75**, and 0.4/2 mM **76t**, or 11.0 mM monomer equivalents to a mixture of 9.1/2 mM **75** and 1.5/2 mM **76t**, or 10.6 mM total, so that the conversion was quantitative within experimental error (no new signals appeared).

To test the effect of oxygen on the decay rate of **3**, a solution of **2** in CD₂Cl₂ containing mesitylene as an internal standard was divided between two

sample tubes, and each sample was photolyzed (using filter combination #1, Table 3-3) at $-95\text{ }^{\circ}\text{C}$. One tube was filled with 0.8 atm of O_2 , and the decay of **3** was monitored by ^1H NMR at $-40\text{ }^{\circ}\text{C}$ for each sample by the procedure elaborated upon below. With the caveat that the absolute rates are critically dependent on measuring the concentration of **3** accurately (see below), the rate constants were $4.65 (\pm 0.35)\text{ M}^{-1}\text{ s}^{-1}$ for the degassed sample and $4.99 (\pm 0.25)\text{ M}^{-1}\text{ s}^{-1}$ for the oxygenated. (The error limits are standard deviations of the slopes of the eight-point $1/[\mathbf{3}]$ vs t plots.) Given the error ranges on the rate constants and the potential effect of oxygen in alleviating possible spin-lattice relaxation problems¹²⁶ (see below), there appears to be no experimentally significant difference between the two values.

A sample of *ca.* 8 mM **2** and 0.1 M Ph_2CO in CD_2Cl_2 , identical to the first sample used in section b (above), was placed under 0.8 atm of O_2 . The sample was irradiated using filter combination #3 as described in section b (above) for *ca.* 2 min. The photolysis destroyed 80% of the diazene, but no **77t** was observed by ^1H NMR, and there was no detectable increase – and perhaps even a slight decrease – in the small amounts of adventitious **75** and **76t** present before the photolysis. In addition, new signals were found to grow in to a small extent during the reaction. These appeared as sharp peaks at δ 9.5-9.8 (6 peaks), 8.9, 6.9, 6.7, 6.5 (2), 6.3 (3-4) and 5.0 (2).

Decomposition kinetics of diazene 2. Samples of *ca.* 10 mM **2** and *ca.* 5 mM mesitylene in CD_2Cl_2 were inserted in the NMR probe and allowed to equilibrate for *ca.* 5 min at the temperature of the experiment. Typically 12 to 16 spectra were recorded during each run over the time intervals listed in

Table 3-5, each spectrum being acquired with 8 scans *ca.* 9 sec apart. (The 223 K rate was obtained from only 10 points and with a shorter pulse delay.) The decays were all cleanly first-order over several half-lives and the error attached to each rate constant listed in Table 3-5 represents the standard

Table 3-5. Decay kinetics of diazene 2.^a

T	k_1^b	t (final)	half-lives
229.3 K	$3.431 (\pm 0.076) \times 10^{-3} \text{ s}^{-1}$	0.3 h	4.8
225.1	$1.603 (\pm 0.026) \times 10^{-3}$	0.5	4.3
224.8	$1.555 (\pm 0.025) \times 10^{-3}$	0.5	4.2
220.5	$6.964 (\pm 0.21) \times 10^{-4}$	1.0	3.6
220.4	$6.904 (\pm 0.12) \times 10^{-4}$	1.0	3.7
216.5	$3.174 (\pm 0.029) \times 10^{-4}$	3.0	5.0
212.2	$1.345 (\pm 0.012) \times 10^{-4}$	4.0	2.8
208.2	$6.009 (\pm 0.075) \times 10^{-5}$	5.5	1.7

^a in CD₂Cl₂. ^b error limits represent standard deviations of the $\ln [2](\text{rel})$ vs t plots.

deviation of the slope of the $-\ln[2](\text{rel})$ vs time plot. The data are plotted as $\ln(k)$ vs $1/T$ in Figure 3-2 ($\ln(k) = -9177(1/T) + 34.35$) to provide activation parameters $\log A = 14.9 (\pm 0.1)$ and $E_a = 18.2 (\pm 0.1) \text{ kcal mol}^{-1}$. The error limits represent standard deviations derived from the plots. Alternatively, an Eyring plot furnishes $\Delta H^\ddagger = 17.8 (\pm 0.1) \text{ kcal mol}^{-1}$ and $\Delta S^\ddagger = 8.3 (\pm 0.3) \text{ eu}$. (An additional point at 212.2 K fell well off the line for an unknown reason and was rejected.)

Dimerization kinetics of dimethylenebicyclobutane (3). Samples of 2 (*ca.* 10 mM) were made by dissolving the solid diazene in a cold solution of mesitylene in CD_2Cl_2 , then dividing the solution among 8 sample tubes. The standard solution consisted of 1.60 μl (1.38 mg, 11.5 mmol) of mesitylene in 2.80 ml of CD_2Cl_2 , for a concentration of 4.11 mM at room temperature. In order to determine the concentration at low temperature, the solvent volume contraction was measured by the height of a sample of CH_2Cl_2 in an NMR tube. At -81°C the volume was measured as 0.87 and at -29°C 0.93 relative to that at room temperature, and the volume change was assumed to be linear with temperature.

Each sample was irradiated at -95°C (liq. N_2/MeOH bath) using filter combination #1 (Table 3-3) for 20-30 min, the progress of the photolysis being monitored intermittently by UV spectroscopy. The samples were stored in liq. N_2 prior to the kinetics runs. We note that the samples contained an impurity that was later established to be a byproduct from the synthesis of 2, tentatively assigned as a coupling product of two molecules of the semicarbazide precursor of 2 (**67**, see Chapter 2). We have no reason to suspect that this impurity interferes in any way with the chemistry of interest, and we have reproduced the present experiments with samples free of this contaminant (see below).

The samples were inserted into the NMR probe and allowed to equilibrate for a few minutes at the desired temperature. The initial NMR spectrum revealed the presence of *ca.* 3 mM 3 at the lower and *ca.* 1 mM 3 at the higher temperatures. Ten to 14 spectra were recorded during each run, and each spectrum was obtained with 8 scans *ca.* 7 sec apart (*ca.* 60° pulses). (The 249.4

K rate was obtained from 8 points and with 4 scans per spectrum.) The decays were all cleanly second-order, as illustrated in Figure 3-3 for two runs. The data were analyzed by plotting the ratio of the integrated intensities of the mesitylene aryl peak and the methylene peak of **3**, r (eqn 3-10)

$$r = \frac{I(\text{mesitylene ArH})}{I(3 \text{ CH}_2)} \quad (3-10)$$

(which is proportional to $1/[3]$), vs time. The slopes of these plots and their standard deviations are listed in Table 3-6. The second order rate constants,

Table 3-6. Dimerization kinetics of **3**.^a

T	slope ^b	k_2 ^c	t (final)	half-lives
249.4 K	$2.618 (\pm 0.178) \times 10^{-2}$	$3.99 (\pm 0.27) \text{ M}^{-1} \text{ s}^{-1}$	0.2 h	2.0
243.3	$2.272 (\pm 0.088) \times 10^{-2}$	$3.43 (\pm 0.14)$	0.3	3.1
235.0	$1.140 (\pm 0.020) \times 10^{-2}$	$1.70 (\pm 0.03)$	0.5	3.2
227.0	$6.266 (\pm 0.179) \times 10^{-3}$	$0.925 (\pm 0.027)$	1.0	3.4
218.4	$3.749 (\pm 0.055) \times 10^{-3}$	$0.548 (\pm 0.008)$	1.7	3.8
210.2	$1.979 (\pm 0.038) \times 10^{-3}$	$0.286 (\pm 0.006)$	1.8	2.9
202.2	$9.235 (\pm 0.317) \times 10^{-4}$	$0.132 (\pm 0.005)$	4.5	2.9
194.0	$4.719 (\pm 0.115) \times 10^{-4}$	$0.0666 (\pm 0.0016)$	4.0	2.6

^a in CD_2Cl_2 . ^b the slopes of the integral ratio r (eqn 2) vs time plots (see text) and their standard deviations. ^c second-order rate constants derived from the slopes by eqn 3 (see text). The errors were propagated by simply applying eqn 3 to the errors in the slopes.

k_2 , were derived by eqn 3-11,

$$k_2 = \frac{1}{2} \times \text{slope} \times \frac{4}{3} \times \frac{1}{c_m} \quad (3-11)$$

where c_m is the mesitylene concentration, 4.11×10^{-3} M at room temperature divided by the appropriate volume ratio (see above). The factor of $\frac{1}{2}$ is required by the rate law (Scheme 3-2a). The errors in the slopes were also propagated by eqn 3-11. That is, the uncertainty in mesitylene concentration was not included in the errors attached to the rate constants in Table 3-6 or those implied by the error bars in Figure 3-4. The errors on k_2 are therefore equivalent to the standard deviations in the slopes of $1/[3]$ vs t plots.

The Eyring plot of Figure 3-4 ($\ln(k/T) = -3445 (1/T) + 9.76$) provides activation parameters $\Delta H^\ddagger = 6.8$ kcal mol⁻¹ and $\Delta S^\ddagger = -28$ eu. Although the standard deviations in the slope and intercept of the Eyring plot suggest that error limits of ± 0.1 kcal mol⁻¹ and ± 1 eu be attached to these quantities, we prefer more conservative estimates to allow for possible systematic errors. We note first that even a 10% error in the concentration of the internal standard, mesitylene, changes the absolute rate constants by 10%, but causes only a ± 0.2 eu change in ΔS^\ddagger and no change in ΔH^\ddagger . More significant is the potential effect of incomplete relaxation on the integrals of the ¹H NMR signals. We have checked for such problems at -80 °C, the lower end of the kinetic range, by simply varying the delay between scans and have found no significant relaxation problems under the conditions used in the present experiment. However, at -25 °C, the upper end of the range, **3** decays much too fast to make such an measurement. An error could be introduced by either mesitylene or **3** being incompletely relaxed and therefore displaying an artificially small ¹H NMR signal, which would cause a corresponding change in the rate constant (eqn 3-11). If we assume that relaxation problems introduce a 30% error in the rate constant at the upper end of the Eyring plot,

we find a ± 0.6 kcal mol⁻¹ change in ΔH^\ddagger and a ± 3 eu change in ΔS^\ddagger . This problem is not easily circumvented because of the need to acquire a sufficient number of scans in a time period short compared to the decay rate. We believe that 30% is probably an upper limit on the error in the higher rate constant, so that the error limits quoted above are reasonably conservative estimates.

Another potential source of error in this experiment is a perturbation of the decay kinetics by the impurity mentioned above or by adventitious acid. We therefore repeated the experiment with 5 clean (*i.e.*, free of the coupled semicarbazide contaminant) samples prepared with CD₂Cl₂ that had been distilled from CaH₂ and containing 0.02 M 2,6-lutidine. The decays remained cleanly second-order, and the 5 rate constants measured between -73 and -33 °C provided activation parameters $\Delta H^\ddagger = 7.4$ kcal mol⁻¹ and $\Delta S^\ddagger = -25$ eu. The error limits determined from the standard deviations in the slope and intercept of the Eyring plot were ± 0.3 kcal mol⁻¹ and ± 2 eu. That the activation parameters obtained in the presence of lutidine are reasonably close to those determined in its absence establishes that adventitious acid had no effect on the experiment discussed above (either by not influencing the decay rates or by simply not being present). Because the rate data presented above are intrinsically more reliable, we report the activation parameters derived from the 8-point Eyring plot.

Secondary deuterium kinetic isotope effect. A stock solution of mesitylene in CD₂Cl₂ (distilled from CaH₂) was used to make two samples each of **2** and **2-*d*₂**, and the samples were irradiated as described above. Decay rates for **3** and **3-*d*₂** were determined as described above at -38 and -71 °C.

At $-38\text{ }^{\circ}\text{C}$, $k_{\text{H}}/k_{\text{D}}$ was determined to be $2.33 (\pm 0.18) \text{ M}^{-1} \text{ s}^{-1} / 1.89 (\pm 0.07) \text{ M}^{-1} \text{ s}^{-1} = 1.23 (\pm 0.10)$; at $-71\text{ }^{\circ}\text{C}$, $0.193 (\pm 0.005) \text{ M}^{-1} \text{ s}^{-1} / 0.137 (\pm 0.010) \text{ M}^{-1} \text{ s}^{-1} = 1.41 (\pm 0.11)$. (As above, the error limits are derived only from the standard deviations of the slopes of the $1/[3](\text{rel})$ vs time plots.)

The experiment was later repeated at $-49\text{ }^{\circ}\text{C}$ to provide $k_{\text{H}}/k_{\text{D}}$ of $1.104 (\pm 0.036) \text{ M}^{-1} \text{ s}^{-1} / 0.850 (\pm 0.037) \text{ M}^{-1} \text{ s}^{-1} = 1.30 (\pm 0.07)$, and at $-73\text{ }^{\circ}\text{C}$ to provide a $k_{\text{H}}/k_{\text{D}}$ of $0.144 (\pm 0.003) \text{ M}^{-1} \text{ s}^{-1} / 0.118 (\pm 0.003) \text{ M}^{-1} \text{ s}^{-1} = 1.22 (\pm 0.04)$. All four $k_{\text{H}}/k_{\text{D}}$ values are greater than unity to an experimentally significant extent. Extrapolated to a common temperature of $-60\text{ }^{\circ}\text{C}$, these values become $1.26 (\pm 0.10)$, $1.39 (\pm 0.11)$, $1.32 (\pm 0.07)$, and $1.21 (\pm 0.04)$, for an average of 1.3.

Time evolution of [3] during thermolysis of 2. Two samples were made by dissolving diazene **2** in a solution of CD_2Cl_2 containing $1.22 \times 10^{-2} \text{ M}$ mesitylene and $1.15 \times 10^{-2} \text{ M}$ 2-methoxynaphthalene, both as internal standards. (These concentrations include a factor of $1/0.90$ to account for the volume contraction upon cooling the solution from room temperature to the temperature range of interest, -48 to $-61\text{ }^{\circ}\text{C}$.) One sample was placed in the NMR probe and allowed to equilibrate at $-48.4\text{ }^{\circ}\text{C}$ (224.8 K), the other at $-61.0\text{ }^{\circ}\text{C}$ (212.2 K). ^1H NMR spectra were recorded with 8 scans at the higher temperature and 16 at the lower, and by using *ca.* 50° pulses. 9 sec apart. Twelve spectra were recorded over 30 min during the $-48.4\text{ }^{\circ}\text{C}$ thermolysis and 14 spectra spanned 4 hrs during the $-61.0\text{ }^{\circ}\text{C}$ thermolysis. The concentrations of **2**, **3**, **75**, and **76t** were determined by comparison of their integrated ^1H NMR signals with those of the internal standards. The

integrals of the aryl singlet of mesitylene and all the signals of 2-methoxynaphthalene were found to be consistent with their relative concentrations to within 5%. The measured concentrations of the four species of interest are plotted as Figure 3-5a and b.

The time evolution of the concentration of 3 was calculated with the aid of a simple FORTRAN program ("KINB" – Appendix 3) written for the IBM-PC/AT. The program required as input the rate constants k_1 (for loss of 2) and k_2 (for dimerization of 3), determined from the plots of Figures 3-2 and 3-4, and the initial concentration of 3 was varied arbitrarily within the error range of the first experimental point to provide the best fit to the data. The program then changed the concentrations of 2 and 3 incrementally by small time intervals dt , so that the curves of Figure 3-6 each comprise 100 points. Thus, the concentration of 2 was progressively decreased by $k_1[2]dt$, while the concentration of 3 was increased by $(k_1[2] - 2k_2[3]^2)dt$. For the -48.4°C plot of Figure 3-6a, $k_1 = 1.545 \times 10^{-3} \text{ s}^{-1}$, $k_2 = 0.8611 \text{ M}^{-1} \text{ s}^{-1}$, $[2]_0 = 8.51 \times 10^{-3} \text{ M}$, and $[3]_0 = 1.6 \times 10^{-3} \text{ M}$. For the -61.0°C plot of Figure 3-6b, $k_1 = 1.368 \times 10^{-4} \text{ s}^{-1}$, $k_2 = 0.3272 \text{ M}^{-1} \text{ s}^{-1}$, $[2]_0 = 8.99 \times 10^{-3} \text{ M}$, $[3]_0 = 5.6 \times 10^{-4} \text{ M}$. The error bars attached to the data points in Figure 3-6 represent the probable error in measuring the integrals of the olefinic methylene signal of 3. Increasing the rate constants k_2 by 10-15% provides the optimal fit to the experimental data points.

Attempted trapping of singlet 1. *Ca.* 0.35 ml of a solution of diazene 2 and mesitylene in acetone- d_6 was added to each of two sample tubes, one containing 34.3 mg of maleic anhydride and the other 27.3 mg of

fumaronitrile. The samples were degassed and the tubes were sealed. In order to dissolve the solid the sample tubes were completely submerged in a $\text{CO}_2/\text{Me}_2\text{CO}$ bath then removed, shaken quickly, and returned to the bath. All the maleic anhydride dissolved, but a small amount of fumaronitrile remained undissolved. (Comparison of the ^1H NMR integrals for these compounds with that for mesitylene indicated that the concentrations of maleic and anhydride and fumaronitrile were respectively 1.0 M and 0.9 M.) The samples were analyzed by ^1H NMR, thermolyzed at $-50 \pm 5^\circ\text{C}$ for *ca.* 1 hr, then analyzed again to determine the amounts of dimers **75** and **76t** formed.

In the maleic anhydride sample 8.18 mM **2**, 0.36 mM **3**, 1.35/2 mM **75**, and *ca.* 0.20/2 mM **76t** were converted, upon thermolysis, to 3.65/2 mM **75** and *ca.* 0.50/2 mM **76t**, so that 8.5 mM **2** + **3** formed 2.6/2 mM dimers for a 30% yield. Allowing for errors in integration of the dimer signals, we estimate the error in this value as $\pm 10\%$. In the fumaronitrile sample 8.69 mM **2**, 0.89 mM **3**, 1.79/2 mM **75**, and *ca.* 0.25/2 mM **76t** formed 8.15/2 mM **75** and 0.88/2 mM **76t**, so that 9.6 mM **2** + **3** was converted to 7.0/2 mM dimers, for a 70% yield. Again, we estimate the error as *ca.* $\pm 10\%$.

In a more qualitative trapping experiment, 0.9 ml portions of a solution of diazene **2** and mesitylene in CH_2Cl_2 were added via cannula to stirred solutions of olefins in 2 ml of CH_2Cl_2 under N_2 at 0°C . For each solution an amount of olefin was used so as to provide a concentration of 1 M after addition of the diazene solution. After *ca.* 5 min at 0°C the solutions were allowed to warm to room temperature and were analyzed by GC. A sample of the original diazene solution was diluted appropriately and warmed to room

temperature to serve as a blank, and the amount of **75** *vs* the mesitylene standard in the olefin solutions was compared to that in the blank solution. The olefins used and the relative yields of **75** (some of which was undoubtedly formed upon adventitious decomposition of the diazene solution) were as follows (**76t** was also present, and in the usual ratio *vs* **75**, but is omitted for convenience): 1,3-cyclohexadiene, 25%; methyl acrylate, 28%; dimethyl fumarate, 33%; fumaronitrile, 10%; methacrylonitrile, 67%; ethyl vinyl ether, 78%; dihydropyran, 67%. Some very small, new GC peaks were observed, but no effort was made toward isolating or characterizing the new compounds.

Dimer ratios vs temperature. Samples of diazene **2** in CD_2Cl_2 were analyzed before and after thermolysis by ^1H NMR. The amounts of dimers **75** and **76t** formed upon thermolysis of samples at -78°C , -51°C , and -32°C can easily be extracted from the data presented in part a of the section on thermal and photochemical reactions of **2** above. These data are presented in Table 3-7 with error limits determined by estimating the the accuracy of the NMR integrations and propagating these errors through the calculations. The ratios at higher temperature were determined by GC analysis of samples prepared by cannulating *ca.* 100-200 μl of diazene solution into an N_2 -filled flask, which was swirled rapidly and held at a constant temperature. The cold solution was added via 30-gauge teflon tubing at a rate of *ca.* 2 drops sec^{-1} — rapidly enough so that after the first dew drops the cannula remained sufficiently cold to prevent premature decomposition of the diazene, but slowly enough to allow rapid thermal equilibration. That the high temperature points of Figure 3-7 fall nicely in line suggests that thermal

equilibrium was probably reached quickly enough, but this problem remains a potential source of systematic error for the higher temperature points. Because it was felt that the ratio of dimers formed upon transfer through warm tubing would more adversely effect the lower temperature ratios, these data were obtained by NMR measurements. Conversely, the higher temperature points were not measured by NMR because thermal equilibration of an NMR sample would probably not have been rapid enough. That the GC and NMR measurements give fairly consistent results is demonstrated by the -32 and -35 °C points of Figure 3-7. A least-squares analysis provided a slope of 460 and an intercept of -0.24 , which imply (eqn 3-2) $E_a(76t) - E_a(75) = 0.9 (\pm 0.2) \text{ kcal mol}^{-1}$ and $A_{75}/A_{76t} = 0.8 (\pm 0.3)$. The error limits were estimated by tipping the line of Figure 3-7 to intersect most of the error bars.

Table 3-7. Dimer ratios *vs* temperature.

T	ratio 75/76t	
195 K	8.5 ± 0.9^a	
222	6.7 ± 1.0^a	
241	5.1 ± 0.5^a	
238	5.0 ± 0.3^b	
273	4.2 ± 0.3^b	
297	3.4 ± 0.3^b	3.9 ± 0.3^b
313	3.6 ± 0.3^b	3.5 ± 0.3^b

a by NMR b by GC

Photochemistry of triplet 1 at 77 K. A sample of diazene 2 was dissolved in a cold (-78°C) solution of 0.85 mg of mesitylene, 20 μl of acetophenone (distilled), and 100 μl of 3-methylpentane (3-MP) in 750 μl of toluene- d_8 , and *ca.* 500 μl of the solution was placed in a 5-mm o.d., 3.5 mm i.d. sample tube, degassed, and sealed. (When a typical sample made with toluene alone is frozen in liq. N_2 the solvent forms a glass that tends to stress-fracture violently, often with enough force to break the sample tube. Thus, the 3-MP was included in the minimum amount required to moderate the fracturing so that the sample tube would survive repeated immersion in liq. N_2 .)

A 4.27×10^{-4} M solution of 2,2,6,6-tetramethylpiperidinyloxy (TEMPO) in 12% 3-MP/toluene was placed in a sample tube to serve as an EPR spin standard. By measuring the height of the solution in the tube, the relative volume upon cooling from room temperature was measured as 0.875 at -78°C and 0.84 at 77 K. The concentration of TEMPO at 77 K was therefore 5.08×10^{-4} M.

The volume of the diazene solution was estimated (again by measuring the height of the solution) as 440 μl at -78°C and 420 μl at 77 K. Applying the appropriate volume contraction, the concentration of mesitylene was 9.51×10^{-3} M at -78°C . (The acetophenone concentration was *ca.* 0.24 M at 77 K.) ^1H NMR spectroscopy at -80°C revealed that the diazene sample contained 12.1 mM 2, 1.8 mM 3, 5.7/2 mM 75, and 0.9/2 mM 76t, for a total of 20.5 mM monomer equivalents.

EPR spectra were recorded at 77 K as described in Chapter 2, the sample resting in a quartz finger dewar mounted in the microwave cavity. The dewar

was positioned so that the hemispherical bottom of the tube was below the cavity. The cavity height was measured as 2.3 cm, so that the sample volume inside the cavity was 220 μl .

The diazene sample was irradiated with light from the 1000-W Hg(Xe) arc lamp, which was directed alternately through filter combinations #4 (Table 3-3) for 30 sec to generate triplet 1 and #5 for 10 sec to destroy it. The sample was subjected to 150 such cycles in 15-20-cycle sets, being thawed (*ca.* 1-2 sec at -78°C) between each set. The signal intensity was monitored at a single field setting during each photolysis cycle. The first and last spectra of each set were recorded and later numerically double-integrated¹⁰¹ and scaled to a common receiver gain. The average of the two double-integrals (*di*) was multiplied by the number of cycles in the set, and the total *di* values for each set were combined to yield a relative *di* value of 1.86×10^4 .

Spectra of the standard TEMPO sample were recorded before and after the experiment, and *di* values of 640 and 665 were obtained. The instrument response factor for doublet (free radical) signals, $c_D = [\text{TEMPO}]/\text{di} = 7.79 \times 10^{-7}$. Triplet signals are inherently $4/3$ as intense per electron as doublet signals, or $8/3$ as intense per paramagnet.⁶⁷ Accordingly, the triplet response factor, $c_T = 3/8 c_D = 2.91 \times 10^{-7}$.

The total quantity of triplet 1 produced (and photolyzed), in terms of concentration within the 220 μl (see above) portion of the sample in the EPR cavity, is then given by $[1] = c_T(\text{di})$, or $[1] = 5.43 \times 10^{-3} \text{ M}$. Thus, $5.43 \times 10^{-3} \text{ M} \times 0.220 \text{ ml}$, or $1.19 \times 10^{-3} \text{ mmol}$ of triplet 1 was photolyzed; at -80°C a single photoproduct would then be present in a concentration of 1.19×10^{-3}

mmol/0.440 ml (see above) = 2.7×10^{-3} M. Because this value is a lower-limit, we have attached no errors to any of the numbers reported.

^1H NMR spectroscopy at -80°C revealed the presence of 5.2 mM **2**, 3.3 mM **3**, 11.4/2 mM **75**, and 1.90/2 mM **76t**, for a total of 21.8 mM monomer equivalents, or a material balance within 6% of the original sample composition.

No ^1H NMR signals besides those of **2**, **3**, **75**, and **76t** were observed in the region from *ca.* δ 6.8 to 2.3. (Solvent and sensitizer signals and their sidebands and satellites obscured the regions from δ 0.7 to 2.3 and δ 6.8 to 7.8; additionally, no signals were observed beyond these regions, upfield to δ -0.6 and downfield to δ 9.3.) By comparison to the mesitylene aryl peak height, we estimate that a hypothetical photoproduct present in a concentration of 2.7 mM would display singlets of $S/N \approx 10$ -15 per H, if the singlets were as broad as the reference peak. Consequently, even if this hypothetical photoproduct were totally asymmetric, with each signal split somewhat, it should still have been observable in the final ^1H NMR spectrum.

Sensitized photolysis of dimethylenebicyclobutane (3). A *ca.* 1-mM solution of diazene **2** in CH_2Cl_2 (which had been placed under vacuum) was irradiated with light from the Hg(Xe) arc lamp, directed through filter combination #1 (Table 3-3), at -95°C until no diazene remained, as indicated by UV spectroscopy. (While we cannot rule out the presence of a small amount of **2**, control experiments (see below) have established that it is not responsible for the chemistry of interest.) The vessel was then pressurized with nitrogen, and the solution was quickly cannulated through 30-gauge

teflon tubing with *ca.* 400 μ l being delivered to each of 8 N₂-purged sample tubes. To each tube had been added the requisite amount of sensitizer to make a *ca.* 0.04 M solution (due to its large ϵ and low solubility, enough methylene blue was used to make a *ca.* 0.01 M solution). The sensitizers used and their triplet energies, E_T , are listed in Table 3-8. The samples were immediately

Table 3-8. Sensitized photolysis of 3.

Sensitizer ^a	E_T ^b	$f(77t)$ ^c
Benzophenone	68.5 ^d kcal mol ⁻¹	0.236
Naphthalene	60.9 ^d	0.002
Benzil	53.7 ^d	0.509 ^e
Fluorenone	53.3 ^d	0.181
9-Methylanthracene	41 ^f	0.007
Acridine	45.3 ^f	0.039
Phenazine	43.8 ^f	0.042
Methylene blue ^g	<i>ca.</i> 32 ^h	0.015

^a *ca.* 0.04 M, in CH₂Cl₂. ^b triplet energy. ^c by GC: $77t/(75+76t+77t)$. ^d ref 75. ^e the amount of 75 present was anomalously low (13%), presumably due to reaction with the sensitizer. ^f ref 76. ^g *ca.* 0.01 M. ^h ref 77.

placed in liq. N₂ and later evacuated and sealed with a flame. Each sample, in turn, was thawed carefully, submerged in a CO₂/Me₂CO bath, withdrawn briefly and shaken to dissolve all or most of the sensitizer, irradiated at -78 °C for 1 min using filter combination #3 (Table 3-3), and finally warmed to room temperature. The methylene blue sample was irradiated instead for 2 min using filter combination #6. The solutions were analyzed by GC, and the

fraction of total dimers constituted by **77t** is reported in Table 3-8 for each sensitizer used. In addition, a small, unidentified peak at r.t. 7.37 min (relative to those reported above) was observed in each of the last 5 samples (the peak was quite large in the benzil sample). The control experiments described below demonstrated that this species is produced upon sensitized photolysis of a mixture of **75** and **76t**.

Control experiments were conducted to establish that the source of the **77t** observed was neither diazene **2** nor the dimers (**75** and **76t**). Thus, a solution of **2** in CH_2Cl_2 of similar concentration to that used above was transferred to sample tubes containing the sensitizers listed in Table 3-8. *Ca.* 250 μl of solution was added to each tube, so that the sensitizer concentrations were *ca.* 0.06 M (again, the methylene blue sample was *ca.* 0.01 M). The samples were degassed thoroughly by three freeze-pump-thaw cycles (liq. N_2 – $\text{CO}_2/\text{Me}_2\text{CO}$), and sealed with a flame. The samples were then stored at -100°C for 2.5 weeks to allow any **3** present to dimerize. The samples were submerged in a $\text{CO}_2/\text{Me}_2\text{CO}$ bath, shaken briefly to promote dissolution of the sensitizers, then photolyzed exactly as described above and warmed to room temperature. After standing overnight, the samples were opened inside an Ar-filled balloon, analyzed by GC, then irradiated again at -78°C and reanalyzed. The GC analyses revealed no **77t** (the fraction of **77t** was \leq *ca.* 0.001 under the conditions used) except in the case of the Ph_2CO sample, which was found to contain **77t** as *ca.* 30-40% of the total quantity of dimers present, as anticipated. (This established that the samples did, in fact, contain a significant amount of diazene **2**, even after sample manipulation and storage.)

Additional evidence for photosensitized destruction of **3** is provided by a separate ^1H NMR experiment. A sample of **2** in 3:1 (*v/v*) $\text{Et}_2\text{O}-d_{10}/\text{EtOH}-d_6$, containing mesitylene and saturated with Ph_2CO , was irradiated at 77 K with light from the 1000-W Hg(Xe) arc lamp directed through filter combination #7 (Table 3-3; $\lambda > 341$ nm). The photolysis was continued for a total of *ca.* 2 hrs. ^1H NMR spectroscopy at -80°C revealed the presence of 2.0 mM **2** and 8.5 mM **3**, as well as the usual dimer signals. The sample was stored in liq. N_2 . (This experiment had been conceived to probe the photochemistry of triplet **1**, which was presumably generated by sensitized photolysis and destroyed by direct photolysis in the same experimental step. As in the experiment described in the previous section, no ^1H NMR peaks were observed other than those attributed to **2**, **3**, and the dimers, although this experiment, of course, provided no direct measure of the amount of triplet **1** generated and photolyzed.)

The sample was irradiated for 2 min at -105°C using filter combination #4 (Table 3-3) then returned to liq. N_2 . The ^1H NMR spectrum (at -80°C) revealed that the sample contained 1.0 mM **2** and 0.8 mM **3**, so that 1.0 mM **2** and 7.7 mM **3** were consumed. Assuming that all the **2** lost was converted to triplet **1**, and this then reacted with **3**, the loss of 6.7 mM **3** would remain unaccounted for. This material must therefore have been destroyed by either sensitized photolysis or thermolysis. We estimate that the sample spent at most 20 min at -80°C between the times at which the two NMR spectra were recorded. Barring a substantial solvent effect, the concentration of **3** should have decreased from 7.5 mM (8.5-1.0 hypothetically destroyed by diazene-generated triplet **1**) to 3.6 mM in this time period, leaving the loss of 2.8 mM **3**

unaccounted for. (Qualitative observations suggest that dimerization of **3** is not unusually rapid in this solvent; in fact, in order to account for the observed decrease in [**3**] from 7.5 to 0.8 mM at -80°C in 20 min, the second-order rate constant would have to be larger by a factor of 8 than that derived from the Eyring plot of Figure 3-4.) It would appear, therefore, that at least some of the **3** lost was destroyed by photosensitization consistent with the results of the experiment described above.

Attempted photolysis of **3 at 77 K.** A *ca.* 10-mM sample of **2** in MTHF at 77 K in a quartz finger dewar was irradiated with monochromatic 334 (± 5) nm light from the 1000-W Hg(Xe) arc lamp for 30-40 min to generate *ca.* 0.2 mM triplet 1^{101} and leave *ca.* 2 mM diazene **2**, as indicated by UV-vis spectroscopy. The rest of the **2** photolyzed had presumably been converted to **3** via singlet diazene photochemistry or by adventitious photolysis of the triplet biradical by scattered visible light.⁷² The biradical was subsequently photolyzed in the course of another experiment, and the sample was finally irradiated for *ca.* 1 hr using filter combination #1 (Table 3-3). UV-vis spectroscopy showed no triplet **1** present at the end of the photolysis.

The sample, still at 77 K, and now presumed to contain a large amount of **3**, was placed in the quartz finger dewar, which had been mounted in a light-tight box, and irradiated with light from a low-pressure Hg arc lamp (Ultra-Violet Products UVG-11; nominally 0.3 mW cm^{-2} (unfiltered) at the distance used) directed through a UG-5 UV-transmitting, visible-absorbing filter (#8, Table 3-3) for *ca.* 1 hr. Unfortunately, no triplet **1** was observed by UV-vis spectroscopy.

Several attempts were made to effect the conversion of **3** to triplet **1** by sensitized photolysis in rigid media 77 K. The experimental strategy was to use a sensitizer of sufficiently low energy that it would not induce decomposition of **2**, but would effect opening of **3** (generated by direct photolysis of **2**) to triplet **1**, whose absorption spectrum is easily observable.¹⁰¹ The sensitizer is required to be soluble to the extent of *ca.* 0.1-0.2 M¹²⁷ in a glass-forming solvent at -78°C , optically transparent in the region that triplet **1** absorbs (ideally λ 400-510 nm),¹⁰¹ and non-emissive in this spectral region so as not to destroy the biradical photochemically. Of the sensitizers listed in Table 3-8, only phenazine and methylene blue were judged to be acceptable with respect to the last criterion, but methylene blue fails the first two miserably. (A variety of others were rejected primarily on the basis of solubility.) Phenazine appeared promising, except that at -78°C it precipitates from the glass-forming solvents tried (Et_2O , EtOH , C_7H_8 , MTHF). Although phenazine precipitates relatively slowly from MTHF, we were unable to make diazene samples of adequate optical quality with such supersaturated solutions. However, an attempt was made to conduct the experiment by using MTHF samples saturated with phenazine at -78°C (<0.1 M). The samples were immersed in liq. N_2 and irradiated with light from the 1000-W Hg(Xe) arc lamp directed through filter combination #1 (Table 3-3) for *ca.* 2 hrs to generate **3**, then through combination #3 for *ca.* 30 min in the hope of converting **3** to triplet **1**; however, no biradical was observed by UV-vis spectroscopy.

Thermal decay kinetics of triplet 1. EPR spectra were recorded on a Varian E-Line Century Series X-band spectrometer equipped with a cavity having a photolysis grating.¹⁰¹ The room lights were dimmed and the cavity was shrouded with black cloth. Temperature control above 77 K was provided by a Varian model V-4540 temperature controller. The temperature in the sample region was measured with a Lake Shore Cryotronics CGR-1-1000 carbon glass resistor immersed in ethylene glycol in a standard sample tube.¹⁰¹ The VT system was allowed to stabilize for 5-10 min, and the sample temperature was measured several times (*i.e.*, by removing and replacing the sensor) both before and after each kinetics run. These measurements implied an uncertainty in temperature of $\pm 2^\circ$.

Three diazene samples of *ca.* 6, 5, and 3 mM **2** and *ca.* 0.25 M Ph₂CO in CH₂Cl₂ were used. These were thawed at -78°C between runs. After having reached thermal equilibrium, each sample was irradiated for 10 sec with light from the 1000-W Hg(Xe) arc lamp, which was directed through filter combination #1 (Table 3-3) and focused into the microwave cavity. The rise and decay of the EPR signal of triplet 1 was monitored at the low-field *z*-transition, and 0.1 mW power was used. The baseline was periodically checked for drift by switching to 1000 G lower field, and the intensity measurements were corrected accordingly. The decays were followed for ≤ 1 hr. Approximately 15 intensity measurements were taken from each decay curve and plotted as $-\ln(I/I_0)$ vs $t^{1/2}$.⁸³ These plots are presented in Figure 3-12.

The temperature and rate data are presented in Table 3-9. Because the decays were non-exponential, the lower-temperature rate constants were

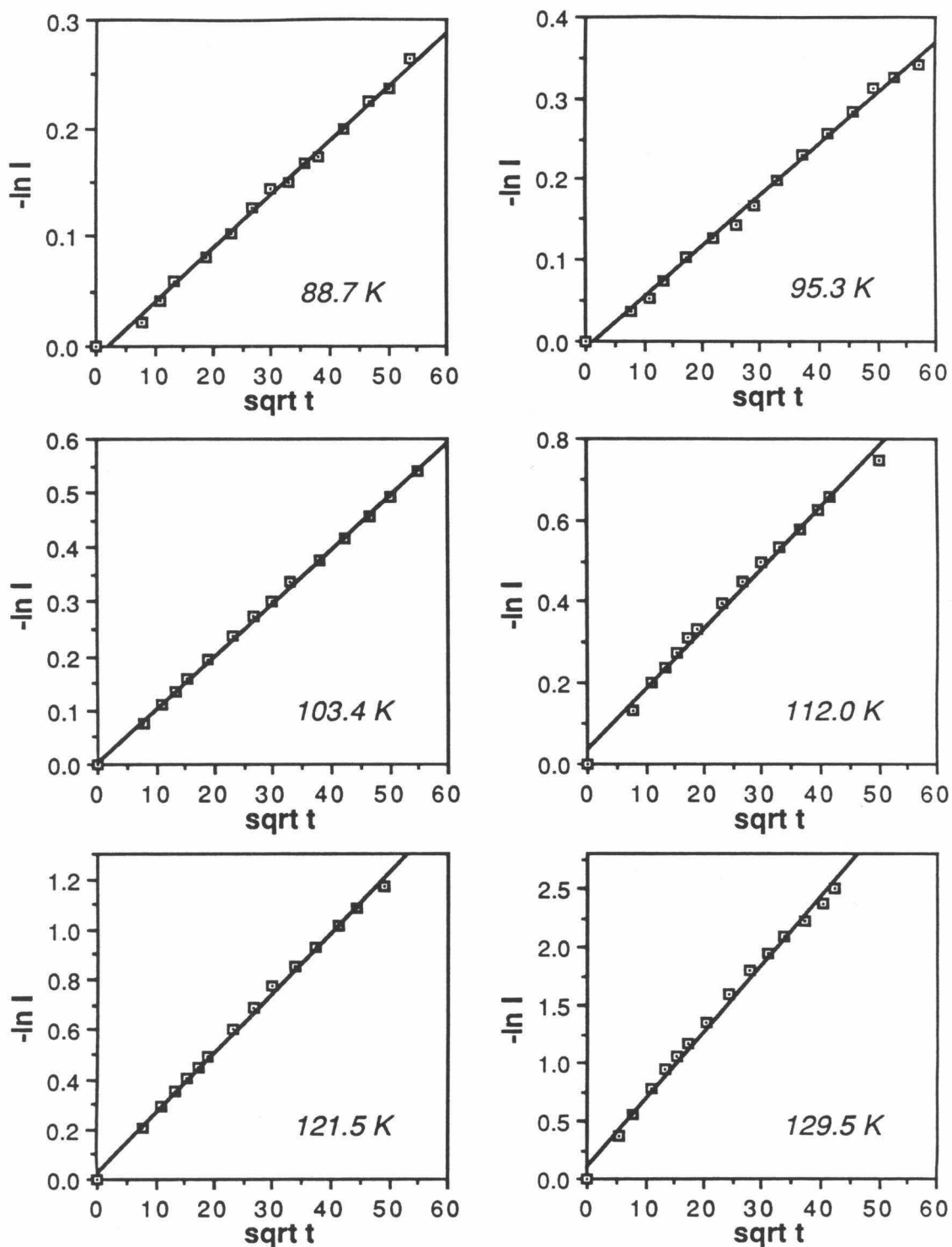


Figure 3-12. Triplet 1 EPR signal intensity (in CH_2Cl_2) vs time (s) data plotted as $-\ln I$ vs $t^{1/2}$ (s^{1/2}).

extracted from data that covered less than one half-life. Such decays begin rapidly, as species in "fast" matrix sites are lost, then slow considerably. Following the decays longer, say for 2 hr, would therefore not significantly improve the accuracy of the rates. A point at 84.8 K ($k = 4.92 \times 10^{-6} \text{ s}^{-1}$) was rejected because temperature control was lost during the run. Additional points at 136.5 K (*ca.* 95% decay in 2.3 min), 138.8 K (*ca.* 94% decay in 13 min), and 145.4 K (*ca.* 90% decay in 7.5 min; very low signal intensity) were rejected for the following reasons: (1) The $-\ln(I/I_0)$ vs $t^{\frac{1}{2}}$ plots were quite noticeably curved (as were plots recast as $1/(I/I_0)$ vs t and as $-\ln(I/I_0)$ vs t , the latter of which was severely curved). This suggests that some process other than unimolecular decay may have contributing to the loss of triplet 1 at these temperatures. (2) Samples of diazene 10 in CH_2Cl_2 containing *ca.* 0.25 M Ph_2CO , were subjected to the same experiment as a test for bimolecular decay, since biradical 9 has been demonstrated to be stable with respect to unimolecular reactions to near room temperature.⁸⁵ At temperatures of 123.5-145 K the EPR signal of 9 was found to decay appreciably, in most cases providing strongly curved $-\ln(I/I_0)$ vs $t^{\frac{1}{2}}$ plots (a $1/(I/I_0)$ vs t plot of the 145 K data showed even more curvature). The 123.5 K data, however, provided a linear $-\ln(I/I_0)$ vs $t^{\frac{1}{2}}$ plot, which furnished a rate constant of $8.3 (\pm 0.4) \times 10^{-3} \text{ s}^{-1}$ (11% decay over 3.5 min). Regardless of what type of process this rate constant corresponds to, this value is two orders of magnitude slower than the decay of triplet 1 at the same temperature (*cf.* the 121.5 K rate). In addition, we have found that triplet 9 does not decay measurably in CH_2Cl_2 at *ca.* 110 K. These observations suggest that the process by which triplet 9 decays is

not significant in the decay of triplet 1 below *ca.* 125 K, and these data probably represent unimolecular decay of the triplet biradical.

Table 3-9. Thermal decay kinetics of triplet 1 in solid CH₂Cl₂.

T ^a	k ^b	time	I _f /I ₀ ^c
88.7 K	4.15 (±0.14) × 10 ⁻⁶ s ⁻¹	0.8 h	0.77
95.3	6.60 (±0.21) × 10 ⁻⁶	1.0	0.71
103.4	1.605 (±0.027) × 10 ⁻⁵	0.8	0.58
112.0	3.73 (±0.17) × 10 ⁻⁵ ^d	0.7	0.47
121.5	9.64 (±0.26) × 10 ⁻⁵	0.7	0.31
129.5	5.58 (±0.25) × 10 ⁻⁴ ^d	0.5	0.08

^a errors are estimated as ±2°. ^b $k = (\text{slope of } -\ln(I/I_0) \text{ vs } t \text{ plot})^{2/6}$; ⁸³ deviations in the slopes of the plots. ^c ratio of final and initial signal intensities. ^d slight curvature was observed in the plots from which these values were derived (correlation coefficients for these two points were 0.9965, while those for the other points were generally 0.9985 or better).

The data are plotted as $\ln k$ vs $1/T$ in Figure 3-9. The Arrhenius "activation parameters," $E_a = 2.1 (\pm 0.2)$ kcal mol⁻¹ and $\log A = -0.3 (\pm 0.3)$, were obtained by a least-squares analysis using only the first five points; the 129.5 K rate appears abnormally high, most likely due to the onset of diffusion (or whatever process is responsible for the curvature in the $-\ln(I/I_0)$ vs t plots and the decay of triplet 9 in this temperature range; see above), and was therefore excluded.

Finally, full spectra of triplet 1 were recorded at the end of the 88.7, 112.0, and 129.5 K runs. None of these spectra showed any trace of doublet (free radical) signal, ruling out H-atom abstraction as the decay process.

References and notes.

1. Most notably, the compound forms **75** and **76t** with second-order kinetics (see below). A dimer with D_{2h} symmetry (**74** or **78**) could be responsible for the ^1H NMR signals observed, but if it rearranged to **75** and/or **76t** it would almost certainly do so by a first-order process.

2. Gordon, A.J.; Ford, R.A. *The Chemist's Companion*; Wiley: New York; 1972, pp 258-261.

3. (a) Wiberg, K.B. *Adv. Alicyclic. Chem.* **1968**, *2*, 185-205. (b) Wiberg, K.B.; Lampman, G.M.; Ciula, R.P.; Connor, D.S.; Schertler, P.; Lavanish, J. *Tetrahedron* **1965**, *21*, 2749-2769.

4. For comparison, the bridgehead protons of 5-isopropylidenebicyclopentane (**42**) appear at δ 1.99.⁵ An analysis similar to that of Scheme 3-1 (the bridgehead protons of bicyclo[2.1.0]pentane appear at δ 1.50⁶) leads to estimates of $1.50 + 0.77 = 2.27$ ppm and $0.99 + 1.28 = 2.27$ ppm. Also, the olefinic protons of a 5-methylenebicyclopentane derivative appear at δ 5.25.⁷

5. Rule, M.; Mondo, J.A.; Berson, J.A. *J. Am. Chem. Soc.* **1982**, *104*, 2209-2216. Rule, M.; Lazzara, M.G.; Berson, J.A. *J. Am. Chem. Soc.* **1979**, *101*, 7091-7092.

6. Roth, W.R.; Martin, M. *Lieb. Ann. Chem.* **1967**, *702*, 1-7.

7. Lazzara, M.G.; Harrison, J.J.; Rule, M.; Hilinski, E.F.; Berson, J.A. *J. Am. Chem. Soc.* **1982**, *104*, 2233-2243.

8. Billups, W.E.; Lin, L.-J.; Casserly, E.W. *J. Am. Chem. Soc.* **1984**, *106*, 3698-3699. Staley, S.W.; Norden, T.D. *J. Am. Chem. Soc.* **1984**, *106*, 3699-3700.

9. Budzelaar, P.H.M.; Kraka, E.; Cremer, D.; Schleyer, P.v.R. *J. Am. Chem. Soc.* **1986**, *108*, 561-567.
10. Feller, D.; Davidson, E.R.; Borden, W.T. *J. Am. Chem. Soc.* **1982**, *104*, 1216-1218.
11. Allinger, N.L. *J. Am. Chem. Soc.* **1977**, *99*, 8127-8134.
12. See ref. 13, pp. 176-177. A cobalt-capped relative of **78** has recently been reported. Gleiter, R.; Karcher, M.; Ziegler, M.L.; Nuber, B. *Tet. Lett.* **1987**, *28*, 195-198.
13. Greenberg, A.; Liebman, J.F. *Strained Organic Molecules*, Academic: New York, 1978.
14. Several new ^1H NMR signals, primarily around δ 9-10 and δ 6-7, grow in to a small extent during the course of the photolysis, in addition to numerous broad lumps.
15. We have observed no CIDNP in the ^1H NMR signals of **75** and **76t** produced by thermolysis of **2**. Cf. the observation of CIDNP in the dimerization of **9**: Berson, J.A.; Bushby, R.J.; McBride, J.M.; Tremelling, M. *J. Am. Chem. Soc.* **1971**, *93*, 1544-1546 and ref 16a.
16. (a) Corwin, L.R.; McDaniel, D.M.; Busby, R.J.; Berson, J.A. *J. Am. Chem. Soc.* **1980**, *102*, 276-287. (b) Duncan, C.D.; Corwin, L.R.; Davis, J.H.; Berson, J.A. *J. Am. Chem. Soc.* **1980**, *102*, 2350-2358.
17. The rate constant for dimerization of **3** at -38°C was also found to be unaffected by the addition of oxygen.
18. See, for example, Wilson, R.M.; Geiser, F. *J. Am. Chem. Soc.* **1978**, *100*, 2225-2226. Roth, W.R.; Scholz, B.P. *Chem. Ber.* **1982**, *115*, 1197-1208.

Adam, W.; Hannemann, K.; Wilson, R.M. *J. Am. Chem. Soc.* **1986**, *108*, 929-935. See also ref. 16.

19. (a) Crawford, R.J.; Mishra, A. *J. Am. Chem. Soc.* **1966**, *88*, 3963-3969.
(b) Chang, M.H.; Crawford, R.J. *Can. J. Chem.* **1981**, *59*, 2556-2567.

20. Cichra, D.; Duncan, C.D.; Berson, J.A. *J. Am. Chem. Soc.* **1980**, *102*, 6527-6533. Berson, J.A.; Duncan, C.D.; O'Connell, G.C.; Platz, M.S. *J. Am. Chem. Soc.* **1976**, *98*, 2358-2360.

21. (a) Chang, M.H.; Jain, R.; Dougherty, D. A. *J. Am. Chem. Soc.* **1984**, *106*, 4211-4217. (b) Chang, M.H.; Dougherty, D.A. *J. Org. Chem.* **1981**, *46*, 4092-4093.

22. The activation parameters for deazetation of **10** (Table 3-2) are virtually independent of solvent polarity (*cf.* the parameters in benzene, dielectric constant, $\epsilon = 2.3$,²³ *vs* acetonitrile, $\epsilon = 36.2$ ²³) and there is no indication that the nitrogen extrusion mechanisms differ for **10** and **2** (see below). It is therefore reasonable to compare parameters determined for diazene **2** in methylene chloride ($\epsilon = 8.9$ ²³) to values obtained for thermolyses in the gas phase or in non-polar solvents.

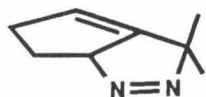
23. Ref 2, p 3, ff.

24. Roth, W.R.; Martin, M. *Tet. Lett.* **1967**, 4695-4698.

25. Chang, M.H.; Dougherty, D.A. *J. Am. Chem. Soc.* **1982**, *104*, 1131-1132.

26. Strong evidence for the intervention of **80** derives from the observation that rearrangement to diazene **82** accompanies thermal (but not photochemical) deazetation of **10**.²⁰ We have found no evidence that **83** is involved in either the thermal or photochemical decomposition of **2**, although

force field calculations suggest that rearrangement of **2** to **83** is

**82****83**

thermodynamically reasonable. Thus, MM2 calculations¹¹ on the alkene analogs²⁷ of **2** and **83**, as well as those of **10** and **82** (less the methyl groups), indicate that rearrangement of **10** to **82** is *ca.* 9 kcal mol⁻¹ downhill, while the conversion of **2** to **83** is exothermic by *ca.* 11 kcal mol⁻¹. The ring system of **83** is therefore not exceptionally strained (relative to that of **2**). The absence of diazene **83** could, of course, be due to other factors, such as unfavorable recyclization energetics for **81** or an exceptionally facile, orbital symmetry allowed nitrogen extrusion by **83**.

27. The strain energies of azo compounds are generally quite similar to those of their alkene analogs: Kao, J.; Huang, T.-N. *J. Am. Chem. Soc.* **1979**, *101*, 5546-5557. The correspondence should be quite good for derivatives of the same bicyclic ring system.

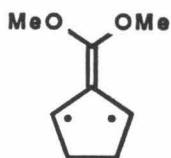
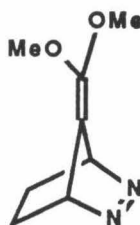
28. See ref. 29 and Trenwith, A.B.; *J. Chem. Soc., Faraday 1* **1982**, *78*, 3131-3136; **1980**, *76*, 266-271.

29. McMillen, D.F.; Golden, D.M. *Ann. Rev. Phys. Chem.* **1982**, *33*, 493-532.

30. See ref. 29 and Rossi, M.; King, K.D.; Golden, D.M. *J. Am. Chem. Soc.* **1979**, *101*, 1223-1230. Rossi, M.; Golden, D.M. *J. Am. Chem. Soc.* **1979**, *101*, 1230-1235.

31. We carried out MM2¹¹ calculations on the alkene analogs²⁷ of **79**, **10**, **46**, and **2**. Addition of a methylene group to norbornene, the analog of **79**, or **79a**, to form (almost) **10a** increases the strain energy by 6.0 kcal mol⁻¹. Addition of the first methylene to **46a** raises the strain energy by 8.4 kcal mol⁻¹; addition of the second raises it by 4.7, for a total of 13.1 kcal mol⁻¹.

32. The regiochemistries of olefin and diene cycloadditions to singlet **9** are best rationalized in terms of frontier orbital-control.^{33,34} (S and A are defined relative to the mirror plane that passes through the exocyclic double bond of **9** and through both double bonds of **1**.) The trapping regiochemistry observed for the methoxy-substituted singlet biradical **84** suggests that its NBMO ordering has been reversed (*i.e.*, A < S) as predicted by simple perturbation theory.³⁶ The change in the symmetry of the biradical HOMO on going from **9** to **84** also manifests itself in an unusually facile loss of nitrogen by diazene **85**. This is presumably because a concerted extrusion of nitrogen

**84****85**

from **85** is orbital symmetry allowed, while that from **10** is forbidden.^{33a,20} Thus, **85** decomposes with an E_a *ca.* 5-6 kcal mol⁻¹³⁷ lower than that for **10**. That the E_a for decomposition of **2** is nicely rationalized in terms of a stepwise mechanism is therefore consistent with S < A for **1**; A < S would presumably have led to a substantially more facile loss of nitrogen.

33. (a) Siemionko, R.; Shaw, A.; O'Connell, G.; Little, R.D.; Carpenter, B.K.; Shen, L.; Berson, J.A. *Tet. Lett.* **1978**, 3529-3582. (b) Siemionko, R.K.; Berson, J.A. *J. Am. Chem. Soc.* **1980**, *102*, 3870-3882.
34. Berson, J.A. In ref. 35; Ch 4, pp. 151-194.
35. *Diradicals*; Borden, W.T., Ed.; Wiley: New York, 1982.
36. Carpenter, B.K.; Little, R.D.; Berson, J.A. *J. Am. Chem. Soc.* **1976**, *98*, 5723-5725.
37. Diazene **85** is reported to expel nitrogen 10^4 - 10^5 times faster than diazene **10**.^{36,34} If the preexponential factors are comparable, this corresponds to an E_a of 21-23 kcal mol⁻¹ for **85**.
38. Snyder, G.J.; Goddard, W.A., III; Dougherty, D.A., unpublished results.
39. The error limits represent conservative estimates based on potential systematic errors rather than the spread of the experimental data (see **Experimental**).
40. Gassman, P.G. *Acc. Chem. Res.* **1971**, *4*, 128-136.
41. Near -60°C a k_H/k_D of 1.3 implies a ΔE_a of ca. 110 cal mol⁻¹, which corresponds to a room temperature k_H/k_D of 1.2.
42. Notwithstanding the trace amounts of the characteristic "triplet" dimers observed (Table 3-1).
43. The decay rate at -100°C in ca. 10:1 CF₂Cl₂/CD₂Cl₂ is 0.01 M⁻¹s⁻¹.
44. For example, see Carpenter, B.K. *Determination of Organic Reaction Mechanisms*; Wiley: New York, 1984, p 3.

45. The condition $k_{-1} \gg k_2[1]$ provides the expression $-d[3]/dt = k_1k_2[3][1]/k_{-1}$. If 3 and 1 are in equilibrium, $[1] = k_1[3]/k_{-1}$. Substituting this for [1] leads to the expression of Scheme 3-2c.

46. Competition studies have suggested that this is the case at 60 °C.^{47,16b,34} For the purposes of the present analysis, we felt that it was crucial to verify that the trapping is also diffusion-controlled under the conditions of our experiments, and we therefore present the following supporting arguments. (Although only maleic anhydride trapping is addressed, fumaronitrile is just 30% less reactive toward singlet 9.^{16b})

(1) Mazur and Berson have studied the kinetics of trapping of 5-isopropylidenebicyclo[2.1.0]pentane (42) with maleic anhydride and acrylonitrile under pseudo-first-order conditions in acetone-*d*₆ at -55 °C.⁴⁸ A plot of the reciprocal of k_{obs} , the pseudo-first-order rate constant, vs the reciprocal of the maleic anhydride concentration was found to have a slope within experimental error of zero, indicating that every singlet biradical 9 formed by opening of 42 was intercepted before it could recyclize.⁴⁸ We can place a lower limit on the trapping rate by asking how slow the competing reclosure can be. If we draw the line with the maximum slope permitted by the error bars on $1/k_{\text{obs}}$ shown in Figure 1 of ref. 48, we find an intercept of 600 s, corresponding to $1/k_0$ (the rate constant for opening of 42)⁴⁸ and a slope of 500 Ms, corresponding to k_c/k_0k_T (k_c and k_T are respectively the rate constants for closure and trapping of singlet 9).⁴⁸ Rate constant k_T must then be at least $(0.83 \text{ M}^{-1})k_c$. We can place a reasonable lower limit on k_c by assuming $E_a = 3 \text{ kcal mol}^{-1}$ (the value determined by Berson and coworkers is $2.3 \text{ kcal mol}^{-1}$ ^{48,34}) and $A = 10^{12} \text{ s}^{-1}$ (the reaction is a spin-allowed, unimolecular process).

Thus, $k_c = 1 \times 10^9 \text{ s}^{-1}$ at -55°C , and $k_T \geq 8 \times 10^8 \text{ M}^{-1} \text{ s}^{-1}$, whereas the diffusion rate, $k_d = 5 \times 10^9 \text{ M}^{-1} \text{ s}^{-1}$.⁴⁹ (Conveniently, our trapping experiment was conducted at almost the same temperature, so this result is directly relevant to the issue at hand.)

(2) Photolysis of diazene **10** at -78°C in acetone containing 1 M maleic anhydride affords $> 95\%$ cycloadducts and $< 5\%$ **42**.⁴⁸ Again, this is a competition between cyclization and trapping of singlet **9**, but under conditions that do not allow ring opening of **42**.⁴⁸ The activation parameters above for closure of the singlet biradical provide $k_c = 4 \times 10^8 \text{ s}^{-1}$ at -78°C . The product ratios require that $k_T(1 \text{ M}) > 19 k_c$, or $k_T > 8 \times 10^9 \text{ M}^{-1} \text{ s}^{-1}$, and $k_d = 3 \times 10^9 \text{ M}^{-1} \text{ s}^{-1}$ ⁴⁹ at this temperature.

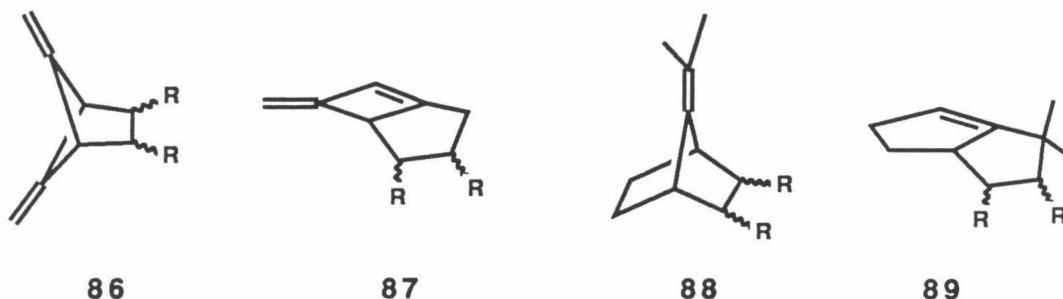
47. Berson, J.A. *Acc. Chem. Rec.* **1978**, *11*, 446-453.

48. Mazur, M.; Berson, J.A. *J. Am. Chem. Soc.* **1982**, *104*, 2217-2222; **1981**, *103*, 684,686.

49. At -55°C the viscosity of acetone, $\eta = 0.9 \text{ cp}$; at -78°C , 1.5 cp . *CRC Handbook of Chemistry and Physics*, 60th ed.; CRC Press: Boca Raton, FL; p. F-52. The diffusion rate constant is given by $k_d = (2.2 \times 10^7 \text{ cp K}^{-1} \text{ M}^{-1} \text{ s}^{-1})T/\eta$. See ref 2, p.137.

50. If the frontier orbitals (i.e., the nominal NBMOs) of singlets **9** and **1** bear the expected anatomical and energetic similarities (see ref 32), one would not expect a large electronically-based reactivity change. Experimentally, we have found that substantial amounts of dimers **75** and **76t** are formed upon thermolysis of **2** at 0°C in the presence of 1 M dihydropyran or ethyl vinyl ether, suggesting that either electron-rich olefins are not effective traps for the singlet biradical, or it is not involved in the reaction. (see Experimental)

51. The potential olefin-trapping products of **1** are **86** and **87**, and the actual products of **9** are **88** and **89**. Our calculated (MM2) heats of formation



and strain energies (in kcal mol⁻¹) for these ring systems less the Me and R groups are as follows: **86**: 65.3, 50.2; **87**: 65.7, 54.7; **88**: 12.8, 23.9; **89**: 8.2, 19.7. We can estimate ΔH_f° for singlets **1** and **9** by using a combination of Benson group increments (Ref. 52, p. 272; including the value 37.45 kcal mol⁻¹ for a localized secondary radical center: O'Neal, H.E.; Benson, S.W. In *Free Radicals*, vol. 2; Kochi, J.K., Ed.; Wiley: New York, 1973; pp. 338-340) and the strain and resonance energies as discussed previously. Thus, for **9**, the sum of the group increments is 81.6 kcal mol⁻¹. Adding 5 kcal mol⁻¹ for strain energy,⁵³ subtracting 24 for the TMM resonance energy,⁵⁵ and adding 15 for promotion of triplet **9** to the singlet state,^{48,34} we find that ΔH_f° for singlet **9** is 77.6 kcal mol⁻¹. Taking ΔH_f° for ethylene as 12.5 kcal mol⁻¹, the cycloadditions to form **88** and **89** have $\Delta H^\circ = -77$ and -82 kcal mol⁻¹, respectively. For **1**, the group increments add to 108.1 kcal mol⁻¹. As above, we add 32 kcal mol⁻¹ for strain⁵⁶ and 15 for the S-T gap¹⁰ and subtract 41 for resonance energy,⁵⁵ for an estimated ΔH_f° of 114 kcal mol⁻¹ for singlet **1**. Thus, the cycloadditions to form **86** and **87** each have $\Delta H^\circ = -61$ kcal mol⁻¹.

52. Benson, S.W. *Thermochemical Kinetics*, 2nd ed.; Wiley: NY, 1976; p. 309.

53. This value is an average of the strain energies for cyclopentane, 6.2 and cyclopentene, 4.1 kcal mol⁻¹.⁵⁴

54. Wiberg, K.B. *Angew. Chem., Int. Ed. Engl.* 1986, 25, 312-322.

55. See Chapter 1 of this thesis.

56. This estimate derives from the observation that each sp² center incorporated into the cyclobutane ring system adds ca. 1.5 kcal mol⁻¹ to the strain energy.^{54,57}

57. Schleyer, P.v.R.; Williams, J.F.; Blanchard, K.R. *J. Am. Chem. Soc.* 1970, 92, 2377-2386.

58. One might consider the possibility that triplet 1 ring-closes to 3 at this temperature before it can undergo bimolecular reaction to form 77t. An upper limit on the closure rate is derived by assuming, for the sake of argument, that the 77 K decay rate of the triplet EPR signal of 1, ca. 10⁻⁶ s⁻¹ (see Chapter 2), corresponds to an activated cyclization with A = 10¹¹ s⁻¹ (an upper limit on the pre-exponential factor for closure of triplet TMM, 459). The E_a for closure would then be 6 kcal mol⁻¹, and the closure rate at -78 °C would be at most 2 x 10⁴ s⁻¹. (The closure rate could easily be several orders of magnitude lower than this.) A triplet biradical should encounter molecules of 3 at 10⁷ s⁻¹, more than 500 times the closure rate. Such encounters can almost certainly produce 77t, and a measurable amount of this dimer should therefore have been formed.

59. Dowd, P.; Chow, M. *Tetrahedron* 1982, 38, 799-807; *J. Am. Chem. Soc.* 1977, 99, 6438-6440.

60. Turro, N.J. *Modern Molecular Photochemistry*; Benjamin/Cummings: Menlo Park, CA, 1978; p.186.

61. Chang, M.H.; Jain, R.; Dougherty, D.A. *J. Am. Chem. Soc.* **1984**, *108*, 4211-4217. Chang, M.H.; Dougherty, D.A. *J. Am. Chem. Soc.* **1982**, *104*, 1131-1132.

62. See, for example, Newton, M.D.; Schulman, J.M. *J. Am. Chem. Soc.* **1972**, *94*, 767-773. Jorgensen, W.L.; Salem, L. *The Organic Chemist's Book of Orbitals*; Academic: New York, 1973; pp. 203-205.

63. The bond dissociation energies for Et-Et, Et-*n*Pr, Et-*i*Pr, *n*Pr-*i*Pr, and *i*Pr-*i*Pr are all within 2 kcal mol⁻¹ of this value.^{52,29}

64. Ref. 44, pp. 96-97.

65. Dervan, P.B.; Santilli, D.S. *J. Am. Chem. Soc.* **1980**, *102*, 3863-3870.

66. See, for example, Eliel, E.L. *Stereochemistry of Carbon Compounds*; McGraw-Hill: New York; 1962, pp. 151-152.

67. Platz, M.S.; Berson, J.A. *J. Am. Chem. Soc.*, **1980**, *102*, 2358-2364.

68. In addition, when a sample of **2** containing 0.10 M Ph₂CO was photolyzed with a higher light intensity, which may have significantly increased the amount of adventitious photolysis of triplet **1**, a plot similar to that of Figure 3-8b was obtained (see **Experimental**).

69. Such abstractions have been observed, for example, upon photolysis of triplet diphenylcarbene in alcoholic matrices at 77 K⁷⁰ and upon photolysis of triplet 1,3-cyclopentanediyI in cylcohexane at 5.5 K.⁷¹

70. Leyva, E.; Barcus, R.L.; Platz, M.S. *J. Am. Chem. Soc.* **1986**, *108*, 7786-7788.

71. Buchwalter, S.L.; Closs, G.L. *J. Am. Chem. Soc.* **1979**, *101*, 4688-4694.

72. The intensity of the scattered light depends on λ^{-4} . Berne, B.J.; Pecora, R. *Dynamic Light Scattering*; Wiley: New York, 1976; p. 37.

73. In a separate experiment, a sample of **2** in 3:1 Et₂O-*d*₁₀/EtOH-*d*₆ saturated with Ph₂CO was irradiated with light of $\lambda > 340$ nm for ca. 2 hrs at 77 K. This sample was also found to contain no new species, as indicated by ¹H NMR.

74. Of course, we can rigorously rule out neither the presence of a small amount of another photoproduct nor the possibility that the photoproduct is a labile species that is converted (thermally or photochemically) to **3** or (thermally) to dimers **75** and **76t**.

75. Herkstroeter, W.G.; Lamola, A.A.; Hammond, G.S. *J. Am. Chem. Soc.* **1964**, *86*, 4537-4540.

76. Engel, P.S.; Monroe, B.M. *Adv. Photochem.* **1971**, *8*, 245-313.

77. Denny, R.W.; Nickon, A. *Org. Reactions* **1973**, *20*, 133-336.

78. In addition, when a Ph₂CO-saturated sample of **3** in 3:1 Et₂O-*d*₁₀/EtOH-*d*₆ was irradiated ($\lambda > 340$ nm) at -105 °C, more **3** was found to have been destroyed than can be accounted for by thermal dimerization alone (see **Experimental**).

79. Viscosity data for a number of organic glasses have been reported. Fischer, G.; Fischer, E. *Molec. Photochem.* **1977**, *8*, 279-281. Hutzler, J.S.; Colton, R.J.; Ling, A.C. *J. Chem. Eng. Data* **1972**, *17*, 324-327. Ling, A.C.; Willard, J.E. *J. Phys. Chem.* **1968**, *72*, 1918-1923; 3349-4451.

80. We also attempted to cocrystallize diazene **10** and Ph₂CO by dissolving them in Me₂O or CFCl₃ and pumping off the solvent at -78 °C, but this failed to provide viable EPR samples.

81. Such abstractions are observed in the chemistry of methyl radicals and carbenes in rigid media near 77 K. See, for example, ref. 82 and Platz, M.S.; Senthilnathan, V.P.; Wright, B.B.; McCurdy, C.W., Jr. *J. Am. Chem. Soc.* **1982**, *104*, 6494-6501.

82. Doba, T.; Ingold, K.U.; Siebrand, W. *Chem. Phys. Lett.* **1984**, 339-342.
Doba, T.; Ingold, K.U.; Siebrand, W.; Wildman, T.A. *J. Phys. Chem.* **1984**, *88*, 3165-3167.

83. A linear $\ln I$ vs $t^{\frac{1}{2}}$ plot implies a distribution of rate constants whose most probable rate constant, k_0 , is given by $k_0 = c^2/6$, where c is the slope of the plot.⁸² The half-life is then given by $t^{\frac{1}{2}} = (\ln 2)^{2/6} / k_0$.

84. Triplet biradical **9**, which is reportedly stable with respect toward unimolecular reaction up to near room temperature⁸⁵ is found to decay in this solvent at $\geq ca.$ 120 K, suggesting that diffusion may be occurring. This biradical is stable at 110 K in CH_2Cl_2 , though, and its decay is *ca.* two orders of magnitude slower than that of **1** at 122 K (the last data point on the line in Figure 3-9; see Experimental).

85. Platz, M.S.; Berson, J.A. *J. Am. Chem. Soc.* **1980**, *102*, 2358-2364.
Platz, M.S.; McBride, J.M.; Little, R.D.; Harrison, J.J.; Shaw, A.; Potter, S.E.; Berson, J.A. *J. Am. Chem. Soc.* **1976**, *98*, 5725-5726.

86. Feller, D.; Davidson, E.R.; Borden, W.T. *Isr. J. Chem.* **1983**, *23*, 105-108.

87. Possibly the best estimate of $\log A$ for closure of singlet **9** comes from the ratio of closure to isc at 77 K. Thus, $5k_c \approx k_{isc}$ at this temperature.⁵ If $k_{isc} = 109.5$,⁸⁸ and E_a for closure is 2.3 kcal mol⁻¹,⁴⁸ $\log A$ for closure is found

to be 15. Allowing for some uncertainty in the k_{isc} and E_a values used, we use 12 as a probable lower limit on $\log A$ for closure of singlet 9.

88. The Arrhenius preexponential factor for dimerization of 42 provides an estimate of $\log A$ for isc as 9.5. Since isc is assumed to have $E_a \approx 0$, $k_{isc} \approx 109.5_{.48}$

89. The photochemical generation of triplet 9 from diazene 10 occurs exclusively via the singlet biradical rather than the diazene triplet state. Platz, M.S.; Kelsey, D.R.; Berson, J.A.; Turro, N.J.; Mirbach, M. *J. Am. Chem. Soc.* 1977, 99, 2009-2010.

90. This limit is based on the estimate of k_{isc} for 9⁸⁸ as well as the range of values observed for aromatic hydrocarbons.⁶⁰

91. Turro, N.J.; Renner, C.A.; Waddell, W.H.; Katz, T.J. *J. Am. Chem. Soc.* 1976, 98, 4320-4322. Engel, P.S.; Nalepa, C.J.; Leckonby, R.A.; Chae, W.-K. *J. Am. Chem. Soc.* 1979, 101, 6435-6437. Mirbach, M.F.; Mirbach, M.J.; Liu, K.-C.; Turro, N.J. *J. Photochem.* 1978, 8, 299-306.

92. Chang, M.H.; Dougherty, D.A. *J. Am. Chem. Soc.* 1982, 104, 2333-2334.

93. We can place an upper limit on k_c for triplet 1 at 40 °C as in ref. 58. Thus, $k_c \leq 6 \times 10^6 \text{ s}^{-1}$; however, given the assumptions used,⁵⁸ this value could easily be several orders of magnitude higher than the actual rate constant. For example, if $E_a = 9 \text{ kcal mol}^{-1}$ and $\log A = 9$, $k_c = 5 \times 10^2 \text{ s}^{-1}$. If the reaction of 3¹ and 3 occurs at the diffusion rate, $10^{10} \text{ M}^{-1} \text{ s}^{-1}$, then $k_T[3]$ would be about 10^6 s^{-1} . While the assumption that $k_c \gg k_T[3]$ is probably valid, it remains a point of some uncertainty.

94. To the amounts of **77t**, **D**₁, and **D**₂ reported in Table 3-1, *ca.* 0.3%, we add 0.1% to allow for a small amount of **75** originating via triplet chemistry.

95. An E_a of 13.7 kcal mol⁻¹ provides $k_0 = 1.75 \times 10^{-6}$ s⁻¹ (with $\log A = 9.6$) at -78 °C. Rate constant $k_2 = 0.0718$ M⁻¹ s⁻¹, so the ratio $k_0/2k_2$ (*ca.* 10⁻³ M) = 0.012. This is several orders of magnitude above the amount required for GC detection. Using $E_a = 20$ kcal mol⁻¹; one obtains a ratio of 10⁻⁹, which is well below the detection limit.

96. The triplet is favored by a factor of 3 because of its spin state and an additional factor of 2 by its higher symmetry.⁹⁷ The factor $(R \ln \sigma)T$ thus contributes *ca.* 1 kcal mol⁻¹ to ΔG at room temperature.

97. Ref. 52 p. 47-50.

98. Applying our usual thermochemical estimates, we subtract the strain energy of **2 45s**, 2 x 64 kcal mol⁻¹,⁵⁴ from 2 x 28⁵⁶ + 80⁶³ for the strain and "missing C - C bond" energy of **93**. Thus, $\Delta H = 8$ kcal mol⁻¹.

99. This value is obtained by 80⁶³ + 2 x 55³ - 2 x 12³⁰ = 66 kcal mol⁻¹ for **94**, minus 2 x (27⁵⁴ + 41⁵⁴) for **42**, or $\Delta H = -70$ kcal mol⁻¹.

100. Note that if $\log A$ for dimerization of **42** were also *ca.* 7, this reaction would be even more unfavorable compared to ring opening ($\log A = 9.648$) at higher temperatures.

101. See Chapter 2 of this thesis.

102. Pranata, J.; Dougherty, D.A. *J. Am. Chem. Soc.* **1987**, *109*, 1621-1627.

103. Salem, L.; Rowland, C. *Angew. Chem., Int. Ed. Engl.* **1972**, *11*, 92-111.

104. Schmidt, S.P.; Pinhas, A.R.; Hammons, J.H.; Berson, J.A. *J. Am. Chem. Soc.* **1982**, *104*, 6822-6823.
105. Turro, N.J.; Mirbach, M.J.; Harrit, N.; Berson, J.A.; Platz, M.S. *J. Am. Chem. Soc.* **1978**, *100*, 7653-7658. See also Davis, J.H.; Goddard, W.A., III *J. Am. Chem. Soc.* **1977**, *99*, 4242-4247; **1976**, *98*, 303-304.
106. The product of a sequence analogous to that of eqn 3-8, 3-methylenepent-4-ene-1-yne, has a ^1H NMR spectrum that would have been easily observed under the conditions of the experiment. Hopf, H. *Chem. Ber.* **1971**, *104*, 1499-1506.
107. See ref 82 and 81. See also ref 108.
108. Sponsler, M.B.; Jain, R.; Coms, F.D.; Dougherty, D.A. Manuscript in preparation.
109. Jain, R.; Ph.D. thesis, California Institute of Technology, 1987.
110. The flame was kept well away from the cold bath. Both bath solvents were well below their flash points, which are reported as 12 °C for both MeOH and iPrOH. *The Merck Index*, 9th ed.; Windholz, M., Ed.; Merck: Rahway, NJ, 1976.
111. Van Geet, A.L. *Anal. Chem.* **1970**, *42*, 679-680. The T vs $\Delta\nu$ equation for 60 MHz data is claimed to be accurate to within 0.8 K; however, Raiford, D.S.; Fisk, C.L.; Becker, E.D. *Anal. Chem.* **1979**, *51*, 2050-2051 report that the equation can be scaled to higher field without loss of accuracy.
112. Crystalline **2** will not dissolve in CF_2Cl_2 , whether for thermodynamic or kinetic reasons, but it will stay in such a solution once dissolved.
113. Sørensen, O.W.; Ernst, R.R. *J. Magn. Res.* **1983**, *51*, 477-489. Doddrell, D.M.; Pegg, D.T.; Bendall, M.R. *J. Magn. Res.* **1982**, *48*, 323-327.

114. For example, see the force field method described in Kao, J.; Allinger, N.L. *J. Am. Chem. Soc.* **1977**, *99*, 975-986.

115. Tai, J.C.; Allinger, N.L. *J. Am. Chem. Soc.* **1976**, *98*, 7928-7932.

116. Cox, J.D.; Pilcher, G. *Thermochemistry of Organic and Organometallic Compounds*; Academic: NY, 1970; pp. 140 ff.

117. The ΔH_f° for the olefin was found to be 48.0, while those of *cis*- and *trans*-1,3-dimethylcyclobutane were -10.3 and -9.7 kcal mol⁻¹, respectively.

118. Caserio, F.F., Jr.; Parker, S.H.; Piccolini, R.; Roberts, J.D. *J. Am. Chem. Soc.* **1958**, *80*, 5507-13. The measurement was made in HOAc solution by the method of Turner, R.B.; Meador, W.R.; Winkler, R.E. *J. Am. Chem. Soc.* **1957**, *79*, 4116-4121. However, Rogers, D.W.; Dagdagan, D.A.; Allinger, N.L. *J. Am. Chem. Soc.* **1979**, *101*, 671-676, contend that values determined by this method are not exothermic enough because the differential heats of solution of the alkene and alkane are neglected.

119. The last two are tentatively assigned to the C-3 (cyclobutene) methylene group by their proximity to the olefinic singlets of 76t and 77t (see below).

120. The chemical shifts are in accord with those observed for model compounds. Specifically, 5,6-bismethylenebicyclo[2.1.1]hexane displays methylene and bridgehead proton signals at δ 4.33 and 3.03 respectively;¹²¹ 3-methylene- cyclobutene and 1-methyl-3-methylenecyclobutene display methylene signals at δ 4.3-4.5, while the olefinic (C-2) and allylic methylene protons appear at δ 6.2 and 2.8, respectively.¹²²

121. Martin, H.-D.; Eckert-Maksic, M.; Mayer, B. *Angew Chem., Int. Ed. Engl.* **1980**, *19*, 807-809.

122. Wu, C.C.; Lenz, R.W. *J. Polym. Sci., Polym. Chem. Ed.* **1972**, *10*, 3529-3553.

123. The peaks of **75** and **76t** were distinguished on the basis of the intensity differences between similar carbons in the two compounds.

124. The δ 2.58 and 2.23 signals of **76t** and the δ 2.75 and 2.13 signals of **77t** are tentatively assigned as equatorial and axial, respectively for each compound. For **77t** the relative coupling constants expected on the basis of the dihedral angles clearly support this assignment. See Silverstein, R.M.; Bassler, G.C.; Morrill, T.C. *Spectrometric Identification of Organic Compounds*, 4th ed.; Wiley: New York, 1981; p.189.

125. The peak list beyond the semicolon has been abbreviated.

126. Günther, H. *NMR Spectroscopy*, Wiley: New York, 1980; pp. 218-220.

127. Triplet-triplet energy transfer is thought to occur over distances of $\leq 15\text{\AA}$.¹²⁸ A concentration of 0.1 M places one sensitizer molecule in each 16\AA sphere surrounding the species to which energy is to be transferred; a concentration of 0.2 M places one in each 13\AA sphere.

128. Ref. 60; pp 329 ff.

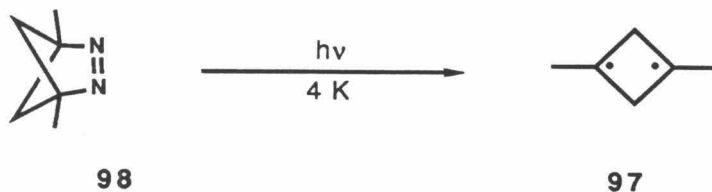
129. Balzani, V.; Bolletta, F.; Scandola, F. *J. Am. Chem. Soc.* **1980**, *102*, 2152-2163.

130. While the observed activation parameters suggest a concerted dimerization, they are not inconsistent with a stepwise mechanism. Similar activation parameters have been observed in the stepwise dimerization of 2,3-dimethylene-2,3-dihydrofuran: Chou, C.-H.; Trahanovsky, W.S. *J. Am. Chem. Soc.* **1986**, *108*, 4138-4144.

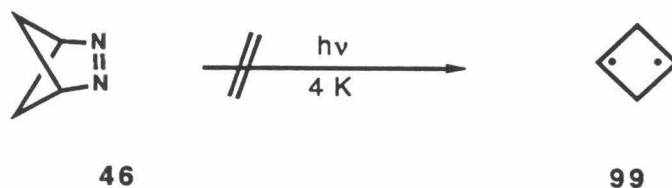
Appendix 1

Attempted Preparation of 2,4-Dialkyl-1,3-cyclobutanediyls

Several years ago we generated the localized triplet biradical 1,3-dimethyl-1,3-cyclobutanediyl (**97**) by photolysis of diazene **98** and directly observed it by EPR spectroscopy. Photolysis of diazene **46**, on the other hand,



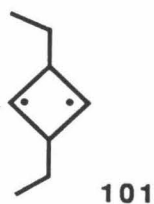
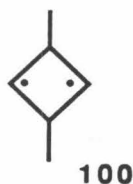
had earlier been found not to produce an EPR signal corresponding to the parent biradical **99**.² The observation of a triplet EPR signal for **97** at



temperatures as low as 4 K¹ strongly supports the theoretical prediction of triplet ground states for cyclobutanediyls. Biradical **97** is not indefinitely stable, even at 4 K, however, and it decays by ring closure to 1,3-dimethylbicyclobutane.¹ The ring closure rates for **97** were found to be quite insensitive to temperature from 4-25 K, implying that the decay involves heavy-atom tunnelling.¹ Tunnelling rates are critically dependent on the mass of the tunnelling particle.⁴ Since all the atoms of **97** move during ring closure, the tunnelling mass is effectively that of the entire molecule. One could argue, therefore, that the failure to observe **99** results from its smaller mass and greatly accelerated ring closure rate.⁵ Diazene **46** undergoes primarily β C—C bond cleavage from its T_1 state,² as does diazene **98**.⁵ Thus, another possibility is that the radical-stabilizing methyl groups allow some

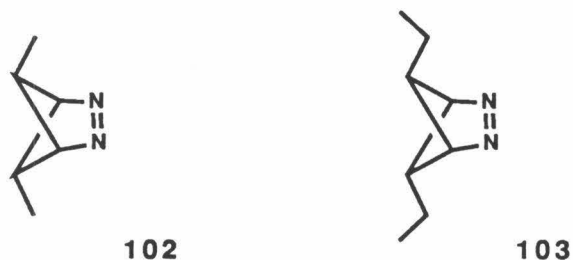
C—N bond cleavage to occur for **98**, whereas perhaps none occurs in the case of **46**.

We wondered what effect placing methyl groups at the 2 and 4 positions of the cyclobutanediyl ring would have on the decay rate of the biradical. Biradical **100** might then provide an interesting comparison to **97** in terms of the heavy-atom tunneling process. Similarly, the diethyl analog, **101**, was expected to be of interest in relation to its 1,3 isomer.^{5,6}

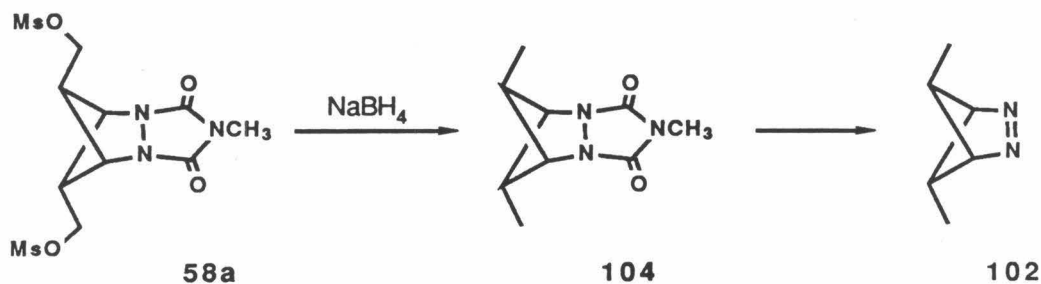


Results.

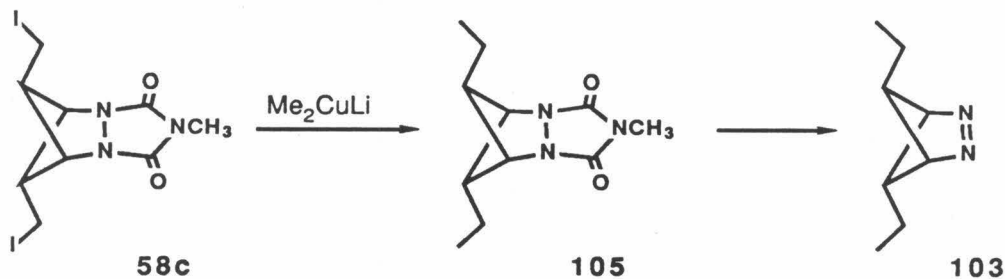
The synthesis described in Chapter 2 provided an easy route to the azo precursors to **100** and **101**, diazenes **102** and **103**, respectively. The



preparation of diazene **102** involved hydride displacement of the mesylate groups of **58a** to provide **104**. The standard hydrolysis/oxidation sequence



then afforded diazene **102**. Diazene **103** was prepared by treating diiodide **58c** with Me_2CuLi to produce **105**, which was easily converted to **103**.



Unfortunately, prolonged irradiation of neither **102** nor **103** at or near 4 K in the cavity of an EPR spectrometer produced a triplet EPR signal.

Experimental.

Descriptions of general procedures and instrumentation can be found in Chapters 2 and 3.

Exo,exo-8,9-dimethyl-4-methyl-2,4,6-triazatricyclo[5.1.1.0^{2,6}]nonane-3,5-dione (104). Mesylate 58a (0.20 g, 0.52 mmol), *ca.* 2.5 ml. of HMPA, and NaBH₄ (100 mg, 2.64 mmol) were combined and stirred magnetically at room temperature for 3.5 hrs.⁷ The solution was poured cautiously into 10 ml of half-sat'd NaCl, the product was extracted with Et₂O (3 x 10 ml), and the Et₂O solution was washed with 15 ml of half-sat'd NaCl and dried (MgSO₄). Removal of the solvent provided a small volume of HMPA solution. This was taken up in Et₂O and flash chromatographed on a 2-cm x 5-in silica column with 200 ml of Et₂O as eluent to afford 74 mg (74%) of 104 as a colorless oil: ¹H NMR (90 MHz, CDCl₃) δ 4.41 (t, *J*=1.7 Hz, 2 H, H-1,7), 3.01 (s, 3 H, NCH₃), 2.30 (qt, *J*=6.4, 1.7 Hz, 2 H, H-8,9), 0.79 (d, *J*=6.4 Hz, 6 H, CH₃). ¹³C NMR (22.6 MHz, CDCl₃) δ 159.5 (C=O), 66.3 (C-1,7), 45.9 (C-8,9), 25.7 (NCH₃), 9.6 (CH₃). MS (EI) *m/e* 195 (M⁺), 180 (M⁺ - CH₃), 138 (M⁺ - CH₃NCO), 128 (M⁺ - CH₃NCO,CH₃), 111, 110 (M⁺ - CH₃NCO,CO), 96, 95 (M⁺ - CH₃NCO,CO,CH₃), 94, 83, 82 (M⁺ - CH₃NCO,CO,N₂), 81, 80, 69, 68, 67 (M⁺ - CH₃NCO,CO,N₂,CH₃). Anal. Calc'd for C₉H₁₃O₂N₃: C, 55.37%; H, 6.71%; N, 21.52%. Found: C, 54.00%; H, 6.59%; N, 21.65%.

Exo,exo-5,6-dimethyl-2,3-diazabicyclo[2.1.1]hex-2-ene (102). Following the standard procedure,⁸ urazole 104 (45 mg, 0.23 mmol), 150 mg (2.33 mmol) of 87% KOH, and *ca.* 2 ml of isopropanol were combined, and Ar was

bubbled through the mixture for *ca.* 10 min. With magnetic stirring the reaction mixture was heated at *ca.* 90 °C for 9 hrs. After the cloudy mixture had cooled, most of the isopropanol was removed with a stream of N₂, the solids were dissolved in *ca.* 1 ml of (degassed) water, and the solution was acidified with (degassed) 3 M HCl, which caused gas evolution. The solution was warmed to *ca.* 40 °C for 10-15 min and cooled, and the pH was adjusted to 5-6 with (degassed) 1 M NH₄OH. A solution of CuBr₂ (130 mg, 0.58 mmol) in *ca.* 0.5 ml of water was introduced, causing the rapid formation of a red-brown precipitate. The solid was isolated by suction filtration and washed with water (2-3 ml), MeOH (1 ml) and Et₂O (1 ml). Air drying afforded 69 mg (53%) of the CuBr complex of **102** as a rust-colored solid.

The solid was suspended in 3-4 ml of Et₂O, the stirred slurry was cooled in an ice bath, and *ca.* 3 ml of 1 M NH₄OH was added. After *ca.* 15 min the Et₂O layer was removed, the blue aqueous layer was extracted with an additional 3 x 4 ml of Et₂O, and the combined ether extracts were dried over MgSO₄. The solvent was removed by careful distillation (bath temp. 41-42 °C), and the pot residue, which GC analysis (DB-5 capillary, 50 °C) indicated to be primarily **102**, was dissolved in CDCl₃. The diazene (**102**) was subsequently isolated by preparative-GC (0.25 in x 15 ft 10% UCW 982; 65 °C; 50 ml min⁻¹; r.t. *ca.* 20 min) to provide 10.4 mg (41%) of **102** as a liquid (mp *ca.* -10 °C): ¹H NMR (90 MHz, CDCl₃) δ 4.90 (t, *J* ≈ 2 Hz, 2 H, H-1,4), 2.48 (qt, *J* ≈ 7,2 Hz, 2 H, H-5,6), 0.80 (d, *J* ≈ 7 Hz, 6 H, CH₃). UV (cyclohexane) λ_{max} 341 nm (ε 555 M⁻¹ cm⁻¹), 329 (130).

Exo,exo-8,9-diethyl-4-methyl-2,4,6-triazatricyclo[5.1.1.0^{2,6}]nonane-3,5-diene (105). To a well-stirred slurry of CuBr-Me₂S complex (460 mg, 2.24 mmol) in 2.5 ml of Et₂O under Ar at 0 °C, was added 2.5 ml (4.5 mmol) of 1.8 M methyllithium in Et₂O via syringe over *ca.* 5 min.^{9,5} (A small amount of yellow MeCu remained after the addition was complete.) After another 15-20 min a solution of diiodide 58c (50 mg, 0.112 mmol) in 1.5 ml of CH₂Cl₂-Et₂O (1:1 *v/v*) was added over *ca.* 3 min, and the yellow mixture was allowed to stir under Ar at 0 °C for *ca.* 1.5 hrs. The mixture was poured into 40 ml of sat'd NH₄Cl, the product was extracted from the blue aqueous layer with Et₂O (3 x 40 ml), and the ether solution was dried (MgSO₄). Removal of the solvent (in a fume hood) afforded a yellow solid. The CH₂Cl₂-soluble material was flash chromatographed on a 1 cm x 5.5 in silica column with 30 ml of 10:1 (*v/v*) CH₂Cl₂-Et₂O as eluent to afford 5.3 mg (21%) of 105 as a colorless residue: ¹H NMR (400 MHz, CDCl₃) δ 4.56 (t, *J* = 1.7 Hz, 2 H, H-1,7), 3.02 (s, 3 H, NCH₃), 2.08 (tt, *J* = 1.7, 7.3 Hz, 2 H, H-8,9), 1.15 (pseudo-quintet, *J* = 7.3 Hz, 4 H, CH₂), 0.83 (t, *J* = 7.3 Hz, 6 H, CH₃).

Exo,exo-5,6,-diethyl-2,3-diazabicyclo[2.1.1]hex-2-ene (103). The procedure above for the preparation of diazene 102 was employed. The hydrolysis was conducted in a sealed tube, and the orange-red copper complex was isolated by centrifugation, washed, and air-dried. Liberation of the diazene by treatment of the complex with NH₄OH afforded 103 as a slightly yellow oil with a distinctive odor: UV (MTHF) λ_{max} 341, 329 nm.

EPR experiments. Samples of diazene **102** in cyclohexane and MTHF at 5-6 K were irradiated for *ca.* 30 min with the pyrex-filtered output of an Oriel 200-W Hg(Xe) arc lamp (conditions that typically provided a large signal for biradical **97**), but no EPR signal was observed. Samples of diazene **103** in MTHF with and without Ph₂CO were irradiated at 4 K with UV light from a 1000-W Xe arc lamp, but no triplet EPR signal was observed.

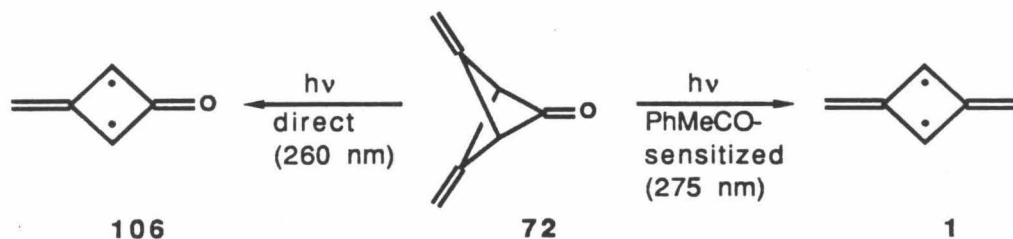
References and notes.

1. Jain, R.; Snyder, G.J.; Dougherty, D.A. *J. Am. Chem. Soc.* **1984**, *106*, 7294-7295.
2. Chang, M.H.; Dougherty, D.A. *J. Am. Chem. Soc.* **1982**, *104*, 2333-2334.
3. Goldberg, A.H.; Dougherty, D.A. *J. Am. Chem. Soc.* **1983**, *105*, 284-290.
4. For example, see Bell, R.P. *The Tunnel Effect in Chemistry*; Chapman and Hall: New York, 1980.
5. Jain, R., Ph.D. thesis, California Institute of Technology, 1987.
6. Jain, R.; Sponsler, M.B.; Coms, F.D.; Dougherty, D.A. *J. Am. Chem. Soc.*, submitted.
7. Hutchins, R.O.; Kandasamy, D.; Dux, F., III; Maryanoff, C.A.; Rotstein, D.; Goldsmith, B.; Burgoyne, W.; Cistone, F.; Dalesandro, J.; Puglis, J. *J. Org. Chem.* **1978**, *43*, 2259-2267.
8. Chang, M.H.; Jain, R.; Dougherty, D.A. *J. Am. Chem. Soc.* **1984**, *106*, 4211-4217.
9. See, for example, Ireland, R.E.; Daub, J.P. *J. Org. Chem.* **1981**, *46*, 479-485.

Appendix 2

Concerning 2-Oxo-4-methylene-1,3-cyclobutanediyl

After we initially reported the generation of biradical **1** ($D=0.0204$, $E=0.0028\text{ cm}^{-1}$) by photolysis of diazene **2** under cryogenic, matrix-isolation conditions¹ (see Chapter 2), Dowd and Paik reported the preparation of **1** by photolysis of ketone **72**.² Interestingly, direct photolysis provided a different triplet EPR signal ($D=0.018$, $E=0.006\text{ cm}^{-1}$).² Dowd and Paik suggested that this new signal be ascribed to biradical **106**, the product of vinylidene extrusion from photoexcited **72**.² The generation of a biradical by such a reaction is to our knowledge without literature precedent.



The D value observed for this species is clearly consistent with the EPR signal carrier being a delocalized triplet biradical. Dowd and Paik's assignment of this signal to **106**, however, seems to rely primarily on the large E value observed, although little justification is offered for expecting an increase in E on going from **1** to **106**.²

Reassignment of the reported EPR spectrum.

We believe that the D value for a triplet EPR spectrum is a far better indicator of structure than the E value. Use of the previously described computational method³ consistently finds that the D value should increase noticeably upon oxygen-substitution at the spin center of a non-Kekulé hydrocarbon. Table A2-1 lists the D values calculated (by using Hückel wavefunctions) for such biradical pairs. Experimentally, the D values for 12 (0.011 cm^{-1} 4) and 15 (0.027 cm^{-1} 3) support this expectation. However, spin polarization can have a large influence of the zero-field splitting, and one must therefore be cautious in the use of low-level wavefunctions to calculate D values for delocalized biradicals.⁵

There are three principal reasons that oxygen-substitution should increase the D value for delocalized biradicals, and each effect operates by decreasing the separation between the unpaired spins. (1) C—O bonds are shorter than the corresponding C—C bonds, (2) oxygen holds its electrons more tightly than carbon, and (3) incorporation of an oxygen atom polarizes the NBMOs so as to place AO coefficients on formerly inactive carbons. This last point is illustrated below for 1 vs 106. The non-bonding electrons of 106 experience several short-range 1,2-interactions, while those of 1 experience (to first

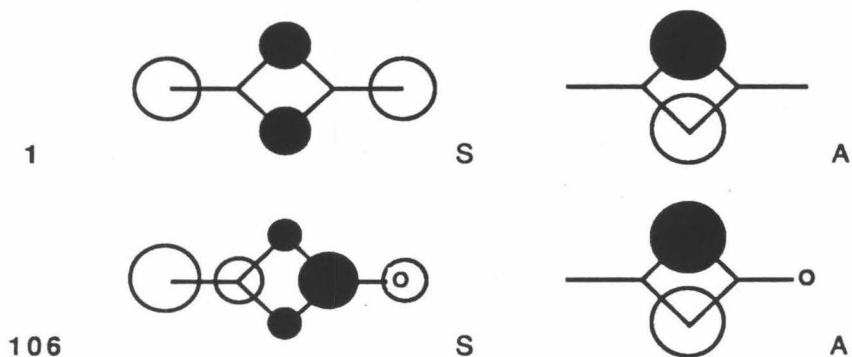
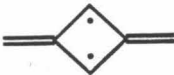

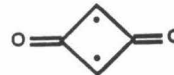

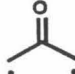
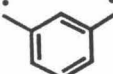
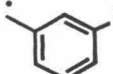


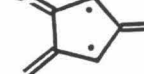


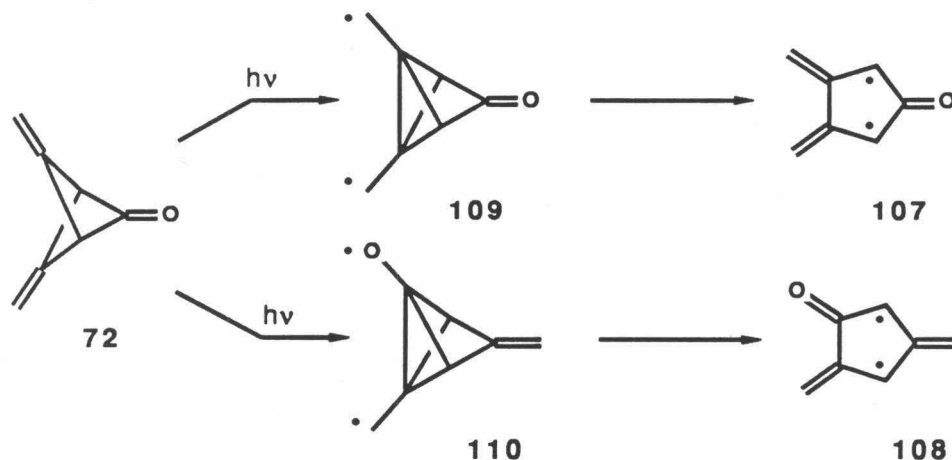
Table A2-1. Calculated *D* values for non-Kekulé hydrocarbons and their oxo analogs.

<i>D</i> ^a (calc.b)		
	1	0.051
	106	0.091
	111	0.084
	4	0.052 ^c
		0.135
	12	0.034 ^{c,d}
	15	0.057 ^{c,d}
		0.030
	107	0.059
	108	0.043

^ain cm⁻¹. ^bbased on Hückel wavefunctions; 1.41 Å C=C bonds, 1.27 Å C=O bonds. ^cref. 3. ^dbased on INDO wavefunctions.³

order) only 1,3-interactions. One would expect these three factors to be generally operative in such systems, and the calculated D values of Table A2-1 clearly bear out this expectation. Given the magnitude of the increase in D upon oxygen-substitution, one would expect this effect to survive the influence of spin polarization. Thus, there is good reason to expect the D value for 106 to be larger than that for 1.

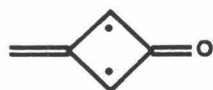
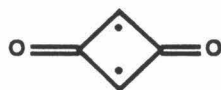
While the assignment of the mystery EPR signal to 106² may be correct, we believe an alternative assignment is well worth considering. We propose that this signal might arise from biradical 107 or 108. These species could be produced as shown below. Photolysis of ketone 72 might reasonably be expected to induce the initial step of a di- π -methane or oxa-di- π -methane rearrangement⁶ to produce 109 or 110. Each of these species could then



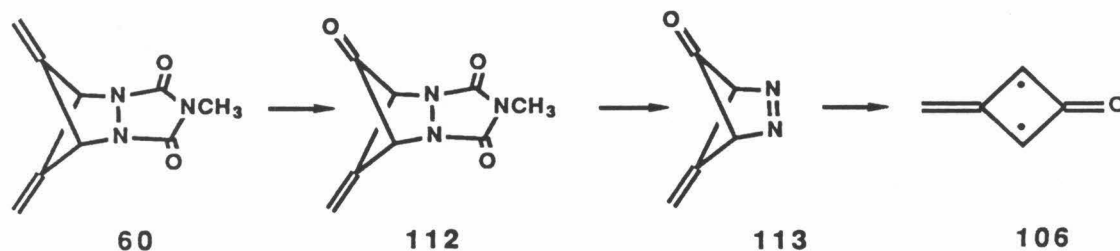
undergo two cyclopropylcarbinyl-type cleavages, either sequentially or simultaneously, to provide 107 or 108. The apparent viability of this route — especially as compared to an extrusion of vinylidene from 72 — suggests that the assignment of the mystery EPR signal to biradical 106² was perhaps a bit premature.

Attempted synthesis.

Biradicals **106** and **111**⁷ are intrinsically interesting species that should serve as important tests of ground state spin multiplicity predictions.⁸ The recent report of the EPR spectrum of **106** (see above)² provided us additional motivation to attempt the preparation of these biradicals.

**106****111**

Our synthesis of **1** (Chapter 2) appeared to furnish an easy route to **106** (and/or **111**). This involved oxidative cleavage of one double bond of diene **60** to provide **112**, which could be converted to the corresponding diazene (**113**), a viable precursor to **106**. Various methods to effect the transformation of **60** to **112** were attempted, but without success. These included ozonolysis under a variety of conditions, RuO_4 and OsO_4 oxidations, and routes involving initial bromohydrin formation or epoxidation with MCPBA, $\text{H}_2\text{O}_2/\text{CH}_3\text{CN}$, and $\text{CF}_3\text{CO}_3\text{H}$ (to be followed by conversion to the vicinal diol and NaIO_4 cleavage). Attempts to prepare **112** by various other routes are currently being undertaken in our laboratory.



References and notes.

1. Snyder, G.J.; Dougherty, D.A. *J. Am. Chem. Soc.* **1985**, *107*, 1774-1775.
2. Dowd, P.; Paik, Y.H. *J. Am. Chem. Soc.* **1986**, *108*, 2788-2790.
3. Rule, M.; Matlin, A.R.; Seeger, D.E.; Hilinski, E.F.; Dougherty, D.A.; Berson, J.A. *Tetrahedron* **1982**, *38*, 787-798.
4. Wright, B.B.; Platz, M.S. *J. Am. Chem. Soc.* **1983**, *105*, 628-630.
Goodman, J.L.; Berson, J.A. *J. Am. Chem. Soc.* **1985**, *107*, 5409-5424; **1984**, *106*, 1867-1868.
5. See the discussion in Chapter 2 of this thesis.
6. Hixson, S.S.; Mariano, P.S.; Zimmerman, H.E. *Chem. Rev.* **1973**, *73*, 531-551.
7. (a) Gleiter, R.; Hoffmann, R. *Angew. Chem., Int. Ed. Engl.* **1969**, *8*, 214-215. (b) Budzelaar, P.H.M.; Kraka, E.; Cremer, D.; Schleyer, P.v.R. *J. Am. Chem. Soc.* **1986**, *108*, 561-567. Schleyer, P.v.R.; Budzelaar, P.H.M.; Cremer, D.; Kraka, E. *Angew. Chem., Int. Ed. Engl.* **1984**, *23*, 374-375.
8. See the discussion in refs. 3 and 7a.

Appendix 3

Source Listing of Computer Programs

Programs "CURIE", "UVESRDV", and "KINB" are written in FORTRAN for the IBM-PC/AT. "CURIE" calculates a triplet EPR signal intensity vs $100/T$ curve for a value of the S-T gap specified by the user. "UVESRDV" generates a photochemical action spectrum from EPR intensity $vs.$ λ data by smoothing and differentiating the data, then dividing by signal intensity and incident light intensity. "KINB" calculates the concentration of **3** at specific time intervals by using the values of k_1 , k_2 , $[2]_0$ and $[3]_0$ provided by the user.

Programs "ABS" and "OSCIL" are written in BASIC for the HP-85A interfaced with the HP-8451A UV-vis spectrophotometer. "ABS" determines the absorbance at a given λ vs a baseline drawn between two reference λ s. "OSCIL" determines an absorption oscillator strength by numerically integrating a spectrum and by using an ϵ provided by the user.

Program "CURIE"

```

C      THIS PROGRAM READS A FOUR-LINE DATA FILE "CURIE.PAR" THAT CONTAINS:
C      ES -- THE S-T GAP (ES-ET, IN CAL/MOL)
C      TL,TH -- THE TEMPERATURE LIMITS FOR THE CALCULATED CURVE
C      C1,C2 -- THE SLOPE AND INTERCEPT OF THE I VS 100/T LINE
C      MODE -- SWITCH: 0 -- USE CURVE DETERMINED BY C1,C2 INPUT
C          1 -- SET CURVE TO INTERSECT LINE AT 20 K
C          2 -- SET CURVE TO INTERSECT LINE AT 20 AND 80 K
C      THE OUTPUT IS PRINTED TO "CURIE.CAL" AS INTENSITY, 100/T
      DIMENSION TI(50),I(50)
      REAL IT,I
      OPEN(5,FILE='CURIE.PAR',STATUS='OLD')
      OPEN(6,FILE='CURIE.CAL',STATUS='UNKNOWN')
      READ(5,*) ES
      READ(5,*) TL,TH
      READ(5,*) C1,C2
      READ(5,*) MODE
      MODE = MODE-1
      IF (MODE) 87,73,74
C      FIND NEW INTERCEPT (C2) SO THAT CURVE INTERSECTS LINE AT 20 K
73  YI = C1*100/20 + C2
      C2 = YI - (300*C1)/(20*(3.0+EXP((-1)*ES/(20*1.987))))
C      SCALE SLOPE (C1) FROM 100/T DATA
      C1 = C1*100
      GOTO 87
C      CALCULATE C1 AND C2 SO THAT CURVE INTERSECTS LINE AT 20 AND 80 K
74  YI1 = C1*100/20 + C2
      YI2 = C1*100/80 + C2
      X1 = 3/(20*(3.0+EXP((-1)*ES/(20*1.987))))
      X2 = 3/(80*(3.0+EXP((-1)*ES/(80*1.987))))
      C1 = (YI1-YI2)/(X1-X2)
      C2 = YI1 - (3*C1)/(20*(3.0+EXP((-1)*ES/(20*1.987))))
C      CALCULATE CURVE
87  SIT = 1/TL - 1/TH
      DIT = SIT/49
      IT = 1/TH + DIT
      DO 517 J=1,50
      DENOM = 3.0 + EXP((-1)*ES*IT/1.987)
      I(J) = 3*C1*IT/DENOM + C2
      TI(J) = 100*IT
      IT = IT + DIT
517 CONTINUE
      WRITE(6,17) (I(K),TI(K),K=1,50)
17  FORMAT(' ',F6.2,',',F7.4)
      STOP
      END

```

Program "UVESRDV"

C Written by Gary J. Snyder (adapted to the IBM PC/AT by Michael B. Sponsler)
 C 5/16/87 --- copyright 1987 GJS, Inc.

C
 C This program reads data from an ESR data file (ASCII format),
 C smoothes the data by a quadratic/cubic least squares procedure,
 C and differentiates the data using a quadratic filter.
 C The smoothing and differentiation procedures are described in:
 C A.Savitzky,M.J.E.Golay, AnalChem, 36, 1627-1639 (1964), and
 C R.R.Ernst, AdvMagRes, 2, 1-135 (1966), esp. p. 45.
 C Parts of the program are patterned after QEPR by Jeff Gelles
 C (and Craig Martin).

C
 C Input data file --- for004 UVE.DAT
 C Input lamp intensity file --- for003 XE1000.INT
 C Smoothed data output --- for007 UVESM.DAT
 C Deriv. data $((-1/I)*dI/dt)$ output --- for008 UVEDV.DAT

C
 C The program is designed to produce an electronic absorption
 C spectrum from a photochemical action spectrum -- $dI/d\lambda$,
 C then correct for variation in lamp output with wavelength.
 C The output files can be used directly as input for the plotting
 C program DUV written by Michael B. Sponsler.

C
 C The program also reads input parameters interactively as follows:

C
 C 1 ----- NBL -- baseline value (full scale 4100).
 C
 C 2,3 ----- NSM, NDV -- number of adjacent points to be used
 C for smoothing and differentiation,
 C respectively. These must be ODD
 C integral values, typically 15-45.
 C For deriv. only, enter 01 for NSM;
 C an output file "UVESM.DAT" will not be
 C written.
 C
 C 4,5 ----- DPL, DPR -- first and last data points to be used
 C (full spectral width 1000 dp).
 C
 C 6,7 ----- LL, LR -- wavelengths at the left and right sides
 C of the spectrum, respectively. (These do
 C not need to be ordered $LL < LR$.)
 C
 C 8 ----- LAMP -- scale for lamp intensity variation? (1,0)

-----continued-----

```

C
C 9  ----- BP -- (if LAMP = 1) monochrometer bandpass (nm).
C      For lack of anything better, a Gaussian
C      weighting function is applied with a width
C      at half-height of BP nm. Conveniently,
C      this also allows the intensity data,
C      which has 1 nm spacing, to be "projected"
C      onto the ESR data point space.
C
C *****
C
C      DIMENSION PAR(23), CFIL(35), DFIL(35), CX(18), C1(18), C2(18),
C      *AAINT(500), BINT(1005)
C      CHARACTER NAME*8
C      INTEGER*4 FI, A(1005), B(1005), D(15), LINT(500), DPL, DPR
C      REAL*8 C(1005)
C      DATA FILE/4HFILE/
C
C      Read data from input file _____
C
C      OPEN(UNIT=4, FILE='UVE.DAT', STATUS='OLD')
C      READ(4,992) TEST, FI
C      IF (TEST.NE.FILE) GO TO 999
C      READ(4,1042,ERR=1047) A
C      READ(4,1042,ERR=1047) D
C      READ(4,603,ERR=607) (PAR(I), I=1,23)
C      READ(4,2042,ERR=2047) (CX(I),I=1,18)
C      READ(4,2042,ERR=2047) (C1(I),I=1,18)
C      READ(4,2042,ERR=2047) (C2(I),I=1,18)
C      992 FORMAT(1X,A4,2X,I2)
C      1042 FORMAT(1X,15I4)
C      603 FORMAT(1X,1P5E14.7)
C      2042 FORMAT(1X,18A4)
C
C      Read parameters interactively _____
C
C      WRITE (6,11)
C      11 FORMAT (/' Please enter baseline level. ')
C      READ (5,*) NBL
C      WRITE (6,12)
C      12 FORMAT (/ ' Smoothing and derivative windows? (typ. 15-45, odd) ')
C      READ (5,*) NSM,NDV
C      10 WRITE (6,13)
C      13 FORMAT (/ ' Please enter first and last data points to be used. ')
C      READ (5,*) DPL,DPR

```

-----continued-----

```

NDP = DPR - DPL + 1
IF (NDP.LT.0) GO TO 10
WRITE (6,14)
14 FORMAT (' To what wavelengths do these correspond? ')
READ (5,*) LL,LR
IF (LL.LT.LR) THEN
    LSTART = LL - 1
ELSE
    LSTART = LR - 1
ENDIF
LRNG = LR - LL
WRITE (6,15)
15 FORMAT (' Would you prefer that I scale your action spectrum')
WRITE (6,16)
16 FORMAT (' for the variation in lamp intensity with wavelength?')
WRITE (6,17)
17 FORMAT (' If so, please enter "1"; if not, "0". ')
READ (5,*) LAMP
IF (LAMP.NE.1) GO TO 9
WRITE (6,18)
18 FORMAT (' Please enter monochrometer bandpass in nm.')
WRITE (6,19)
19 FORMAT (' A Gaussian with this width at half-height will be')
WRITE (6,20)
20 FORMAT (' applied to the lamp intensity data. ')
READ (5,*) BP
9 WRITE (6,21)
21 FORMAT (' Thank you so much -- you have been very cooperative.')
WRITE (6,22)
22 FORMAT (//////' .... Igor, take these data to my study.')
WRITE (6,23)
23 FORMAT (//'          (grunt) Yaath, Maathtaaa (drool).////)
GO TO 5713

```

C
C
C

Error messages

```

999 WRITE(6,998)
998 FORMAT('0 NO "FILE" STATEMENT FOUND')
STOP
607 WRITE(6,608)
608 FORMAT('0 ERROR IN READING PARAMETERS')
STOP
1047 WRITE(6,1048)
1048 FORMAT('0 ERROR IN READING ESR DATA')
STOP

```

continued

```

2047 WRITE(6,2048)
2048 FORMAT('0 ERROR IN READING COMMENTS')
STOP

```

C

C

```

Lamp intensity matrix _____

```

C

```

1 Read appropriate data from file _____

```

C

```

5713 IF (LAMP.NE.1) GO TO 7
      OPEN (UNIT=3, FILE='XE1000.INT', STATUS='OLD')
      READ (3,73) IPTS
      73 FORMAT (/I3)
807 READ (3,74) LTEST, ATEST
      74 FORMAT (I3,1X,F6.4)
      IF (LTEST.NE.LSTART) GO TO 807
      DIR = LRNG/ABS(LRNG)
      LDP = ABS(LRNG) + 1
      XHLF = (LR - LL)/2
      N1 = ABS(XHLF) + 1 - XHLF
      N2 = ABS(XHLF) + 1 + XHLF
      READ (3,74) (LINT(J), AAINT(J), J=N1,N2,DIR)

```

C

C

```

2 Determine Gaussian weighting function and project

```

C

```

intensity data onto points of EPR data set _____

```

C

```

XLDP = FLOAT(LDP)
CONV = (XLDP-1.0)/(NDP-1)
BPP = BP/CONV
A1 = (-2.7726)/BPP**2
K = INT(1.2888*BPP + 1)
XK = K*CONV
KX = 2*NINT(XK) + 1
NST = DPL + INT((NINT(XK) - 0.5)/CONV + 2)
NFN = DPR - NST + DPL + 1
DO 1118 J=NST,NFN
  XINDM = (J - DPL)*CONV + 1
  NINDL = NINT(XINDM) - NINT(XK)
  BINT(J) = 0.0
  DO 1123 I=NINDL,NINDL+KX-1
    DISPL = ((I - 1)/CONV + DPL) - J
    COEFF = EXP(A1*DISPL**2)
    BINT(J) = BINT(J) + COEFF*AAINT(I)
1123 CONTINUE
1118 CONTINUE
      DO 1203 J=DPL,NST-1
120 BINT(J) = BINT(NST)

```

_____continued_____

```

      DO 1204 J=NFN+1,DPR
1204 BINT(J) = BINT(NFN)
C
C   Determination of convolution functions
C
      7 MSM=(NSM-1)/2
      MDV=(NDV-1)/2
      CNORM=0
      DNORM=0
      DO 1017 I=1,NSM
      J=I-MSM-1
      CFIL(I) = 3*MSM**2 + 3*MSM - 1 - 5*J**2
      CNORM=CNORM + CFIL(I)
1017 CONTINUE
      DO 9743 I=1,NDV
      J=I-MDV-1
      DFIL(I) = J
      DNORM=DNORM + J**2
9743 CONTINUE
C
C   Quadratic/Cubic Smoothing in NSM window
C
      DO 88 K=DPL+MSM,DPR-MSM
      B(K)=0
      M=0
      DO 119 L=K-MSM,K+MSM
      M=M+1
      B(K) = B(K) + A(L)*CFIL(M)
119 CONTINUE
      B(K) = B(K)/CNORM
      88 CONTINUE
      DO 741 N=DPL,DPL+MSM-1
741 B(N) = B(DPL+MSM)
      DO 742 N=DPR-MSM+1,DPR
742 B(N) = B(DPR-MSM)
C
C   Quadratic Filter and Derivative in NDV window
C
      DO 417 K=DPL+MDV+MSM,DPR-MDV-MSM
      C(K)=0
      M=0
      DO 428 L=K-MDV,K+MDV
      M=M+1
      C(K) = C(K) + B(L)*DFIL(M)
428 CONTINUE

```

-----continued-----

```

      C(K) = C(K)/DNORM
417  CONTINUE
      DO 5334 I=DPL,DPL+MSM+MDV-1
5334 C(K) = C(DPL+MSM+MDV)
      DO 5335 I=DPR-MSM-NDV+1,DPR
5335 C(K) = C(DPR-MSM-MDV)
C
C      Find  $(-1/I)*dl/dt$ 
C
      CMAX=0
      CMIN=100
      DO 766 N=DPL,DPR
      FINT = B(N) - NBL
      C(N) = (-1000)*C(N)/FINT
      IF(C(N).GT.CMAX) CMAX=C(N)
      IF(C(N).LT.CMIN) CMIN=C(N)
766  CONTINUE
      IF (LAMP.NE.1) GO TO 1705
C
C      Scale for lamp intensity
C
      CMAX = 0
      CMIN = 100
      DO 57 I=DPL,DPR
      C(I) = 1000*C(I)/BINT(I)
      IF (C(I).GT.CMAX) CMAX = C(I)
      IF (C(I).LT.CMIN) CMIN = C(I)
57  CONTINUE
C
C      Scale differentiated data in y-direction
C
1705 CFACT=4000/(CMAX-CMIN)
      DO 2 L=DPL,DPR
2  A(L) = (C(L)-CMIN)*CFACT
C
C      Write data to output files
C
      IF (DPR.GE.1000) DPR = 999
      D(1) = DPL
      D(2) = DPR
      D(3) = LL
      D(4) = LR
      IF (NSM.EQ.1) GO TO 798
      J=7
      NAME='SMOOTHED'

```

—————continued—————


```

      OPEN (UNIT=J, FILE='UVESM.DAT')
5011 WRITE(J,501,ERR=599) FI,NAME
      501 FORMAT(' FILE #',I2,5X,A8)
      IF (J.EQ.7) THEN
      WRITE(J,504,ERR=599) B
      ELSE
      WRITE(J,504,ERR=599) A
      ENDIF
      WRITE(J,504,ERR=599) D
504  FORMAT(1X,15I4)
      WRITE(J,507,ERR=599) (PAR(I),I=1,23)
507  FORMAT(1X,1P5E14.7)
      WRITE(J,509,ERR=599) (CX(I),I=1,18)
      WRITE(J,509,ERR=599) (C1(I),I=1,18)
      WRITE(J,509,ERR=599) (C2(I),I=1,18)
509  FORMAT(1X,18A4)
      WRITE(J,333)
333  FORMAT(/)
798  IF (J.EQ.8) GO TO 441
      J=8
      NAME='DERIV'
      OPEN(UNIT=J, FILE='UVEDV.DAT')
      GO TO 5011
599  WRITE(6,600)
600  FORMAT('0 ERROR IN WRITING OUTPUT. OHNOOOOOOOOOO!!')
441  WRITE (6,7738)
7738 FORMAT (' I have placed your data in the files UVESM.DAT and')
      WRITE (6,7740)
7740 FORMAT (' UVEDV.DAT. Thank you and good evening....Come, Igor.')
      WRITE (6,7742)
7742 FORMAT (/ '      Yaaaaath...Gooood eeeeeevening.'//)
      STOP
      END

```

Program "KINB"

```

C   INPUT FILE "KIN.PAR" -- GRRR INPUT + k1/k2/[A]0/[B]0/FINAL TIME/
C   NCALCPTS/SWITCH: 0=NORMAL PLOT; 1=EXTRAPOLATION TO [B]=0
      DIMENSION TEX(30),BEX(30),TC(500),BC(500)
      CHARACTER*60 TITLE,SUBT,XAX,YAX
      INTEGER TF,TC,TEX
      OPEN(5,FILE='KIN.PAR',STATUS='OLD')
      OPEN(6,FILE='KIN.FIT',STATUS='UNKNOWN')
      READ(5,17) TITLE,SUBT,XAX,YAX
      READ(5,19) NEXPT
      READ(5,*) (BEX(I),TEX(I),I=1,NEXPT)
      READ(5,*) AK,BK,ACONC,BCONC,TF,NCP,KSW
      JSW = 0
      DELT=TF/NCP
      ACC=ACONC
      BCC=BCONC
      TCC=0
      IF (KSW.EQ.1) GO TO 5309
1998 DO 2217 J=1,NCP
      TC(J)=TCC
      BC(J)=BCC
2042 TCC = TCC+DELT
      ACC = ACC - AK*ACC*DELT
      DELB = (AK*ACC - 2*BK*BCC**2)*DELT
      BCC = BCC + DELB
      IF (JSW.EQ.0) GO TO 2217
      IF (BCC.LE.0.0) GO TO 5817
      GO TO 2042
2217 CONTINUE
      NLINE = 2
      WRITE(6,18)TITLE,SUBT,XAX,YAX
      WRITE(6,25)NLINE,NCP,NEXPT
      WRITE(6,29) (BC(I),TC(I),I=1,NCP)
      WRITE(6,29) (BEX(I),TEX(I),I=1,NEXPT)
17  FORMAT(A60/A60/A60/A60)
18  FORMAT(' ',A60/1X,A60/1X,A60/1X,A60)
19  FORMAT(/I2)
21  FORMAT(E10.4/F6.4/E10.4/E10.4/I7/I1)
25  FORMAT(1X,I1/1X,I3/1X,I2)
29  FORMAT(1X,E10.4,',',I7)
      GO TO 42
C   BACKTRACK ROUTINE
5309 JSW = 1
      DELT = -DELT

```

continued

```

      GO TO 1998
5817 DELT = (TF-TCC)/NCP
      JSW = 0
      GO TO 1998
42  STOP
    END

```

Sample input deck —

```

BCB concentration by NMR
224.8 K -- experimental data
Old Man Time (sec)
[bcbl (M)
1
12
1.46e-03,0
2.21e-03,105
2.52e-03,210
2.42e-03,315
2.26e-03,420
2.12e-03,540
1.91e-03,660
1.65e-03,840
1.57e-03,1020
1.33e-03,1200
1.22e-03,1500
8.66e-04,1800
1.545e-03
0.8611
8.51e-03
1.60e-03
0002500
100
0

```

Headings

Axis labels (for plotting program GRRR)

Number of data sets (for GRRR)

Number of data points

Concentration (M), time (sec)

Rate constant k_1 (s^{-1})

Rate constant k_2 ($M^{-1} s^{-1}$)

Initial diazene concentration (M)

Initial bicyclobutane concentration (M)

Final time (s)

Number of calculated points

Switch (see above)

Program "ABS"

```

10 ON KEY# 1,"2 PT" GOTO 150
20 ON KEY# 2,"3 PT" GOTO 250
30 ON KEY# 3,"PLOTTER" GOTO 360
40 ON KEY# 4,"EXIT" GOTO 390
50 CLEAR @ KEY LABEL
60 DISP
70 DISP "USE THE FUNCTION KEYS
   TO SELECT"
80 DISP
90 DISP "2 PT"
100 DISP "    ---ABS(λ) vs ABS(RE
   F λ)"
110 DISP "3 PT"
120 DISP "    ---ABS(λ) vs BASELI
   NE DRAWN"
130 DISP "    BETWEEN TWO REF
   λs"
140 GOTO 140
150 CLEAR @ BEEP 1500,20
160 DISP
170 DISP "ENTER λ"
180 INPUT L
190 DISP "ENTER REFERENCE λ"
200 INPUT R
210 I=VALUE(L)-VALUE(R)
220 PRINT USING "2/,2X,3D,8A,3D,
   8A" ; L," nm (vs ",R," nm RE
   F)"
230 PRINT USING "/6A,D.5D,2/" ;
   "ABS = ",I
240 GOTO 50
250 CLEAR @ BEEP 1500,15 @ WAIT
   1500 @ BEEP 1500,5
260 DISP
270 DISP "ENTER λ"
280 INPUT L
290 DISP "ENTER REFERENCE λs [R1
   ,R2]"
300 INPUT R1,R2
310 F=(L-R1)/(R2-R1)
320 I=(VALUE(R1)-VALUE(R2))*F+VA
   LUE(L)-VALUE(R1)
330 PRINT USING "2/,2X,3D,8A,3D,
   A,3D,8A" ; L," nm (vs ",R1,"
   ",R2," nm REF)"
340 PRINT USING "/6A,D.5D,2/" ;
   "ABS = ",I
350 GOTO 50
360 PLOTTER
370 WAIT 8000
380 GOTO 50

```

 continued

```

390 CLEAR
400 PLOTTER
410 FOR N=80 TO 10 STEP -1
420 BEEP N,100/N
430 NEXT N
440 PRINT USING "5/"
450 END

```

Program "OSCIL"

```

10 CLEAR
20 DISP "THIS PROGRAM IS DESIGN
   ED TO"
30 DISP "NUMERICALLY INTEGRATE
   AN"
40 DISP "ABSORPTION SPECTRUM (I
   N TERMS"
50 DISP "OF ENERGY) AND DETERMI
   NE AN"
60 DISP "OSCILLATOR STRENGTH."
70 DISP "BASELINE EXTRAPOL IS U
   SED."
80 DISP
90 DISP "see NJTurro, 'Modern Mo
   lecular"
100 DISP "Photochem', p. 87."
110 INTEGER Z1,Z2,L
120 DIM X(820),Y(820)
130 DISP
140 DISP "ENTER INTEGR LIMITS ( $\lambda$ 
   1, $\lambda$ 2)"
150 INPUT Z1,Z2
160 I1=VALUE(Z1)
170 I2=VALUE(Z2)
180 DISP
190 DISP "ENTER  $\lambda$  AND epsilon ( $\lambda$ 
   ,e)"
200 INPUT L,E
210 DISP
220 DISP "THANK YOU FOR THE YUMM
   IE DATA!"
230 FOR I=Z1 TO Z2 STEP 2
240 X(I)=10000000/I
250 Y(I)=VALUE(I)
260 NEXT I
270 A=0
280 FOR J=Z1+1 TO Z2-1 STEP 2
290 F=(J-Z1)/(Z2-Z1)
300 B=I1-F*(I1-I2)

```

—continued—

```

310 A=A+(Y(J-1)+Y(J+1)-2*B)*(X(J
    -1)-X(J+1))/2
320 NEXT J
330 F=(L-Z1)/(Z2-Z1)
340 R2=F*(I1-I2)-I1+VALUE(L)
350 R=E/R2
360 CLEAR
370 PRINT "NUMERICAL INTEGRATION
    "
380 PRINT USING "5A,3D,4A,3D,3A"
    ; "FROM ",Z1," TO ",Z2," nm
    "
390 PRINT USING "/4X,7A,D.3DE,5A
    " ; "AREA = ",A," cm-1"
400 PRINT USING "2/"
410 PRINT USING "2X,14A,5D,8A" ;
    "SCALED TO e = ",E," M-1cm-
    1"
420 PRINT USING "2X,7A,3D,4A" ;
    "AT  $\lambda$  = ",L," nm:"
430 A=A*R
440 PRINT USING "/4X,7A,D.3DE,8A
    " ; "AREA = ",A," M-1cm-2"
450 F7=A*.0000000043
460 PRINT USING "2/"
470 PRINT "OSCILLATOR STRENGTH,"
480 PRINT USING "2X,4A,D.3DE" ;
    "f = ",F7
490 PRINT USING "5/"
500 END

```